ANALYSIS AND NUMERICAL SIMULATION

OF TUMOR GROWTH MODELS

By

Daniel Acosta Soba

J. Rafael Rodríguez Galván
Professor of Mathematics
Universidad de Cádiz
(Advisor)

Jin Wang
Professor of Mathematics
University of Tennessee at Chattanooga
(Advisor)

Francisco Guillén González
Professor of Mathematics
Universidad de Sevilla
(Advisor)

Christopher Cox
Professor of Mathematics and Department Head
University of Tennessee at Chattanooga
(Committee Member)

Concepción García Vázquez
Professor of Mathematics and Department Head
Universidad de Cádiz
(Committee Member)

Kristoffer van der Zee
Professor of Mathematics
University of Nottingham
(Committee Member)

ANALYSIS AND NUMERICAL SIMULATION

OF TUMOR GROWTH MODELS

By

Daniel Acosta Soba

A Thesis Submitted to the Faculties of
the Universidad de Cádiz and the University of Tennessee at Chattanooga
in Partial Fulfillment of the Requirements of the Degree of Doctor of Philosophy
in Mathematics (Universidad de Cádiz) and in Computational Science:
Computational and Applied Mathematics (University of Tennessee at Chattanooga),
under the Joint Supervision Program in place between both institutions.

Universidad de Cádiz
Puerto Real, Cádiz, Spain

The University of Tennessee at Chattanooga
Chattanooga, Tennessee, USA

May 2024

ABSTRACT

In this dissertation we focus on the numerical analysis of tumor growth models. Due to the difficulty of developing physically meaningful approximations of such models, we divide the main problem into more simple pieces of work that are addressed in the different chapters.

First, in Chapter 2 we present a new upwind discontinuous Galerkin (DG) scheme for the convective Cahn-Hilliard model with degenerate mobility which preserves the pointwise bounds and prevents non-physical spurious oscillations. These ideas are based on a well-suited piecewise constant approximation of convection equations. The proposed numerical scheme is contrasted with other approaches in several numerical experiments.

Afterwards, in Chapter 3, we extend the previous ideas to a mass-conservative, positive and energy-dissipative approximation of the Keller–Segel model for chemotaxis. Then we carry out several numerical tests in regimes of chemotactic collapse. These ideas are used later in Chapter 4 to develop a well-suited approximation of two different models related to chemotaxis: a generalization of the classical Keller-Segel model and a model of the neuroblast migration process to the olfactory bulb in rodents' brains.

Now we propose and study a phase-field tumor growth model in Chapter 5. Then, we develop an upwind DG scheme preserving the mass conservation, pointwise bounds and energy stability of the continuous model and we show both the good properties of the approximation and the qualitative behavior of the model in several numerical tests.

Next, in Chapter 6, we present two new coupled and decoupled approximations of a Cahn–Hilliard–Navier–Stokes model with variable densities and degenerate mobility that preserve the physical properties of the model. Both approaches are compared in different computational tests including benchmark problems.

Consequently, we propose, in Chapter 7, an extension of the previous tumor model including the effects of the surrounding fluid by means of a Cahn–Hilliard–Darcy model for which obtaining a physically meaningful approximation seems rather plausible using the previous ideas.

Finally, this and other future lines of research are described, along with the conclusions and the scientific production of the dissertation, in Chapter 8.

RESUMEN

En esta tesis nos centramos en el análisis numérico de modelos de crecimiento tumoral. Debido a la dificultad para desarrollar aproximaciones físicamente significativas de dichos modelos, dividimos el problema principal en trabajos más sencillos que se abordan en los diferentes capítulos.

En primer lugar, en el Capítulo 2 presentamos un nuevo esquema aguas arriba de tipo Galerkin discontinuo (DG) para el modelo de Cahn–Hilliard convectivo con movilidad degenerada que preserva las cotas puntuales y evita las oscilaciones espurias no físicas. Estas ideas se basan en una aproximación adecuada, usando funciones constantes a trozos, de ecuaciones de convección. El esquema numérico propuesto se compara con otras técnicas en varios experimentos numéricos.

Después, en el Capítulo 3, extendemos las ideas anteriores a una aproximación que conserva la masa, es positiva y disipa la energía del modelo de Keller–Segel para la quimiotaxis. Posteriormente, realizamos varios experimentos numéricos en situaciones de colapso quimiotáctico. Estas ideas se utilizan más adelante en el Capítulo 4 para desarrollar una aproximación adecuada de dos modelos diferentes relacionados con la quimiotaxis: una generalización del modelo clásico de Keller–Segel y un modelo del proceso de migración de neuroblastos al bulbo olfatorio en el cerebro de roedores.

Tras esto, proponemos y estudiamos un modelo de crecimiento tumoral de tipo campo de fases en el Capítulo 5. A continuación, desarrollamos un esquema DG aguas arriba que preserva la conservación de la masa, las cotas puntuales y la estabilidad energética del modelo continuo y mostramos tanto las buenas propiedades de la aproximación como el comportamiento cualitativo del modelo en varios experimentos numéricos.

Más adelante, en el Capítulo 6, presentamos dos nuevas aproximaciones, acoplada y desacoplada, de un modelo Cahn–Hilliard–Navier–Stokes con densidades variables y movilidad degenerada que preservan las propiedades físicas del modelo. Ambas aproximaciones se comparan en diferentes tests computacionales que incluyen problemas de referencia.

Luego, proponemos, en el Capítulo 7, una extensión del modelo de tumor anterior incluyendo los efectos del fluido que se encuentra en el entorno mediante un modelo Cahn–Hilliard–Darcy para el que la

obtención de una aproximación físicamente significativa parece bastante plausible utilizando las ideas anteriores.

Finalmente, se describen esta y otras futuras líneas de investigación, junto con las conclusiones y la producción científica de la tesis, en el Capítulo 8.

DEDICATION

To the little me that once dreamt of becoming a scientist.

ACKNOWLEDGEMENTS

I cannot start these words without giving credit to the person who pushed me to start a scientific career and enroll into the doctoral program at the Universidad de Cádiz: J. Rafael Rodríguez Galván. Rafa, as we friendly know him, started as my professor but has soon become a friend – a really good friend – whose support extends far beyond the academic scope. Thank you for being the pillar of my short academic career.

In this sense, I also have to mention Francisco Guillén González, Kisko, another close source of support and vast knowledge in mathematics, who never doubted about becoming my PhD advisor once we first contacted him. After these few years of collaboration, the academic relationship that we started has turned into a good friendship that will last many years more.

Also, I have to thank the third fundamental person behind this project, Jin Wang, who jumped at the chance of joining this project when the opportunity of starting the joint doctoral program with the University of Tennessee at Chattanooga arose. Thank you for every effort you have made to make this work possible providing the best help throughout the way.

Thanks to all the amazing people that have collaborated with me in this project. In particular, Noelia Ortega Román has been really important since the beginning as we joined the research group almost at the same time and we have been working side by side for several years now. In addition, I would like to thank Carmen Castro González and her research group *INIBICA INCO-5* for the insightful discussions that arose everytime this group of neuroscientists and our group of mathematicians have met. Finally, I have to mention Giuseppe Viglialoro, Silvia Frassu and Alessandro Columbu, who made Cagliari feel like home and who soon became part of the best friends that academia has put into my life.

Then, I would like to thank some other really important people who have tried to make this experience through the doctoral program the least tough they possibly could. In this sense, I must mention the names of Francisco Ortegón Gallego and Juan Carlos García Galindo at the Universidad de Cádiz and Joanne Romagni, Ethan Carver and Christopher L. Cox at the University of Tennessee at Chattanooga. Moreover, although he is not any more in the academia, I will always remember the good conversations

with Michael Colvin who always had some really interesting story and some wise piece of advice to tell. Thank you all for somehow becoming part of this project and contribute to its success.

Now, I have to give credit to the people who have always been my first and unconditional support, my family, with special mention to my mum Maricarmen, my dad José, my grandparents Uchi and Pepe and my dear partner Laura. They have always been there to hold my hand every time I needed them and to celebrate each of the milestones I have reached on the way. Many times they have told me they are proud of what I have done but I must say, and it is difficult to find the right words, that it is me who has to be proud of them as I have never been on my own – all my little successes are not more than a small part of their own great achievements.

Finally, I must talk about my friends, both those who I have made along the process and those who have always been there since the very beginning. I am not going to mention each of their names as I do not want to forget any because, most fortunately, I can say I have dozens of them. Thank you all for the really good moments and the help you have always provided me every time I needed it. I think I will never be able to give you back all the love you have showed to me.

All in all, even though it seems that God plays dice in the end, this chaos has somehow guided me to bump into the right people along the way. People who not only made this process enjoyable and fruitful but who are the reason why I am writing these lines today with the biggest smile on my face – and this is far more important than the result itself. Thank you.

TABLE OF CONTENTS

LIST OF TABLES

LIST OF FIGURES

LIST OF ABBREVIATIONS

CC, Corpus Callosum

CCH, Convective Cahn–Hilliard

CFL, Courant–Friedrichs–Lewy

CH, Cahn–Hilliard

CHNS, Cahn–Hilliard–Navier–Stokes

DG, Discontinous Galerkin

EQ, Energy Quadratization

FE, Finite Element

FV, Finite Volume

GMRES, Generalized Minimal Residual Method

ILU, Incomplete LU

IP, Interior Penalty

LHS, Left-Hand Side

NSC, Neural Stem Cells

NZ, Narrowing Zone

OB, Olfactory Bulb

ODE, Ordinary Differential Equation

PDE, Partial Differential Equation

RHS, Right-Hand Side

RMS, Rostral Migratory Stream

SAV, Scalar Auxiliary Variable

SIP, Symmetric Interior Penalty

SSP, Strong Stability Preserving

SVZ, Subventricular Zone

UPW, Upwind

LIST OF SYMBOLS

Ω, bounded domain

$\partial\Omega$, boundary of the domain Ω

$\overline{\Omega}$, closure of the domain Ω

$\boldsymbol{n}$, unit normal vector to Ω

h, mesh size

$\mathcal{T}_h$, triangular mesh of size h

$\mathcal{E}_h$, set of edges of the mesh

$\mathcal{E}_h^{\mathsf{b}}$, set of boundary edges

$\mathcal{E}_h^{\mathsf{i}}$, set of interior edges

$\boldsymbol{n}_e$, unit normal vector to the edge e

$\{\!\{ \cdot \}\!\}$, average of piecewise discontinuous function

$[\![\cdot]\!]$, jump of piecewise discontinuous function

$\mathcal{D}_e(T_h)$, distance between the baricenters of the elements of $\mathcal{T}_h$ sharing the edge e

$\mathbb{P}_k^{\mathsf{cont}}(\mathcal{T}_h)$, space of continuous piecewise polynomials of degree $k \geq 0$ on $\mathcal{T}_h$

$\mathbb{P}_k^{\mathsf{disc}}(\mathcal{T}_h)$, space of discontinuous piecewise polynomials of degree $k \geq 0$ on $\mathcal{T}_h$

T, upper bound of the time interval

Δt, time step size

δ_t, discrete Euler derivative

$(\cdot)_{\oplus}$, positive part

$(\cdot)_{\ominus}$, negative part

$\approx$, approximately equal for real numbers

$\simeq$, approximately equal for functions

$\nabla(\,\cdot\,)$, gradient of a function

$\nabla\cdot(\,\cdot\,)$, divergence of a function

$\boldsymbol{D}(\,\cdot\,)$, strain tensor operator

$\Delta(\,\cdot\,)$, Laplacian of a function

$\partial_u(\,\cdot\,)$, derivative with respect to u

$\dfrac{d}{dt}(\,\cdot\,)$, derivative with respect to t

$\|\cdot\|_X$, norm in the space X

$|\cdot|$, absolute value of a scalar, norm 2 or of a vector or measure of a set

X_+, subset of all the nonnegative elements (scalars of functions) of the set X

X', algebraic dual of the vector space X

$(\cdot,\cdot)$, usual scalar product in $L^2(\Omega)$ or in $L^2(\Omega)^d$

$(\cdot,\cdot)_h$, usual scalar product in $L^2(\Omega)$ or in $L^2(\Omega)^d$ with mass lumping

$\langle\cdot,\cdot\rangle$, duality product in an algebraic dual space

$\log(\,\cdot\,)$, natural logarithm

Π_0, projection operator on $\mathbb{P}_0^{\text{disc}}(\mathcal{T}_h)$

Π_1, projection operator on $\mathbb{P}_1^{\text{cont}}(\mathcal{T}_h)$

Π_1^h, regularization operator on $\mathbb{P}_1^{\text{cont}}(\mathcal{T}_h)$ using mass-lumping

$\fint_\Omega(\,\cdot\,)$, average of function on the domain Ω

$\triangle ABC$, triangle with vertices A, B, C

CHAPTER 1

INTRODUCTION

Cancer is the first or the second leading cause of death before the age of 70 years in at least 112 countries, according to the estimates of the World Health Organization (WHO) in 2019, [176]. This overwhelming issue has led the scientists of a vast number of disciplines to make an enormous effort towards the understanding of its mechanism with the purpose of fighting and overcoming the disease. In particular, mathematics has acquired an increasingly important role as it has been postulated as a discipline that can shed light on the prediction of the development of tumors and their consequences, therefore filling gaps that other more experimental sciences have not been able to address yet.

Lately, significant work on the mathematical modeling of tumor growth has been carried out. As a result, many different models have arisen, some of which have even been applied to predict the response of the tumor to its surrounding environment and possible medical treatments. Most of these models can be classified into micro-scale discrete models, macro-scale continuum models or hybrid models, [57, 145]. Regarding the continuum models, different approaches has been developed among which we can find models using both ODE, for instance, [46, 147], and PDE, for example, [79, 164].

In this sense, phase field models such as the Cahn-Hilliard (CH) equation have become a very popular tool. This model describes the evolution of a thin, diffuse, interface between two different phases or states of a process [36, 154] through a so-called phase-field variable, which minimizes an adequate free energy. Sometimes, this CH model is coupled with a degenerate mobility to impose phase-related pointwise bounds on this variable.

In particular, in the context of tumor modeling, the phase-field variable u is usually interpreted as a tumor volume-fraction (with $0 \leq u \leq 1$) and this model is coupled with other equations describing the interaction between the tumor and the surrounding environment. The complexity of these models vary depending on their constitutive assumptions and intrinsic limitations, but most of them are based on multicomponent mixture theory which accounts for the mass, momentum and energy balances for each of the constituents. One can trace back these kind of thermodynamically consistent mixture models to the

work of Wise et al., [189] and the references therein. As a consequence of this pioneering work, many other models have arisen taking into account different kind of processes and proposing simplifications. For instance, we can find [85] where the model in [189] is extended to describe angiogenesis and tumor invasion, the work by [113] where the nutrients are included as a component of the mixture, or the more recent model in [94] where mechanical effects are also taken into account, just to mention a few.

In this regard, considerable effort has been made in describing a general framework for the correct modeling and calibration of the diffuse-interface models of tumor growth, oriented to their possible physical application, as summarized in [88, 112, 156, 157] and the references therein. So far, there are several examples of success in this direction as different approaches have been capable of providing accurate enough results to be compared with real clinical data. Among these celebrated models we can find the work by Pozzi et al. [160] where a Cahn–Hilliard equation is coupled with a Keller–Segel system; the works by Agosti et al. [7, 8, 9] where a Cahn-Hilliard equation for the tumor with nonsymmetric degenerate mobility (as the one shown in Chapter 5) is coupled with a diffusion-reaction equation for the nutrients; or the works of Lima et al. [137, 138] where phase-field models are compared against reaction-diffusion models regarding data prediction.

In this context of tumor modeling, chemotaxis, a biological process through which organisms (e.g. cells) migrate in response to a chemical stimulus, often plays an important role, see for instance [91, 113]. The classical chemotaxis model was introduced in the 70' by E. F. Keller and L. A. Segel, [125, 126] attracting huge interest from the mathematical community due to both its interesting analytical properties and its possible application to describing real phenomena (as shown in Section 4.4.1).

Also, among the existing literature, one can find different works which have tried to model the tumor tissue immersed in a fluid that transports the mixture of cells and nutrients. On the one hand, as initially proposed in [189], some authors have derived models relying on the Cahn–Hilliard–Darcy equations, [86, 92, 93, 95], where the tissue is assumed to behave as a porous medium. On the other hand, some alternatives have arisen for the cases where the tissue cannot be modeled as porous medium, for instance, a Cahn–Hilliard–Brinkman model [54, 67, 68] and, very recently, a Cahn–Hilliard–Navier–Stokes system [69]. In this sense, even more general models have been proposed where the previous approaches have been generalized to satisfy the Darcy–Forchheimer–Brinkman law, [89], or to introduce viscoelastic effects, [91].

Regarding the numerical approximation of these equations, significant advances have been done both with respect to the time and the spatial discretizations.

On the one hand, the classical approach for the time discretization of the phase-field models is the convex-splitting decomposition introduced in [77] which preserves the energy stability. Nonetheless, other time-discrete schemes have been introduced in the literature (see, for instance, [105, 106, 180]). Among these time approximations we find the idea of introducing a Lagrange multiplier in the potential term in [24] which was extended in [105, 106, 180]. This idea led to the popular energy quadratization (EQ) schemes [192, 193, 194], later extended to the scalar auxiliary variable (SAV) approach [169].

On the other hand, in the case of the Cahn-Hilliard equation with degenerate mobility, designing a suitable spatial discretization consistent with the physical properties of the model, specially the pointwise bounds, is a difficult task and only a few works have been published in this regard. Among the currently available structure-preserving schemes we can find some schemes based on finite volumes, [25, 118], and on finite elements, [27, 103].

In addition, the main difficulty from the point of view of the numerical approximation in the context of chemotaxis is dealing with the cross-diffusion term. Not only for its non-linearity, but due to its convective nature, which makes particularly difficult to deal with using the finite element (FE) method. This difficulty is specifically significant in steep-gradient regions for v, which are precisely relevant in blow-up settings. Furthermore, preserving the physical properties of the continuous model (mass conservation, positivity and energy dissipation) in the discrete case adds an extra level of complication when it comes to designing a well-suited approximation. Despite that, many interesting works have been published on numerical simulation of chemotaxis equations using different kinds of approaches, see [23, 41, 45, 72, 73, 104, 108, 111, 117, 120, 136, 165, 168, 195].

The difficulties of the discretization are emphasized in the case of phase-field tumor models. In particular, in [113] an energy-stable finite element scheme with a first-order convex-splitting scheme in time is proposed for (5.1) and extended in [190] to a second-order time discretization. Other types of approximations of this model (5.1) using meshless collocation methods, [62], stabilized element-free Galerkin method, [151], and SAV Fourier-spectral method, [171], can be found in the literature. However, no bounds are obtained on the discrete variables whatsoever.

As a consequence, not many works have been able to provide a successful, unconditionally physically meaningful approximation of more complicated tumor models as the ones involving tumor-

nutrient interactions and fluid flows. In this context, the transport of the diffuse interface by the velocity of the fluid is typically modeled by means of a convective term that is introduced into the Cahn-Hilliard equation which may lead to numerical instabilities in highly convective regimes if it is not treated carefully. In this regard, the works [68, 93, 95] propose a finite element bound-preserving discretization that involves solving a discrete variational inequality following the ideas in [27] whereas [91] introduce a finite element approximation that mimic some entropies of the model at the discrete level. On the contrary, in [69], a combination of a suitable phase-field variable transformation, the time-discrete SAV approach and an upwind finite volume spatial discretization is used to preserve the pointwise bounds and the energy-stability in their approximations, although a CFL condition that is difficult to check beforehand is required.

In this work, we aim to develop a suitable discretization of diffuse-interface tumor models that can be useful for approximating not complicated models and extended to models describing more complex phenomena as the interaction with fluid flows. Moreover, we provide some notions on how some of the tumor models existing in the literature can be modified to ensure the physical meaning of the variables. To this purpose, we apply the "divide and conquer" principle and we address separately the different problems involved in the tumor models existing in the literature. Finally, we pretend to extend the ideas resulting from this work to other fields where we will obtain really good results. The outline of this PhD thesis and the notation that we are going to follow are presented below.

This work is divided in eight chapters, each of which treats specific topics that we will summarize now.

In Chapter 2 we develop numerical schemes for the convective Cahn-Hilliard (CCH) problem (2.1) which guarantee punctual estimates of the phase at the discrete level, in addition to maintaining the rest of continuous properties of (2.1). The main idea is to introduce an upwind DG discretization associated to the transport of the phase by the convective velocity $\boldsymbol{v}$, but also associated to the degenerate mobility $M(u)$. These ideas are first applied to the linear convection equation itself in Sections 2.3.2 and 2.3.3, and then, further extended to the more complex CCH model in Section 2.4. The main result in this work is Theorem 2.4.11, where we show that, for a piecewise constant approximation of the phase, our DG scheme preserves the maximum principle, that is the discrete phase is also bounded in $[0, 1]$. In addition, we present several numerical tests in Section 2.5 comparing our DG scheme with two different

space discretizations found in the literature: classical continuous P_1 finite elements and the SIP+upwind sigmoid DG approximation proposed in [81].

In Chapter 3, we propose a new upwind DG scheme for the Keller-Segel model (3.1) that preserves the mass-conservation, positivity (Theorem 3.4.7) and energy stability (Theorem 3.4.13) properties of the continuous problem. As in [168], the proposed discretization takes advantage of the gradient flow structure of the model. This idea follows from the work introduced in Chapter 2 in the case of the convective Cahn-Hilliard system, where now we introduce a particular approximation of the normal derivative of the flux to ensure the energy stability in Section 3.4.1. Moreover, in Section 3.5, we reproduce several benchmark numerical tests that endorse the good behavior of the approximation obtained with the new scheme, which allows us to capture very steep gradients at the discrete level.

Then, in Chapter 4, we extend the ideas in Chapters 2 and 3 and provide some insight on the mathematical analysis of generalized chemotaxis models and the modeling and computational simulation of real-life processes involving chemotaxis.

On the one hand, we study some extensions of the Keller-Segel model (3.1) describing population dynamics, (4.1) and (4.2), in Section 4.3. In this regard, we first state some results about the existence and regularity of the solution of these models in Section 4.3.2. Then, in Section 4.3.3, we present and analyze the properties of a discrete approximation of the models using the upwind DG ideas previously introduced in Chapters 2 and 3. Finally, we implement this scheme in the computer and carry out some tests in Section 4.3.4, whose results are in accordance with the previous theoretical analysis concerning the global in time existence and regularity of the solutions under certain constraints on the parameters.

On the other hand, we present a mathematical model of neuroblast migration in Section 4.4. Neuroblasts are primitive nerve cells which develop into neurons after a migration phase, particularly to the olfactory bulb in a rodent's brain. This model, inspired in chemotaxis, supplements a transport equation with some extra reaction terms modeling the birth of neuroblasts and their disappearance due to evolution in mature neurons. Moreover, in Section 4.4.2, we develop a discrete approximation of this model using a discrete upwind DG scheme inspired in the one given in Chapter 2. In this sense, in Section 4.4.3, we show several numerical simulations of the neuroblasts migration process where the model has been calibrated and validated using real data experimentally obtained by the research group *INIBICA INCO-5*, led by Dr. Carmen Castro-González.

Afterwards, in Chapter 5, we consider the diffuse-interface model (5.1) presented by Hawkins-Daarud et al. in [113], which describes the interaction between a tumor and the nutrients in the extracellular water. In this sense, in Section 5.3, we propose a modification of the model using possibly nonsymmetric mobility and proliferation functions, see (5.3) below, in accordance with its physical interpretation. This modification leads us to obtain pointwise bounds on the tumor and the nutrient volume fractions which are consistent with the physical meaning of the variables and which may be helpful to a future application of this model (or a variant of it) for real tumor growth prediction.

In addition, we introduce a well-suited convex-splitting upwind DG scheme of the proposed model (5.3), based on [120] and the previous work in Chapters 2 and 3, in Section 5.4. This approximation preserves the physical properties of the phase-field tumor model (mass conservation, pointwise bounds and energy stability), as shown in Theorems 5.4.9 and 5.4.11, and prevent numerical spurious oscillations. Finally, we carry out a numerical comparison between the new robust DG scheme and a standard FE discretization of (5.12) in Section 5.5, the latter of which fails in the case of strong cross-diffusion and we show the behavior of the model under different choices of parameters and mobility/proliferation functions.

Next, in Chapter 6, we provide a fully-coupled upwind DG approximation (6.10) of the Cahn–Hilliard–Navier–Stokes (CHNS) model by Abels et al. [1] with variable densities and degenerate mobility in Section 6.4. This approximation preserves all the mass-conservation, pointwise bounds (Theorem 6.4.5) and energy-stability properties (Theorem 6.4.8). Moreover, using similar ideas, a decoupled approximation of this model, (6.34), is developed by means of the well-known projection method in Section 6.5. This decoupled approximation lacks the energy-stability property but is much more computationally efficient than the coupled counterpart. Finally, in Section 6.6 we conduct several numerical experiments in which we compare both the coupled and the decoupled approaches both through simple test and well-known benchmark problems. Furthermore, we compute a preliminary accuracy test that suggests that both schemes may have similar convergence order for all the variables.

Subsequently, in Chapter 7, we introduce a possible extension of the results presented in both Chapters 5 and 6 with the purpose of developing a physically meaningful approximation for a tumor system coupled with a fluid equation. In this sense, in Section 7.3, we derive a mass-conservative, pointwise-bounded and energy-stable Cahn–Hilliard–Darcy model from the more general model introduced by Garcke et al. in [95] under certain constitutive assumptions by means of the non-symmetric

mobility and proliferation functions used in Chapter 5 to modify the tumor model in [113]. The resulting model lies in the framework of the previous tumor model studied in Chapter 5 and the CHNS studied in Chapter 6, hence a successful approximation using the upwind DG ideas developed throughout this work is likely to be obtained.

Finally, in Chapter 8, we briefly summarize the results presented in the different chapters of this dissertation providing the scientific publications that have been derived from this work. In addition, we present the lines of research that we are currently exploring as a consequence of this dissertation and we discuss the possible extensions of this work.

1.1 Notation

Let $\Omega \subset \mathbb{R}^d$ with $d \in \mathbb{N}$ be a regular-enough bounded domain, e.g. polygonal, with $\boldsymbol{n}$ its unit normal vector.

We consider a finite element shape-regular triangular mesh $\mathcal{T}_h = \{K\}_{K\in\mathcal{T}_h}$ in the sense of Ciarlet, [48], of size h over Ω. We denote by $\mathcal{E}_h$ the set of the edges of $\mathcal{T}_h$ (faces if $d = 3$) with $\mathcal{E}_h^{\mathsf{i}}$ the set of the *interior edges* and $\mathcal{E}_h^{\mathsf{b}}$ the *boundary edges*, thus $\mathcal{E}_h = \mathcal{E}_h^{\mathsf{i}} \cup \mathcal{E}_h^{\mathsf{b}}$.

Now, we fix the following orientation over the mesh $\mathcal{T}_h$:

- For any interior edge $e \in \mathcal{E}_h^{\mathsf{i}}$ we set the associated unit normal vector $\boldsymbol{n}_e$. In this sense, when refering to edge $e \in \mathcal{E}_h^{\mathsf{i}}$ we will denote by K_e and L_e the elements of $\mathcal{T}_h$ with $e = \partial K_e \cap \partial L_e$ and so that $\boldsymbol{n}_e$ is exterior to K_e pointing to L_e.

  If there is no ambiguity, to abbreviate the notation we will denote the previous elements K_e and L_e simply by K and L, respectively, with the assumption that their naming is always with respect to the edge $e \in \mathcal{E}_h^{\mathsf{i}}$ and it may vary if we consider a different edge of $\mathcal{E}_h^{\mathsf{i}}$. See Figure 1.1.

- For any boundary edge $e \in \mathcal{E}_h^{\mathsf{b}}$, the unit normal vector $\boldsymbol{n}_e$ points outwards of the domain Ω.

Therefore, we can define the *average* $\{\!\{\cdot\}\!\}$ and the *jump* $[\![\cdot]\!]$ of a function v on an edge $e \in \mathcal{E}_h$ as follows:

$$\{\!\{v\}\!\} \coloneqq \begin{cases} \dfrac{v_K + v_L}{2} & \text{if } e \in \mathcal{E}_h^{\mathsf{i}},\ e = K \cap L, \\ v_K & \text{if } e \in \mathcal{E}_h^{\mathsf{b}},\ e \subset K, \end{cases} \qquad [\![v]\!] \coloneqq \begin{cases} v_K - v_L & \text{if } e \in \mathcal{E}_h^{\mathsf{i}},\ e = K \cap L, \\ v_K & \text{if } e \in \mathcal{E}_h^{\mathsf{b}},\ e \subset K. \end{cases}$$

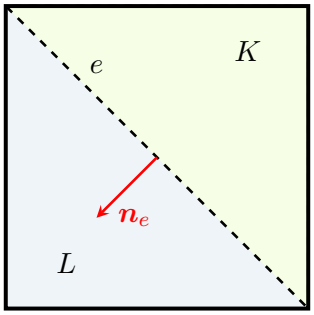

Figure 1.1 Orientation of the unit normal vector $\boldsymbol{n}_e$

We denote by $\mathbb{P}_k^{\text{disc}}(\mathcal{T}_h)$ and $\mathbb{P}_k^{\text{cont}}(\mathcal{T}_h)$ the spaces of finite element discontinuous and continuous functions, respectively, which are polynomials of degree $k \geq 0$ when restricted to the elements K of $\mathcal{T}_h$. In this sense, we will denote the broken differential operators (see [63, 163]) the same way than the standard differential operators in the absence of ambiguity.

We refer the reader to [34, 74] and to [63, 66, 163] for a further insight on continuous and discontinuous finite elements, respectively.

Moreover, we take an equispaced partition $0 = t_0 < t_1 < \cdots < t_N = T$ of the time domain $[0, T]$ with $\Delta t = t_{m+1} - t_m$ the time step. If v is a function depending on space and time, e.g. defined in $\overline{\Omega} \times [0, T]$, we set $v(t) := v(\cdot, t)$ for every t in the time domain $[0, T]$. Also, for any function v depending on time, we denote $v^{m+1} \simeq v(t_{m+1})$ and the discrete time derivative operator $v_t(t_{m+1}) \simeq \delta_t v^{m+1} := (v^{m+1} - v^m)/\Delta t$.

We denote by $(\cdot, \cdot)$ and $(\cdot, \cdot)_h$ the standard and the mass-lumped scalar products in $L^2(\Omega)$ (or $L^2(\Omega)^d$ as there is no ambiguity), respectively. Also, $\langle \cdot, \cdot \rangle$ denotes a duality product in an algebraic dual space.

Finally, we set the following notation for the positive and negative parts of a function v:

$$v_\oplus := \frac{|v| + v}{2} = \max\{v, 0\}, \quad v_\ominus := \frac{|v| - v}{2} = -\min\{v, 0\}, \quad v = v_\oplus - v_\ominus.$$

CHAPTER 2

AN UPWIND DG SCHEME PRESERVING THE MAXIMUM PRINCIPLE FOR THE CONVECTIVE CAHN–HILLIARD MODEL

2.1 Abstract

The design of numerical approximations of the Cahn-Hilliard model preserving the maximum principle is a challenging problem, even more if considering additional transport terms. In this chapter we present a new upwind discontinuous Galerkin scheme for the convective Cahn-Hilliard model with degenerate mobility which preserves the maximum principle and prevents non-physical spurious oscillations. Furthermore, we show some numerical experiments in agreement with the previous theoretical results. Finally, numerical comparisons with other schemes found in the literature are also carried out. The results shown in this chapter have already been published in [4].

2.2 Introduction

This chapter is concerned with the development of discontinuous Galerkin (DG) numerical schemes for the following convective Cahn-Hilliard (CCH) problem (written as a second order system): Given an incompressible velocity field $\boldsymbol{v} \in C(\overline{\Omega})^d$ with $\nabla \cdot \boldsymbol{v} = 0$ in Ω, such that $\boldsymbol{v} \cdot \boldsymbol{n} = 0$ on $\partial\Omega$, find two real valued functions, the phase u and the chemical potential μ, defined in $\Omega \times [0, T]$ such that:

$$\partial_t u = \frac{1}{\mathsf{Pe}} \nabla \cdot (M(u) \nabla \mu) - \nabla \cdot (u \boldsymbol{v}) \qquad \text{in } \Omega \times (0, T), \tag{2.1a}$$

$$\mu = F'(u) - \varepsilon^2 \Delta u \qquad \text{in } \Omega \times (0, T), \tag{2.1b}$$

$$\nabla u \cdot \boldsymbol{n} = (M(u) \nabla \mu - u \boldsymbol{v}) \cdot \boldsymbol{n} = 0 \qquad \text{on } \partial\Omega \times (0, T), \tag{2.1c}$$

$$u(0) = u_0 \qquad \text{in } \Omega. \tag{2.1d}$$

The phase field variable u localizes the two different phases at the values $u = 0$ and $u = 1$, while the interface occurs when $0 < u < 1$. Parameters are $\mathsf{Pe} > 0$ the Péclet number of the flow and $\varepsilon > 0$ related

to the width interface. For simplicity, we take $\mathsf{Pe} = 1$. The given initial phase is denoted by u_0. The classical Cahn–Hilliard equation (CH) corresponds to the case without convection, i.e. $\boldsymbol{v} = 0$.

We consider the double-well Ginzburg-Landau potential

$$F(u) = \frac{1}{4}u^2(1-u)^2$$

and the *degenerate mobility*

$$M(u) = u(1-u). \tag{2.2}$$

This type of degenerate mobility, vanishing at the pure phases $u = 0$ and $u = 1$, implies the following maximum principle property (see [71] for the CH equation): if $0 \leq u_0 \leq 1$ in $\overline{\Omega}$ then $0 \leq u(\cdot, t) \leq 1$ in $\overline{\Omega}$ for $t \in (0, T)$. This property does not hold for constant mobility, and in general for fourth-order parabolic equations. We are concerned in numerical schemes maintaining this property at the discrete level.

Cahn-Hilliard equation was originally introduced in [35, 36] as a phenomenological model of phase separation in a binary alloy and it has been successfully applied in different contexts as a model which characterizes phase segregation and interface dynamics. Applications include tumor tissues [189, 190], image processing [29] and multi-phase fluid systems, see e.g. the review [128]. The dynamics of this equation comprises a first stage in which a rapid separation process takes place, leading to the creation of interfaces, followed by a second stage where aggregation and development of bulk phases separated by thin diffuse interfaces take place. These two phenomena (separation and aggregation) are characterized by different temporal and spatial scales which, together with the non-linear and fourth-order nature of CH, makes efficiently solving this equation an interesting computational challenge.

The interface is represented as a layer of small thickness of order ε and the auxiliary function u (the phase-field function) is used to localize the (pure) phases $u = 0$ and $u = 1$. The chemical potential μ is the variational derivative of the Helmholtz free energy $E(u)$ with respect to u, $\mu = \partial_u E(u)$, where

$$E(u) = \int_\Omega \left(\frac{\varepsilon^2}{2}|\nabla u|^2 + F(u) \right) dx. \tag{2.3}$$

Then the dynamics of CH correspond to the physical energy dissipation of $u_t = -\nabla \cdot J(u)$, where $J(u) = -M(u)\nabla\mu = -M(u)\nabla\partial_u E(u)$. For existence of solution for CH equation with a

degenerate mobility of the type (2.2), besides bounds for the phase over time, we can refer to [71]. A review and many variants can be read in [149].

Numerical approximation of CH is a research topic of great interest due to the wide spectrum of its applications, as well as a source of interesting mathematical challenges due to the computational issues referred above. Time approximations include both linear schemes [105] and nonlinear ones, where a Newton method is usually employed. Although some authors (see e.g. [70]) consider the fourth-order equation obtained by substitution in the equation (2.1a) of the expression of μ given in (2.1b), the spatial discretization is usually based on the mixed phase field/chemical potential formulation presented in (2.1). These equations can be approximated by classical numerical methods, including: (a) Finite differences, see e.g. [44, 90] for constant mobility $M(u) \equiv 1$ and [127] for degenerate mobility similar to (2.2), see also [184] for applications in crystallography. (b) Finite volumes, see e.g. [25, 58] for degenerate mobility schemes. (c) And, above all, finite elements see the precursory papers [70] (constant mobility) and [27] (degenerate mobility).

In recent years, an increasing number of advances has been published exploring the use of discontinuous Galerkin (DG) methods both for constant [20, 124] and degenerate mobility [81, 141, 185, 191]. Although DG methods lead in general to more complex algorithms and to bigger amounts of degrees of freedom, they exhibit some benefits of which one can take advantage also in CH equations, for instance doing mesh refining and adaptivity [20]. In this chapter we are interested in the following relevant point: the possibility of designing conservative schemes preserving the maximum-principle $0 \leq u(t,x) \leq 1$ at the discrete level, even for the CCH variant of CH equations, namely where a convective term models the convection or transport of the phase-field.

The idea of introducing a convection term in the CH equations modeling a phase-field driven by a flow, arriving at the CCH problem (2.1), arouses great interest. Specially, in the case where the phase field is coupled with fluid equations.

To design adequate numerical approximations of these CCH equations is an extremely challenging problem because it adds the hyperbolic nature of convective terms to the inherent difficulties of the CH equation. There are not many numerical methods in the literature on this topic, although some interesting contributions can be found. The first of them [22] is worth mentioning for the application of high-resolution spectral Fourier schemes. We also underline the papers [33, 133], based on finite volume

approximations, and also [43, 109], where finite difference techniques are applied for Navier-Stokes CH equations.

Some authors have recently worked in DG methods for spatial discretization of the CCH problem. Using DG schemes in this context is natural because they are well-suited in convection-dominated problems, even when the Péclet number is substantially large. For instance, the work of [124] is focused on construction and convergence analysis of a DG method for the CCH equations with constant mobility, applying an interior penalty technique to the second order terms and an upwind operator for discretization of the convection term. Authors of [81] consider CCH with degenerate mobility applying also an interior penalty to second order terms in the mixed form (2.1) and a more elaborated upwinding technique, based on a sigmoid function, to the convective term.

These previous works show that DG methods are well suited for the approximation of CCH equations, obtaining optimal convergence order and maintaining most of the properties of the continuous model. But they have room for improvement in one specific question: getting a maximum principle for the phase in the discrete case. Although there are some works in which the maximum principle for the CH model is preserved at the discrete level using finite volumes [25] and flux limiting for DG [82], to the best knowledge of the authors, no scheme has been published in which an upwind DG technique is used to obtain a discrete maximum principle property.

Our main contribution in this chapter is made in this regard: the development of numerical schemes which guarantee punctual estimates of the phase at the discrete level, in addition to maintaining the rest of continuous properties of (2.1). The main idea is to introduce an upwind DG discretization associated to the transport of the phase by the convective velocity $\boldsymbol{v}$, but also associated to the degenerate mobility $M(u)$. The main result in this work is Theorem 2.4.11, where we show that, for a piecewise constant approximation of the phase, our DG scheme preserves the maximum principle, that is the discrete phase is also bounded in $[0, 1]$.

Our scheme is specifically designed for the CH equation with non-singular (polynomial) chemical potential and degenerate mobility. For the CH equation with the logarithmic Flory-Huggins potential, a strict maximum principle is satisfied without the need of degenerate mobility. In this case, designing maximum principle-preserving numerical schemes is a different issue. See, for instance, the paper [42] where a finite difference numerical is proposed in this regard.

The chapter is organized as follows: In Section 2.3, we fix notation ax/nd review DG techniques for discretization of conservative laws. We consider the linear convection given by a velocity field and show that the usual linear upwind DG numerical scheme with P_0 approximation preserves positivity in general, and the maximum principle in the divergence-free case. In Section 2.4, we consider the CCH problem (2.1). Using a truncated potential and a convex-splitting time discretization we obtain a scheme satisfying an energy law, which is decreasing for the CH case ($\boldsymbol{v} = 0$). Then we introduce our fully discrete scheme (2.30) providing a maximum principle for the discrete phase variable. Finally, in Section 2.5 we present several numerical tests, comparing our DG scheme with two different space discretizations found in the literature: classical continuous P_1 finite elements and the SIP+upwind sigmoid DG approximation proposed in [81]. We show error order tests and also we present qualitative comparisons where the maximum principle of our scheme is confirmed (and it is not conserved by the other ones).

The results shown in this chapter have already been published in [4].

2.3 DG discretization of conservative laws

Throughout this section we are going to study the problem of approximating linear and nonlinear conservative laws preserving the positivity of the continuous models. To this purpose, we introduce an upwinding DG scheme which follows the ideas of the paper [120] based on an upwinding finite volume method.

2.3.1 Conservative laws

We consider the following non-linear conservative problem for v:

$$v_t + \nabla \cdot \boldsymbol{F}(v) = 0 \quad \text{en } \Omega \times (0,T), \tag{2.4}$$

where the flux $\boldsymbol{F}(\cdot)$ is a vectorial continuous function.

Let $S_h = \mathbb{P}_k^{\text{disc}}(\mathcal{T}_h)$. Multiplying by any $\overline{v} \in \mathcal{S}_h$ and using the Green Formula in each element $K \in \mathcal{T}_h$:

$$\int_\Omega \partial_t v \, \overline{v} - \sum_{K \in \mathcal{T}_h} \int_K \boldsymbol{F}(v) \cdot \nabla \overline{v} + \sum_{K \in \mathcal{T}_h} \int_{\partial K} \big(\boldsymbol{F}(v) \cdot \boldsymbol{n}_K\big) \, \overline{v} = 0,$$

where $\boldsymbol{n}_K$ is the normal vector to ∂K pointing outwards K. If v is a strong solution of (2.4), such that v is continuous over $e \in \mathcal{E}_h$, we get:

$$\int_\Omega \partial_t v\ \overline{v} - \sum_{K\in\mathcal{T}_h} \int_K \boldsymbol{F}(v)\cdot\nabla\overline{v} + \sum_{e\in\mathcal{E}_h} \int_e \left(\boldsymbol{F}(v)\cdot\boldsymbol{n}_e\right)\ [\![\overline{v}]\!] = 0. \tag{2.5}$$

But, if we look for functions $v \in \mathcal{S}_h$ which are discontinuous over $e \in \mathcal{E}_h$, then the term $\boldsymbol{F}(v)\cdot\boldsymbol{n}_e$ in the last integral of (2.5) is not well defined and we need to approach it. Hence, the concept of numerical flux is used, taking expressions like $\boldsymbol{\Phi}(v_K, v_L, \boldsymbol{n}_e)$ such that:

$$\int_e \left(\boldsymbol{F}(v)\cdot\boldsymbol{n}_e\right)\ [\![\overline{v}]\!] \approx \int_e \boldsymbol{\Phi}(v_K, v_L, \boldsymbol{n}_e)\ [\![\overline{v}]\!]\,.$$

From now on we will consider fluxes of the form

$$\boldsymbol{F}(v) = M(v)\boldsymbol{\beta},$$

with $M = M(v) \in \mathbb{R}$ and $\boldsymbol{\beta} = \boldsymbol{\beta}(x,t) \in \mathbb{R}^d$. Since in this chapter we are interested in studying conservative problems defined over isolated domains, we impose from now on that the transport vector $\boldsymbol{\beta}$ satisfies the slip condition

$$\boldsymbol{\beta}\cdot\boldsymbol{n} = 0 \quad \text{on } \partial\Omega. \tag{2.6}$$

Remark 2.3.1. *We will have to take into consideration the sign of $M'(v)$, i.e. if $M(v)$ is nonincreasing or nondecreasing, in order to work out a well-suited upwinding scheme. This is due to*

$$\nabla\cdot\boldsymbol{F}(v) = \nabla\cdot(M(v)\boldsymbol{\beta}) = M'(v)\boldsymbol{\beta}\cdot\nabla v + M(v)\nabla\cdot\boldsymbol{\beta}. \tag{2.7}$$

where

- *The first term $M'(v)\boldsymbol{\beta}\cdot\nabla v$ is a transport of v in the direction of $M'(v)\boldsymbol{\beta}$.*
- *The second term $M(v)\nabla\cdot\boldsymbol{\beta}$ can be seen as a reaction term with coefficient $\nabla\cdot\boldsymbol{\beta}$.*

It may be specially interesting the case $\boldsymbol{\beta} = -\nabla v$, where the whole term $\nabla\cdot(M(v)\boldsymbol{\beta}) = -\nabla\cdot(M(v)\nabla v)$ is a nonlinear diffusion term.

2.3.2 *Linear convection and positivity*

Taking $M(v) = v$, we arrive at the linear conservative problem:

$$v_t + \nabla \cdot (v\boldsymbol{\beta}) = 0 \qquad \text{in } \Omega \times (0,T), \tag{2.8a}$$

$$v(0) = v_0 \qquad \text{in } \Omega, \tag{2.8b}$$

where $\boldsymbol{\beta}\colon \overline{\Omega} \to \mathbb{R}^d$ is continuous.

Remark 2.3.2. *The problem* (2.8) *is well-posed without imposing boundary conditions due to the slip condition (2.6) (it can be derived writing an integral expression of solution in terms of the characteristic curves, see for example [158]). In particular, this integral expression implies the positivity of the solution, namely, if $v_0 \geq 0$ in $\overline{\Omega}$, then the solution v of* (2.8) *satisfies $v \geq 0$ in $\overline{\Omega} \times (0,T)$.*

For the linear problem (2.8a), we introduce the upwind numerical flux

$$\boldsymbol{\Phi}(v_K, v_L, \boldsymbol{n}_e) \coloneqq (\boldsymbol{\beta} \cdot \boldsymbol{n}_e)_{\oplus} v_K - (\boldsymbol{\beta} \cdot \boldsymbol{n}_e)_{\ominus} v_L, \tag{2.9}$$

which leads to the following discrete scheme for (2.8a): Given $v^m \in \mathcal{S}_h$, find $v^{m+1} \in \mathcal{S}_h$ solving

$$\int_\Omega \delta_t v^{m+1} \overline{v} + a_h^{\text{upw}}(\boldsymbol{\beta}; v_{\oplus}^{m+1}, \overline{v}) = 0, \quad \forall \overline{v} \in \mathcal{S}_h, \tag{2.10}$$

where

$$a_h^{\text{upw}}(\boldsymbol{\beta}; v, \overline{v}) \coloneqq -\sum_{K \in \mathcal{T}_h} \int_K v(\boldsymbol{\beta} \cdot \nabla \overline{v}) + \sum_{e \in \mathcal{E}_h^{\text{i}}, e = K \cap L} \int_e \left((\boldsymbol{\beta} \cdot \boldsymbol{n}_e)_{\oplus} v_K - (\boldsymbol{\beta} \cdot \boldsymbol{n}_e)_{\ominus} v_L \right) [\![\overline{v}]\!] \tag{2.11}$$

and $\delta_t v^{m+1} = (v^{m+1} - v^m)/\Delta t$ denotes a discrete time derivative.

Notice that we have truncated v by its positive part $v_{\oplus}$, taking into account that the solution of the continuous model (2.8a) is positive.

Remark 2.3.3. *The numerical flux $\boldsymbol{\Phi}(v_K, v_L, \boldsymbol{n}_e)$ giving in* (2.9) *can be rewritten as follows:*

$$\boldsymbol{\Phi}(v_K, v_L, \boldsymbol{n}_e) = (\boldsymbol{\beta} \cdot \boldsymbol{n}_e) \{\!\{ v \}\!\} + \frac{1}{2} |\boldsymbol{\beta} \cdot \boldsymbol{n}_e| [\![v]\!],$$

where $(\boldsymbol{\beta} \cdot \boldsymbol{n}_e) \{\!\{ v \}\!\}$ is a centered-flux term and $\frac{1}{2}|\boldsymbol{\beta} \cdot \boldsymbol{n}_e| [\![v]\!]$ is the upwind term.

Now we will prove that if we set $\mathcal{S}_h = \mathbb{P}_0^{\text{disc}}(\mathcal{T}_h)$, the scheme (2.10) preserves the positivity of the continuous model. In this case, since $\sum_{K\in\mathcal{T}_h}\int_K(\boldsymbol{\beta}\cdot\nabla\overline{v})v = 0$, the upwind term (2.11) reduces to

$$a_h^{\text{upw}}(\boldsymbol{\beta}; v, \overline{v}) = \sum_{e\in\mathcal{E}_h^{\text{i}}, e=K\cap L}\int_e \left((\boldsymbol{\beta}\cdot\boldsymbol{n}_e)_\oplus v_K - (\boldsymbol{\beta}\cdot\boldsymbol{n}_e)_\ominus v_L\right)[\![\overline{v}]\!]\,. \tag{2.12}$$

Theorem 2.3.4 (DG scheme (2.10) preserves positivity)**.** *If $\mathcal{S}_h = \mathbb{P}_0^{disc}(\mathcal{T}_h)$, then the scheme* (2.10) *preserves positivity, that is, for any $v^m \in \mathcal{S}_h$ with $v^m \geq 0$ in $\overline{\Omega}$, then any solution v^{m+1} of* (2.10) *satisfies $v^{m+1} \geq 0$ in $\overline{\Omega}$.*

Proof. Taking the following test function

$$\overline{v} = \begin{cases} (v_{K^*}^{m+1})_\ominus & \text{in } K^*, \\ 0 & \text{out of } K^*, \end{cases} \qquad \overline{v}\in\mathcal{S}_h,$$

where K^* is an element of $\mathcal{T}_h$ such that $v_{K^*}^{m+1} = \min_{K\in\mathcal{T}_h} v_K^{m+1}$, the scheme (2.10) becomes

$$|K^*|\left(\delta_t v_{K^*}^{m+1}\right)(v_{K^*}^{m+1})_\ominus = -a_h^{\text{upw}}(\boldsymbol{\beta}; v_\oplus^{m+1}, \mathbb{1}_{K^*}(v_{K^*}^{m+1})_\ominus). \tag{2.13}$$

By applying for all $L\in\mathcal{T}_h$, $v_L^{m+1} \geq v_{K^*}^{m+1}$ hence in particular $(v_L^{m+1})_\oplus \geq (v_{K^*}^{m+1})_\oplus$ (the positive part is a non-decreasing function), we deduce

$$\begin{aligned} a_h^{\text{upw}}(\boldsymbol{\beta}; v_\oplus^{m+1}, \mathbb{1}_{K^*}(v_{K^*}^{m+1})_\ominus) &= \sum_{e\in\mathcal{E}_h^{\text{i}}, e=K^*\cap L}\int_e \left((\boldsymbol{\beta}\cdot\boldsymbol{n}_e)_\oplus(v_{K^*}^{m+1})_\oplus - (\boldsymbol{\beta}\cdot\boldsymbol{n}_e)_\ominus(v_L^{m+1})_\oplus\right)(v_{K^*}^{m+1})_\ominus \\ &\leq \sum_{e\in\mathcal{E}_h^{\text{i}}, e=K^*\cap L}\int_e \left((\boldsymbol{\beta}\cdot\boldsymbol{n}_e)_\oplus(v_{K^*}^{m+1})_\oplus - (\boldsymbol{\beta}\cdot\boldsymbol{n}_e)_\ominus(v_{K^*}^{m+1})_\oplus\right)(v_{K^*}^{m+1})_\ominus. \end{aligned}$$

Since $(v_{K^*}^{m+1})_\oplus(v_{K^*}^{m+1})_\ominus = 0$ then

$$a_h^{\text{upw}}(\boldsymbol{\beta}; v_\oplus^{m+1}, \mathbb{1}_{K^*}(v_{K^*}^{m+1})_\ominus) \leq 0.$$

Therefore, from (2.13),

$$|K^*|\left(\delta_t v_{K^*}^{m+1}\right)(v_{K^*}^{m+1})_\ominus \geq 0.$$

On the other hand,

$$0 \leq |K^*| \left(\delta_t v_{K^*}^{m+1}\right) (v_{K^*}^{m+1})_{\ominus} = -\frac{|K^*|}{\Delta t} \left((v_{K^*}^{m+1})_{\ominus}^2 + v_{K^*}^m (v_{K^*}^{m+1})_{\ominus}\right) \leq 0,$$

hence $(v_{K^*}^{m+1})_{\ominus} = 0$. Thanks to the choice of K^*, we can assure that $v^{m+1} \geq 0$. □

Theorem 2.3.5 (Existence of DG scheme (2.10))**.** *Assume that $\mathcal{S}_h = \mathbb{P}_0^{disc}(\mathcal{T}_h)$. For any $v^m \in \mathcal{S}_h$, there is at least one solution $v^{m+1} \in \mathcal{S}_h$ of the scheme* (2.10)*.*

Proof. Consider the following well-known theorem:

Theorem 2.3.6 (Leray-Schauder fixed point theorem)**.** *Let χ be a Banach space and let $T\colon \chi \longrightarrow \chi$ be a continuous and compact operator. If the set*

$$\{x \in \chi\colon x = \alpha\, T(x) \quad \textit{for some } 0 \leq \alpha \leq 1\}$$

is bounded (uniformly with respect to α), then T has at least one fixed point.

Given a function $w \in \mathbb{P}_0^{\text{disc}}(\mathcal{T}_h)$ with $w \geq 0$, we are going to define the operator $T\colon \mathbb{P}_0^{\text{disc}}(\mathcal{T}_h) \longrightarrow \mathbb{P}_0^{\text{disc}}(\mathcal{T}_h)$ such that $T(\widehat{v}) = v$ where v is the unique solution of the linear scheme:

$$v \in \mathbb{P}_0^{\text{disc}}(\mathcal{T}_h), \quad \int_\Omega \frac{v - w}{\Delta t} \overline{v} = -a_h^{\text{upw}}(\boldsymbol{\beta}; \widehat{v}_{\oplus}, \overline{v}), \quad \forall \overline{v} \in \mathbb{P}_0^{\text{disc}}(\mathcal{T}_h). \tag{2.14}$$

The idea is to use the Leray-Schauder fixed point theorem 2.3.6 to the operator T. First of all, T is well defined.

Secondly, we will check that T is continuous. Let $\{\widehat{v}_j\}_{j\in\mathbb{N}} \subset \mathbb{P}_0^{\text{disc}}(\mathcal{T}_h)$ be a sequence such that $\lim_{j\to\infty} \widehat{v}_j = \widehat{v}$. Taking into account that all norms are equivalent in $\mathbb{P}_0^{\text{disc}}(\mathcal{T}_h)$ since it is a finite-dimensional space, the convergence $\widehat{v}_j \to \widehat{v}$ is equivalent to the convergence elementwise $(\widehat{v}_j)_K \to \widehat{v}_K$ for every $K \in \mathcal{T}_h$ (this may be seen, for instance, by using the norm $\|\cdot\|_{L^\infty(\Omega)}$). Taking limits when $j \to \infty$ in the scheme (2.14) (with $\widehat{v} := \widehat{v}_j$ and $v := T(\widehat{v}_j)$), and using the notion of convergence elementwise, we get that

$$\lim_{j\to\infty} T(\widehat{v}_j) = T(\widehat{v}) = T\left(\lim_{j\to\infty} \widehat{v}_j\right),$$

hence T is continuous.

In particular, as T is a continuous operator defined over $\mathbb{P}_0^{\text{disc}}(\mathcal{T}_h)$, which is finite-dimensional, T is also compact.

Finally, let us prove that the set

$$B = \{v \in \mathbb{P}_0^{\text{disc}}(\mathcal{T}_h) \colon v = \alpha\, T(v) \quad \text{for some } 0 \leq \alpha \leq 1\}$$

is bounded. The case $\alpha = 0$ is trivial so we will assume that $\alpha \in (0, 1]$. If $v \in B$, then v is the solution of the scheme

$$v \in \mathbb{P}_0^{\text{disc}}(\mathcal{T}_h), \quad \int_\Omega \frac{v - \alpha w}{\Delta t}\overline{v} = -\alpha\, a_h^{\text{upw}}(\boldsymbol{\beta}; v_\oplus, \overline{v}), \quad \forall \overline{v} \in \mathbb{P}_0^{\text{disc}}(\mathcal{T}_h). \tag{2.15}$$

Now, testing (2.15) by $\overline{v} = 1$, we get that

$$\int_\Omega v = \alpha \int_\Omega w,$$

and, since $w \geq 0$, and since it can be proved that $v \geq 0$ using the same arguments than in Theorem 2.3.4, we get that

$$\|v\|_{L^1(\Omega)} \leq \|w\|_{L^1(\Omega)}.$$

Hence, since $\mathbb{P}_0^{\text{disc}}(\mathcal{T}_h)$ is a finite-dimensional space where the norms are equivalent, we have proved that B is bounded. Thus, using the Leray-Schauder fixed point theorem 2.3.6, there is a solution of the scheme (2.10). □

Let us focus on the the following linear scheme (without truncating v by its positive part, $v_\oplus$): Given $v^m \in \mathbb{P}_0^{\text{disc}}(\mathcal{T}_h)$, find $v^{m+1} \in \mathbb{P}_0^{\text{disc}}(\mathcal{T}_h)$ such that, for every $\overline{v} \in \mathbb{P}_0^{\text{disc}}(\mathcal{T}_h)$:

$$\int_\Omega \delta_t v^{m+1}\overline{v} + a_h^{\text{upw}}(\boldsymbol{\beta}; v^{m+1}, \overline{v}) = 0. \tag{2.16}$$

It is well-known (see e.g. [63] and references therein) that (2.16) has a unique solution at least for Δt small enough so that the following constraint is satisfied: there is $\gamma > 0$ such that

$$1 + \frac{\Delta t}{2}\nabla \cdot \boldsymbol{\beta} \geq \gamma > 0 \text{ in } \Omega. \tag{2.17}$$

Hence, if we assume that the scheme (2.16) has a unique solution and since we have shown positivity of the nonlinear truncated scheme (2.10), then any solution of (2.10) is the unique solution of (2.16). This argument implies uniqueness of (2.10) and positivity of (2.16).

Corollary 2.3.7 (Linear DG scheme (2.16) preserves positivity)**.** *For any $v^m \in \mathbb{P}_0^{disc}(\mathcal{T}_h)$ with $v^m \geq 0$ in $\overline{\Omega}$, the unique solution v^{m+1} of the linear scheme* (2.16) *is positive, i.e. $v^{m+1} \geq 0$ in $\overline{\Omega}$.*

Remark 2.3.8. *Also, following the steps in Proposition 2.3.9 below, one can show that, if $\nabla \cdot \boldsymbol{\beta} < 0$ in Ω, then all the solutions of* (2.16) *are positive. Hence, since we have shown that there is at least one solution of* (2.16) *and the scheme is linear, this implies that there is a unique solution of* (2.16) *which, in addition, is positive.*

2.3.3 Linear convection with incompressible velocity and maximum principle

Now let us focus on the particular case of the conservation problem (2.8) where $\boldsymbol{\beta}\colon \overline{\Omega} \to \mathbb{R}^d$ is continuous and **incompressible**, i.e. $\nabla \cdot \boldsymbol{\beta} = 0$ in Ω. In this case, the solution of the problem (2.8), satisfies the following maximum principle (it can be proved, for instance, using the characteristics method as in Remark 2.3.2):

$$\min_{\overline{\Omega}} v_0 \leq v \leq \max_{\overline{\Omega}} v_0 \quad \text{in } \overline{\Omega} \times (0, T).$$

We are going to show that the solution of the linear scheme 2.16 (without truncating v) preserves this maximum principle. The proof is based on the fact that, as consequence of the divergence theorem, one has

$$\int_{\partial K} \boldsymbol{\beta} \cdot \boldsymbol{n}_K = 0, \quad \forall K \in \mathcal{T}_h. \tag{2.18}$$

Proposition 2.3.9 (Linear DG (2.16) preserves the maximum principle)**.** *For any $v^m \in \mathbb{P}_0^{disc}(\mathcal{T}_h)$, the solution $v^{m+1} \in \mathbb{P}_0^{disc}(\mathcal{T}_h)$ of the scheme* (2.16) *satisfies the maximum principle, that is*

$$\min_{\overline{\Omega}} v^m \leq v^{m+1} \leq \max_{\overline{\Omega}} v^m \quad \textit{in } \overline{\Omega}.$$

Proof. First, we will prove that $v^{m+1} \geq \min_{\overline{\Omega}} v^m$. Let us denote $v_{min} = \min_{\overline{\Omega}} v^m$. Taking the following test function

$$\overline{v} = \begin{cases} (v_{K^*}^{m+1} - v_{min})_{\ominus} & \text{in } K^*, \\ 0 & \text{out of } K^*, \end{cases}$$

where K^* is an element of $\mathcal{T}_h$ such that the value $v_{K^*}^{m+1} = \min_{K \in \mathcal{T}_h} v_K^{m+1}$, the scheme (2.16) becomes

$$|K^*| \delta_t v_{K^*}^{m+1} (v_{K^*}^{m+1} - v_{min})_{\ominus} = -a_h^{\text{upw}}(\boldsymbol{\beta}; v^{m+1}, \mathbb{1}_{K^*}(v_{K^*}^{m+1} - v_{min})_{\ominus}).$$

Now, as we have chosen K^* we can assure that $v_L^{m+1} \geq v_{K^*}^{m+1}$ for all $L \in \mathcal{T}_h$. Hence, using (2.18), one has

$$\begin{aligned} a_h^{\text{upw}}(\boldsymbol{\beta}; v^{m+1}, \mathbb{1}_{K^*}(v_{K^*}^{m+1} - v_{min})_{\ominus}) = \\ &= \sum_{e \in \mathcal{E}_h^{\text{i}}, e = K^* \cap L} \int_e \left((\boldsymbol{\beta} \cdot \boldsymbol{n}_e)_{\oplus} v_{K^*}^{m+1} - (\boldsymbol{\beta} \cdot \boldsymbol{n}_e)_{\ominus} v_L^{m+1} \right) (v_{K^*}^{m+1} - v_{min})_{\ominus} \\ &\leq \sum_{e \in \mathcal{E}_h^{\text{i}}, e = K^* \cap L} \int_e \left((\boldsymbol{\beta} \cdot \boldsymbol{n}_e)_{\oplus} v_{K^*}^{m+1} - (\boldsymbol{\beta} \cdot \boldsymbol{n}_e)_{\ominus} v_{K^*}^{m+1} \right) (v_{K^*}^{m+1} - v_{min})_{\ominus} \\ &= v_{K^*}^{m+1} (v_{K^*}^{m+1} - v_{min})_{\ominus} \sum_{e \in \mathcal{E}_h^{\text{i}}, e = K^* \cap L} \int_e (\boldsymbol{\beta} \cdot \boldsymbol{n}_e) = 0. \end{aligned}$$

Therefore,

$$|K^*| \delta_t v_{K^*}^{m+1} (v_{K^*}^{m+1} - v_{min})_{\ominus} \geq 0.$$

Moreover,

$$\begin{aligned} 0 &\leq |K^*| (\delta_t v_{K^*}^{m+1}) (v_{K^*}^{m+1} - v_{min})_{\ominus} \\ &= \frac{|K^*|}{\Delta t} \left((v_{K^*}^{m+1} - v_{min}) + (v_{min} - v_{K^*}^m) \right) (v_{K^*}^{m+1} - v_{min})_{\ominus} \\ &= \frac{|K^*|}{\Delta t} \left(-(v_{K^*}^{m+1} - v_{min})_{\ominus}^2 + (v_{min} - v_{K^*}^m)(v_{K^*}^{m+1} - v_{min})_{\ominus} \right) \leq 0, \end{aligned}$$

then we have proved that $(v_{K^*}^{m+1} - v_{min})_{\ominus} = 0$. Hence, from the choice of K^*, we can assure $v^{m+1} \geq \min_{\overline{\Omega}} v^m$.

Now, we will prove that $v^{m+1} \leq \max_{\overline{\Omega}} v^m$. Let us denote $v_{max} = \max_{\overline{\Omega}} v^m$. Taking the following test function

$$\overline{v} = \begin{cases} (v_{K^*}^{m+1} - v_{max})_{\oplus} & \text{in } K^*, \\ 0 & \text{out of } K^*, \end{cases}$$

where K^* is an element of $\mathcal{T}_h$ such that the value $v_{K^*}^{m+1} = \max_{K \in \mathcal{T}_h} v_K^{m+1}$ and using similar arguments to those above, we arrive at

$$|K^*| \delta_t v_{K^*}^{m+1} (v_{K^*}^{m+1} - v_{max})_{\oplus} \leq 0.$$

Moreover,

$$\begin{aligned} 0 &\leq \frac{|K^*|}{\Delta t} \left((v_{K^*}^{m+1} - v_{max})_{\oplus}^2 + (v_{max} - v_{K^*}^m)(v_{K^*}^{m+1} - v_{max})_{\oplus} \right) \\ &= \frac{|K^*|}{\Delta t} \left((v_{K^*}^{m+1} - v_{max}) + (v_{max} - v_{K^*}^m) \right) (v_{K^*}^{m+1} - v_{max})_{\oplus} \\ &= |K^*| \delta_t v_{K^*}^{m+1} (v_{K^*}^{m+1} - v_{max})_{\oplus} \leq 0, \end{aligned}$$

then we have proved that $(v_{K^*}^{m+1} - v_{max})_{\oplus} = 0$. From the choice of K^*, we can assure that $v^{m+1} \leq \max_{\overline{\Omega}} v^m$. □

2.4 Cahn-Hilliard with degenerate mobility and incompressible convection

At this point, given $\boldsymbol{v} \colon \Omega \times (0,T) \longrightarrow \mathbb{R}^d$ a continuous incompressible velocity field satisfying the slip condition (2.6), we are in position to consider the CCH problem (2.1).

Remark 2.4.1. *Any smooth enough solution (u, μ) of the CCH model (2.1) satisfies the maximum principle $0 \leq u \leq 1$ in $\overline{\Omega} \times (0,T)$ whenever $0 \leq u_0 \leq 1$ in $\overline{\Omega}$. The proof of this statement is a straightforward consequence of Remark 2.3.2.*

- *To prove that $u \geq 0$, it is enough to notice that u is the solution of (2.8) with $\boldsymbol{\beta} \coloneqq -(1-u)\nabla\mu + \boldsymbol{v}$ and to use Remark 2.3.2.*
- *To check that $u \leq 1$ we make the change of variables $w \coloneqq 1 - u$ and, using that $\nabla \cdot \boldsymbol{v} = 0$, notice that w is the solution of (2.8) with $\boldsymbol{\beta} \coloneqq (1-w)(\nabla\mu + \boldsymbol{v})$. Then, we just use Remark 2.3.2.*

Owing to this maximum principle, the following $C^2(\mathbb{R})$ truncated potential is considered

$$F(u) \coloneqq \frac{1}{4}\begin{cases} u^2 & u < 0, \\ u^2(1-u)^2 & u \in [0,1], \\ (u-1)^2 & u > 1. \end{cases} \tag{2.19}$$

This truncated potential will allow us to define a linear time discrete convex-splitting scheme satisfying an energy law (where the energy is decreasing in the case $\boldsymbol{v} = 0$), see Section 2.4.1.

Assume $0 \leq u_0 \leq 1$ in $\overline{\Omega}$. The weak formulation of problem (2.1) consists of finding (u, μ) such that, $u(t) \in H^1(\Omega)$, $\mu(t) \in H^1(\Omega)$ with $\partial_t u(t) \in H^1(\Omega)'$, $M(u(t))\nabla\mu(t) \in L^2(\Omega)$ a.e. $t \in (0,T)$, and satisfying the following variational problem a.e. $t \in (0,T)$ for every $\overline{\mu}, \overline{u} \in H^1(\Omega)$:

$$\langle \partial_t u(t), \overline{\mu} \rangle = -\left(M(u(t))\nabla\mu(t) - u(t)\boldsymbol{v}(t), \nabla\overline{\mu}\right), \tag{2.20a}$$

$$(\mu(t), \overline{u}) = \varepsilon^2 \left(\nabla u(t), \nabla\overline{u}\right) + \left(F'(u(t)), \overline{u}\right), \tag{2.20b}$$

with the initial condition $u(0) = u_0$ in Ω. We denote by $\langle \cdot, \cdot \rangle$ the duality product in $H^1(\Omega)'$.

Remark 2.4.2. *By taking $\overline{\mu} = 1$ in* (2.20a)*, any solution u of* (2.20) *conserves the mass, because*

$$\frac{d}{dt}\int_\Omega u(x,t)dx = 0.$$

Remark 2.4.3. *By taking $\overline{\mu} = \mu(t)$ and $\overline{u} = \partial_t u(t)$ in* (2.20)*, and adding the resulting expressions, one has that any solution (u, μ) of* (2.20) *satisfies the following energy law*

$$\frac{d}{dt}E(u(t)) + \int_\Omega M(u(x,t))|\nabla\mu(x,t)|^2 dx = \int_\Omega u(x,t)\,\boldsymbol{v}(x,t)\cdot\nabla\mu(x,t)dx, \tag{2.21}$$

where $E\colon H^1(\Omega) \longrightarrow \mathbb{R}$ is the Helmholtz free energy

$$E(u) \coloneqq \int_\Omega \left(\frac{\varepsilon^2}{2}|\nabla u|^2 + F(u)\right) dx. \tag{2.22}$$

Indeed, by applying the chain rule we get

$$\begin{aligned}\frac{d}{dt}E(u(t)) &= \langle \frac{\delta E}{\delta u}(u(t)), \partial_t u(t)\rangle = \int_\Omega \mu(x,t)\partial_t u(x,t)dx \\ &= -\int_\Omega M(u(x,t))|\nabla\mu(x,t)|^2 dx + \int_\Omega u(x,t)\,\boldsymbol{v}(x,t)\cdot\nabla\mu(x,t)dx.\end{aligned}$$

In particular, in the CH case ($\boldsymbol{v}=0$), the energy $E(u(t))$ is dissipative. Contrarily, to the best knowledge of the authors, for the CCH problem with $\boldsymbol{v}\neq 0$, there is no evidence of the existence of a dissipative energy.

2.4.1 Convex splitting time discretization

Now we are ready to focus on a convex splitting time discretization (of Eyre's type [77]) of (2.20). Specially, we decompose the truncated potential (2.19) as follows:

$$F(u) = F_{\mathrm{i}}(u) + F_{\mathrm{e}}(u),$$

where

$$F_{\mathrm{i}}(u) \coloneqq \frac{3}{8}u^2, \qquad F_{\mathrm{e}}(u) \coloneqq \frac{1}{4}\begin{cases} -\frac{1}{2}u^2 & u<0, \\ u^4-2u^3-\frac{1}{2}u^2 & u\in[0,1], \\ 1-2u-\frac{1}{2}u^2 & u>1. \end{cases}$$

It can be easily proved that $F_{\mathrm{i}}(u)$ is a convex operator, which will be treated implicitly whereas $F_{\mathrm{e}}(u)$ is a concave operator that will be treated explicitly. Then we consider the following convex $E_{\mathrm{i}}(u(t))$ and concave $E_{\mathrm{e}}(u(t))$ energy terms:

$$\begin{aligned}E_{\mathrm{i}}(u) &\coloneqq \frac{\varepsilon^2}{2}\int_\Omega |\nabla u(x)|^2 dx + \int_\Omega F_{\mathrm{i}}(u(x))dx, \\ E_{\mathrm{e}}(u) &\coloneqq \int_\Omega F_{\mathrm{e}}(u(x))dx,\end{aligned}$$

such that the free energy (2.22) is split as $E(u) = E_{\mathrm{i}}(u) + E_{\mathrm{e}}(u)$.

Finally we define the following time discretization of (2.20): find $u^{m+1} \in H^1(\Omega)$ and $\mu^{m+1} \in H^1(\Omega)$ such that, for every $\overline{\mu}, \overline{u} \in H^1(\Omega)$:

$$\left(\delta_t u^{m+1}, \overline{\mu}\right) = -\left(M(u^{m+1})_{\oplus} \nabla \mu^{m+1} - u^{m+1} \boldsymbol{v}(t_{m+1}), \nabla \overline{\mu}\right), \tag{2.23a}$$

$$\left(\mu^{m+1}, \overline{u}\right) = \varepsilon^2 \left(\nabla u^{m+1}, \nabla \overline{u}\right) + \left(f(u^{m+1}, u^m), \overline{u}\right), \tag{2.23b}$$

where we denote the convex-implicit and concave-explicit linear approximation of the potential as follows

$$f(u^{m+1}, u^m) \coloneqq F_{\mathrm{i}}'(u^{m+1}) + F_{\mathrm{e}}'(u^m) = \frac{3}{4} u^{m+1} + \frac{1}{4} \begin{cases} -u^m, & u^m \in (-\infty, 0), \\ 4(u^m)^3 - 6(u^m)^2 - u^m, & u^m \in [0, 1], \\ -\left(u^m + 2\right), & u^m \in (1, +\infty). \end{cases} \tag{2.24}$$

Notice that the positive part of the mobilitity has been taken in (2.23a), regarding the Remark 2.4.1, in order to prevent possible overshoots of the solution u^{m+1} beyond the interval $[0, 1]$.

2.4.1.1 Discrete energy law

By adding (2.23a) and (2.23b) for $\overline{\mu} = \mu^{m+1}$ and $\overline{u} = \delta_t u^{m+1}$ in (2.23), we get:

$$\int_\Omega M(u^{m+1})_{\oplus} |\nabla \mu^{m+1}|^2 + \varepsilon^2 \left(\nabla u^{m+1}, \delta_t \nabla u^{m+1}\right) + \left(f(u^{m+1}, u^m), \delta_t u^{m+1}\right) = \int_\Omega u^{m+1} \boldsymbol{v}(\cdot, t_{m+1}) \cdot \nabla \mu^{m+1}. \tag{2.25}$$

Taking into account that

$$\varepsilon^2 \left(\nabla u^{m+1}, \delta_t \nabla u^{m+1}\right) = \frac{\varepsilon^2}{2} \delta_t \int_\Omega |\nabla u^{m+1}|^2 + \frac{k\varepsilon^2}{2} \int_\Omega |\delta_t \nabla u^{m+1}|^2,$$

by adding and substracting $\delta_t \int_\Omega F(u^{m+1})$ we get the following equality where $E(u)$ is defined in (2.22):

$$\delta_t E(u^{m+1}) + \int_\Omega M(u^{m+1})_{\oplus} |\nabla \mu^{m+1}|^2 + \frac{k\varepsilon^2}{2} \int_\Omega |\delta_t \nabla u^{m+1}|^2 + \left(f(u^{m+1}, u^m), \delta_t u^{m+1}\right) - \delta_t \int_\Omega F(u^{m+1}) = \int_\Omega u^{m+1} \boldsymbol{v}(\cdot, t_{m+1}) \cdot \nabla \mu^{m+1}.$$

Then, using the Taylor theorem we get

$$F_{\mathrm{i}}(u^m) = F_{\mathrm{i}}(u^{m+1}) + F_{\mathrm{i}}'(u^{m+1})(u^m - u^{m+1}) + \frac{F_{\mathrm{i}}''(u^{m+\xi})}{2}(u^m - u^{m+1})^2,$$
$$F_{\mathrm{e}}(u^{m+1}) = F_{\mathrm{e}}(u^m) + F_{\mathrm{e}}'(u^m)(u^{m+1} - u^m) + \frac{F_{\mathrm{e}}''(u^{m+\eta})}{2}(u^{m+1} - u^m)^2,$$

for certain $\xi, \eta \in (0,1)$ with $u^{m+\xi} = \xi u^{m+1} + (1-\xi)u^m$, $u^{m+\eta} = \eta u^{m+1} + (1-\eta)u^m$. Hence, adding these expressions and taking into consideration that $F(u) = F_{\mathrm{i}}(u) + F_{\mathrm{e}}(u)$ for every $u \in \mathbb{R}$, we arrive at

$$F(u^{m+1}) - F(u^m) = f(u^{m+1}, u^m)(u^{m+1} - u^m) - \frac{F_i''(u^{m+\xi}) - F_e''(u^{m+\eta})}{2}(u^{m+1} - u^m)^2.$$

Furthermore, as

$$\frac{F_i''(u^{m+\xi}) - F_e''(u^{m+\eta})}{2k} = \begin{cases} \frac{1}{2k}, & u^{m+\eta} \in (-\infty, 0) \cup (1, +\infty), \\ \dfrac{3 - 12(u^{m+\eta})^2 + 12(u^{m+\eta}) + 1}{8k}, & u^{m+\eta} \in [0,1], \end{cases}$$
$$= \begin{cases} \frac{1}{2k} \geq 0, & u^{m+\eta} \in (-\infty, 0) \cup (1, +\infty), \\ \frac{1}{2k}\left(1 - 3u^{m+\eta}(u^{m+\eta} - 1)\right) \geq 0, & u^{m+\eta} \in [0,1], \end{cases}$$

we have

$$\frac{F_i''(u^{m+\xi}) - F_e''(u^{m+\eta})}{2k} \geq 0,$$

and finally

$$\left(f(u^{m+1}, u^m), \delta_t u^{m+1}\right) - \int_\Omega \delta_t F(u^{m+1}) \geq 0.$$

Therefore, we arrive at the following result:

Theorem 2.4.4. *Any solution of the scheme* (2.23) *satisfies the following* ***discrete energy law***

$$\delta_t E(u^{m+1}) + \int_\Omega M(u^{m+1})_\oplus |\nabla \mu^{m+1}|^2 + \frac{k\varepsilon^2}{2}\int_\Omega |\delta_t \nabla u^{m+1}|^2 \leq \int_\Omega u^{m+1} \boldsymbol{v}(\cdot, t_{m+1}) \cdot \nabla \mu^{m+1}. \tag{2.26}$$

In particular, if $\boldsymbol{v} = 0$ *the time-discrete scheme is unconditionally energy stable, because* $E(u^{m+1}) \leq E(u^m)$.

2.4.2 Fully discrete scheme

At this point we are going to introduce the key idea for the spatial approximation: to treat equation (2.1a) as a conservative problem where there are two different fluxes (linear and nonlinear). In this sense, we propose an upwind DG scheme approximating the nonlinear flux $\boldsymbol{F}(u) = M(u)\nabla\mu$ properly.

To this aim, we take for values $v \in \mathbb{R}$ the increasing and decreasing part of $M(v)_\oplus$, denoted respectively by $M^\uparrow(v)$ and $M^\downarrow(v)$, as follows:

$$M^\uparrow(v) = \int_0^v \left(\partial_s \left(M(s)_\oplus\right)\right)_\oplus ds = \int_0^{\min(v,1)} M'(s)_\oplus ds = \int_0^{\min(v,1)} (1-2s)_\oplus ds,$$
$$M^\downarrow(v) = -\int_0^v \left(\partial_s \left(M(s)_\oplus\right)\right)_\ominus ds = -\int_0^{\min(v,1)} M'(s)_\ominus ds = -\int_0^{\min(v,1)} (1-2s)_\ominus ds.$$

Therefore,

$$M^\uparrow(v) = \begin{cases} M(v)_\oplus & \text{if } v \le \frac{1}{2}, \\ M\left(\frac{1}{2}\right) & \text{if } v > \frac{1}{2}, \end{cases} \qquad M^\downarrow(v) = \begin{cases} 0 & \text{if } v \le \frac{1}{2}, \\ M(v)_\oplus - M\left(\frac{1}{2}\right) & \text{if } v > \frac{1}{2}. \end{cases} \tag{2.28}$$

Notice that $M^\uparrow(v) + M^\downarrow(v) = M(v)_\oplus$. We define the followig generalized upwind bilinear form to be applied for the nonlinear flux $\boldsymbol{F}(u) = M(u)\boldsymbol{\beta}$ where now $\boldsymbol{\beta}$ can be discontinuous over $\mathcal{E}_h^{\mathrm{i}}$ (in fact we will take $\boldsymbol{\beta} = \nabla\mu$):

$$\begin{aligned} a_h^{\mathrm{upw}}(\boldsymbol{\beta}; M(v)_\oplus, \overline{v}) \coloneqq & -\int_\Omega (\boldsymbol{\beta}\cdot\nabla\overline{v}) M(v)_\oplus \\ & + \sum_{e\in\mathcal{E}_h^{\mathrm{i}}, e=K\cap L} \int_e \Big((\{\!\{\boldsymbol{\beta}\}\!\}\cdot\boldsymbol{n}_e)_\oplus (M^\uparrow(v_K) + M^\downarrow(v_L)) \\ & \qquad -(\{\!\{\boldsymbol{\beta}\}\!\}\cdot\boldsymbol{n}_e)_\ominus (M^\uparrow(v_L) + M^\downarrow(v_K)) \Big) [\![\overline{v}]\!]. \end{aligned} \tag{2.29}$$

Remark 2.4.5. *We refer to* (2.29) *as a generalized bilinear form since it generalizes the definition of* (2.11) *considering the case where $\boldsymbol{\beta}$ may be discontinuous. If $\boldsymbol{\beta}$ is continuous both definitions are equivalent.*

Then, we propose the following fully discrete DG+Eyre scheme (named **DG-UPW**) for the model (2.1):

Find $u^{m+1} \in \mathbb{P}_0^{\text{disc}}(\mathcal{T}_h)$, with $\mu^{m+1}, w^{m+1} \in \mathbb{P}_1^{\text{cont}}(\mathcal{T}_h)$, solving

$$\left(\delta_t u^{m+1}, \overline{u}\right) + a_h^{\text{upw}}(-\nabla\mu^{m+1}; M(u^{m+1})_{\oplus}, \overline{u}) + a_h^{\text{upw}}(\boldsymbol{v}(t_{m+1}); u^{m+1}, \overline{u}) = 0, \tag{2.30a}$$

$$\left(\mu^{m+1}, \overline{\mu}\right) = \varepsilon^2 \left(\nabla w^{m+1}, \nabla\overline{\mu}\right) + \left(f(u^{m+1}, u^m), \overline{\mu}\right), \tag{2.30b}$$

$$\left(w^{m+1}, \overline{w}\right) = \left(u^{m+1}, \overline{w}\right), \tag{2.30c}$$

for all $\overline{u} \in \mathbb{P}_0^{\text{disc}}(\mathcal{T}_h)$ and $\overline{\mu}, \overline{w} \in \mathbb{P}_1^{\text{cont}}(\mathcal{T}_h)$. Following the notation of the Section 2.3.2,

$$a_h^{\text{upw}}(\boldsymbol{v}; u, \overline{u}) = \sum_{e \in \mathcal{E}_h^{\text{i}}, e = K|L} \int_e \left((\boldsymbol{v}\cdot\boldsymbol{n}_e)_{\oplus} u_K - (\boldsymbol{v}\cdot\boldsymbol{n}_e)_{\ominus} u_L\right) [\![\overline{u}]\!] .$$

In this scheme we have introduced a truncation of the function $M(u)$ taking its positive part $M(u)_{\oplus}$, which is consistent as the solution of the continuous model (2.1) satisfies $0 \leq u \leq 1$.

Notice that we have introduced a new continuous variable $w \in \mathbb{P}_1^{\text{cont}}(\mathcal{T}_h)$ in (2.30c). It can be seen as a regularization of the variable $u \in \mathbb{P}_0^{\text{cont}}(\mathcal{T}_h)$, which is used in the diffusion term in (2.30b) (which corresponds to the philic term in the energy of the model (2.22)). In fact, both variables w^{m+1} and u^{m+1} are approximations of $u(t_{m+1})$.

Remark 2.4.6. *We are using the same notation in the fully discrete scheme* (2.30) *than the one we have used in the time-discrete scheme* (2.23) *given in the Section 2.4.1.1, satisfying an energy law.*

Nevertheless, in this case we are changing the meaning of the equations since we are treating (2.30a) *as the u-equation and* (2.30b) *as the μ-equation, contrary to computations done to reach the energy law. This has been done for the purpose of preserving the maximum principle in the equation* (2.30a) *and adequately approximating the laplacian term of the equation* (2.30b)*.*

Remark 2.4.7. *The boundary condition $\nabla w^{m+1} \cdot \boldsymbol{n} = 0$ on $\partial\Omega \times (0, T)$ is imposed implicitly by the term $\left(\nabla w^{m+1}, \nabla\overline{\mu}\right)$ in* (2.30b)*.*

Remark 2.4.8. *Since $f(\cdot, u^m)$ is linear, we have the following equality of the potential term of* (2.30b)*:*

$$\left(f(w^{m+1}, u^m), \overline{\mu}\right) = \left(f(u^{m+1}, u^m), \overline{\mu}\right).$$

Remark 2.4.9. *The scheme* (2.30) *is nonlinear, hence we will have to use an iterative procedure, the Newton's method, to approach its solution.*

Proposition 2.4.10. *The scheme* (2.30) *conserves the mass of both* u^{m+1} *and* w^{m+1} *variables:*

$$\int_\Omega u^{m+1} = \int_\Omega u^m \quad \textit{and} \quad \int_\Omega w^{m+1} = \int_\Omega w^m.$$

Proof. Just need to take $\overline{u} = 1$ in (2.30a) and $\overline{w} = 1$ in (2.30c). □

Theorem 2.4.11 (DG (2.30) preserves the maximum principle)**.** *For any* $u^m \in \mathbb{P}_0^{disc}(\mathcal{T}_h)$ *with* $0 \leq u^m \leq 1$ *in* $\overline{\Omega}$*, then any solution* u^{m+1} *of* (2.30) *satisfies* $0 \leq u^{m+1} \leq 1$ *in* $\overline{\Omega}$*.*

Proof. Firstly, we prove that $u^{m+1} \geq 0$. Taking the following $\mathbb{P}_0^{\text{disc}}(\mathcal{T}_h)$ test function

$$\overline{u} = \begin{cases} (u_{K^*}^{m+1})_\ominus & \text{in } K^*, \\ 0 & \text{out of } K^*, \end{cases}$$

where K^* is an element of $\mathcal{T}_h$ such that $u_{K^*}^{m+1} = \min_{K\in\mathcal{T}_h} u_K^{m+1}$, equation (2.30a) becomes

$$|K^*|\delta_t u_{K^*}^{m+1}(u_{K^*}^{m+1})_\ominus \quad = \quad -a_h^{\text{upw}}(-\nabla\mu^{m+1}; M(u^{m+1})_\oplus, \overline{u}) \;-\; a_h^{\text{upw}}(\boldsymbol{v}(t_{m+1}); u^{m+1}, \overline{u}). \quad (2.31)$$

Now, since $u_L^{m+1} \geq u_{K^*}^{m+1}$ for all $L \in \mathcal{T}_h$, we can assure that

$$M^\uparrow(u_L^{m+1}) \geq M^\uparrow(u_{K^*}^{m+1}) \quad \text{and} \quad M^\downarrow(u_L^{m+1}) \leq M^\downarrow(u_{K^*}^{m+1}).$$

Then, we can bound as follows:

$$\begin{aligned} a_h^{\text{upw}}(-\nabla\mu^{m+1}; M(u^{m+1})_\oplus, \overline{u}) &= \sum_{e\in\mathcal{E}_h^{\text{i}}, e=K^*\cap L} \int_e \Big((\{\!\{-\nabla\mu^{m+1}\}\!\} \cdot \boldsymbol{n}_e)_\oplus (M^\uparrow(u_{K^*}^{m+1}) + M^\downarrow(u_L^{m+1})) \\ &\qquad -(\{\!\{-\nabla\mu^{m+1}\}\!\} \cdot \boldsymbol{n}_e)_\ominus (M^\uparrow(u_L^{m+1}) + M^\downarrow(u_{K^*}^{m+1}))\Big) (u_{K^*}^{m+1})_\ominus \\ &\leq \sum_{e\in\mathcal{E}_h^{\text{i}}, e=K^*\cap L} \int_e \Big((\{\!\{-\nabla\mu^{m+1}\}\!\} \cdot \boldsymbol{n}_e)_\oplus (M^\uparrow(u_{K^*}^{m+1}) + M^\downarrow(u_{K^*}^{m+1})) \\ &\qquad -(\{\!\{-\nabla\mu^{m+1}\}\!\} \cdot \boldsymbol{n}_e)_\ominus (M^\uparrow(u_{K^*}^{m+1}) + M^\downarrow(u_{K^*}^{m+1}))\Big) (u_{K^*}^{m+1})_\ominus \\ &= \sum_{e\in\mathcal{E}_h^{\text{i}}, e=K^*\cap L} \int_e (\{\!\{-\nabla\mu^{m+1}\}\!\} \cdot \boldsymbol{n}_e) \left(M(u_{K^*}^{m+1})\right)_\oplus (u_{K^*}^{m+1})_\ominus = 0. \end{aligned}$$

On the other hand, applying the incompressibility of $\boldsymbol{v}$ and proceeding as in Section 2.3.3, one has that

$$a_h^{\text{upw}}(\boldsymbol{v}(t_{m+1}); u^{m+1}, \overline{u}) \leq 0.$$

Therefore, from (2.31)

$$|K^*|\delta_t u_{K^*}^{m+1}(u_{K^*}^{m+1})_{\ominus} \geq 0.$$

Consequently, it is satisfied that

$$0 \leq |K^*|(\delta_t u_{K^*}^{m+1})(u_{K^*}^{m+1})_{\ominus} = -\frac{|K^*|}{\Delta t}\left((u_{K^*}^{m+1})_{\ominus}^2 + u_{K^*}^m (u_{K^*}^{m+1})_{\ominus}\right) \leq 0,$$

hence, since $u_{K^*}^m \geq 0$, we prove that $(u_{K^*}^{m+1})_{\ominus} = 0$. Hence $u^{m+1} \geq 0$.

Secondly, we prove that $u^{m+1} \leq 1$. Taking the following test function

$$\overline{u} = \begin{cases} (u_{K^*}^{m+1} - 1)_{\oplus} & \text{in } K^*, \\ 0 & \text{out of } K^*, \end{cases}$$

where K^* is an element of $\mathcal{T}_h$ such that $u_{K^*}^{m+1} = \max_{K \in \mathcal{T}_h} u_K^{m+1}$ and using similar arguments than above, we arrive at

$$|K^*|\delta_t u_{K^*}^{m+1}(u_{K^*}^{m+1} - 1)_{\oplus} \leq 0.$$

Besides, it is satisfied that

$$\begin{aligned} 0 \geq |K^*|\delta_t u_{K^*}^{m+1}(u_{K^*}^{m+1} - 1)_{\oplus} &= \frac{|K^*|}{\Delta t}\left((u_{K^*}^{m+1} - 1) + (1 - u_{K^*}^m)\right)(u_{K^*}^{m+1} - 1)_{\oplus} \\ &= \frac{|K^*|}{\Delta t}\left((u_{K^*}^{m+1} - 1)_{\oplus}^2 + (1 - u_{K^*}^m)(u_{K^*}^{m+1} - 1)_{\oplus}\right) \geq 0, \end{aligned}$$

hence we deduce that $(u_{K^*}^{m+1} - 1)_{\oplus} = 0$ and, therefore, $u^{m+1} \leq 1$. □

The following result is a direct consequence of Theorem 2.4.11.

Corollary 2.4.12. *If we use mass-lumping to compute w^{m+1} in* (2.30c)*, then $0 \leq w^{m+1} \leq 1$ in $\overline{\Omega}$ for $m \geq 0$.*

Theorem 2.4.13. *There is at least one solution of the scheme* (2.30).

Proof. Given a function $z \in \mathbb{P}_0^{\text{disc}}(\mathcal{T}_h)$ with $0 \leq z \leq 1$, we define the map

$$T\colon \mathbb{P}_0^{\text{disc}}(\mathcal{T}_h) \times \mathbb{P}_1^{\text{cont}}(\mathcal{T}_h) \times \mathbb{P}_1^{\text{cont}}(\mathcal{T}_h) \longrightarrow \mathbb{P}_0^{\text{disc}}(\mathcal{T}_h) \times \mathbb{P}_1^{\text{cont}}(\mathcal{T}_h) \times \mathbb{P}_1^{\text{cont}}(\mathcal{T}_h)$$

such that $T(\widehat{u}, \widehat{\mu}, \widehat{w}) = (u, \mu, w) \in \mathbb{P}_0^{\text{disc}}(\mathcal{T}_h) \times \mathbb{P}_1^{\text{cont}}(\mathcal{T}_h) \times \mathbb{P}_1^{\text{cont}}(\mathcal{T}_h)$ is the unique solution, for every $\overline{u} \in \mathbb{P}_0^{\text{disc}}(\mathcal{T}_h)$, $\overline{\mu}, \overline{w} \in \mathbb{P}_1^{\text{cont}}(\mathcal{T}_h)$, of the linear (and decoupled) scheme:

$$\frac{1}{\Delta t}\,(u - z, \overline{u}) + a_h^{\text{upw}}(\boldsymbol{v}; u, \overline{u}) = -a_h^{\text{upw}}(-\nabla\widehat{\mu}; M(\widehat{u})_{\oplus}, \overline{u}), \tag{2.32a}$$

$$(\mu, \overline{\mu}) = \varepsilon^2\,(\nabla w, \nabla\overline{\mu}) + (f(u, z), \overline{\mu})\,, \tag{2.32b}$$

$$(w, \overline{w}) = (u, \overline{w})\,, \tag{2.32c}$$

To check that T is well defined, one may use the following steps. First, it is easy to prove that there is a unique solution u of (2.32a) which implies that there is a unique solution w of (2.32c) using, for instance, the Lax-Milgram theorem. Then, it is straightforward to see that the solution μ of (2.32b) is unique, which implies its existence as $\mathbb{P}_1^{\text{cont}}(\mathcal{T}_h)$ is a finite-dimensional space.

It can be proved, using the notion of convergence elementwise, as it was done in Theorem 2.3.5 and taking into consideration that $\nabla\widehat{\mu} \in \left(\mathbb{P}_0^{\text{disc}}(\mathcal{T}_h)\right)^d$, that the operator T is continuous, and, therefore, it is compact since $\mathbb{P}_0^{\text{disc}}(\mathcal{T}_h)$ and $\mathbb{P}_1^{\text{cont}}(\mathcal{T}_h)$ have finite dimension.

Finally, let us prove that the set

$$B = \{(u, \mu, w) \in \mathbb{P}_0^{\text{disc}}(\mathcal{T}_h) \times \mathbb{P}_1^{\text{cont}}(\mathcal{T}_h) \times \mathbb{P}_1^{\text{cont}}(\mathcal{T}_h)\colon (u, \mu, w) = \alpha T(u, \mu, w) \text{ for some } 0 \leq \alpha \leq 1\}$$

is bounded (independent of α). The case $\alpha = 0$ is trivial so we will assume that $\alpha \in (0, 1]$.

If $(u, \mu, w) \in B$, then $u \in \mathbb{P}_0^{\text{disc}}(\mathcal{T}_h)$ is the solution, for every $\overline{u} \in \mathbb{P}_0^{\text{disc}}(\mathcal{T}_h)$, of

$$\frac{1}{\Delta t}\,(u - \alpha z, \overline{u}) + a_h^{\text{upw}}(\boldsymbol{v}; u, \overline{u}) = -\alpha\, a_h^{\text{upw}}(-\nabla\mu; M(u)_{\oplus}, \overline{u}). \tag{2.33}$$

Now, testing (2.33) by $\overline{u} = 1$, we get that

$$\int_\Omega u = \alpha \int_\Omega z,$$

and, since $0 \leq z \leq 1$, and since it can be proved that $0 \leq u \leq 1$ using the same arguments than in Theorem 2.4.11, we get that

$$\|u\|_{L^1(\Omega)} \leq \|z\|_{L^1(\Omega)}.$$

Moreover, $w \in \mathbb{P}_1^{\text{cont}}(\mathcal{T}_h)$ is the solution of the equation

$$(w, \overline{w}) = (u, \overline{w}), \quad \forall \overline{w} \in \mathbb{P}_1^{\text{cont}}(\mathcal{T}_h). \tag{2.34}$$

Testing with $\overline{w} = w$ and using that $u \leq 1$ and that the norms are equivalent in $\mathbb{P}_1^{\text{cont}}(\mathcal{T}_h)$, we obtain

$$\|w\|^2_{L^2(\Omega)} = (u, w) \leq \|w\|_{L^1(\Omega)} \leq |\Omega|^{1/2} \|w\|_{L^2(\Omega)},$$

hence $\|w\|_{L^2(\Omega)} \leq |\Omega|^{1/2}$ holds.

Finally, we will check that μ is bounded. Regarding that, $\mu \in \mathbb{P}_1^{\text{cont}}(\mathcal{T}_h)$ is the solution of

$$(\mu, \overline{\mu}) = \varepsilon^2 (\nabla w, \nabla \overline{\mu}) + (f(u, z), \overline{\mu}), \quad \forall \overline{\mu} \in \mathbb{P}_1^{\text{cont}}(\mathcal{T}_h), \tag{2.35}$$

by testing by $\overline{\mu} = \mu$ we get that

$$\begin{aligned} \|\mu\|^2_{L^2(\Omega)} &\leq \varepsilon^2 \|\nabla w\|_{L^2(\Omega)^d} \|\nabla \mu\|_{L^2(\Omega)^d} + \|f(u, z)\|_{L^2(\Omega)} \|\mu\|_{L^2(\Omega)} \\ &\leq \varepsilon^2 \|w\|_{H^1(\Omega)} \|\mu\|_{H^1(\Omega)} + \|f(u, z)\|_{L^2(\Omega)} \|\mu\|_{L^2(\Omega)}. \end{aligned}$$

The norms are equivalent in the finite-dimensional space $\mathbb{P}_1^{\text{cont}}(\mathcal{T}_h)$, therefore, there is $C_{\text{cont}} \geq 0$ such that

$$\|\mu\|_{L^2(\Omega)} \leq \varepsilon^2 C_{\text{cont}} \|w\|_{L^2(\Omega)} + \|f(u, z)\|_{L^2(\Omega)}.$$

Hence, as $0 \leq u, z \leq 1$, we know that $\|f(u, z)\|_{L^2(\Omega)}$ is bounded, and therefore $\|\mu\|_{L^2(\Omega)}$ is bounded.

Since $\mathbb{P}_0^{\text{disc}}(\mathcal{T}_h)$ and $\mathbb{P}_1^{\text{cont}}(\mathcal{T}_h)$ are finite-dimensional spaces where all the norms are equivalent, we have proved that B is bounded.

Thus, using the Leray-Schauder fixed point theorem 2.3.6, there is a solution (u, μ, w) of the scheme (2.30). □

Corollary 2.4.14. *There is at least one solution of the following (non-truncated) scheme:*

Find $u^{m+1} \in \mathbb{P}_0^{disc}(\mathcal{T}_h)$ *with* $0 \leq u^{m+1} \leq 1$ *and* $\mu^{m+1}, w^{m+1} \in \mathbb{P}_1^{cont}(\mathcal{T}_h)$ *with* $0 \leq w^{m+1} \leq 1$*, solving*

$$\left(\delta_t u^{m+1}, \overline{u}\right) + a_h^{upw}(-\nabla\mu^{m+1}; M(u^{m+1}), \overline{u}) + a_h^{upw}(\boldsymbol{v}(t_{m+1}); u^{m+1}, \overline{u}) = 0, \tag{2.36a}$$

$$\left(\mu^{m+1}, \overline{\mu}\right) = \varepsilon^2 \left(\nabla w^{m+1}, \nabla\overline{\mu}\right) + \left(f(u^{m+1}, u^m), \overline{\mu}\right), \tag{2.36b}$$

$$\left(w^{m+1}, \overline{w}\right) = \left(u^{m+1}, \overline{w}\right). \tag{2.36c}$$

for all $\overline{u} \in \mathbb{P}_0^{disc}(\mathcal{T}_h)$ *and* $\overline{\mu}, \overline{w} \in \mathbb{P}_1^{cont}(\mathcal{T}_h)$*. Here, we have considered* $M(u^{m+1})$ *instead of* $M(u^{m+1})_{\oplus}$*.*

Proof. By Theorems 2.4.11 and 2.4.13 we know that there is a solution of the scheme (2.30) such that $0 \leq u^m \leq 1$ in $\overline{\Omega}$ for every $m \geq 0$. Hence, $M(u^m) = M(u^m)_{\oplus}$ for every $m \geq 0$, and therefore the solution of (2.30) is also a solution of (2.36), which moreover satisfies the discrete maximum principle. □

2.5 Numerical experiments

We now present several numerical tests in which we explore the behavior of the new upwind DG scheme presented in this work (**DG-UPW**) (2.30) and compare it with two other space semidiscretizations found in the literature: firstly a classical finite element discretization (**FE**) and secondly the DG scheme proposed in [81], based on an SIP + (sigmoid upwind) technique, that we call (**DG-SIP**). We use P_1 piecewise polynomials for both schemes unless otherwise specified.

For the DG-UPW scheme, we use mass lumping to compute w^{m+1} in (2.30c) so that $w^{m+1} \in [0, 1]$ by the Corollary 2.4.12. This w^{m+1}, which is a regularization of the primal variable u^{m+1}, is considered as the main phase-field variable, which is used when showing the results of the numerical experiments. Moreover, we consider $\mathsf{Pe} = 1$ unless another value is specified.

2.5.1 Qualitative tests and comparisons

Our first numerical tests are devoted to qualitative experiments about our DG-UPW scheme in rectangular and circular domains with different kinds of velocity fields. We also inspect the discrete energy and the maximum principle property, confirming that the latter one holds for our scheme but not for the two aforementioned ones, FE and DG-SIP.

2.5.1.1 Agreggation of circular regions without convection

First, we consider the Cahn–Hilliard equation without convection ($\boldsymbol{v} = 0$) in the squared domain $\Omega = (0,1)^2$ and the following initial condition (two small circles of radius 0.2, see Figure 2.1, left) :

$$u_0 = \frac{1}{2}\left(\frac{\tanh\left(0.2 - \sqrt{(x-x_1)^2 + (y-y_1)^2}\right)}{\sqrt{2}\varepsilon} + 1\right) + \frac{1}{2}\left(\frac{\tanh\left(0.2 - \sqrt{(x-x_2)^2 + (y-y_2)^2}\right)}{\sqrt{2}\varepsilon} + 1\right), \quad (2.37)$$

with centers $(x_1, y_1) = (0.3, 0.5)$ and $(x_2, y_2) = (0.7, 0.5)$. We take a structured mesh with $h \approx 2.8284 \cdot 10^{-2}$ and run time iterations with $\Delta t = 10^{-6}$. Each iteration consists of solving a nonlinear system for computing $(u^{n+1}, \mu^{n+1}, w^{n+1})$, for which we use Newton's method iterations, programmed on the `FEniCS` finite element library [14, 142]. For linear systems we used a MPI parallel solver (GMRES) in the computing cluster of the Universidad de Cádiz.

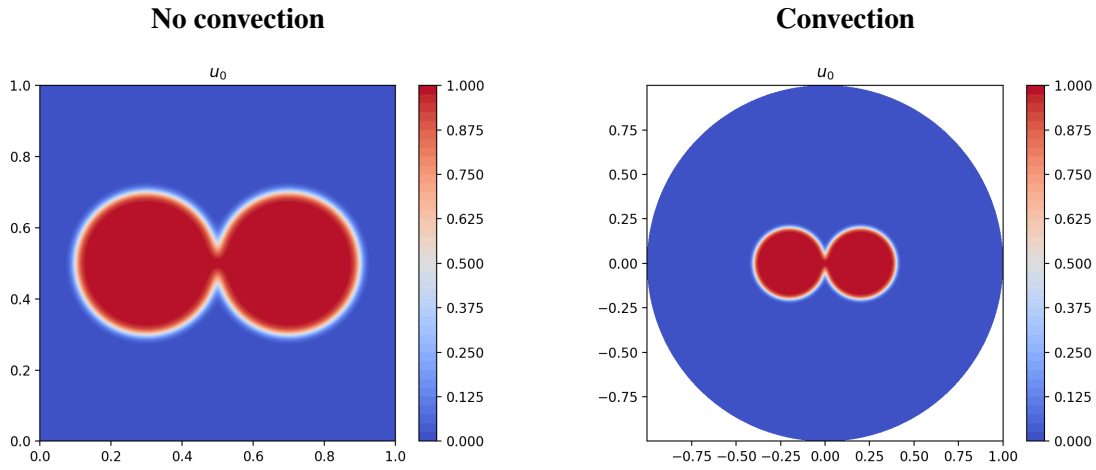

Figure 2.1 Left: initial condition in the case $\boldsymbol{v} = 0$. Right: initial condition in the case $\boldsymbol{v} = 100(y, -x)$

In Figure 2.2 we show a 3D view of the phase field function at the time step $T = 0.001$, when the aggregation process has started. It is interesting to notice that for our upwind DG scheme (2.30) there are no spurious oscillations meanwhile for the FE and DG-SIP schemes we obtain several numerical issues (vertical fluctuations in the 3D graphics).

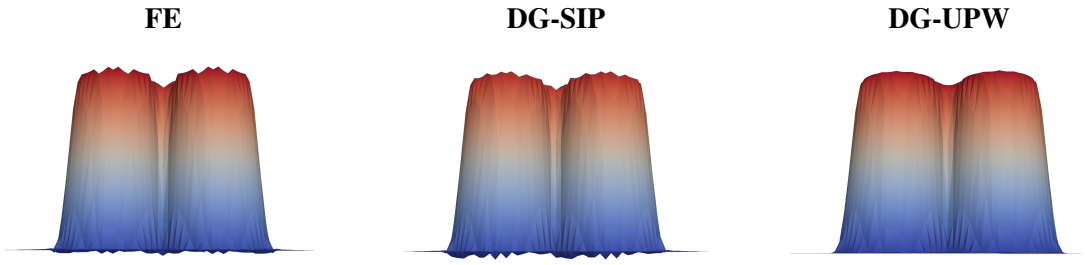

Figure 2.2 Aggregation of circular regions at $T = 0.001$ without convection, 3D view (height represents the value of the phase variable on each point of the squared domain)

Moreover, in the Figure 2.3 we can clearly observe how the maximum principle is preserved by DG-UPW scheme (and not by the two other ones). Regarding the energy, we obtain a non-increasing behavior as expected from the continuous model. An analytical proof of this property in the discrete case is left as future work.

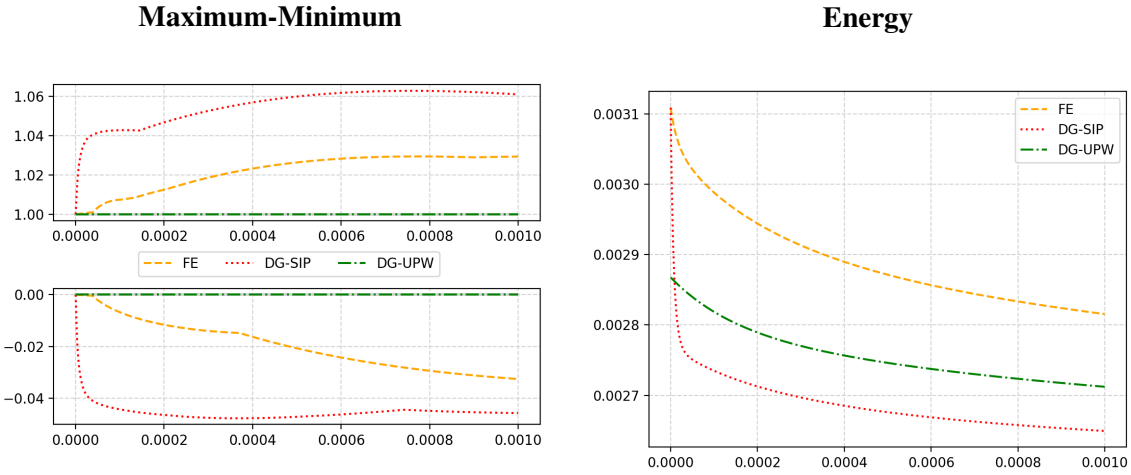

Figure 2.3 Aggregation of circular phases. On the left, maximum (top) and minimum (bottom) of the phase field variable over time without convection ($\boldsymbol{v} = 0$). On the right, energy over time

2.5.1.2 Agreggation of circular regions with convection

Second, we define Ω as the unit ball in $\mathbb{R}^2$ and, again, the initial condition (2.37) (two small circles of radius 0.2), with centers $(x_1, y_1) = (-0.2, 0)$ and $(x_2, y_2) = (0.2, 0)$, see Figure 2.1 (right). Moreover, for testing the effect of convection in our scheme, we take $\varepsilon = 0.001$ and $\boldsymbol{v} = 100(y, -x)$, so that $\boldsymbol{v} \cdot \boldsymbol{n} = 0$ on $\partial\Omega$. We take an unstructured mesh with $h \approx 4 \cdot 10^{-2}$ and run time iterations with $\Delta t = 10^{-3}$. Figure 2.4 shows the values of the phase field function at different time steps. We

can observe that, despite of our election of a highly significant convection term, the results of scheme DG-UPW are qualitatively correct. Nevertheless, we can observe how the spurious oscillations become more important and the solution begins to have an unexpected behavior when using both the FE and DG-SIP schemes.

Concerning the maximum principle, in Figure 2.5 we can see how this property is preserved by the DG-UPW scheme (2.30), while the phase field variable reaches nonphysical values, very far from $[0, 1]$, when using the other aforementioned schemes. Moreover, it is interesting to observe the approximation of the steady state of the schemes, represented by the quantity $\frac{\|u^{m+1}-u^m\|_{L^\infty(\Omega)}}{\|u^m\|_{L^\infty(\Omega)}}$, which tends to 0 in the case DG-UPW. This fact indicates that the solution converges to a stationary state, while for the other schemes it remains in an oscillatory state.

The computational time spent to obtain the results (computed sequentially) with each of these schemes is 2:32min using DG-UPW, 1:10min using FE and 3:24min using DG-SIP.

For the fairness of comparisons, we redo the tests using both FE and DG-SIP reducing the step size of the mesh, on the one hand, and using higher order polynomials, on the other hand. First, if we reduce the mesh size to $h/2 \approx 2 \cdot 10^{-2}$ and we use P_1 polynomials, the FE scheme does not converge (the linear solver, GMRES, fails to converge) while the DG-SIP scheme gives us the results shown in Figure 2.6 (left), requiring 35:20min to complete the computations sequentially. Second, if we keep the mesh size $h \approx 4 \cdot 10^{-2}$ and we use P_2 polynomials, the FE scheme does not converge either (Newton's method does not converge) while the DG-SIP scheme gives us the results shown in Figure 2.6 (right), requiring 11min to complete the computations sequentially. Therefore, the FE scheme does not even converge if we try to improve the results above and, while the DG-SIP scheme does converge, the results still show spurious oscillations and require a much longer computational time to be completed than those shown in Figure 2.4 (right) using our DG-UPW scheme.

2.5.1.3 Spinoidal decomposition driven by Stokes cavity flow

We show the results from a spinoidal decomposition test, in which the initial condition is a small uniformly distributed random perturbation around 0.5, $u_0(x) \in [0.49, 0.51]$ for $x \in \Omega$ as shown in Figure 2.7.

As convection vector $\boldsymbol{v}$, we take the flow resulting from solving a cavity test for the Stokes equations in the domain $\Omega = [0, 2] \times [0, 1]$ with Dirichlet boundary conditions given by a parabolic

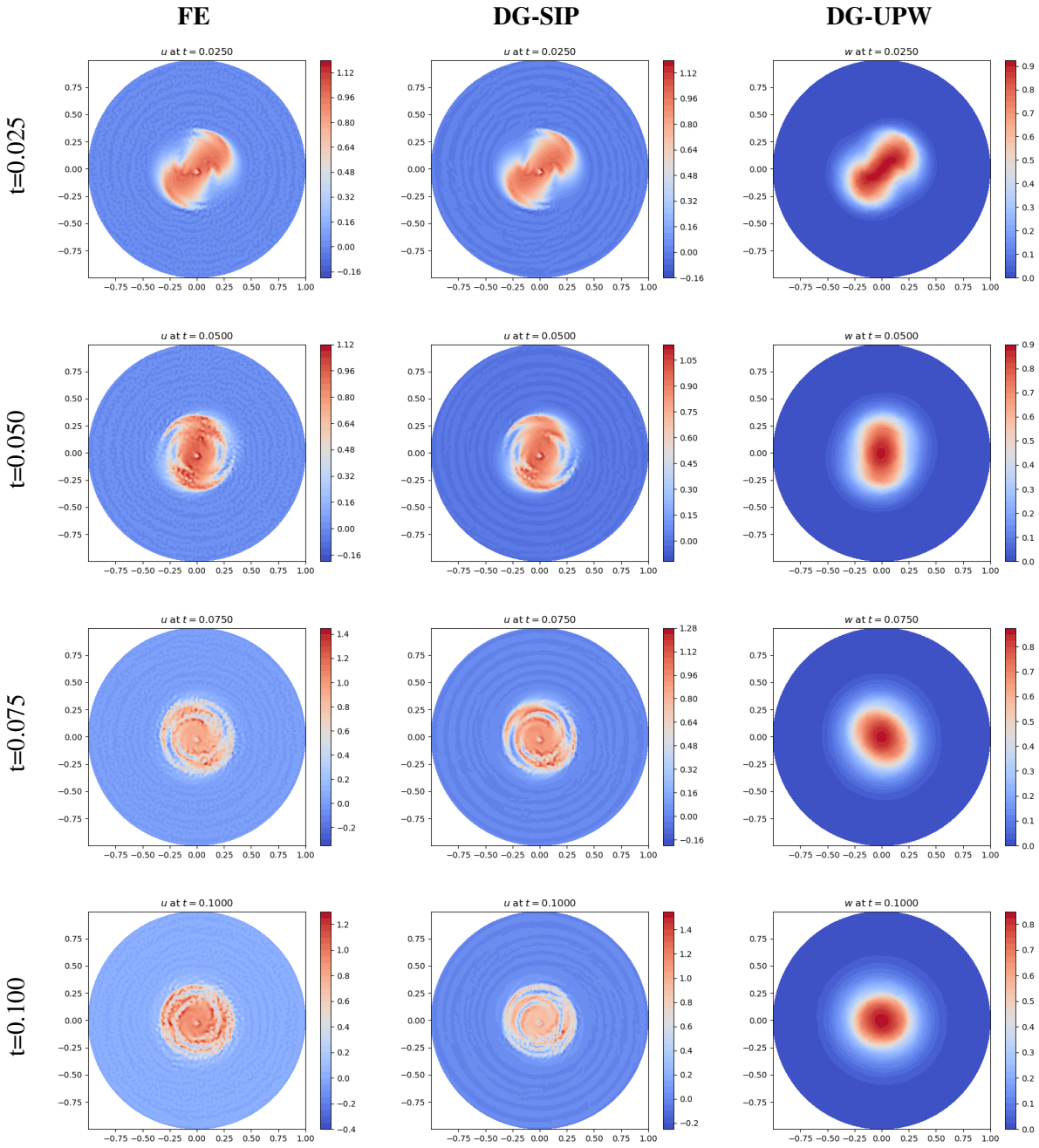

Figure 2.4 Aggregation of circular regions over time with a strong convection ($\boldsymbol{v} = 100(y, -x)$)

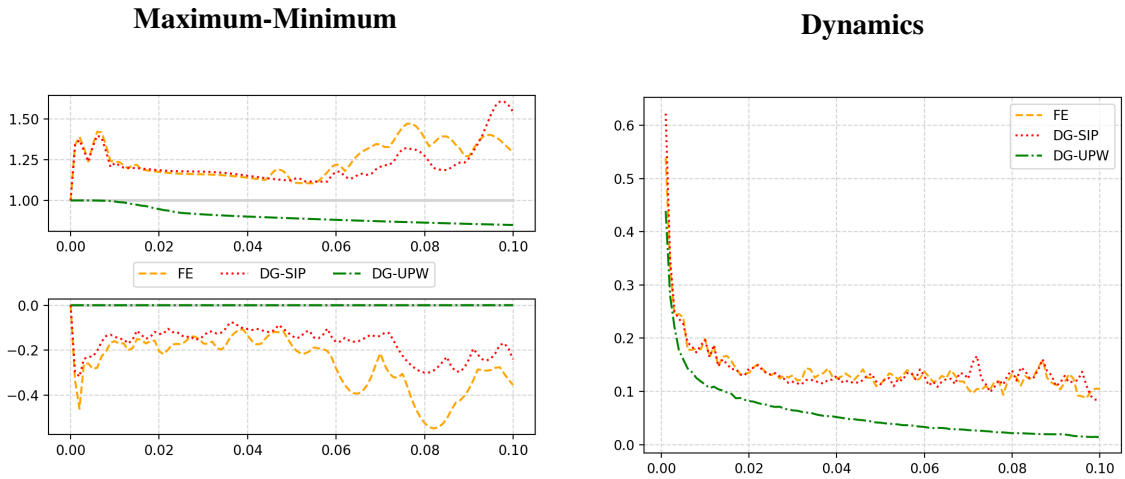

Figure 2.5 Aggregation of circular phases with strong convection ($\boldsymbol{v} = 100(y, -x)$). On the left, maximum and minimum of the phase field variable over time. On the right, we plot $\frac{\|u^{m+1}-u^m\|_{L^\infty(\Omega)}}{\|u^m\|_{L^\infty(\Omega)}}$ to observe the dynamics of the approximations

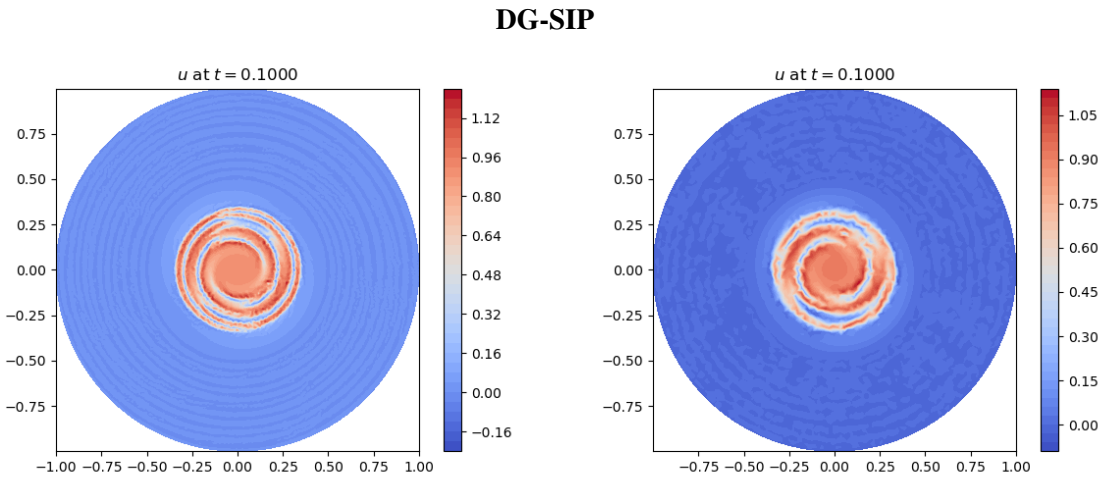

Figure 2.6 Aggregation of circular phases with strong convection ($\boldsymbol{v} = 100(y, -x)$) using the DG-SIP scheme. On the left, the result obtained with $h/2 \approx 2 \cdot 10^{-2}$ and $\mathbb{P}_1^{\text{disc}}(\mathcal{T}_h)$. On the right, the result obtained with $h \approx 4 \cdot 10^{-2}$ and $\mathbb{P}_2^{\text{disc}}(\mathcal{T}_h)$

Random perturbation

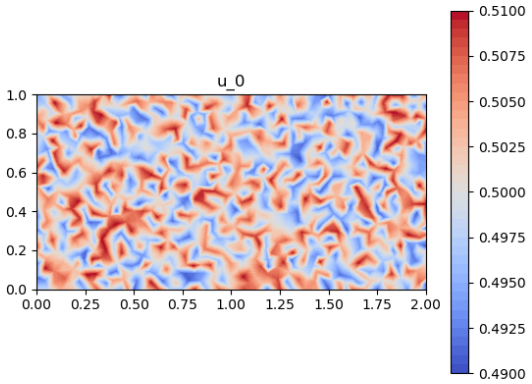

Figure 2.7 Random initial perturbation for the spinoidal decomposition test

profile

$$\boldsymbol{v}(x,y) = (x(2-x), 0), \quad \forall (x,y) \in \Gamma_{\text{top}} = \{(x,1) \in \mathbb{R}^2 \colon x \in [0,2]\}.$$

We used this parabolic profile in order to avoid the discontinuities of the Stokes velocity for a standard boundary condition $\boldsymbol{v} = 1$ on Γ_{top}, which produces a non vanishing divergence in the corners where the discontinuities arise. In fact we have checked that, in this particular case where $\boldsymbol{v} = 1$ on Γ_{top}, the scheme DG-UPW does not preserve the upper bound $u^m \leq 1$, although it does preserve the lower bound $0 \leq u^m$ (recall that, for compressible velocity, positivity is the only property of the solution, see Remark 2.3.2).

We set $\varepsilon = 0.005$, $\Delta t = 0.001$, $h \approx 0.07$ and, in this case, we take $\mathsf{Pe} = 10$ in order to emphasize the convection effect. We can observe in the Figures 2.8 and 2.9 how the maximum principle is preserved by our DG-UPW scheme (2.30) while for the other schemes the solution takes values out of the interval $[0, 1]$ (to notice that, we must take into account the scale of the values shown on the right-hand side of each picture).

Furthermore, in Figure 2.9 we can also notice that the approximation obtained using the DG-UPW scheme converges to a stationary state, while it remains in an nonphysical oscillatory state when we use the other schemes.

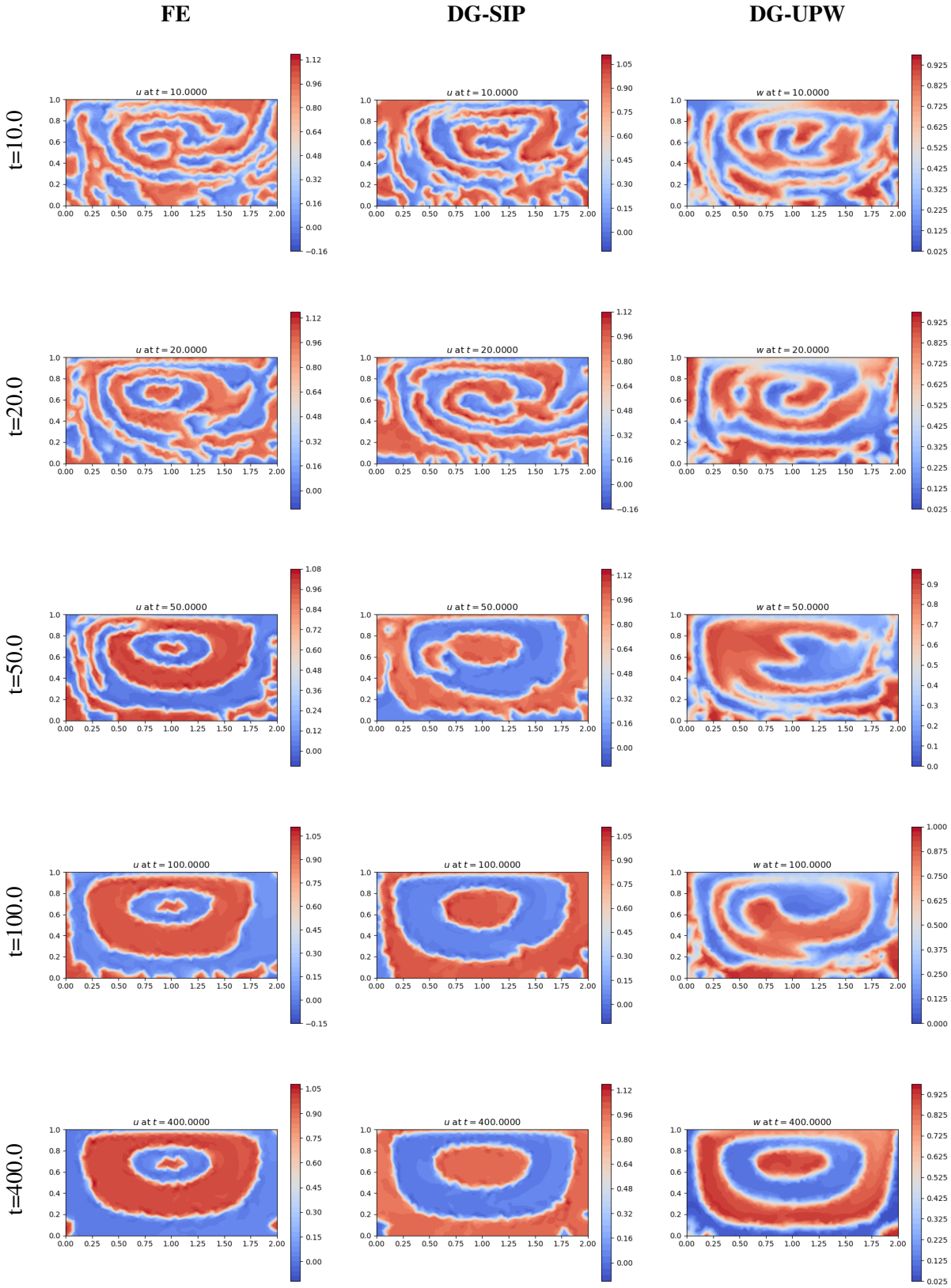

Figure 2.8 Spinoidal decomposition over time with convection vector obtained from a cavity test

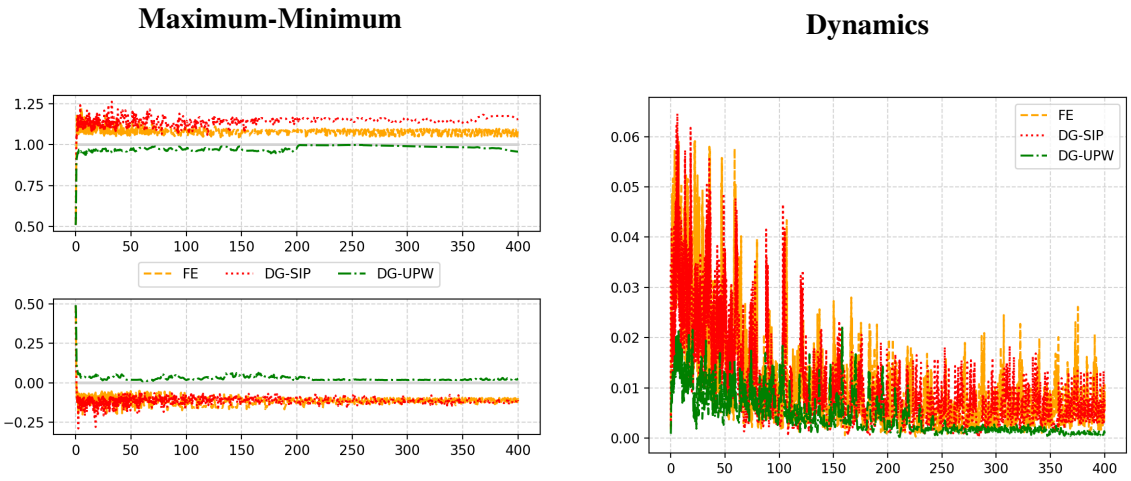

Figure 2.9 Spinoidal decomposition with convection vector obtained from a cavity test. On the left, maximum and minimum of the phase field variable over time. On the right, we plot $\frac{\|u^{m+1}-u^m\|_{L^\infty(\Omega)}}{\|u^m\|_{L^\infty(\Omega)}}$ to observe the dynamics of the approximations

2.5.2 Error order test

We now introduce the results of a numerical test in which we study the convergence order of our numerical scheme DG-UPW, verifying experimentally that the expected order is obtained. For the sake of completeness, we also compare the convergence orders of the two others aforementioned space semidiscretizations: FE, DG-SIP. We consider again the same initial conditions than in Section 2.5.1.1 with $\varepsilon = 0.01$, see Figure 2.1.

First, in the nonconvective case, errors and convergence order are compared with respect to an approximate solution which is computed using the FE scheme in a very fine mesh of size $h = 1.414 \cdot 10^{-3}$ and a time step $\Delta t = 10^{-6}$ (which is taken as the "exact solution"). In this case we have used conforming structured meshes for the space discretization. The results for the DG-UPW scheme, which are shown in the first row of Table 2.1, confirm order 1 (in fact, slightly over 1) in norm $\|\cdot\|_{L^2(\Omega)}$. These results match our expectations for the P_0 approximation of u^{m+1}, with the upwind discretization of the nonlinear second-order term. It is interesting to emphasize that, unexpectedly, the scheme produces kind results in $\|\cdot\|_{H^1(\Omega)}$, reaching order 1. On the other hand, the FE and DG-SIP schemes reach order 2 in L^2 and order 1 in H^1 norms, as expected (see also Table 2.1).

Next, we focus on the case with convection, where we take $\boldsymbol{v} = (y, -x)$ in the unit ball. The resulting errors and convergence orders computed using the three different schemes over a conforming

Table 2.1 Errors and convergence orders in $T = 0.001$ without convection ($\boldsymbol{v} = 0$)

Scheme	Norm	$h \approx 2.83 \cdot 10^{-2}$	$h/2 \approx 1.41 \cdot 10^{-2}$		$h/3 \approx 9.43 \cdot 10^{-3}$		$h/4 \approx 7.07 \cdot 10^{-3}$	
		Error	Error	Order	Error	Order	Error	Order
DG-UPW	$\|\cdot\|_{L^2}$	$8.53 \cdot 10^{-3}$	$3.09 \cdot 10^{-3}$	1.46	$1.76 \cdot 10^{-3}$	1.38	$1.21 \cdot 10^{-3}$	1.30
	$\|\cdot\|_{H^1}$	$8.00 \cdot 10^{-1}$	$4.02 \cdot 10^{-1}$	0.99	$2.61 \cdot 10^{-1}$	1.07	$1.88 \cdot 10^{-1}$	1.13
FE	$\|\cdot\|_{L^2}$	$5.32 \cdot 10^{-3}$	$1.57 \cdot 10^{-3}$	1.76	$6.99 \cdot 10^{-4}$	1.99	$4.02 \cdot 10^{-4}$	1.93
	$\|\cdot\|_{H^1}$	$9.00 \cdot 10^{-1}$	$4.10 \cdot 10^{-1}$	1.13	$2.53 \cdot 10^{-1}$	1.2	$1.78 \cdot 10^{-1}$	1.22
DG-SIP	$\|\cdot\|_{L^2}$	$4.65 \cdot 10^{-3}$	$1.30 \cdot 10^{-3}$	1.84	$5.89 \cdot 10^{-4}$	1.96	$3.27 \cdot 10^{-4}$	2.05
	$\|\cdot\|_{H^1}$	1.18	$5.83 \cdot 10^{-1}$	1.01	$3.63 \cdot 10^{-1}$	1.17	$2.60 \cdot 10^{-1}$	1.15

unstructured mesh are shown in Table 2.2. In this case, the errors are computed with respect to the solution obtained for the FE scheme in a mesh of size $h = 4 \cdot 10^{-3}$.

In this case, it is interesting to notice that the error order in $\|\cdot\|_{L^2(\Omega)}$ of the DG-UPW scheme is improved and it approaches the order 2 of the other schemes, while order in $\|\cdot\|_{H^1(\Omega)}$ slightly beats the other schemes.

As a technical comment, notice that, in order to compute the errors, we projected on a $\mathbb{P}_1^{\text{cont}}$ space both the exact and the DG solution obtained when using the DG-SIP. In the case of the DG-UPW scheme we have taken w as the continuous solution.

Table 2.2 Errors and convergence orders in $T = 0.001$ with convection ($\boldsymbol{v} = (y, -x)$)

Scheme	Norm	$h \approx 4 \cdot 10^{-2}$	$h/2 \approx 2 \cdot 10^{-2}$		$h/3 \approx 1.33 \cdot 10^{-2}$		$h/4 \approx 1 \cdot 10^{-2}$	
		Error	Error	Order	Error	Order	Error	Order
DG-UPW	$\|\cdot\|_{L^2}$	$1.73 \cdot 10^{-2}$	$6.94 \cdot 10^{-3}$	1.32	$3.31 \cdot 10^{-3}$	1.83	$2.06 \cdot 10^{-3}$	1.65
	$\|\cdot\|_{H^1}$	1.45	$6.03 \cdot 10^{-1}$	1.27	$3.02 \cdot 10^{-1}$	1.71	$2.03 \cdot 10^{-1}$	1.38
FE	$\|\cdot\|_{L^2}$	$6.83 \cdot 10^{-3}$	$2.12 \cdot 10^{-3}$	1.69	$9.77 \cdot 10^{-4}$	1.91	$5.39 \cdot 10^{-4}$	2.07
	$\|\cdot\|_{H^1}$	$8.31 \cdot 10^{-1}$	$3.81 \cdot 10^{-1}$	1.13	$2.19 \cdot 10^{-1}$	1.36	$1.50 \cdot 10^{-1}$	1.32
DG-SIP	$\|\cdot\|_{L^2}$	$6.52 \cdot 10^{-3}$	$1.96 \cdot 10^{-3}$	1.74	$8.95 \cdot 10^{-4}$	1.93	$5.03 \cdot 10^{-4}$	2.00
	$\|\cdot\|_{H^1}$	1.20	$6.16 \cdot 10^{-1}$	0.96	$3.85 \cdot 10^{-1}$	1.16	$2.74 \cdot 10^{-1}$	1.17

CHAPTER 3

AN UNCONDITIONALLY ENERGY STABLE AND POSITIVE UPWIND DG SCHEME FOR THE KELLER–SEGEL MODEL

3.1 Abstract

The well-suited discretization of the Keller-Segel equations for chemotaxis has become a very challenging problem due to the convective nature inherent to them. This chapter aims to introduce a new upwind, mass-conservative, positive and energy-dissipative discontinuous Galerkin scheme for the Keller-Segel model. This approach is based on the gradient-flow structure of the equations. In addition, we show some numerical experiments in accordance with the aforementioned properties of the discretization. The numerical results obtained emphasize the really good behavior of the approximation in the case of chemotactic collapse, where very steep gradients appear. The results of this chapter have been already published in [3].

3.2 Introduction

Since the introduction in the 70's of the biological Keller–Segel model for chemotaxis phenomena [125, 126], it and many related variants have attracted a great deal of interest in the mathematical community. Chemotaxis, a biological process through which organisms (e.g. cells) migrate in response to a chemical stimulus, is modelled by means of nonlinear systems of partial differential equations (PDE). The classical one can be written as follows: find two real valued functions, $u = u(\mathbf{x}, t)$ and $v = v(\mathbf{x}, t)$, defined in $\Omega \times [0, T]$ such that:

$$\partial_t u = k_0 \Delta u - k_1 \nabla \cdot (u \nabla v), \qquad \text{in } \Omega \times (0, T), \tag{3.1a}$$

$$\tau \partial_t v = k_2 \Delta v - k_3 v + k_4 u, \qquad \text{in } \Omega \times (0, T), \tag{3.1b}$$

$$\partial_{\mathbf{n}} u := \nabla u \cdot \mathbf{n} = 0, \quad \partial_{\mathbf{n}} v = 0, \qquad \text{on } \partial\Omega \times (0, T), \tag{3.1c}$$

$$u(0) = u_0, \quad v(0) = v_0 \text{ if } \tau > 0, \qquad \text{in } \Omega. \tag{3.1d}$$

Herein the parameters are $k_i > 0$ for $i \in \{0, 1, 2, 3, 4\}$. The mathematical formulation of (3.1) can be interpreted in biological terms as follows: u denotes a certain cell distribution (or population of organisms, in general) at the position $\mathbf{x} \in \Omega$ and time $t \in [0, T]$, whereas v stands for the concentration of chemoattractant (i.e. a chemical signal towards which cells are induced to migrate). Both cells and chemoattractant experiment some diffusion in the spatial domain.

This auto-diffusion phenomena (experimented by cells and chemoattractant) are designed by the terms $-k_0\Delta u$ and $-k_2\Delta v$, while the migration mechanism is modeled by the nonlinear cross-diffusion term $-k_1\nabla \cdot (u\nabla v)$. This term is the major difficulty for theoretical analysis and also for numerical modelling of system 3.1. Further, the degradation and production of chemoattractant are associated with the terms $-k_3 v$ and $k_4 u$, respectively. Note that the production of chemoattractant by the cells, to which cells are attracted, may eventually result in a chemotactic collapse, a phenomenon in which uncontrolled aggregation for u give rise to blowing up or exploding in finite time. This feature is well known and constitutes one of the outstanding characteristics of classical Keller-Segel model, and also one of its main challenges, specifically for numerical methods. Finally, the coefficient $\tau \in \{0, 1\}$ is considered to write at the same time the parabolic system when $\tau = 1$, or the parabolic-elliptic for $\tau = 0$.

Regarding the mathematical analysis for the system (3.1): some results on sufficient conditions to ensure global existence and boundedness of solutions along time can be shown (see e.g. the review of Bellomo et al [28] and the references therein). They are based on mass conservation for u and on an energy dissipation law for this model (see Section 3.3). For dimension $d \geq 2$, these results require the initial density of cells, $\int_\Omega u_0$, to be bigger than certain threshold. On the other hand, considerable research has been done in the direction of finding cases where chemotactic collapse arise. Among them, it is worth mentioning the first result in this direction, due to Herrero and Velázquez [114], where radially symmetric two-dimensional solutions which finite-time blow up are found. Other authors shed light on more general cases, for instance Horstmann and Wang [116] (non symmetric blow-up solutions) or Winkler [186] (higher dimensional case).

In the last decades, a lot of papers have been published dealing with these kinds of theoretical issues both for the classical model (3.1) and for other models based on some extensions or generalizations. In general, they start from the Keller–Segel classical equations and modify them with the purpose of avoiding the non-physical blow up of solutions, producing solutions which are closer to the "real chemotaxis" phenomena observed in biology. Models include logistic, non-linear diffusion or production

terms, chemo-repulsion effects or coupling with fluid equations [39, 83, 177, 178, 188]. See e.g. [21, 28] for more examples. Thus, it is hoped that understanding the classical Keller–Segel equations may open new insights for dealing in depth with those other chemotaxis models.

On the other hand, taking into account the considerable efforts of the mathematical community in the theoretical analysis of Keller-Segel models, the number of papers dedicated to numerical analysis and simulation of chemotaxis equations is much lower, in relative terms. The main difficulty is the numerical approximation of the cross-diffusion term. Not only for its non-linearity, but due to its convective nature, which makes particularly difficult to deal with using the finite element (FE) method (see, for instance, [34, 74] for more details about this method). This difficulty is specifically significant in steep-gradient regions for v, which are precisely relevant in blow-up settings. Furthermore, preserving the physical properties of the continuous model (mass conservation, positivity and energy dissipation) in the discrete case adds an extra level of complication when it comes to designing a well-suited approximation.

Despite that, many interesting works have been published on numerical simulation of chemotaxis equations using different kinds of approaches. For instance, the work by Saito [165] uses FE with upwind stabilization for the parabolic-elliptic Keller–Segel model ($\tau = 0$ in (3.1)) showing mass conservation, positivity and error estimates. Also, Gutiérrez-Santacreu and Rodríguez-Galván demonstrate positivity, an energy law and a priori bounds for their FE scheme on acute meshes in [111]. Recently, Guillén-González and Tierra have presented an energy-stable and approximately positive FE scheme for a chemoattraction and consumption variant of (3.1) in [104]. In addition, other sophisticated techniques have been applied to this problem. This is the case of the finite volume (FV) method (we recommend [132] on this topic) which has become a very popular and successful approach as we can observe in papers like [45] by Chertock and Kurganov in which the authors devised positive preserving methods for the parabolic-parabolic formulation ($\tau = 1$ in (3.1)), with demonstrated high accuracy and robustness, specifically on chemotactic collapse. It might also be pointed out the works of Saad and others, for instance in [120], where a volume finite element scheme for the capture of spatial patterns for a volume-filling chemotaxis is analyzed.

In this sense, it is also worth mentioning the very recent works [23, 41, 117, 168] that show and analyze different techniques to approximate the solution of (3.1) while achieving mass conservation, positivity and energy-dissipation for a strictly positive initial cell condition. In the paper by Badía et al. [23] a discrete scheme using stabilized FE with a graph-Laplacian operator and a shock detector is

proposed. This discretization satisfies, in general, both the mass conservation and positivity properties, and, in the case of acute meshes, it is also energy-dissipative. Otherwise, Huang and Shen develop in [117] a time-discrete approximation, admitting any spatial discretization, that preserves the positivity for the cell distribution u and is energy stable for a modified energy. This latest approach uses a suitable transformation of the solution for the positivity and the scalar auxiliary variable (SAV) technique for the energy stability. Alternatively, Shen and Xu introduced in [168] another general, positive (for the cell distribution u) and energy-dissipative, time-discrete scheme based on the gradient flow structure of the continuous model that admits different kinds of spatial discretization such as FE, spectral methods or even finite-differences. The order of the latest approach and the blow-up phenomenon of the discrete solution, under a CFL condition, is studied in [41] by Chen et al.

Furthermore, discontinuous Galerkin (DG) methods (we refer the reader to [63, 66, 163] for a further insight) aroused the interest of researchers in recent years due to their flexibility for approximating, using standard meshes and computer libraries, different types of PDEs: elliptic, parabolic, hyperbolic. In the chemotaxis context, it is worth mentioning the paper of Y. Epshteyn and A. Kurganov [73], where the FV scheme given in [45] for the 2D Keller-Segel model (3.1) is extended to a DG scheme on cartesian meshes, obtaining good approximations even on blow-up regimes. Y. Epshteyn introduced two other related schemes in [72]. In all cases, different discontinuous Interior Penalty (IP) methods and upwinding techniques were considered for defining DG approximations. The schemes are even applied to the simulation of an haptotaxis model of tumor invasion into healthy tissue. Error estimates are shown but no energy property or maximum principle for the schemes is proven. In fact, spurious oscillations and negative values in the solution are reported.

More recent works make further progress in this direction, for instance in [195], where the classical equations (3.1) are approximated by a positivity-preserving DG method with strong stability preserving (SSP) high order time discretizations. Error order estimates as well as positivity are shown in this work. Finally, in [108, 136], the local discontinuous Galerkin method is applied, showing respectively positivity and energy dissipation.

In this work, we propose a new upwind DG scheme for the Keller-Segel model (3.1) that preserves the mass-conservation, positivity and energy stability properties of the continuous problem. As in [168], the proposed discretization takes advantage of the gradient flow structure of the model. First, in Section 3.3 we discuss the physical properties of the continuous model. Section 3.4 is the main part

of the chapter, in which we introduce the upwind DG scheme (3.8). In particular, in Section 3.4.1, we define the upwind approximation based on the ideas introduced in Chapter 2 along with some geometrical considerations for the mesh family $\mathcal{T}_h$, and we discuss the properties of the scheme in Section 3.4.2. Finally, in Section 3.5, we show several numerical tests in which we reproduce some blow-up results shown in the literature with one steady peak, [45], and a peak moving towards the corner of the domain, [165], as well as pattern formation results with several peaks, [18, 38, 78, 181]. These numerical experiments endorse the good behavior of the approximation obtained with the new scheme, which allows us to capture peaks reaching values up to the order of 10^7. These kinds of numerical results are rare in the literature due to the steep-gradients inherent to such sort of tests.

The results of this chapter have been already published in [3].

3.3 Keller-Segel model

Let us consider the Keller-Segel system (3.1).

Remark 3.3.1. *There is a classical solution of the Keller-Segel problem* (3.1) *at least local in time which is positive, i.e.,* $u, v \geq 0$ *in* $\Omega \times (0,T)$ *whenever* $u_0 \geq 0$ *and* $v_0 \geq 0$ *in* Ω*. See, for instance, [28, 64].*

To our best knowledge, the existence of global solutions in time is still not clear in the literature.

Assume $u_0, v_0 \geq 0$ in Ω. The weak formulation of the problem (3.1) consists of finding $(u,v) : [0,T] \times \Omega \to \mathbb{R}_+ \times \mathbb{R}_+$ regular enough, i.e. $u(t), v(t) \in V$ for a certain regular Sobolev space V (for instance, $V = W^{1,\infty}(\Omega)$), with $\partial_t u(t), \tau \partial_t v(t) \in V'$ a.e. $t \in (0,T)$, satisfying the following variational problem a.e. $t \in (0,T)$:

$$\langle \partial_t u(t), \overline{u} \rangle = -k_0 \left(\nabla u(t), \nabla \overline{u} \right) + k_1 \left(u(t) \nabla v(t), \nabla \overline{u} \right), \qquad \forall \overline{u} \in V, \tag{3.2a}$$

$$\langle \tau \partial_t v(t), \overline{v} \rangle = -k_2 \left(\nabla v(t), \nabla \overline{v} \right) - k_3 \left(v(t), \overline{v} \right) + k_4 \left(u(t), \overline{v} \right), \qquad \forall \overline{v} \in V, \tag{3.2b}$$

and the initial conditions $u(0) = u_0$, $v(0) = v_0$ in Ω. Hereafter, $\langle \cdot, \cdot \rangle$ denotes the duality product in V'.

By taking, formally, the chemical potential of u,

$$\mu = k_0 \log(u) - k_1 v, \tag{3.3}$$

we can rewrite (3.2) as a gradient flow system where the flux direction is given by $-\nabla\mu$ containing the effect of both the diffusion and the chemotaxis terms (see, for instance, [30]). This variational formulation consists of finding $(u, \mu, v) : [0, T] \times \Omega \to \mathbb{R}_+ \times \mathbb{R} \times \mathbb{R}_+$ regular enough, i.e. $u(t), \mu(t), v(t) \in V$ for a certain regular Sobolev space V (for instance, $V = W^{1,\infty}(\Omega)$), with $\partial_t u(t), \tau\partial_t v(t) \in V'$ a.e. $t \in (0, T)$, satisfying the following variational problem a.e. $t \in (0, T)$:

$$\langle \partial_t u(t), \overline{u} \rangle = -\left(u(t)\nabla\mu(t), \nabla\overline{u}\right), \qquad \forall \overline{u} \in V, \tag{3.4a}$$

$$\left(\mu(t), \overline{\mu}\right) = \left(k_0 \log(u(t)) - k_1 v(t), \overline{\mu}\right), \qquad \forall \overline{\mu} \in V, \tag{3.4b}$$

$$\langle \tau\partial_t v(t), \overline{v} \rangle = -k_2\left(\nabla v(t), \nabla\overline{v}\right) - k_3\left(v(t), \overline{v}\right) + k_4\left(u(t), \overline{v}\right), \qquad \forall \overline{v} \in V, \tag{3.4c}$$

and the initial conditions $u(0) = u_0$, $v(0) = v_0$ in Ω.

Remark 3.3.2. *By taking $\overline{u} = 1$ in* (3.2a) *(or* (3.4a)*), any solution u conserves the mass, because*

$$\frac{d}{dt}\int_\Omega u(x, t)dx = 0.$$

Remark 3.3.3. *By taking (formally) $\overline{u} = \mu(t)$, $\overline{\mu} = \partial_t u(t)$ and $\overline{v} = (k_1/k_4)\partial_t v(t)$ in* (3.4)*, and adding the resulting expressions, one has that any solution (u, v) satisfies the following energy law*

$$\frac{d}{dt}E(u(t), v(t)) + \tau\frac{k_1}{k_4}\int_\Omega |\partial_t v(t)|^2 dx + \int_\Omega u(t)\left|\nabla(\mu(t))\right|^2 dx = 0, \tag{3.5}$$

where $E\colon H^1(\Omega)_+ \times H^1(\Omega) \longrightarrow \mathbb{R}$ is the energy functional, defined as follows

$$E(u, v) \coloneqq \int_\Omega \left(k_0 u\log(u) - k_1 uv + \frac{k_1 k_2}{2k_4}|\nabla v|^2 + \frac{k_1 k_3}{2k_4}v^2\right), \tag{3.6}$$

and $H^1(\Omega)_+ = \{u \in H^1(\Omega)\colon u \geq 0\}$.

3.4 Fully discrete scheme

First, we regularize the chemical potential of u, defined in (3.3), by

$$\mu_\varepsilon = k_0 \log(u + \varepsilon) - k_1 v, \tag{3.7}$$

for some $\varepsilon > 0$. Note that ε is a regularization parameter since $\log(u+\varepsilon)$ is regular for all $u \geq 0$. We will take $\varepsilon = \varepsilon(h, \Delta t)$ such that $\varepsilon(h, \Delta t) \to 0$ if $(h, \Delta t) \to 0$, being $h > 0$ the mesh size and $\Delta t > 0$ the time step.

Then, we propose the following decoupled fully discrete first order in time and upwind DG in space scheme for the model (3.1):

Let $v^m \in \mathbb{P}_1^{\text{cont}}(\mathcal{T}_h)$ and $u^m \in \mathbb{P}_0^{\text{disc}}(\mathcal{T}_h)$ such that $v^m \geq 0$ in the case $\tau > 0$ and $u^m \geq 0$ be given.

Step 1: Find $v^{m+1} \in \mathbb{P}_1^{\text{cont}}(\mathcal{T}_h)$ solving

$$\tau \left(\delta_t v^{m+1}, \overline{v}\right)_h + k_2 \left(\nabla v^{m+1}, \nabla \overline{v}\right) + k_3 \left(v^{m+1}, \overline{v}\right)_h - k_4 \left(u^m, \overline{v}\right) = 0, \tag{3.8a}$$

for all $\overline{v} \in \mathbb{P}_1^{\text{cont}}(\mathcal{T}_h)$.

Step 2: Find $(u^{m+1}, \mu^{m+1}) \in \mathbb{P}_0^{\text{disc}}(\mathcal{T}_h) \times \mathbb{P}_0^{\text{disc}}(\mathcal{T}_h)$ with $u^{m+1} \geq 0$ solving the coupled problem

$$\left(\delta_t u^{m+1}, \overline{u}\right) + a_h^{\text{upw}}(\mu^{m+1}; u^{m+1}, \overline{u}) = 0, \tag{3.8b}$$

$$\left(\mu^{m+1}, \overline{\mu}\right) - k_0 \left(\log(u^{m+1} + \varepsilon), \overline{\mu}\right) + k_1 \left(v^{m+1}, \overline{\mu}\right) = 0, \tag{3.8c}$$

for all $\overline{u}, \overline{\mu} \in \mathbb{P}_0^{\text{disc}}(\mathcal{T}_h)$, where $a_h^{\text{upw}}(\cdot;\cdot,\cdot)$ will be defined below in Section 3.4.1.

Notice that 3.8a is a linear problem for v^{m+1} and that (3.8b)–(3.8c) is a coupled nonlinear problem for (u^{m+1}, μ^{m+1}). In fact, we are going to use Newton's method as iterative procedure approximating the scheme (3.8b)–(3.8c).

In order to preserve the positivity of v^{m+1}, we have done mass lumping in the terms $\left(\partial_t v^{m+1}, \overline{v}\right)_h$ and $k_3 \left(v^{m+1}, \overline{v}\right)_h$ in (3.8a).

In Section 3.4.2, we will provide a way of computing the solution of (3.8) enforcing the nonnegativity restriction $u^{m+1} \geq 0$.

3.4.1 Definition of upwind bilinear form $a_h^{upw}(\cdot;\cdot,\cdot)$

Now, we are going to define the upwind bilinear form $a_h^{\text{upw}}(\cdot;\cdot,\cdot)$, introduced in the scheme (3.8).

In order to achieve the energy stability with the scheme (3.8), we must consider the following hypothesis that will let us approximate the flux $-\nabla\mu$ accordingly:

Hypothesis 3.4.1. The mesh $\mathcal{T}_h$ of $\overline{\Omega}$ is structured in the sense that the line between the barycenters of the triangles K and L is orthogonal to the interface $e = K \cap L \in \mathcal{E}_h^i$.

Then, we define the following upwind bilinear form to be applied to the flux $-\nabla\mu$ which may be discontinuous over $\mathcal{E}_h^i$:

$$a_h^{\text{upw}}(\mu; u, \overline{u}) \coloneqq \int_\Omega (\nabla\mu \cdot \nabla\overline{u})u + \sum_{e\in\mathcal{E}_h^i, e=K\cap L} \int_e \left(\left(-\nabla^0_{\boldsymbol{n}_e}\mu\right)_\oplus u_K - \left(-\nabla^0_{\boldsymbol{n}_e}\mu\right)_\ominus u_L \right) [\![\overline{u}]\!], \tag{3.9}$$

where, for every $e \in \mathcal{E}_h^i$ with $e = K \cap L$,

$$\nabla^0_{\boldsymbol{n}_e}\mu = \frac{-[\![\Pi_0\mu]\!]}{\mathcal{D}_e(\mathcal{T}_h)} = \frac{\Pi_0\mu_L - \Pi_0\mu_K}{\mathcal{D}_e(\mathcal{T}_h)}, \tag{3.10}$$

with Π_0 being the projection on $\mathbb{P}_0^{\text{disc}}(\mathcal{T}_h)$ and $\mathcal{D}_e(\mathcal{T}_h)$ the distance between the barycenters of the triangles K and L of the mesh $\mathcal{T}_h$ that share $e \in \mathcal{E}_h^{\text{i}}$, denoted by C_K and C_L, respectively. This way, we can rewrite (3.9) as

$$a_h^{\text{upw}}(\mu; u, \overline{u}) \coloneqq \int_\Omega (\nabla\mu \cdot \nabla\overline{u})u + \sum_{e\in\mathcal{E}_h^i, e=K\cap L} \frac{1}{\mathcal{D}_e(\mathcal{T}_h)} \int_e \left(([\![\Pi_0\mu]\!])_\oplus u_K - ([\![\Pi_0\mu]\!])_\ominus u_L \right) [\![\overline{u}]\!]. \tag{3.11}$$

Remark 3.4.2. *Since the quadrature formula of the barycenter (or centroid) is exact for polynomials of order* 1*, if* $\mu \in \mathbb{P}_1^{disc}(\mathcal{T}_h)$*, we have that*

$$\Pi_0\mu|_K = \fint_K \mu = \frac{1}{|K|}\int_K \mu = \mu(C_K),$$

where C_K *is the barycenter of* $K \in \mathcal{T}_h$*.*

Hence, if $\mu \in \mathbb{P}_1^{disc}(\mathcal{T}_h)$*, the expression* (3.10) *is the slope of the line between the points* $(C_K, \mu(C_K))$ *and* $(C_L, \mu(C_L))$*, which, under the Hypothesis 3.4.1, this line is parallel to the vector* $\boldsymbol{n}_e$*, with* $e = K \cap L \in \mathcal{E}_h^i$*. This expression is considered as an approximation of the discontinuous numerical normal flux* $\nabla\mu \cdot \boldsymbol{n}_e$ *for* $\mu \in \mathbb{P}_1^{disc}(\mathcal{T}_h)$*.*

In addition, observe that, since the barycenters are located $1/3$ *of the median from the side and* $2/3$ *of the median from the vertex of the triangle, the expression* (3.10) *does not degenerate when* $h \to 0$*,*

i.e., $\mathcal{D}_e(\mathcal{T}_h) > 0$ *for every* $e \in \mathcal{E}_h^i$ *and* $h > 0$*. A visual representation of the regular polygonal structure given by the lines between the adjacent barycenters is given in Figure 3.1.*

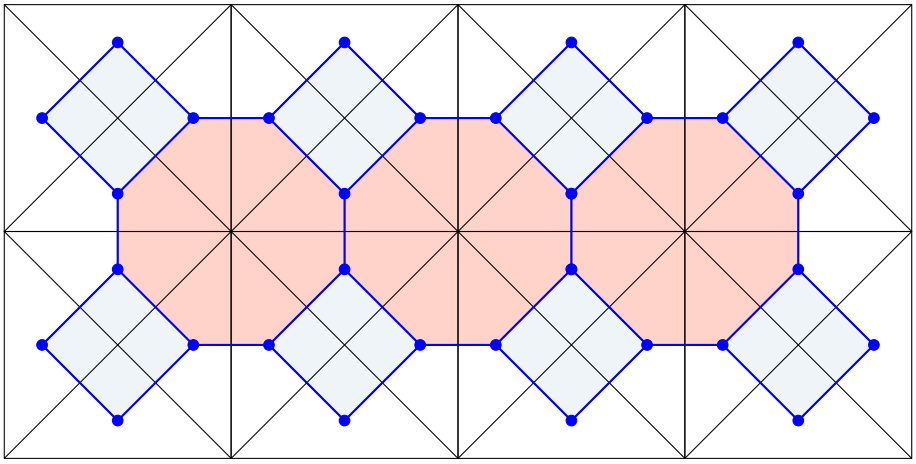

Figure 3.1 Polygonal structure between adjacent barycenters

Furthermore, in order to preserve the positivity of the variable v in our fully discrete scheme, we assume the following hypothesis.

Hypothesis 3.4.3. The mesh $\mathcal{T}_h$ is acute, i.e., the angles of the triangles of $\mathcal{T}_h$ are less than or equal to $\pi/2$.

We give some examples, the meshes represented in Figure 3.2, which satisfy both Hypotheses 3.4.1 and 3.4.3.

Theorem 3.4.4. *Given the meshes represented in Figure 3.2 we can define* $\mathcal{D}_e(T_h)$ *for these meshes as follows*

$$a)\ \underline{\text{Mesh 1}}\text{: } \mathcal{D}_e(\mathcal{T}_h) = \frac{2l^2}{3|e|}, \quad b)\ \underline{\text{Mesh 2}}\text{: } \mathcal{D}_e(\mathcal{T}_h) = \frac{l^2}{3|e|},$$

where l *is the length of the side of the highlighted squares of the mesh.*

Proof. We will only prove the case a) Mesh 1 since the case b) Mesh 2 is analogous.

Observe Mesh 1 in Figure 3.2. The barycenter of the triangles $\triangle OAB$, $\triangle OBC$ and $\triangle OCD$ are, respectively $\frac{O+A+B}{3}$, $\frac{O+B+C}{3}$ and $\frac{O+C+D}{3}$. Hence, if we denote by e_1 the edge between $\triangle OAB$ and $\triangle OBC$ and by e_2 the edge between $\triangle OBC$ and $\triangle OCD$, then

$$\mathcal{D}_{e_1}(\mathcal{T}_h) = \frac{|C-A|}{3} = \frac{2l}{3}, \quad \mathcal{D}_{e_2}(\mathcal{T}_h) = \frac{|D-B|}{3} = \frac{\sqrt{2}l}{3}$$

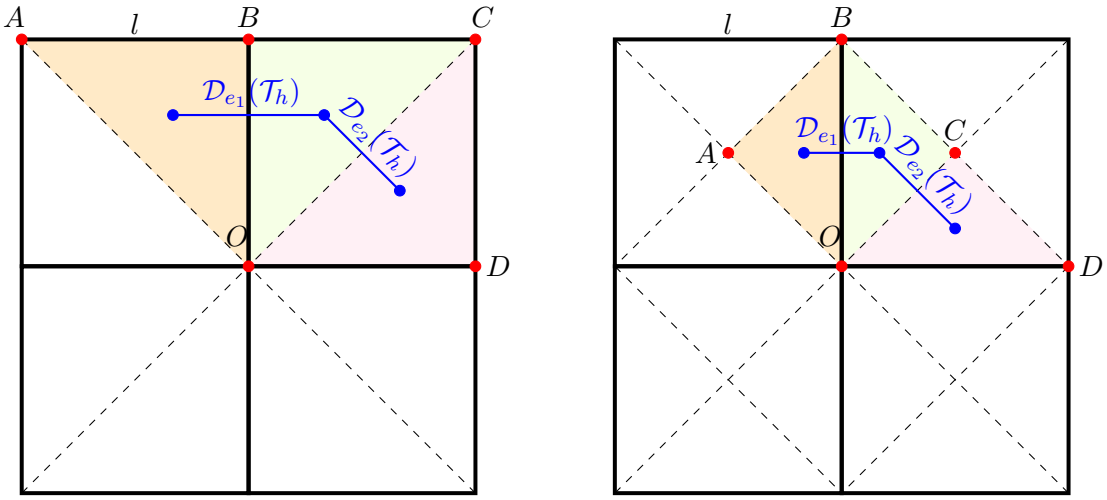

(a) Mesh 1 (b) Mesh 2

Figure 3.2 Representation of $\mathcal{D}_e(\mathcal{T}_h)$

Now, since $l/|e_1| = 1$ and $l/|e_2| = 1/\sqrt{2}$, we can define $\mathcal{D}_e(\mathcal{T}_h)$ for any $e \in \mathcal{E}_h^{\mathrm{i}}$ as

$$\mathcal{D}_e(\mathcal{T}_h) = \frac{2l}{3} \cdot \frac{l}{|e|} = \frac{2l^2}{3|e|}.$$

□

3.4.2 Properties of the scheme

Finally, we discuss the different properties of the scheme (3.8) with the upwind bilinear form defined in (3.9) on meshes under the Hypotheses 3.4.1 and 3.4.3.

With the purpose of proving the existence of solution of the scheme (3.8) and providing a way of computing it enforcing the restriction $u^{m+1} \geq 0$, we define the following auxiliary scheme where a cut-off operator is introduced in (3.8b):

Step 1: Given $v^m \in \mathbb{P}_1^{\mathrm{pcont}}(\mathcal{T}_h)$ such that $v^m \geq 0$ in the case $\tau > 0$, find $v^{m+1} \in \mathbb{P}_1^{\mathrm{pcont}}(\mathcal{T}_h)$ solving

$$\tau \left(\delta_t v^{m+1}, \overline{v}\right)_h + k_2 \left(\nabla v^{m+1}, \nabla \overline{v}\right) + k_3 \left(v^{m+1}, \overline{v}\right)_h - k_4 \left(u^m, \overline{v}\right) = 0, \tag{3.12a}$$

for all $\overline{v} \in \mathbb{P}_1^{\mathrm{pcont}}(\mathcal{T}_h)$.

Step 2: Given $u^m, \mu^m \in \mathbb{P}_0^{\text{disc}}(\mathcal{T}_h)$ such that $u^m \geq 0$, find $u^{m+1}, \mu^{m+1} \in \mathbb{P}_0^{\text{disc}}(\mathcal{T}_h)$ solving

$$\left(\delta_t u^{m+1}, \overline{v}\right) + a_h^{\text{upw}}(\mu^{m+1}; (u^{m+1})_\oplus, \overline{u}) = 0, \tag{3.12b}$$

$$\left(\mu^{m+1}, \overline{\mu}\right) - k_0 \left(\log(u^{m+1} + \varepsilon), \overline{\mu}\right) + k_1 \left(v^{m+1}, \overline{\mu}\right) = 0, \tag{3.12c}$$

for all $\overline{u}, \overline{\mu} \in \mathbb{P}_0^{\text{disc}}(\mathcal{T}_h)$.

Remark 3.4.5. *In order to preserve the positivity of the solution u^{m+1} of* (3.12)*, we have introduced a truncation of this function taking its positive part $(u^{m+1})_\oplus$ in the upwind part of* (3.12b)*, which is consistent as the solution of the continuous model* (3.1) *satisfies $u \geq 0$.*

Since Theorem 3.4.7 below will guarantee that $u^{m+1} \geq 0$, then $\left(\log(u^{m+1} + \varepsilon), \overline{\mu}\right)$ in (3.12b) *is well-defined.*

Proposition 3.4.6. *The schemes* (3.8) *and* (3.12) *conserve the mass of u:*

$$\int_\Omega u^{m+1} = \int_\Omega u^m.$$

Proof. Just need to take $\overline{u} = 1$ in (3.8b) and (3.12b). □

Theorem 3.4.7 (Positivity)**.** *If we assume that $u^m \geq 0$ and, in the case $\tau > 0$, $v^m \geq 0$ in Ω, then any solution of* (3.12) *satisfies that $u^{m+1}, v^{m+1} \geq 0$ in Ω.*

Proof. Proving that if $u^m \geq 0$ and $v^m \geq 0$ (when $\tau > 0$) then $v^{m+1} \geq 0$ using that the mesh is acute is a classic result which can be found, for example, in [47, 80].

Moreover, if $u^m \geq 0$ and $v^m \geq 0$ (when $\tau > 0$) it follows from the equation (3.12b) that $u^{m+1} \geq 0$ using the same arguments that are shown to prove the positivity result in Theorem 2.3.4 since the proof is independent of the flux $\nabla \mu^{m+1}$. □

Proposition 3.4.8. *There is a unique solution v^{m+1} of the linear equation* (3.12a).

Proof. Since we are dealing with a discrete linear problem, existence and unicity of the solution are equivalent. Hence, we just need to assume that there are two solutions of (3.8a), v_1 and v_2, substract the expressions resulting of evaluating both solutions and test with $v_1 - v_2$ to prove unicity of the solution. □

Proposition 3.4.9. *There is at least one solution of* (3.12b)–(3.12c).

Proof. The idea of this proof is to apply the Leray-Schauder fixed point theorem 2.3.6.

Given $u^m \in \mathbb{P}_0^{\text{disc}}(\mathcal{T}_h)$ with $u^m \geq 0$ and the unique solution v^{m+1} of (3.12a), we define the map

$$T\colon \mathbb{P}_0^{\text{disc}}(\mathcal{T}_h) \times \mathbb{P}_0^{\text{disc}}(\mathcal{T}_h) \longrightarrow \mathbb{P}_0^{\text{disc}}(\mathcal{T}_h) \times \mathbb{P}_0^{\text{disc}}(\mathcal{T}_h)$$

such that $T(\widehat{u}, \widehat{\mu}) = (u, \mu) \in \mathbb{P}_0^{\text{disc}}(\mathcal{T}_h) \times \mathbb{P}_0^{\text{disc}}(\mathcal{T}_h)$ is the unique solution of the linear (and decoupled) problem:

$$\frac{1}{\Delta t}\,(u - u^m, \overline{u}) = -a_h^{\text{upw}}(\widehat{\mu}; \widehat{u}_\oplus, \overline{u}), \qquad \forall \overline{u} \in \mathbb{P}_0^{\text{disc}}(\mathcal{T}_h), \tag{3.13a}$$

$$(\mu, \overline{\mu}) = k_0\left(\log((\widehat{u})_\oplus + \varepsilon), \overline{\mu}\right) - k_1\left(v^{m+1}, \overline{\mu}\right), \qquad \forall \overline{\mu} \in \mathbb{P}_0^{\text{disc}}(\mathcal{T}_h). \tag{3.13b}$$

To check that T is well defined, it is straightforward to see that the solutions u of (3.13a) and μ of (3.13b) are unique, which involves their existence as $\mathbb{P}_0^{\text{disc}}(\mathcal{T}_h)$ is a finite-dimensional space.

Secondly, we will check that T is continuous. Let $\{\widehat{u}_j\}_{j\in\mathbb{N}}, \{\widehat{\mu}_j\}_{j\in\mathbb{N}} \subset \mathbb{P}_0^{\text{disc}}(\mathcal{T}_h)$ be sequences such that $\lim_{j\to\infty} \widehat{u}_j = \widehat{u}$ and $\lim_{j\to\infty} \widehat{\mu}_j = \widehat{\mu}$. Taking into account that all norms are equivalent in $\mathbb{P}_0^{\text{disc}}(\mathcal{T}_h)$ since it is a finite-dimensional space, the convergences $\widehat{u}_j \to \widehat{u}$ and $\widehat{\mu}_j \to \widehat{\mu}$ are equivalent to the elementwise convergences $(\widehat{u}_j)_K \to \widehat{u}_K$ and $(\widehat{\mu}_j)_K \to \widehat{\mu}_K$ for every $K \in \mathcal{T}_h$ (this may be seen, for instance, by using the norm $\|\cdot\|_{L^\infty(\Omega)}$). Taking limits when $j \to \infty$ in (3.13) (with $\widehat{u} \coloneqq \widehat{u}_j$, $\widehat{\mu} \coloneqq \widehat{\mu}_j$ and $(u, \mu) \coloneqq T(\widehat{u}_j, \widehat{\mu}_j)$), using the notion of elementwise convergence and the fact that $\log((\widehat{u})_\oplus + \varepsilon)$ is continuous, we get that

$$\lim_{j\to\infty} T(\widehat{u}_j, \widehat{\mu}_j) = T(\widehat{u}, \widehat{\mu}) = T\left(\lim_{j\to\infty} (\widehat{u}_j, \widehat{\mu}_j)\right),$$

hence T is continuous. In addition, T is compact since $\mathbb{P}_0^{\text{disc}}(\mathcal{T}_h)$ have finite dimension.

Finally, let us prove that the set

$$B = \{(u, \mu) \in \mathbb{P}_0^{\text{disc}}(\mathcal{T}_h) \times \mathbb{P}_0^{\text{disc}}(\mathcal{T}_h)\colon (u, \mu) = \alpha T(u, \mu) \text{ for some } 0 \leq \alpha \leq 1\}$$

is bounded (independent of α). The case $\alpha = 0$ is trivial so we will assume that $\alpha \in (0, 1]$.

If $(u,\mu) \in B$, then $u \in \mathbb{P}_0^{\text{disc}}(\mathcal{T}_h)$ is the solution of

$$\frac{1}{\Delta t}\,(u - \alpha u^m, \overline{u}) = -\alpha\, a_h^{\text{upw}}(\mu; u_{\oplus}, \overline{u}), \quad \forall \overline{u} \in \mathbb{P}_0^{\text{disc}}(\mathcal{T}_h). \tag{3.14}$$

Now, testing (3.14) with $\overline{u} = 1$, we get that

$$\int_\Omega u = \alpha \int_\Omega u^m,$$

and, as $u^m \geq 0$ and it can be proved that $u \geq 0$ using the same arguments than in Theorem 3.4.7, we get that

$$\|u\|_{L^1(\Omega)} \leq \|u^m\|_{L^1(\Omega)}.$$

Moreover, since $u \geq 0$, $\mu \in \mathbb{P}_0^{\text{disc}}(\mathcal{T}_h)$ is the solution of the equation

$$(\mu, \overline{\mu}) = \alpha k_0\,(\log(u+\varepsilon), \overline{\mu}) - \alpha k_1\left(v^{m+1}, \overline{\mu}\right), \quad \forall \overline{\mu} \in \mathbb{P}_0^{\text{disc}}(\mathcal{T}_h). \tag{3.15}$$

Hence,

$$\mu = \alpha k_0 \log(u+\varepsilon) - \alpha k_1 \Pi_0 v^{m+1}, \quad \text{in } \mathbb{P}_0^{\text{disc}}(\mathcal{T}_h).$$

Thus, taking into account that u is bounded in $\mathbb{P}_0^{\text{disc}}(\mathcal{T}_h)$, we conclude that μ is bounded in $\mathbb{P}_0^{\text{disc}}(\mathcal{T}_h)$.

Since $\mathbb{P}_0^{\text{disc}}(\mathcal{T}_h)$ is a finite-dimensional space where all the norms are equivalent, we have proved that B is bounded.

Finally, we can apply the Leray-Schauder fixed point theorem 2.3.6 to prove the existence of a fixed point of (3.13a)–(3.13b) and, consequently, the existence of a solution (u^{m+1}, μ^{m+1}) of (3.12b)–(3.12c). □

Since every solution of (3.12) is positive according to Theorem 3.4.7, the schemes (3.12) and (3.8) are equivalent in the sense that any solution of (3.12) is solution of (3.8) and vice versa. Therefore, using Propositions 3.4.8 and 3.4.9 the following result holds.

Corollary 3.4.10. *There is at least one solution of the decoupled non-truncated scheme* (3.8)*. Moreover,* v^{m+1} *is nonnegative and unique.*

Remark 3.4.11. *Obtaining the nonnegative solutions of* (3.8) *can be enforced by solving the scheme* (3.12) *including the cut-off operator* (3.12b)*. In practice, the same solution was found in our numerical experiments using either the auxiliary truncated scheme* (3.12) *or the non-truncated scheme* (3.8) *without explicitly imposing the nonnegativity restriction* $u^{m+1} \geq 0$ *(see Remark 3.5.2).*

Remark 3.4.12. *Showing uniqueness of solution of* (3.8) *is not straightforward and it might require using inverse inequalities that would probably involve some kind of restriction on the time step and mesh size, and this is left to a future work.*

Theorem 3.4.13. *Any solution of the scheme* (3.8) *satisfies the following* ***discrete energy law*** *at the time step* $m+1$*:*

$$\delta_t E_\varepsilon(u^{m+1}, v^{m+1}) + \Delta t \frac{k_1 k_3}{2k_4} \int_\Omega (\delta_t v^{m+1})^2 + \Delta t \frac{k_1 k_2}{2k_4} \int_\Omega |\delta_t \nabla v^{m+1}|^2 \tag{3.16}$$

$$+ \tau \frac{k_1}{k_4} \int_\Omega (\delta_t v^{m+1})^2 + a_h^{upw}(\mu^{m+1}; u^{m+1}, \mu^{m+1}) \leq 0, \tag{3.17}$$

where

$$E_\varepsilon(u, v) \coloneqq \int_\Omega \big(k_0(u+\varepsilon)\log(u+\varepsilon) - k_1 uv + \frac{k_1 k_2}{2k_4}|\nabla v|^2 + \frac{k_1 k_3}{2k_4} v^2\big). \tag{3.18}$$

Proof. Take $\overline{u} = \mu^{m+1}$, $\overline{\mu} = \delta_t u^{m+1}$, $\overline{v} = (k_1/k_4)\delta_t v^{m+1}$ in (3.8) and consider the equalities

$$\delta_t(u^{m+1}v^{m+1}) = u^m \delta_t(v^{m+1}) + \delta_t(u^{m+1})v^{m+1},$$
$$\delta_t(v^{m+1})v^{m+1} = \frac{1}{2}\delta_t(v^{m+1})^2 + \frac{\Delta t}{2}(\delta_t v^{m+1})^2.$$

Then, adding the resulting expressions for (3.8a) and (3.8c) and substracting (3.8b), we obtain

$$\begin{aligned}
0 &= a_h^{\text{upw}}(\mu^{m+1}; u^{m+1}, \mu^{m+1}) + k_0 \int_\Omega \delta_t(u^{m+1}) \log(u^{m+1} + \varepsilon) \\
&\quad - k_1 \int_\Omega \delta_t(u^{m+1}) v^{m+1} - k_1 \int_\Omega u^m \delta_t(v^{m+1}) + \frac{k_1}{k_4} \int_\Omega (\delta_t v^{m+1})^2 \\
&\quad + \frac{k_1 k_2}{k_4} \int_\Omega \nabla v^{m+1} \cdot \nabla(\delta_t v^{m+1}) + \frac{k_1 k_3}{k_4} \int_\Omega v^{m+1} \delta_t(v^{m+1}) \\
&= a_h^{\text{upw}}(\mu^{m+1}; u^{m+1}, \mu^{m+1}) + k_0 \int_\Omega \delta_t(u^{m+1}) \log(u^{m+1} + \varepsilon) \\
&\quad - k_1 \delta_t \int_\Omega u^{m+1} v^{m+1} + \frac{k_1 k_2}{2k_4} \delta_t \int_\Omega |\nabla v^{m+1}|^2 + \frac{\Delta t k_1 k_2}{2k_4} \int_\Omega |\delta_t \nabla v^{m+1}|^2 \\
&\quad + \frac{k_1 k_3}{2k_4} \delta_t \int_\Omega (v^{m+1})^2 + \left(\frac{k_1}{k_4} + \frac{\Delta t k_1 k_3}{2k_4} \right) \int_\Omega (\delta_t v^{m+1})^2. \qquad (3.19)
\end{aligned}$$

Now, using that $\delta_t(u^{m+1}) F'(u^{m+1}) \geq \delta_t(F(u^{m+1}))$ for $F'(u^{m+1}) = \log(u^{m+1} + \varepsilon)$ (owing to the fact that $F(u)$ is convex) we have that

$$\delta_t(u^{m+1}) \log(u^{m+1} + \varepsilon) \geq \delta_t \left((u^{m+1} + \varepsilon) \log(u^{m+1} + \varepsilon) \right) - \delta_t(u^{m+1} + \varepsilon).$$

Hence, using Proposition 3.4.6,

$$\int_\Omega \delta_t(u^{m+1}) \log(u^{m+1} + \varepsilon) \geq \delta_t \left(\int_\Omega \left((u^{m+1} + \varepsilon) \log(u^{m+1} + \varepsilon) \right) \right). \qquad (3.20)$$

Thus, taking into account (3.19) and (3.20), we obtain the discrete energy law (3.16). □

Corollary 3.4.14. *Given a solution of the scheme* (3.8)*, the upwind bilinear form defined in* (3.9) *satisfies*

$$a_h^{upw}(\mu^{m+1}; u^{m+1}, \mu^{m+1}) \geq 0.$$

In consequence, the scheme (3.8) *is unconditionally energy stable with respect to the approximated energy E_ε, that is*

$$E_\varepsilon(u^{m+1}, v^{m+1}) \leq E_\varepsilon(u^m, v^m).$$

Proof. Since we know that the discrete energy satisfies (3.16), to show $\delta_t E_\varepsilon(u^{m+1}, v^{m+1}) \leq 0$ it suffices to prove that

$$a_h^{\text{upw}}(\mu^{m+1}; u^{m+1}, \mu^{m+1}) \geq 0.$$

Now, take $\overline{u} = \mu^{m+1}$ and use the definition (3.11) of the upwind bilinear form to get the following:

$$
\begin{aligned}
a_h^{\text{upw}}(\mu^{m+1};(u^{m+1})_{\oplus},\mu^{m+1}) &= \\
&= \sum_{e\in\mathcal{E}_h^i, e=K\cap L} \frac{1}{\mathcal{D}_e(\mathcal{T}_h)} \int_e \left((\llbracket \mu^{m+1} \rrbracket)_{\oplus} u_K^{m+1} - (\llbracket \mu^{m+1} \rrbracket)_{\ominus} u_L^{m+1} \right) \llbracket \mu^{m+1} \rrbracket \\
&= \sum_{e\in\mathcal{E}_h^i, e=K\cap L} \frac{1}{\mathcal{D}_e(\mathcal{T}_h)} \int_e \left(\left(\llbracket \mu^{m+1} \rrbracket \right)_{\oplus}^2 u_K^{m+1} + \left(\llbracket \mu^{m+1} \rrbracket \right)_{\ominus}^2 u_L^{m+1} \right) \geq 0.
\end{aligned}
$$

□

Remark 3.4.15. *Notice that the energy stability of the scheme* (3.8) *is obtained thanks to the approximation of the flux $-\nabla\mu$ made in the upwind bilinear form $a_h^{upw}(\cdot;\cdot,\cdot)$. In addition, the approximation $-\nabla_{\boldsymbol{n}_e}^0\mu$ on the edges $e \in \mathcal{E}_h^i$ requires the assumption of the Hypothesis 3.4.1 for the mesh $\mathcal{T}_h$ as discussed in the Remark 3.4.2.*

3.5 Numerical experiments

In this section we show some numerical tests whose results are according to the results shown above for the scheme (3.8). For these tests we consider the parameters $k_i = 1$ for $i \in \{0, 1, \ldots, 4\}$, $\tau = 1$, $\varepsilon = 10^{-10}$ and the domain $\Omega = [-1/2, 1/2] \times [-1/2, 1/2]$ unless otherwise specified. Also, the Mesh 3.2a in Figure 3.2 is used to discretize the domain.

In the test 3.5.1 we reproduce the first numerical experiment shown in the paper [45] by A. Chertock and A. Kurganov. In this paper, they use a scheme that preserves the positivity of both variables u and v, although they do not show any energy related result. Hence, in our case, we can improve the results shown in the aforementioned paper assuring that our scheme preserves the energy law of the continuous Keller-Segel model.

Then, in the test 3.5.2 we simulate the qualitative behavior of the solution in the numerical experiment made by N. Saito in [165]. However, since the initial conditions used for the experiment in [165] are not specified we cannot reproduce the exact same test shown in this paper. In the case of our numerical test, the qualitative behavior of the solution is similar to the one in [165] until the mesh is refined enough so that we capture the blow-up phenomenon.

Finally, in the test 3.5.3 we reproduce the qualitative behavior of the results in [18, 38, 181] for different variations of chemotaxis equations and in [78] for the Keller-Segel equations, where pattern formations with multiple peaks are shown.

Remark 3.5.1. *The scheme* (3.8) *preserves the positivity and conserves the mass of* u^{m+1} *which implies* $u^{m+1} \in L^1(\Omega)$. *Therefore, we cannot expect an actual blow-up in the discrete case as it occurs in the continuous model. However, we observe in the numerical tests how the mass accumulates in some elements of* $\mathcal{T}_h$ *leading to the formation of peaks.*

In fact, we are able to capture peaks that reach values up to the order of 10^7 *using the approximation shown in* (3.8). *These kinds of numerical results are not usual in the literature due to the difficulties when approximating the steep gradients that this process involved.*

The numerical results shown in this chapter have been obtained using the Python library `FEniCS`, [14]. In order to improve the efficiency of the code, these have been run in parallel using several CPUs.

For the sake of a better visualization of the results, a $\mathbb{P}_1^{\text{cont}}$-projection of u is represented in 3D using `Paraview`, [10].

Remark 3.5.2. *All the tests were carried out using both the non-truncated equation* (3.8b) *without the restriction* $u^{m+1} \geq 0$ *and the truncated version* (3.12b) *to enforce the nonnegativity. The approximations of* u *and* v *obtained in every case using both versions of the scheme were identical in all the degrees of freedom.*

3.5.1 One bulge of cells

First, we reproduce the results shown in [45]. For this purpose, we consider the radially symmetric initial conditions

$$u_0 = 1000e^{-100(x^2+y^2)}, \quad v_0 = 500e^{-50(x^2+y^2)},$$

which are plotted in Figure 3.3.

As stated in [45], the u and v components of the solution are expected to blow up in a finite time due to the initial conditions chosen. The result of the test using the scheme (3.8) with $h \approx 1.41 \cdot 10^{-3}$ and $\Delta t = 10^{-6}$ is shown in Figures 3.4 and 3.5. In fact, we observe a blow-up phenomenon for a certain finite time in the range conjectured by A. Chertock and A. Kurganov in [45], $t^* \in (4.4 \cdot 10^{-5}, 10^{-4})$, as our discrete approximation reaches values of order 10^6 in this time interval.

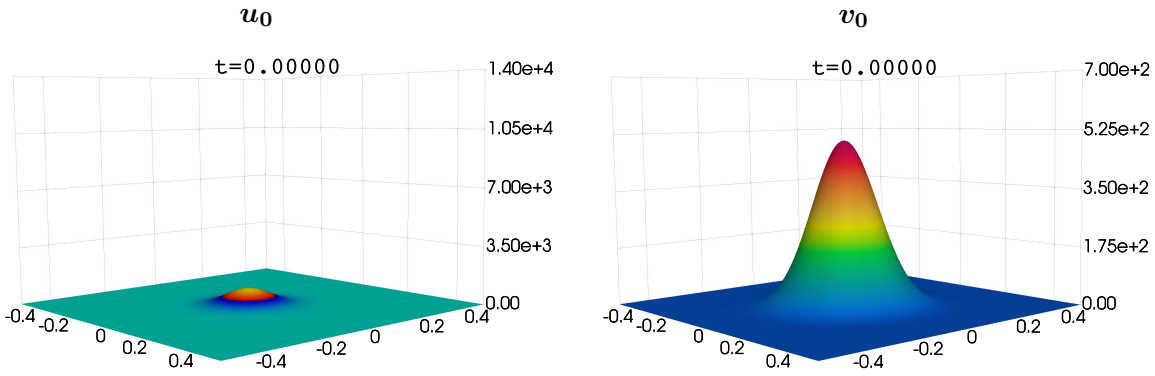

Figure 3.3 Initial conditions for blow-up as in [45] (different scales are used for u and v)

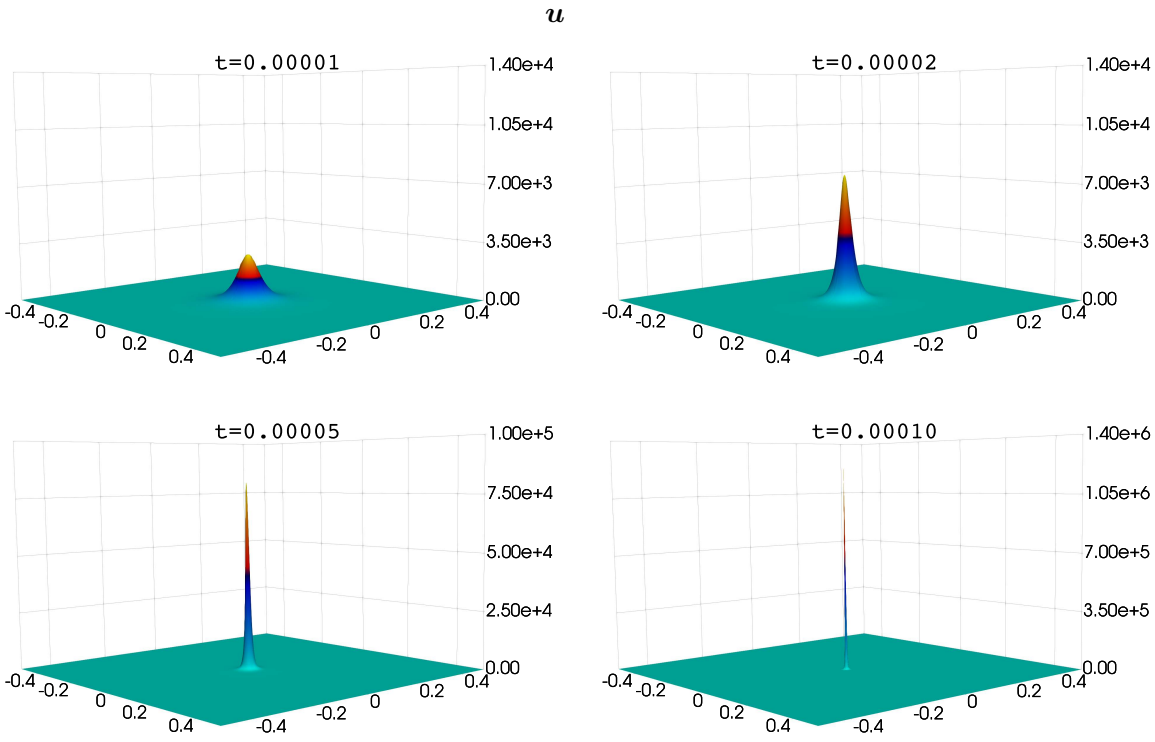

Figure 3.4 Blow-up of u as in [45]

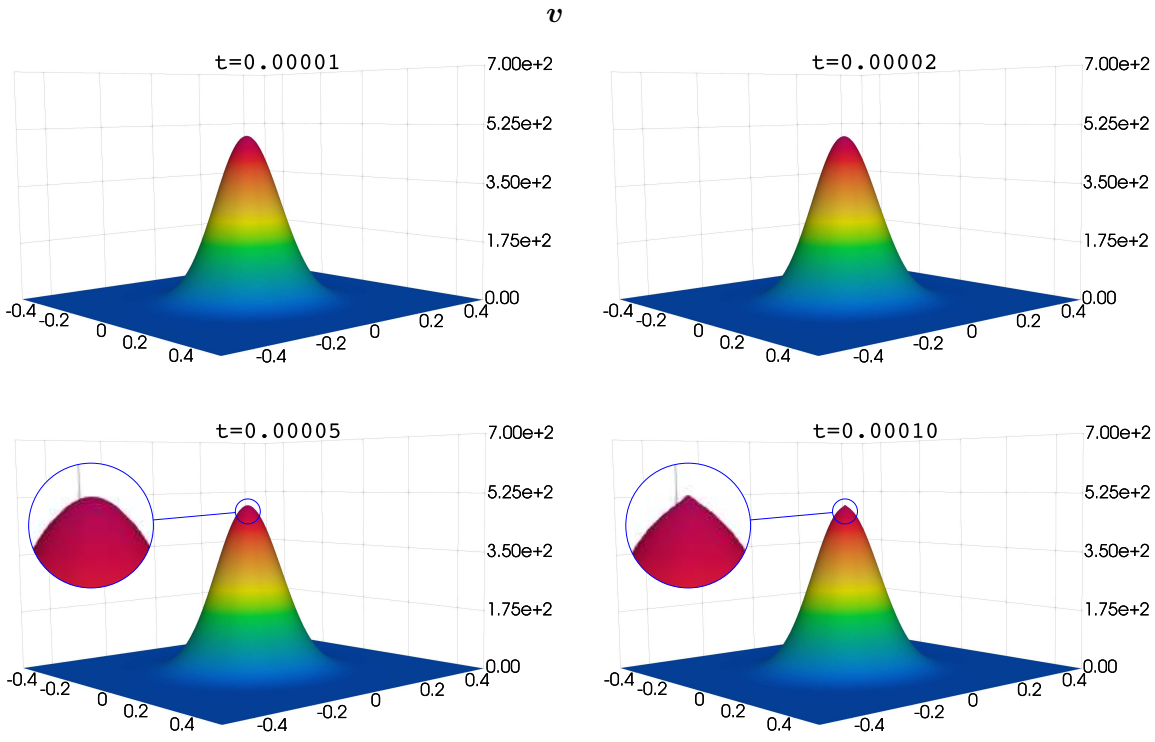

Figure 3.5 Aggregation of v in the test in [45]

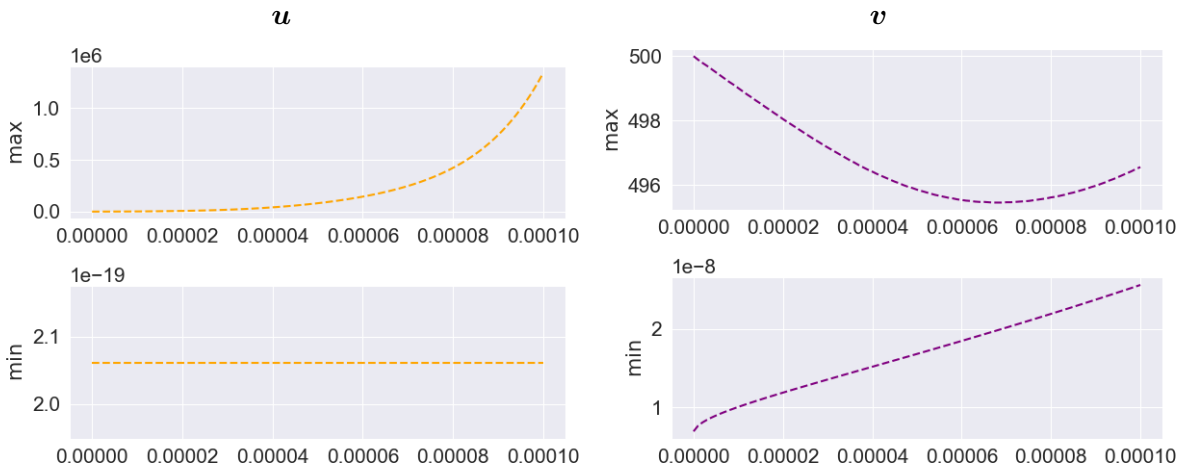

Figure 3.6 Minimum and maximum of u and v over time in the case shown in [45]

Moreover, the positivity is preserved for both u and v as stated in Theorem 3.4.7 and, unlike the scheme presented in [45], we are certain that the discrete energy decreases (both for $E(\cdot,\cdot)$ and $E(\cdot,\cdot)$) using the scheme (3.8) as proved in Theorem 3.4.13. See Figures 3.6 and 3.7.

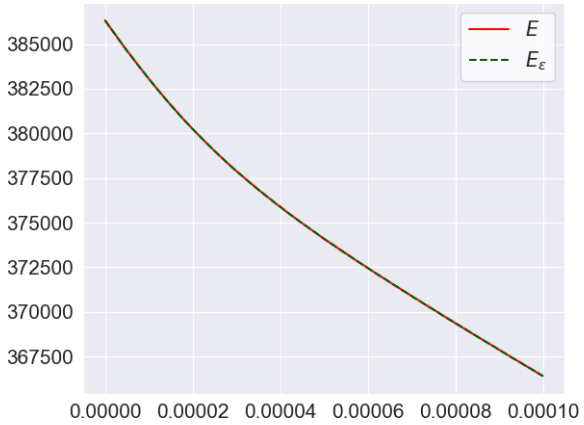

Figure 3.7 Discrete energy over time in the case shown in [45]

Remark 3.5.3. *This test have been computed with greater and lower values of ε including the limiting case $\varepsilon = 0$. The difference in norms L^2 and L^∞ are shown in Table 3.1. From a qualitative point of view, the solutions are indistinguishable.*

In this case, the numerical approximation works with $\varepsilon = 0$ since the minimum of u remains strictly positive and does not tend to 0, it takes values around 10^{-19} during all the iterations computed. Below, in Remark 3.5.4, we show a different test where we do have to take $\varepsilon > 0$ to ensure convergence of the scheme.

Table 3.1 Difference between approximations of the test in Section 3.5.1 at $t = 5 \cdot 10^{-5}$ with respect to the solution with $\varepsilon = 0$

ε	$\|\cdot\|_{L^2(\Omega)}$		$\|\cdot\|_{L^\infty(\Omega)}$	
	u	v	u	v
10^{-6}	$4.81 \cdot 10^{-8}$	$1.01 \cdot 10^{-12}$	$3.52 \cdot 10^{-6}$	$2.90 \cdot 10^{-11}$
10^{-10}	$1.10 \cdot 10^{-10}$	$3.87 \cdot 10^{-13}$	$1.71 \cdot 10^{-8}$	$2.73 \cdot 10^{-12}$
10^{-14}	$8.75 \cdot 10^{-11}$	$6.85 \cdot 10^{-14}$	$1.59 \cdot 10^{-8}$	$8.53 \cdot 10^{-13}$

An accuracy test in space (with $\varepsilon = 10^{-10}$) has been also carried out where the solution obtained with $h \approx 7.071 \cdot 10^{-4}$ and $\Delta t = 10^{-6}$ has been taken as reference solution. The results shown in Tables 3.2 and 3.3 suggest first order of convergence in space in norm L^2 both for u and v.

Table 3.2 Accuracy test in norm L^2 for u (test in Section 3.5.1)

t	$h \approx 1.41 \cdot 10^{-2}$	$5h/7 \approx 1.01 \cdot 10^{-2}$		$5h/9 \approx 7.86 \cdot 10^{-3}$		$5h/11 \approx 6.43 \cdot 10^{-3}$	
	Error	Error	Order	Error	Order	Error	Order
10^{-5}	7.01	5.08	1.00	4.13	0.83	3.41	0.95
$2 \cdot 10^{-5}$	$2.38 \cdot 10$	$1.70 \cdot 10$	0.99	$1.42 \cdot 10$	0.71	$1.09 \cdot 10$	1.33
$5 \cdot 10^{-5}$	$3.15 \cdot 10^2$	$2.31 \cdot 10^2$	0.92	$1.84 \cdot 10^2$	0.92	$1.28 \cdot 10^2$	1.81

Table 3.3 Accuracy test in norm L^2 for v (test in Section 3.5.1)

t	$h \approx 1.41 \cdot 10^{-2}$	$5h/7 \approx 1.01 \cdot 10^{-2}$		$5h/9 \approx 7.86 \cdot 10^{-3}$		$5h/11 \approx 6.43 \cdot 10^{-3}$	
	Error	Error	Order	Error	Order	Error	Order
10^{-5}	$1.43 \cdot 10^{-2}$	$1.04 \cdot 10^{-2}$	0.95	$7.36 \cdot 10^{-3}$	1.36	$5.63 \cdot 10^{-3}$	1.33
$2 \cdot 10^{-5}$	$2.04 \cdot 10^{-2}$	$1.27 \cdot 10^{-2}$	1.40	$8.82 \cdot 10^{-3}$	1.46	$6.76 \cdot 10^{-3}$	1.32
$5 \cdot 10^{-5}$	$2.54 \cdot 10^{-2}$	$1.51 \cdot 10^{-2}$	1.55	$1.27 \cdot 10^{-2}$	0.68	$9.94 \cdot 10^{-3}$	1.22

It is remarkable to notice that, although the L^2 errors of the approximation of u may seem huge at first, particularly as it approaches the blow-up time, they are not that big in relative terms. As it can be observed in Figure 3.4, the maximum value reached by u is around 10^3 bigger than the L^2 errors shown in Table 3.2 at each time step. These errors will tend to vanish as the mesh is refined so that the spiky bulge in the middle of the domain is more accurately approximated.

Also, we would like to emphasize the difficulty of achieving such results as obtaining a reference solution in a blow-up situation where the exact solution tends to degenerate and huge gradients appear require a significant computational effort. In this regard, the reference solution has been computed in parallel using a domain decomposition technique.

3.5.2 Three bulges of cells

Now, we show the results for a similar test to the one that appears in [165]. In this case, we take the parabolic-elliptic case ($\tau = 0$) so that the characteristic speed of v is much faster than the

characteristic speed of u. Moreover, we consider the initial condition

$$u_0 = 900e^{-100((x-0.2)^2+y^2)} + 800e^{-100(x^2+(y-0.2)^2)} + 1000e^{-100((x-0.3)^2+(y-0.3)^2)},$$

which is plotted in Figure 3.8. As stated in [165] and the references therein, since $\|u_0\|_{L^1(\Omega)} > 8\pi$, the solution is expected to blow-up in finite time.

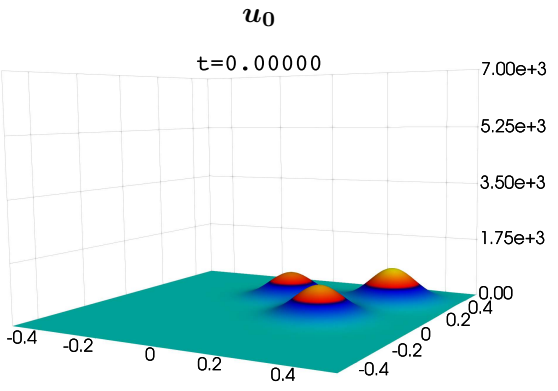

Figure 3.8 Initial condition with three cell bulges (similar to the one in [45])

In Figures 3.9 and 3.10 we can observe the result of the test with $h \approx 2.83 \cdot 10^{-2}$ and $\Delta t = 10^{-5}$. In this case, the qualitative behavior of the solution is similar to the one shown in [165], with the peak of cells moving towards a corner of the domain. However, the qualitative behavior of the solution is different if we take $h \approx 7.07 \cdot 10^{-3}$ and $\Delta t = 10^{-5}$. Now, as represented in Figures 3.11 and 3.12, a blow-up phenomenon seems to occur in finite time and the peak of cells remains motionless far away from the corners of the domain.

In both cases, the positivity is preserved and the energy decreases in the discrete case. See Figures 3.13 and 3.15 (left) for the case $h \approx 2.83 \cdot 10^{-2}$ and Figures 3.14 and 3.15 (right) for the case $h \approx 7.07 \cdot 10^{-3}$.

3.5.3 Pattern formation with multiple peaks

Finally, we show the results for a test in which we obtain a numerical solution describing a pattern with multiple peaks as it occurs, for instance, in the cases that appear in [18, 38, 181] for different variations of chemotaxis equations and in [78] for the Keller-Segel equations. For this purpose, we

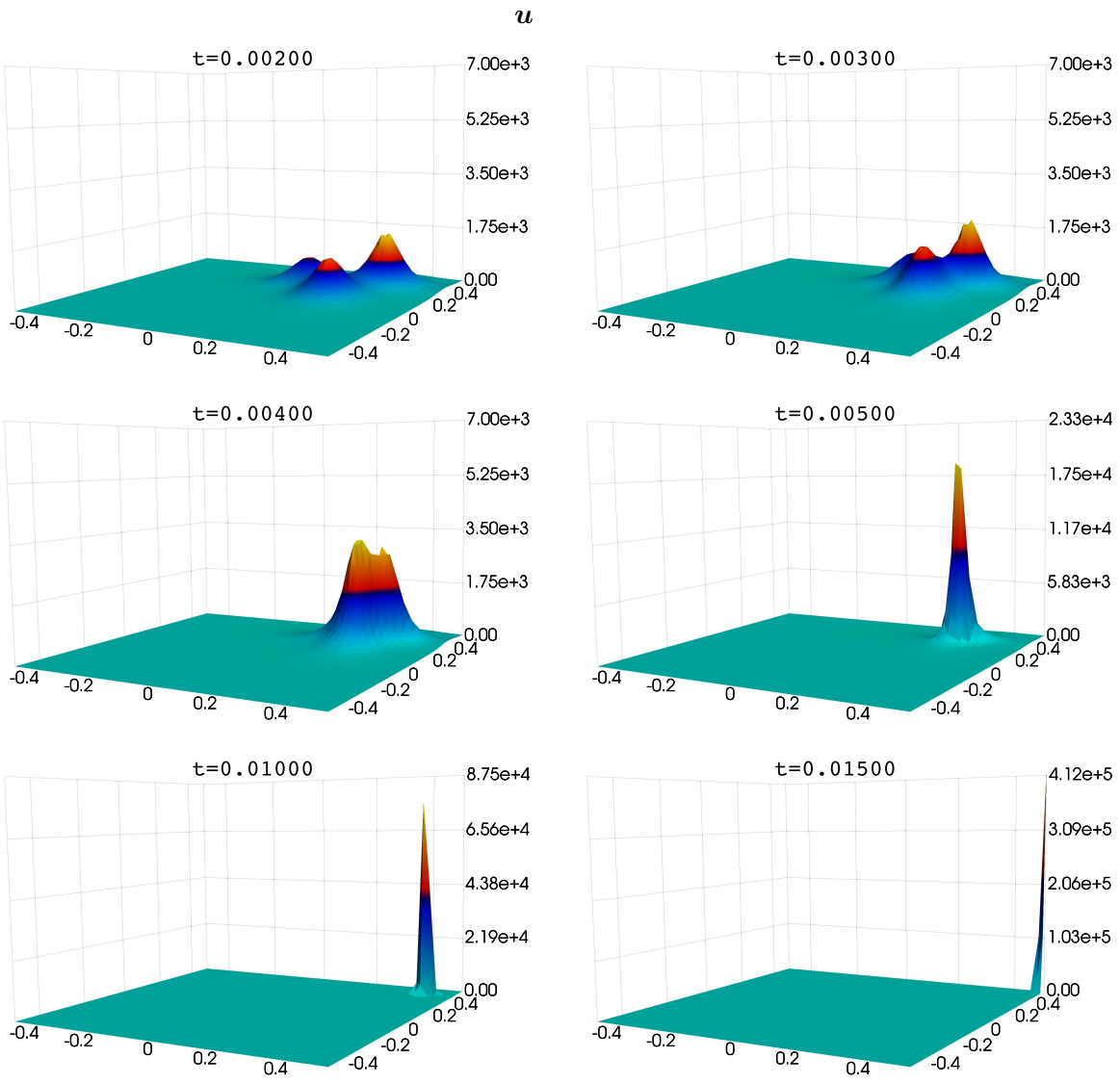

Figure 3.9 Aggregation of three cell bulges with $h \approx 2.83 \cdot 10^{-2}$

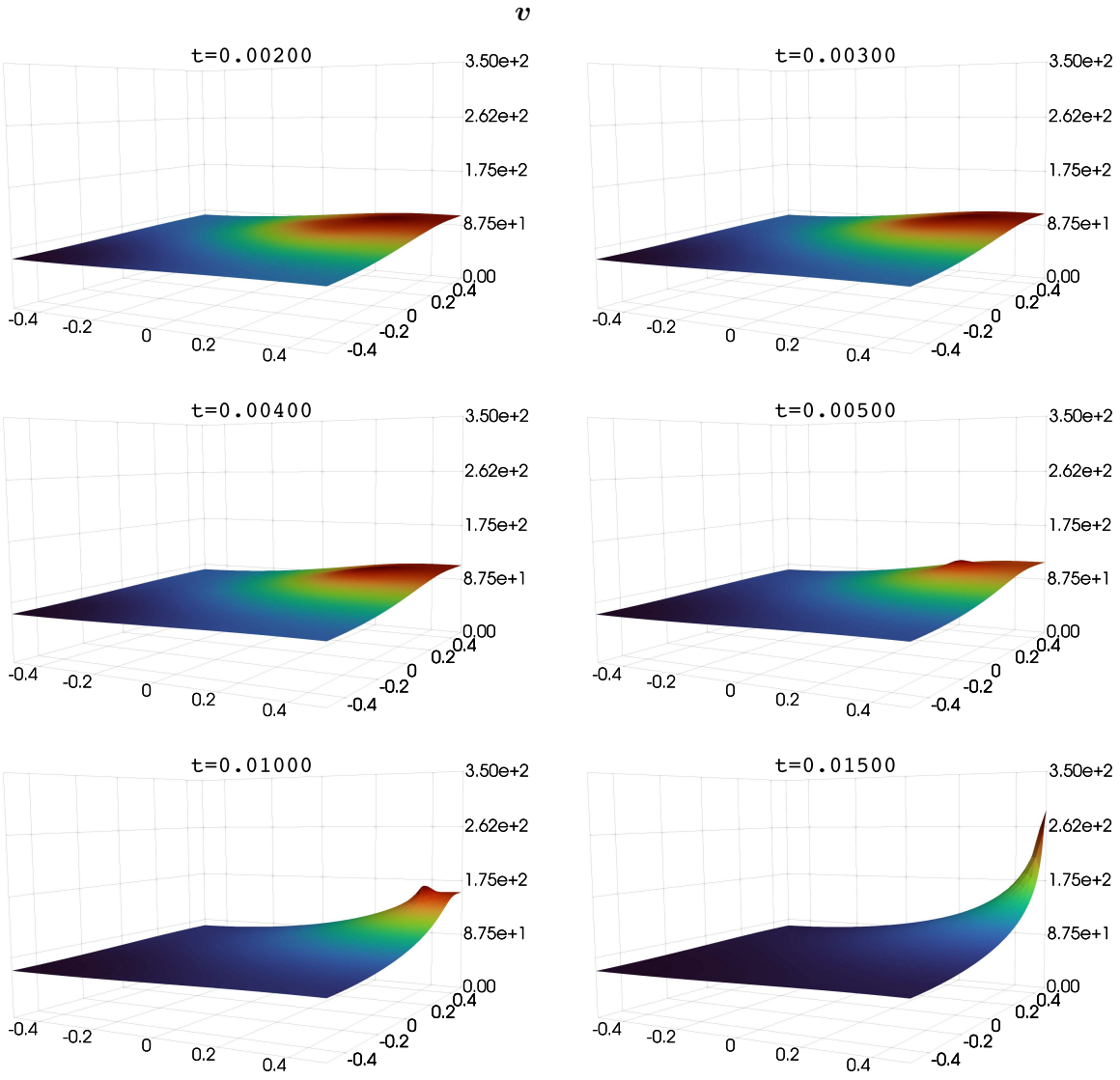

Figure 3.10 Chemoattractant in the case of three cell bulges with $h \approx 2.83 \cdot 10^{-2}$

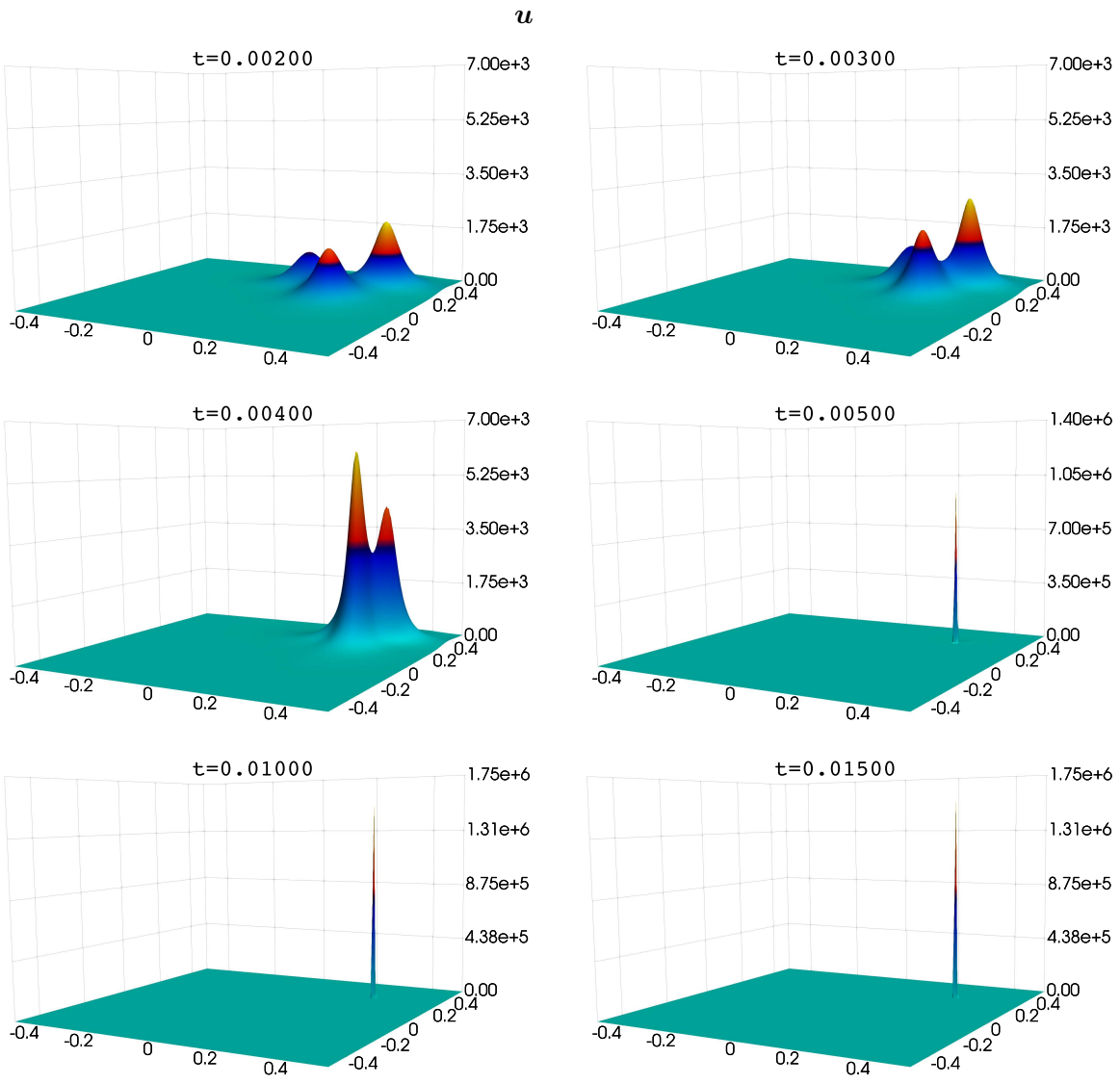

Figure 3.11 Aggregation of three cell bulges with $h \approx 7.07 \cdot 10^{-3}$

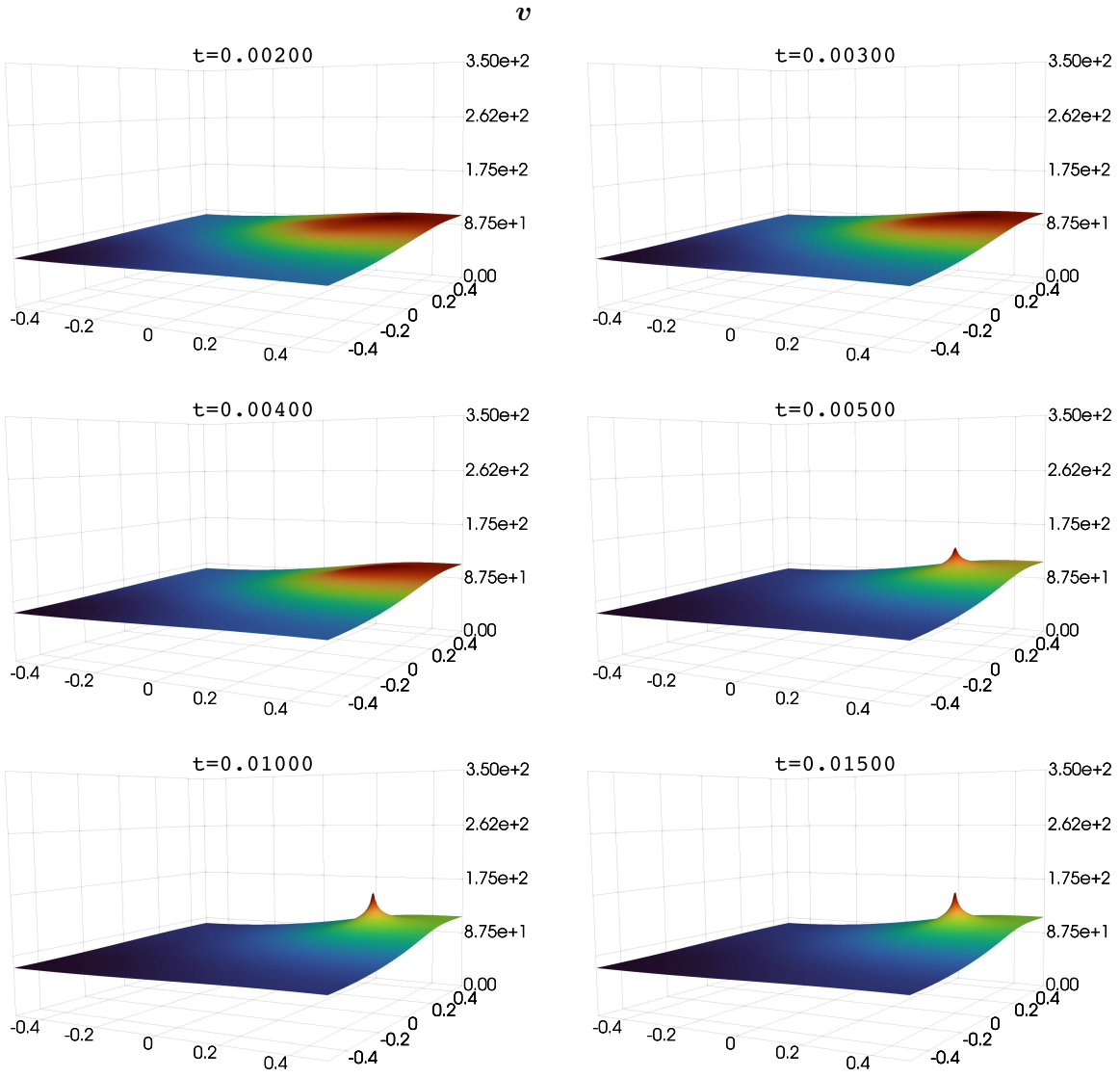

Figure 3.12 Chemoattractant in the case of three cell bulges with $h \approx 7.07 \cdot 10^{-3}$

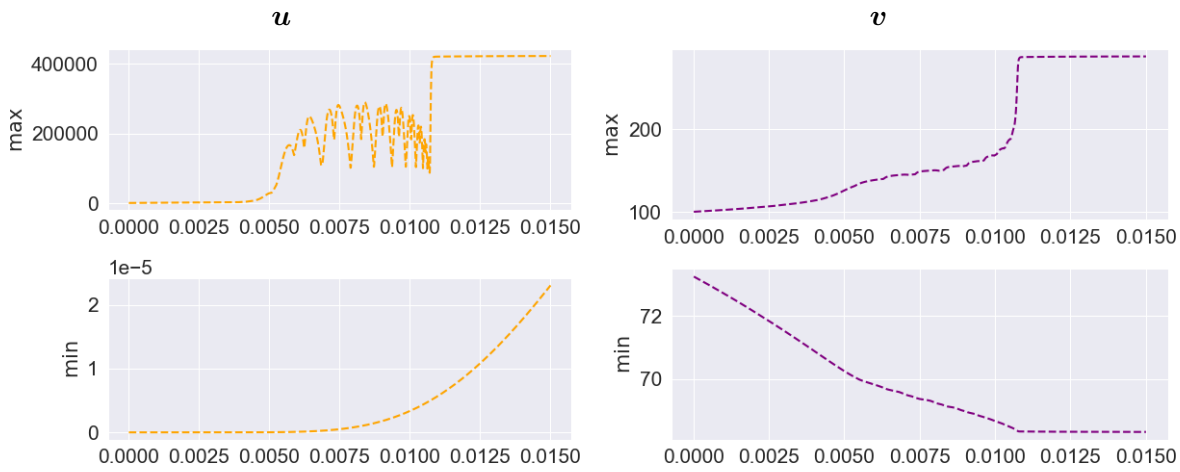

Figure 3.13 Minimum and maximum of u and v in the case of aggregation of three cell bulges with $h \approx 2.83 \cdot 10^{-2}$

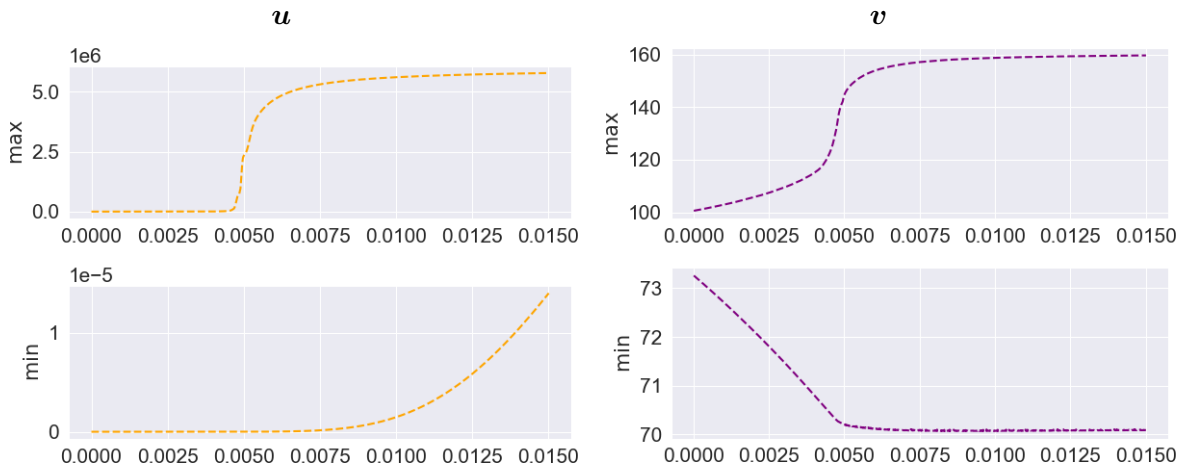

Figure 3.14 Minimum and maximum of u and v in the case of aggregation of three cell bulges with $h \approx 7.07 \cdot 10^{-3}$

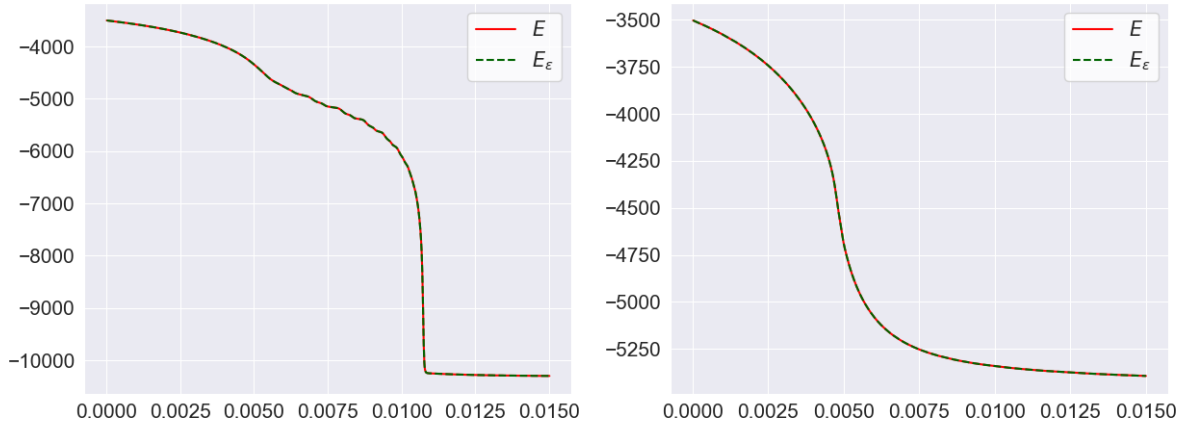

Figure 3.15 Discrete energy over time in the case of aggregation of three cell bulges. On the left, $h \approx 2.83 \cdot 10^{-2}$. On the right, $h \approx 7.07 \cdot 10^{-3}$

consider the initial conditions

$$u_0 = 1000(\cos(2\pi x)\cos(2\pi y) + 1), \quad v_0 = 500(\sin(3\pi x)\sin(3\pi y) + 1),$$

which are plotted in Figure 3.16.

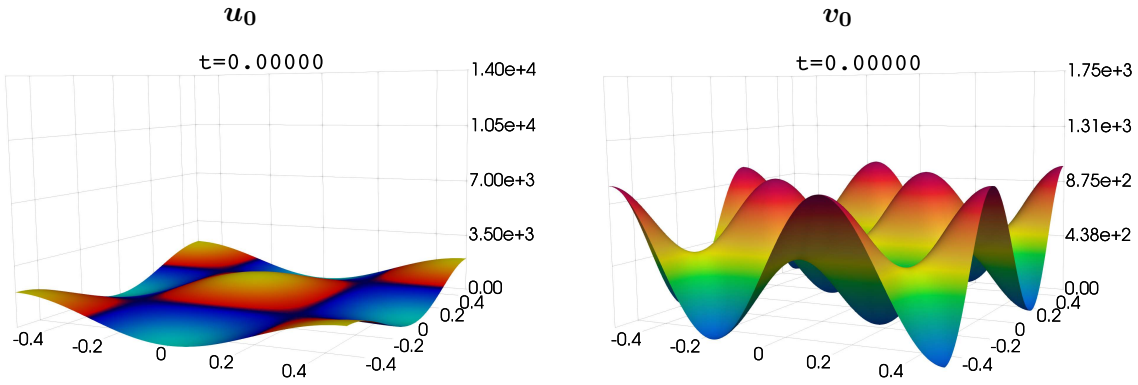

Figure 3.16 Initial conditions for the pattern formation with multiple peaks (different scales are used for u and v)

In Figures 3.17 and 3.18 we can observe the result of the test with $h \approx 3.54 \cdot 10^{-3}$ and $\Delta t = 10^{-7}$. Notice that we obtain 8 peaks of cells that reach very high values (up to values of order 10^7), which may be due to a blow-up phenomenon occurring at a certain finite time t^* close to 10^{-4}.

u

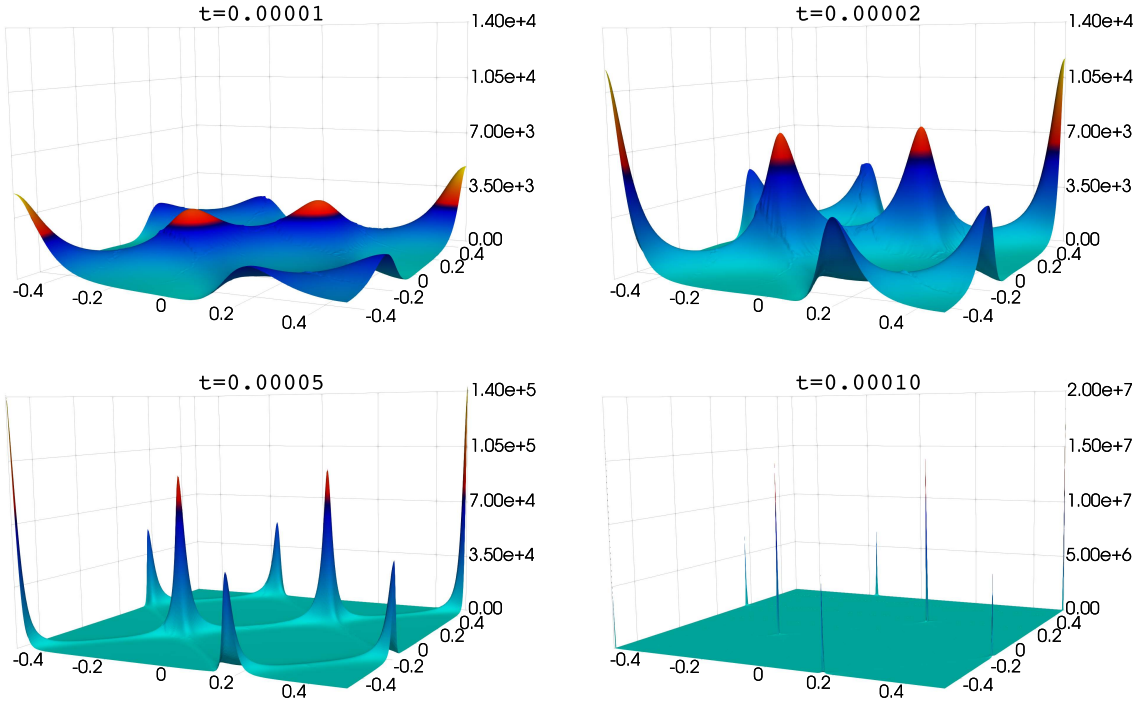

Figure 3.17 Pattern formation of u with multiple peaks

v

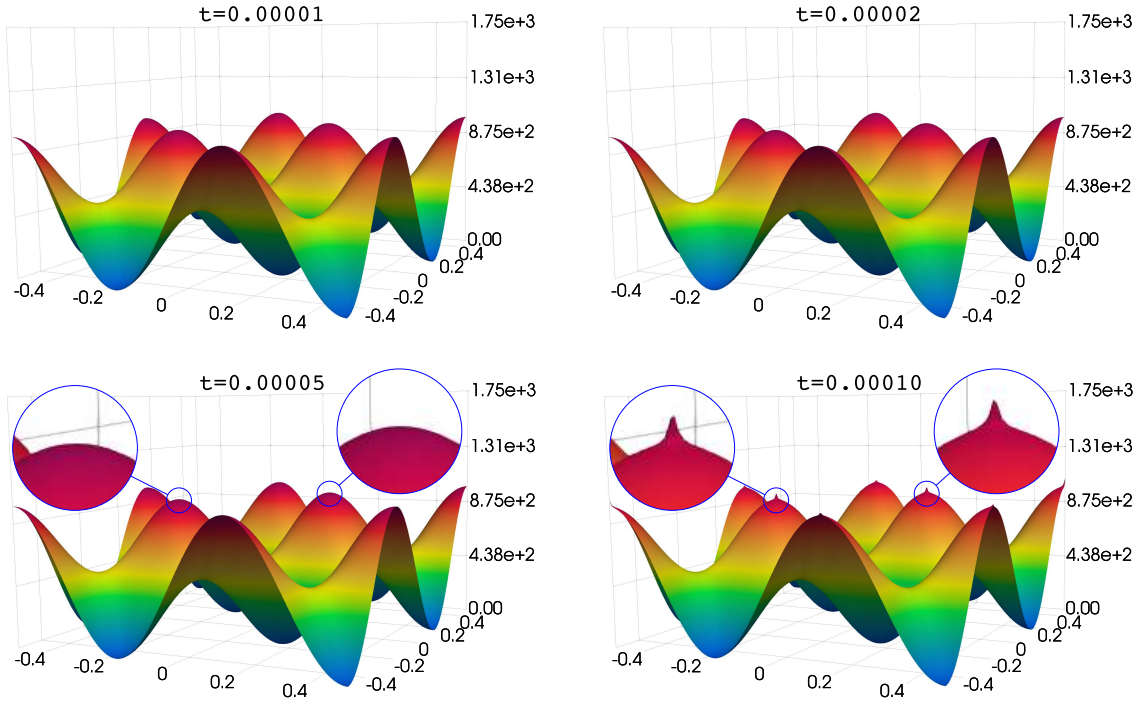

Figure 3.18 Pattern formation of v with multiple peaks

Again, the positivity is preserved as shown in Figure 3.19 and the energy decreases in the discrete case as in Figure 3.20.

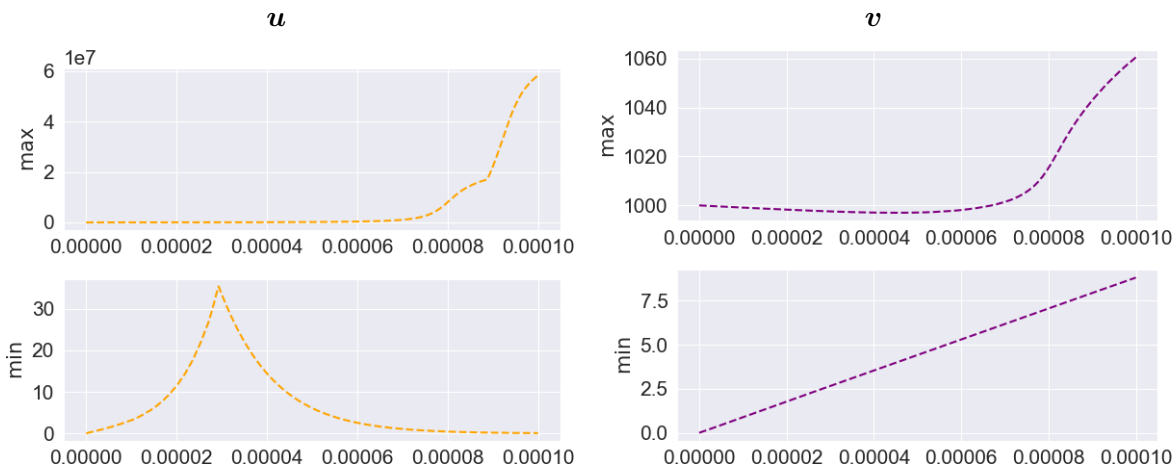

Figure 3.19 Minimum and maximum of u and v in the case of multiple peaks

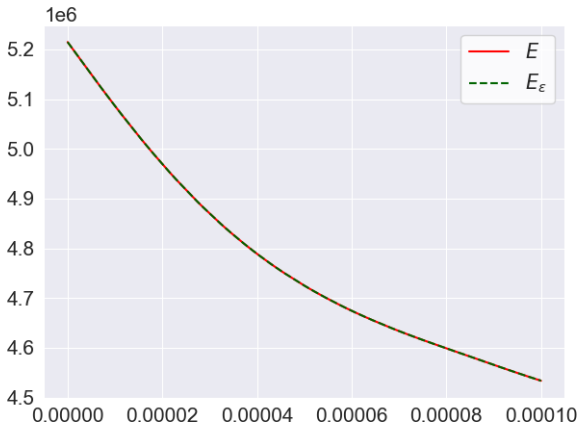

Figure 3.20 Discrete energy over time in the case of multiple peaks

Remark 3.5.4. *This test was also computed with* $h \approx 2.828 \cdot 10^{-2}$, $\Delta t = 2.5 \cdot 10^{-6}$ *and values of* ε *lower than* 10^{-10}. *In this case, the minimum value of* u *tends to* 0 *(see Figure 3.19), hence* (3.8) *is not well suited for too small values of* ε *and the convergence of Newton's method (or other iterative methods) to approximate the solution of the nonlinear schemes is not guaranteed as* $\lim_{u \to 0} \log(u) = \infty$. *Therefore, regularizing the chemical potential of* u *eases the convergence of the numerical method while only introducing a small error as shown by the results in Table 3.4.*

In this table, the difference in L^2 and L^∞ norms between the approximation with $\varepsilon = 0$ and the approximations with greater values of ε at $t = 2.5 \cdot 10^{-4}$ and $t = 5.25 \cdot 10^{-4}$ (last time step before Newton's method stop converging with $\varepsilon = 0$) are shown. In the range of values for ε taken, $\varepsilon = 10^{-12}$ is the lowest value for which Newton's method converges during the 4000 time iterations computed. The minimum value of u achieved at $t = 0.01$, the last time step computed, with $\varepsilon = 10^{-12}$ is of order 10^{-167}. Newton's method stops converging with $\varepsilon = 10^{-14}$ at $t = 8.275 \cdot 10^{-4}$ and at $t = 5.525 \cdot 10^{-4}$ with $\varepsilon = 10^{-16}$ (same time step than with smaller ε values including $\varepsilon = 0$).

Table 3.4 Difference between approximations of the test in Section 3.5.3 ($h \approx 2.828 \cdot 10^{-2}$, $\Delta t = 2.5 \cdot 10^{-6}$) with respect to the solution with $\varepsilon = 0$

t	ε	$\|\cdot\|_{L^2(\Omega)}$		$\|\cdot\|_{L^\infty(\Omega)}$	
		u	v	u	v
$2.5 \cdot 10^{-4}$	10^{-10}	$7.41 \cdot 10^{-11}$	$1.87 \cdot 10^{-13}$	$2.71 \cdot 10^{-9}$	$1.14 \cdot 10^{-12}$
	10^{-12}	$3.56 \cdot 10^{-12}$	0.0	$2.33 \cdot 10^{-10}$	0.0
	10^{-14}	$8.24 \cdot 10^{-13}$	0.0	$5.82e \cdot 10^{-11}$	0.0
	10^{-16}	$2.59 \cdot 10^{-14}$	0.0	$1.82e \cdot 10^{-12}$	0.0
$5.25 \cdot 10^{-4}$	10^{-10}	$2.14 \cdot 10^{-10}$	$6.18 \cdot 10^{-13}$	$7.30 \cdot 10^{-9}$	$3.75 \cdot 10^{-12}$
	10^{-12}	$5.44 \cdot 10^{-12}$	$2.55 \cdot 10^{-13}$	$2.33 \cdot 10^{-10}$	$1.71 \cdot 10^{-12}$
	10^{-14}	$1.16 \cdot 10^{-12}$	0.0	$5.82 \cdot 10^{-11}$	0.0
	10^{-16}	$6.70 \cdot 10^{-15}$	0.0	$4.55 \cdot 10^{-13}$	0.0

CHAPTER 4

EXTENSIONS OF THE POSITIVE UPWIND DG SCHEME TO OTHER BIOLOGICAL MODELS

4.1 Abstract

In this chapter, we extend the ideas introduced in Sections 2.3.2 and 3.4 to develop a well-suited approximation of two different models related to chemotaxis. On the one hand, we consider generalized versions of the classical Keller-Segel model. First, we state results concerning the existence and regularity of their solutions under certain conditions. Then, we develop a positive approximation of these models and include computational examples which support the analytical results and shed light on the cases where the aforementioned conditions do not hold. On the other hand, we present a model of the neuroblast migration process to the olfactory bulb in rodents' brains. In this regard, we develop and implement a positive approximation of its solution and compare the qualitative results to an image generated using real data. The results of the first part of this chapter will appear in [134] and those of the second part have been made available online as a preprint in [6].

4.2 Introduction

As discussed in Section 3.2, chemotaxis models have become a problem of increasing interest among the scientific community both for their applications and for the mathematical difficulties that they present. In this sense, using the ideas that have been previously introduced in Chapters 2 and 3, we would like to provide some insight on this kind of models in two different directions: the mathematical analysis of generalized chemotaxis models and the modeling and computational simulation of real-life processes involving chemotaxis.

4.3 Generalized chemotaxis models for population dynamics

Since the early work of E. Keller and L. Segel [125, 126] were published, many different alternatives have been proposed trying to extend their ideas. While this early work was intended to model the movement of cells towards high concentration of a chemical signal, other authors have applied this

system to modeling population dynamics where the predators are attracted by high concentrations of preys, [123].

These models of population dynamics typically include terms describing population growth or decay in terms of the population size (or density) such as logistic growth terms [11, 148]. In addition, some works suggest that the population of predators can decrease due to accidental deaths as a consequence of their displacements in the chase of their preys, which increase their risk to be decimated by other species that can react to their motion (see [12, 97, 183]). This accidental deaths have been modeled in terms of the gradient of the predators' population density, [174].

All the aforementioned effects have been collected in the model presented in [121], where the authors are more interested in the mathematical analysis of its solution than in its biological interest. As mentioned in Chapter 3, the existence and regularity of solutions in chemotaxis models are not clear as, under certain conditions, the so called chemotaxis collapse can occur (see [28] and the references therein). In this regard, conditions involving the logistic growth and the gradient nonlinearity terms are studied in [121] to ensure the existence of a global, in time, and bounded solution and, therefore, the absence of blow-up.

In Section 4.3.1 we present an even more general version of the model in [121] that additionally includes possibly nonlinear diffusion, chemoattraction and chemorepulsion, see (4.1). Also, a similar model including nonlocal effects of the cell density into the chemosensitivities can be considered, see (4.2). Results regarding the local and global in time existence and regularity of the solutions of both the local and nonlocal models under certain constraints on the parameters are stated in Section 4.3.2 without proofs, as they are not object of this work and we have not contributed to them. Then, in Section 4.3.3 we present and analyze the properties of a linear discrete approximation of the models using the upwind DG ideas previously introduced in Sections 2.3.2 and 3.4. Finally, we implement this scheme in the computer and carry out some tests whose results, included in Section 4.3.4, are in accordance with the previous theoretical analysis. In addition we show that suppression of some of the analytical conditions on the parameters (and in particular those associated to the gradient nonlinearities) that ensure global in time existence of the solution may lead to only local solution that exhibit finite time blow-up.

A more detailed discussion on these models and, in particular, the analytical properties of its solution alongside with the proofs of the results presented in Section 4.3.2 will appear in [134].

4.3.1 Chemotaxis models with dampening gradient nonlinearities

First, in this section we consider a more general version of the Keller-Segel model (3.1) which introduces nonlinear diffusion, attraction and repulsion, logistic growth and dampening gradient nonlinearities. In particular, this model extends the one in [121] and consists of finding three real valued functions: $u = u(x,t)$, the cell density, $v = v(x,t)$, the chemoattractant signal, and $w = w(x,t)$, the chemorepulsive signal, defined in $\Omega \times [0,T]$ satisfying the **local model**

$$\begin{aligned}
u_t &= \nabla \cdot \big((u+1)^{n_1-1}\nabla u - \chi u(u+1)^{n_2-1}\nabla v + \xi u(u+1)^{n_3-1}\nabla w\big) \\
&\quad + \lambda u^\rho - \mu u^k - c|\nabla u|^\gamma && \text{in } \Omega\times(0,T), \quad (4.1a)\\
\tau v_t &= \Delta v - av + f_1(u) && \text{in } \Omega\times(0,T), \quad (4.1b)\\
\tau w_t &= \Delta w - dw + f_2(u) && \text{in } \Omega\times(0,T), \quad (4.1c)\\
0 &= \nabla u\cdot \boldsymbol{n} = \nabla v\cdot \boldsymbol{n} = \nabla w\cdot \boldsymbol{n} && \text{on } \partial\Omega\times(0,T), \quad (4.1d)\\
u(0) &= u_0(x), \tau v(0) = \tau v_0(x), \tau w(0) = \tau w_0(x) && \text{in } \Omega. \quad (4.1e)
\end{aligned}$$

Moreover, we consider a **nonlocal model** where the aforementioned variables satisfy

$$\begin{aligned}
u_t &= \nabla \cdot \big((u+1)^{n_1-1}\nabla u - \chi u(u+1)^{n_2-1}\nabla v + \xi u(u+1)^{n_3-1}\nabla w\big) \\
&\quad + \lambda u^\rho - \mu u^k - c|\nabla u|^\gamma && \text{in } \Omega\times(0,T), \quad (4.2a)\\
0 &= \Delta v - \frac{1}{|\Omega|}\int_\Omega f_1(u) + f_1(u) && \text{in } \Omega\times(0,T), \quad (4.2b)\\
0 &= \Delta w - \frac{1}{|\Omega|}\int_\Omega f_2(u) + f_2(u) && \text{in } \Omega\times(0,T), \quad (4.2c)\\
0 &= \nabla u\cdot \boldsymbol{n} = \nabla v\cdot \boldsymbol{n} = \nabla w\cdot \boldsymbol{n} && \text{on } \partial\Omega\times(0,T), \quad (4.2d)\\
u(0) &= u_0(x) && \text{in } \Omega, \quad (4.2e)\\
0 &= \int_\Omega v(x,t)dx = \int_\Omega w(x,t)dx && \text{in } (0,T). \quad (4.2f)
\end{aligned}$$

Here, $\tau \in \{0,1\}$, $\chi, \xi, \lambda, \mu, c \geq 0$, $n_1, n_2, n_3 \in \mathbb{R}$ and $\rho, k, \gamma \geq 1$.

Notice that the local model (4.1) is a direct generalization of the classical Keller–Segel model (3.1) where $v = v(x,t)$ represents the chemoattractant density and a new variable concerning the chemorepulsion density, $w = w(x,t)$, has been considered. In particular, equations (4.1a) or (4.2a) coincide with the equation (3.1a) for $n_1 = n_2 = 1$ and $\xi = \lambda = \mu = c = 0$. In this sense, equations

(4.1a) or (4.2a) include possibly nonlinear diffusion and chemoattraction, in the case $n_1, n_2 \neq 1$, and chemorepulsion if $\xi \neq 0$. In addition, a logistic growth term $\lambda u^\rho - \mu u^k$ and a dampening gradient term $-c|\nabla u|^\gamma$ have been added to equations (4.1a) and (4.2a).

In the considered nonlocal model (4.2), the unknown $v = v(x,t)$ represents the chemoattractant deviation and not its density as in the local model (4.1) or in the classical Keller-Segel model (3.1). In particular, since the deviation measures the difference between the observed value of a specific variable and its mean, we have that v changes sign, contrarily to what occurs to the cell and signal densities (which are nonnegative). Subsequently, the mean of v is zero, exactly as imposed in the equation (4.2f). Naturally, the chemical repellent w behaves similarly. In this sense, we do not make use of a different symbolism for the deviations, since from the context it is clear to which quantity we are referring to.

Remark 4.3.1. *Notice that we assume $\rho, k, \gamma \geq 1$ so that the terms involving these parameters in* (4.1a) *or in* (4.2a) *are regular when $u = 0$ or $|\nabla u| = 0$.*

In this section, given $\delta \in (0,1)$, we denote by $C^{k+\delta}(\overline{\Omega})$ the set of functions that are k-times, with $k \in \mathbb{N} \cup \{0\}$, continuously differentiable and whose k-th derivative satisfies a Hölder condition with index δ (see e.g. [76]). Moreover, $C^{k+\delta,m+\eta}(\overline{\Omega} \times [0,T])$ is defined for certain $\delta, \eta \in (0,1)$, $k, m \in \mathbb{N} \cup \{0\}$, by functions $u(x,t)$ which satisfy $u(\cdot,t) \in C^{k+\delta}(\overline{\Omega})$ and $u(x,\cdot) \in C^{m+\eta}([0,T])$ for every $t \in [0,T]$ and $x \in \overline{\Omega}$.

Hypothesis 4.3.2. Here, we assume that Ω is an open bounded domain of class $C^{2+\delta}$ for some $\delta \in (0,1)$ (see [76] for details), the sources f_1, f_2 are such that $f_1, f_2 : [0,\infty) \to \mathbb{R}_+$, with $f_1, f_2 \in C^1([0,\infty))$ and the initial data $u_0 = u_0(x), \tau v_0 = \tau v_0(x)$ and $\tau w_0 = \tau w_0(x)$ satisfy $u_0, v_0, w_0 : \overline{\Omega} \to \mathbb{R}_+$, with

$$u_0, v_0, w_0 \in \{\psi \in C^{2+\delta}(\overline{\Omega}) : \nabla\psi \cdot \boldsymbol{n} = 0 \text{ on } \partial\Omega\}.$$

Hypothesis 4.3.3. We might suppose that for proper $\alpha, \beta > 0$,

$$f_1(s) \leq k_1(s+1)^\alpha \quad \text{and} \quad k_2(s+1)^\beta \leq f_2(s) \leq k_3(s+1)^\beta, \tag{4.3}$$

where $k_1, k_2, k_3 > 0$ are positive constants.

Remark 4.3.4. *The bounds on f_1 and f_2 in Hypothesis 4.3.3 are required for technical reasons in the proofs of Theorems 4.3.8 and 4.3.9. In fact, these bounds can be relaxed to the following:*

$$f_1(s) \leq k_1(s+\eta)^\alpha \quad \textit{and} \quad k_2(s+\eta)^\beta \leq f_2(s) \leq k_3(s+\eta)^\beta.$$

for $\eta > 0$. Notice that we avoid the case $\eta = 0$ to move away from a possible singularity at $s = 0$ of the functions $f_1(s) = s^\alpha$ and $f_2(s) = s^\beta$ as they have to be in $C^1([0,\infty))$.

4.3.2 Existence and regularity of solutions

Now, we state the conditions that ensure us the global boundedness of the solutions. In particular, we want to bound solutions which blow up by adding the gradient term $-c|\nabla u|^\gamma$ to the logistic and, therefore, we do not focus on the bounding effect that the diffusive term $\nabla\cdot\big((u+1)^{n_1-1}\nabla u\big)$ has. In order to do that, we establish the following relation involving the parameters in the local and the nonlocal models, (4.1) and (4.2), respectively: for any $d \in \mathbb{N}$, $\tau \in \{0,1\}$, $n_1, n_2, n_3 \in \mathbb{R}$ and $\alpha, \beta, \chi, \xi, \lambda, \mu, c > 0$, $1 \leq \rho < k$ and $\gamma \in [1,2]$ we fix

$$\max\left\{1, \frac{d}{d+1}(n_2+\alpha), \tau\frac{d}{d+1}(n_3+\beta)\right\} < \gamma \leq 2. \tag{4.4}$$

Remark 4.3.5. *Here, in condition* (4.4)*, we have assumed that $1 \leq \rho < k$ and $\gamma \in [1,2]$. These two assumptions are required for the statements in Theorems 4.3.8 and 4.3.9.*

On the one hand, $1 \leq \rho < k$ implies that $\lambda u^\rho - \mu u^k$ in (4.1a) *or* (4.2a) *is a logistic term so that the decay becomes stronger than the production when u increases. This assumption, along with the negative sign of the term $-c|\nabla u|^\gamma$, allows us to have a bound on the mass of u as in Proposition 4.3.6.*

On the other hand, we assume $\gamma \in [1,2]$ for technical reasons concerning the results in Theorems 4.3.8 and 4.3.9 when $c > 0$. Intuitively, the idea of this assumption is that, if $\gamma > 2$, the solution might not be global in time due to $\|\nabla u\|_{L^\infty(\Omega)^d}$ not being bounded in finite time even though $\|u\|_{L^\infty(\Omega)}$ is bounded. However, if $\gamma \in [1,2]$, the previous case cannot occur and if the solution is only local in time, i.e, it exists up to some finite time T, then necessarily $\|u\|_{L^\infty(\Omega)}$ blows up at T. More details can be consulted in [121, 134] and the references therein.

The succeeding theorems are stated without proofs as we have not contributed to them. The full discussion and proofs of these results will be available in [134].

Proposition 4.3.6. *Let $\mu > 0$ and $1 \leq \rho < k$. The mass of the cell density u in* (4.1) *or* (4.2) *is bounded as follows:*

$$\int_\Omega u \leq \max\left\{\int_\Omega u_0, \left(\frac{\lambda}{\mu}|\Omega|^{k-\rho}\right)^{\frac{1}{k-\rho}}\right\}, \quad \forall t \in (0,T), \tag{4.5}$$

where T is the upper bound of the time interval where the function u is defined, with $T \leq \infty$.

Theorem 4.3.7 (Local classical solution of (4.1) and (4.2))**.** *For $\tau \in \{0,1\}$ and $\delta \in (0,1)$, let Ω, $f_1, f_2, u_0, \tau v_0, \tau w_0$ comply with Hypothesis 4.3.2. Additionally, let $\chi, \xi, \lambda, \mu > 0$, $n_1, n_2, n_3 \in \mathbb{R}$, $k, \rho, \gamma \geq 1$. Then there exist $T > 0$ and a unique triple of functions (u, v, w), with*

$$(u,v,w) \in C^{2+\delta,1+\frac{\delta}{2}}(\overline{\Omega}\times[0,T]) \times C^{2+\delta,\tau+\frac{\delta}{2}}(\overline{\Omega}\times[0,T]) \times C^{2+\delta,\tau+\frac{\delta}{2}}(\overline{\Omega}\times[0,T]),$$

solving problems (4.1) *and* (4.2)*, where $u \geq 0$ in $\overline{\Omega}\times[0,T]$ and, in the case* (4.1)*, $v, w \geq 0$ in $\overline{\Omega}\times[0,T]$.*

Theorem 4.3.8 (Global and bounded classical solution of (4.1))**.** *For $\tau \in \{0,1\}$, $\delta \in (0,1)$ and $\alpha, \beta > 0$, let Ω, f_1, f_2, u_0 comply with Hypotheses 4.3.2 and 4.3.3. Additionally, let $\chi, \xi, \lambda, \mu, c > 0$, $n_1, n_2, n_3 \in \mathbb{R}$, $1 \leq \rho < k$ and condition* (4.4) *hold true. Then problem* (4.1) *admits a unique solution*

$$(u,v,w) \in C^{2+\delta,1+\frac{\delta}{2}}(\overline{\Omega}\times[0,\infty)) \times C^{2+\delta,\tau+\frac{\delta}{2}}(\overline{\Omega}\times[0,\infty)) \times C^{2+\delta,\tau+\frac{\delta}{2}}(\overline{\Omega}\times[0,\infty))$$

such that $u, v, w \geq 0$ in $\overline{\Omega}\times[0,\infty)$ and $u, v, w \in L^\infty(\Omega\times(0,\infty))$.

Theorem 4.3.9 (Global and bounded classical solution of (4.2))**.** *For $\delta \in (0,1)$ and $\alpha, \beta > 0$,let Ω, f_1, f_2, u_0 comply with Hypotheses 4.3.2 and 4.3.3. Additionally, let $\alpha, \beta, \chi, \xi, \lambda, \mu, c > 0$, $n_1, n_2, n_3 \in \mathbb{R}$, $1 \leq \rho < k$ and condition* (4.4) *hold true. Then problem* (4.2) *admits a unique solution*

$$(u,v,w) \in C^{2+\delta,1+\frac{\delta}{2}}(\overline{\Omega}\times[0,\infty)) \times C^{2+\delta,\frac{\delta}{2}}(\overline{\Omega}\times[0,\infty)) \times C^{2+\delta,\frac{\delta}{2}}(\overline{\Omega}\times[0,\infty))$$

such that $u \geq 0$ in $\overline{\Omega}\times[0,\infty)$ and $u, v, w \in L^\infty(\Omega\times(0,\infty))$.

Remark 4.3.10. *Notice that the values in the condition* (4.4) *are not critical. In fact, the influence of n_1 in this condition has not been taken into consideration in this work. In this sense, it has been studied in previous works (see, for instance, [55, 56, 135]) how the diffusive term $\nabla\cdot\left((u+1)^{n_1-1}\nabla u\right)$ in* (4.1a) *or in* (4.2a) *affects the global in time existence of solution of similar models.*

4.3.3 Fully discrete scheme

We propose a linear, computationally efficient numerical scheme to approximate the local and the nonlocal models, (4.1) and (4.2), that provides a physically meaningful approximation of every variable.

In each time step $m+1$, we decouple the equations for the chemical signals (4.1b)–(4.1c) or (4.2b)–(4.2c) from the equations for the cell density, (4.1a) or (4.2a), respectively. In this way, we first compute an approximation of v and w treating u explicitly in (4.1b)–(4.1c) or in (4.2b)–(4.2c), where $u^m \geq 0$ as shown in Section 4.3.3.1. In fact, we can obtain a linear finite element scheme with a unique nonnegative solution that approximates v and w in (4.1) assuming Hypothesis 3.4.3 and using the same ideas than in Section 3.4. On the other hand, we can compute an approximation of v and w in (4.2) using standard finite elements where the constraint (4.2f) can be enforced by postprocessing. Therefore, hereafter, we will only focus on the approximation of the cell density u.

Next, with the approximations that we have obtained for v and w, with $v^{m+1}, w^{m+1} \geq 0$ in the case (4.1) or $\int_\Omega v^{m+1} = \int_\Omega w^{m+1} = 0$ in the case (4.2), we compute an approximation of u in the current time step $m+1$. Our aim is to develop a linear positive approximation of u using the ideas of Section 3.4 where the equation of the cell density is rewritten as gradient flux using the chemical potential for the particular case of the classical Keller-Segel model. However, although this is no longer possible for this chemotaxis variant, notice that, formally,

$$\nabla \log(u) = \frac{1}{u}\nabla u,$$

so that we can rewrite, for $u \geq 0$,

$$\nabla \cdot ((u+1)^{n_1-1}\nabla u) = \nabla \cdot (u(u+1)^{n_1-1}\nabla \log(u)) \quad \text{and} \quad |\nabla u| = u|\nabla \log(u)|.$$

Hence, regularizing the term $log(u)$ by adding a small parameter $\varepsilon > 0$ and projecting it into the space $\mathbb{P}_1^{\text{cont}}(\mathcal{T}_h)$ by means of the projection operator Π_1, we propose the following implicit-explicit linear discrete scheme:

Given $u^m \in \mathbb{P}_0^{\text{disc}}(\mathcal{T}_h)$ with $u^m \geq 0$ and $v^{m+1}, w^{m+1} \in \mathbb{P}_1^{\text{cont}}(\mathcal{T}_h)$, find $u^{m+1} \in \mathbb{P}_0^{\text{disc}}(\mathcal{T}_h)$ with $u^{m+1} \geq 0$ solving the problem

$$\begin{aligned}
&\left(\delta_t u^{m+1}, \overline{u}\right) + a_h^{\text{upw}}(-(u^m+1)^{n_1-1}\nabla\Pi_1(\log(u^m+\varepsilon)); u^{m+1}, \overline{u}) \\
&\qquad + a_h^{\text{upw}}((u^m+1)^{n_2-1}\nabla v^{m+1}; u^{m+1}, \overline{u}) + a_h^{\text{upw}}(-(u^m+1)^{n_3-1}\nabla w^{m+1}; u^{m+1}, \overline{u}) \\
&\qquad - \lambda\left((u^m)^\rho, \overline{u}\right) + \mu\left(u^{m+1}(u^m)^{k-1}, \overline{u}\right) \\
&\qquad + c\left(u^{m+1}(u^m)^{\gamma-1}|\nabla\Pi_1 \log(u^m+\varepsilon)|^\gamma, \overline{u}\right) = 0,
\end{aligned} \tag{4.6}$$

for all $\overline{u} \in \mathbb{P}_0^{\text{disc}}(\mathcal{T}_h)$, where

$$a_h^{\text{upw}}(\boldsymbol{\beta}; u, \overline{u}) \coloneqq \sum_{e \in \mathcal{E}_h^i, e=K\cap L} \int_e \left((\{\!\{\boldsymbol{\beta}\}\!\} \cdot \boldsymbol{n}_e)_\oplus \, u_K - (\{\!\{\boldsymbol{\beta}\}\!\} \cdot \boldsymbol{n}_e)_\ominus u_L \right) [\![\overline{u}]\!], \tag{4.7}$$

which extends the definition in (2.11) for any vector $\boldsymbol{\beta}$ which can be discontinuous.

The scheme (4.6) is only a first possible linear approach to obtain a positive approximation of the cell density as shown in the next Section 4.3.3.1. However, other smart modifications of the proposed approach might be considered to preserve other properties of the continuous models such as the mass bound (4.5).

In Section 4.3.3.1 we will provide a way of computing the solution of (4.6) enforcing $u^{m+1} \geq 0$.

4.3.3.1 Properties of the scheme

Consider the following auxiliary truncated scheme:

Given $u^m \in \mathbb{P}_0^{\text{disc}}(\mathcal{T}_h)$ with $u^m \geq 0$ and $v^{m+1}, w^{n+1} \in \mathbb{P}_1^{\text{cont}}(\mathcal{T}_h)$, find $u^{m+1} \in \mathbb{P}_0^{\text{disc}}(\mathcal{T}_h)$ solving the problem

$$\begin{aligned}
&\left(\delta_t u^{m+1}, \overline{u}\right) + a_h^{\text{upw}}(-(u^m+1)^{n_1-1}\nabla\Pi_1(\log(u^m+\varepsilon)); u_\oplus^{m+1}, \overline{u}) \\
&\qquad + a_h^{\text{upw}}((u^m+1)^{n_2-1}\nabla v^{m+1}; u_\oplus^{m+1}, \overline{u}) + a_h^{\text{upw}}(-(u^m+1)^{n_3-1}\nabla w^{m+1}; u_\oplus^{m+1}, \overline{u}) \\
&\qquad - \lambda\left((u^m)^\rho, \overline{u}\right) + \mu\left(u_\oplus^{m+1}(u^m)^{k-1}, \overline{u}\right) \\
&\qquad + c\left(u_\oplus^{m+1}(u^m)^{\gamma-1}|\nabla\Pi_1 \log(u^m+\varepsilon)|^\gamma, \overline{u}\right) = 0,
\end{aligned} \tag{4.8}$$

for all $\overline{u} \in \mathbb{P}_0^{\text{disc}}(\mathcal{T}_h)$.

Lemma 4.3.11 (Local mass bounds)**.** *The solution* u^{m+1} *of* (4.8) *satisfies*

$$\int_\Omega u^{m+1} \leq \int_\Omega u^m + \Delta t \lambda \int_\Omega (u^m)^\rho. \tag{4.9}$$

Proof. Just test (4.8) by $\overline{u} = 1$. □

Notice that the bound of the mass of the discrete solution (4.9) is consistent with the bound on the mass of the continuous solution (4.5).

Theorem 4.3.12 (DG scheme (4.8) preserves positivity)**.** *If we assume that* $u^m \geq 0$ *then any solution of* (4.8) *satisfies that* $u^{m+1} \geq 0$ *in* Ω*.*

Proof. To prove that if $u^m \geq 0$ then $u^{m+1} \geq 0$ just take the following test function in (4.8):

$$\overline{u} = \begin{cases} (u_{K^*}^{m+1})_\ominus & \text{in } K^* \in \mathcal{T}_h, \\ 0 & \text{otherwise,} \end{cases}$$

where $K^* = \arg\min_{K \in \mathcal{T}_h} u_K^{m+1}$.

Therefore, we arrive at

$$\begin{aligned} \left(\delta_t u^{m+1}, \overline{u}\right) &+ a_h^{\text{upw}}(-(u^m+1)^{n_1-1}\nabla \Pi_1(\log(u^m+\varepsilon)); u_\oplus^{m+1}, \overline{u}) \\ &+ a_h^{\text{upw}}((u^m+1)^{n_2-1}\nabla v^{m+1}; u_\oplus^{m+1}, \overline{u}) + a_h^{\text{upw}}(-(u^m+1)^{n_3-1}\nabla w^{m+1}; u_\oplus^{m+1}, \overline{u}) \\ &= \lambda\left((u^m)^\rho, \overline{u}\right) \geq 0, \end{aligned}$$

and we can proceed as in Theorem 2.3.4 in the case of the linear convection equation to show that $(u_{K^*}^{m+1})_\ominus = 0$. Therefore, $u^{m+1} \geq 0$. □

Proposition 4.3.13. *There is at least one solution of* (4.8)*.*

Proof. The idea of this proof is to apply the Leray-Schauder fixed point theorem 2.3.6.

Given $u^m \in \mathbb{P}_0^{\text{disc}}(\mathcal{T}_h)$ with $u^m \geq 0$ and and $v^{m+1}, w^{m+1} \in \mathbb{P}_1^{\text{cont}}(\mathcal{T}_h)$, we define the map

$$T \colon \mathbb{P}_0^{\text{disc}}(\mathcal{T}_h) \longrightarrow \mathbb{P}_0^{\text{disc}}(\mathcal{T}_h)$$

such that $T(\widehat{u}) = u \in \mathbb{P}_0^{\text{disc}}(\mathcal{T}_h)$ is the unique solution of the linear problem:

$$\begin{aligned}\frac{1}{\Delta t}\left(u - u^m, \overline{u}\right) = &-a_h^{\text{upw}}(-(u^m+1)^{n_2-1}\nabla\Pi_1 \log(u^m+\varepsilon); \widehat{u}_\oplus, \overline{u}) \\ &- a_h^{\text{upw}}((u^m+1)^{n_2-1}\nabla v^{m+1}; \widehat{u}_\oplus, \overline{u}) - a_h^{\text{upw}}(-(u^m+1)^{n_3-1}\nabla w^{m+1}; \widehat{u}_\oplus, \overline{u}) \\ &+ \lambda\left((u^m)^\rho, \overline{u}\right) - \mu\left(\widehat{u}_\oplus (u^m)^{k-1}, \overline{u}\right) \\ &- c\left(\widehat{u}_\oplus (u^m)^{\gamma-1}|\nabla\Pi_1 \log(u^m+\varepsilon)|^\gamma, \overline{u}\right), \end{aligned} \tag{4.10}$$

for every $\overline{u} \in \mathbb{P}_0^{\text{disc}}(\mathcal{T}_h)$.

It is straightforward to check that there is a unique solution u of (4.10) so T is well defined.

Secondly, we will check that T is continuous. Let $\{\widehat{u}_j\}_{j\in\mathbb{N}} \subset \mathbb{P}_0^{\text{disc}}(\mathcal{T}_h)$ be a sequence such that $\lim_{j\to\infty} \widehat{u}_j = \widehat{u}$. Taking into account that all norms are equivalent in $\mathbb{P}_0^{\text{disc}}(\mathcal{T}_h)$ since it is a finite-dimensional space, the convergence $\widehat{u}_j \to \widehat{u}$ is equivalent to the elementwise convergence $(\widehat{u}_j)_K \to \widehat{u}_K$ for every $K \in \mathcal{T}_h$ (this may be seen, for instance, by using the norm $\|\cdot\|_{L^\infty(\Omega)}$). Taking limits when $j \to \infty$ in (4.10) (with $\widehat{u} \coloneqq \widehat{u}_j$ and $u \coloneqq T(\widehat{u}_j)$), using the notion of elementwise convergence, we get that

$$\lim_{j\to\infty} T(\widehat{u}_j) = T(\widehat{u}) = T\left(\lim_{j\to\infty} \widehat{u}_j\right),$$

hence T is continuous. In addition, T is compact since $\mathbb{P}_0^{\text{disc}}(\mathcal{T}_h)$ has finite dimension.

Finally, let us prove that the set

$$B = \{u \in \mathbb{P}_0^{\text{disc}}(\mathcal{T}_h) \colon u = \alpha T(u) \text{ for some } 0 \le \alpha \le 1\}$$

is bounded (uniformly with respect to α). The case $\alpha = 0$ is trivial so we will assume that $\alpha \in (0, 1]$.

If $u \in B$, then $u \in \mathbb{P}_0^{\text{disc}}(\mathcal{T}_h)$ is the solution of

$$\begin{aligned}\frac{1}{\Delta t}\left(u - \alpha u^m, \overline{u}\right) = &-\alpha a_h^{\text{upw}}(-(u^m+1)^{n_2-1}\nabla\Pi_1 \log(u^m+\varepsilon); u_\oplus, \overline{u}) \\ &- \alpha a_h^{\text{upw}}((u^m+1)^{n_2-1}\nabla v^{m+1}; u_\oplus, \overline{u}) - \alpha a_h^{\text{upw}}(-(u^m+1)^{n_3-1}\nabla w^{m+1}; u_\oplus, \overline{u}) \\ &+ \alpha\lambda\left((u^m)^\rho, \overline{u}\right) - \alpha\mu\left(u_\oplus (u^m)^{k-1}, \overline{u}\right) \\ &- \alpha c\left(u_\oplus (u^m)^{\gamma-1}|\nabla\Pi_1 \log(u^m+\varepsilon)|^\gamma, \overline{u}\right), \end{aligned} \tag{4.11}$$

Now, testing (4.11) with $\overline{u} = 1$, we get that

$$\int_\Omega u \leq \alpha(1 + \Delta t\lambda) \int_\Omega u^m,$$

and, as $u^m \geq 0$ and it can be proved that $u \geq 0$ using the same arguments than in Theorem 4.3.12, we get that

$$\|u\|_{L^1(\Omega)} \leq \int_\Omega u^m + \Delta t\lambda \int_\Omega (u^m)^\rho.$$

Since $\mathbb{P}_0^{\text{disc}}(\mathcal{T}_h)$ is a finite-dimensional space where all the norms are equivalent, we have proved that B is bounded.

Thus, using the Leray-Schauder fixed point theorem 2.3.6, there is a fixed point of (4.10), therefore, we can conclude that there is a solution u^{m+1} of (4.8). □

Since every nonnegative solution of (4.8) is a solution of (4.6), the following result is straightforward.

Corollary 4.3.14. *There is at least one solution u^{m+1} of* (4.6) *satisfying $u^{m+1} \geq 0$ and*

$$\int_\Omega u^{m+1} \leq \int_\Omega u^m + \Delta t\lambda \int_\Omega (u^m)^\rho.$$

Again, as in Section 3.4, obtaining a nonnegative solution of the linear scheme (4.6) can be enforced by solving the truncated nonlinear scheme (4.8). However, in practice, the linear scheme (4.6) has provided a nonnegative approximation of the cell density in every numerical experiment that we have carried out without explicitly enforcing the nonnegativity constraint $u^{m+1} \geq 0$, as shown in Section 4.3.4.

Remark 4.3.15. *Showing uniqueness of solution of the linear scheme* (4.6) *would imply that, as observed in the numerical tests, its solution is nonnegative without explicitly imposing the nonnegativity restriction $u^{m+1} \geq 0$. However, this is not straightforward and it might require using inverse and trace inequalities that would probably involve some kind of restriction on the time step and mesh size, and this is left to a future work.*

In fact, one could probably derive some sort of constraint, similarly to that in (2.17)*, that guarantees uniqueness of solution for small enough Δt. However, in this case it would not be easy to ensure that condition in practice.*

4.3.4 Numerical experiments

We confine our numerical studies to the parabolic-elliptic-elliptic version ($\tau = 0$) of the problem (4.1), since we expect the results to be similar when $\tau = 1$ and for model (4.2). Some tests in similar attraction-repulsion contexts for the case $\tau = 1$ can be found, for instance, in [84], where an algebraic flux correction technique is used for the spatial approximation.

In this sense, we provide numerical examples in accordance to the results in Section 4.3.2. Moreover, we show that suppression of some of the above conditions (and in particular those associated to the gradient nonlinearities), seems to lead to only local solution (i.e., T finite) that blows up at T.

Here, we define $f_1(u) = u^\alpha$, $f_2(u) = u^\beta$ and we assume that all the parameters are set to 1, but $k = 1.1$, unless otherwise specified. For the sake of clarity, we also indicate in the figures any different value of the parameters with respect to those already fixed.

Remark 4.3.16. *Notice that the functions $f_1(u) = u^\alpha$, $f_2(u) = u^\beta$ do not necessarily satisfy Hypotheses 4.3.2 and 4.3.3 for every $\alpha, \beta > 0$. However, these functions are more physically meaningful than other similar choices of the type $f_1(u) = (u + \eta)^\alpha$, $f_2(u) = (u + \eta)^\beta$ for $\eta > 0$ and, ultimately, we expect the behavior of the solution to be similar to the case $\eta > 0$ very small.*

As in Section 3.5, following Remark 3.5.1, we cannot expect an actual blow-up in the discrete case as it occurs in the continuous model. In this sense, since an accurate discrete solution idealizing such blow-up scenario will exhibit a mass accumulation in small regions of the domain, we establish that blow-up occurs when, after that, the norm $\|\cdot\|_{L^\infty(\Omega)}$ of the approximated solutions stabilizes over time (as in Section 3.5 and [23, 168]).

In order to compute the numerical tests, we have used the Python interface of the open source library `FEniCSx` [13, 166, 167] and the open source libraries `PyVista` [175] and `Matplotlib` [119] to generate the plots.

In practice, in each time step, we have first computed a $\mathbb{P}_1^{\text{cont}}(\mathcal{T}_h)$ approximation of the chemical signals v and w following the ideas in Section 4.3.3. Then, we have used the linear scheme (4.6) without explicitly enforcing the nonnegativity constraint $u^{m+1} \geq 0$, obtaining a positive approximation of the cell density, u^{m+1}, for every case below without needing any constraint on the time step or the mesh size. This strategy has allowed us to carry out the computationally demanding three-dimensional tests shown in the following section with not much computational effort.

4.3.4.1 Linear and only attraction model with linear production

In this first example, we consider a three-dimensional version ($d = 3$) of model (4.1) defined in the spatial domain $\Omega = \{(x, y, z) \in \mathbb{R}^3 \colon x^2 + y^2 + z^2 < 1\}$ with the following initial condition

$$u_0(x, y, z) := 500e^{-35(x^2+y^2+z^2)},$$

plotted in Figure 4.1a. Moreover, we take $\chi = 5$ and $\xi = 0$ (no repulsion) and we use a mesh of size $h \approx 4.4 \cdot 10^{-2}$ and a time step $\Delta t = 10^{-5}$.

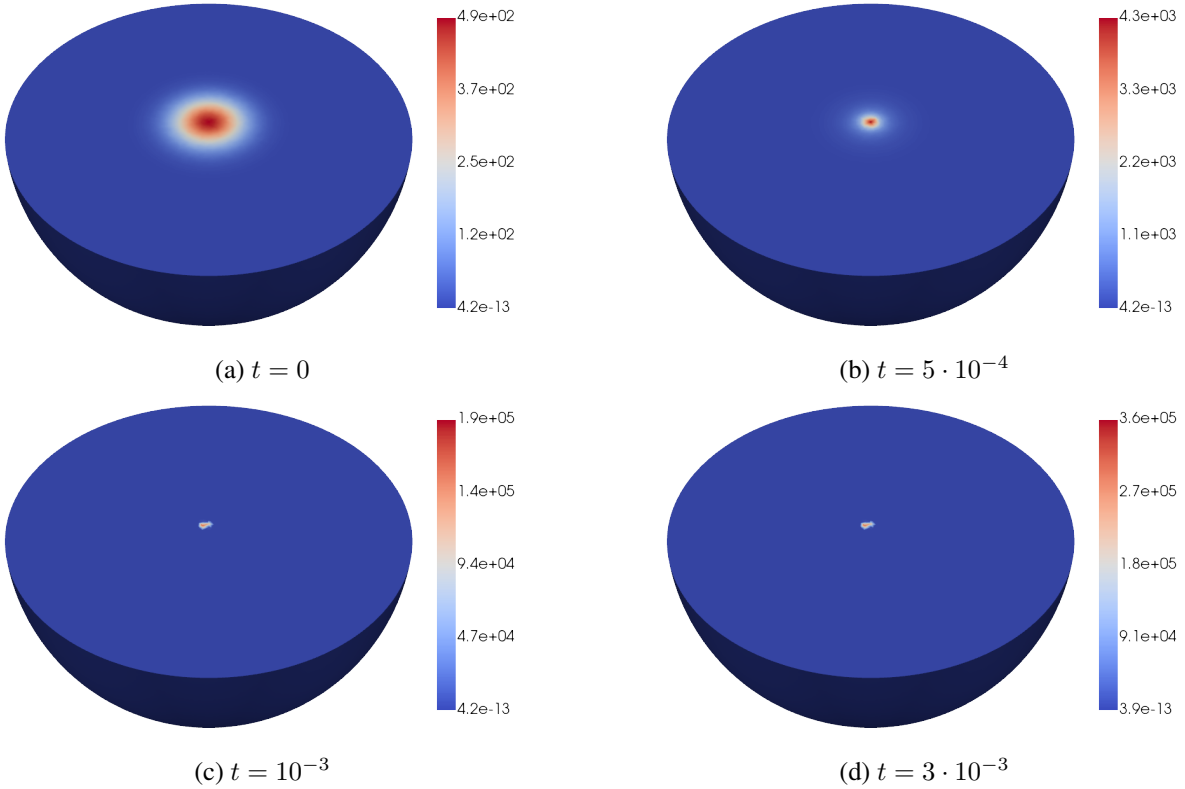

(a) $t = 0$ (b) $t = 5 \cdot 10^{-4}$

(c) $t = 10^{-3}$ (d) $t = 3 \cdot 10^{-3}$

Figure 4.1 Approximation of the solution u at different time steps ($c = 0$, $\chi = 5$, $\xi = 0$)

In Figure 4.1 the approximation obtained with $c = 0$ is plotted at different time steps. We can observe that a blow-up phenomenon seems to appear, according with the analytical results given in [187].

Notice that $k = 1.1 < 7/6 \approx 1.167$ so the condition

$$k < \begin{cases} \frac{7}{6}, & \text{if } d \in \{3, 4\}, \\ 1 + \frac{1}{2(d-1)}, & \text{if } d \geq 5, \end{cases}$$

in [187, Theorem 1.1] is satisfied.

This blow-up phenomenon can be prevented using the dampening gradient as shown in Theorem 4.3.8. In this sense, we show in Figure 4.2 the evolution of the maximum of the approximations for different choices of c and γ. As expected, the blow up is prevented for whatever choice of $c > 0$ (even for small values like $c = 10^{-3}$) if γ satisfies the bound 4.4, i.e., $1.5 < \gamma \leq 2$ (see Figure 4.2a). However, in case that γ does not comply with 4.4, we may require a big enough value of c to prevent the blow-up. This value of c apparently preventing the chemotactic collapse increases as long as γ moves away from the critical value $\gamma^* = 1.5$ for which the equality holds in 4.4 (see Figures 4.2b and 4.2c).

4.3.4.2 Fully nonlinear attraction-repulsion model

Motivated by [55], let us analyze model (4.1) under the assumption that

$$n_2 = n_3, n_1 \in \mathbb{R}, \alpha > \beta \quad \text{and} \quad \begin{cases} n_2 + \alpha > \max\{n_1 + \frac{2}{d}k, k\} & \text{if } n_1 \geq 0, \\ n_2 + \alpha > \max\{\frac{2}{d}k, k\} & \text{if } n_1 < 0. \end{cases} \tag{4.12}$$

In particular, we focus on the 2D case ($n = 2$) in the domain $\Omega = \{(x, y) \colon x^2 + y^2 < 1\}$. We set $\alpha = 1.5$ (in this case $\xi = \chi = 1$) and define the following initial condition

$$u_0(x, y) \coloneqq 500e^{-35(x^2+y^2)},$$

plotted in Figure 4.3a. Also, we take a spatial and a temporal partition of sizes $h \approx 1.37 \cdot 10^{-2}$ and $\Delta t = 10^{-6}$, respectively.

First, in Figure 4.3 we plot the evolution of u over time without the dampening gradient term, i.e. $c = 0$. We observe that due to the choice of the parameters and the initial condition, it seems to occur a blow-up phenomenon, in accordance with the results in [55, Theorem 3] under the restriction (4.12).

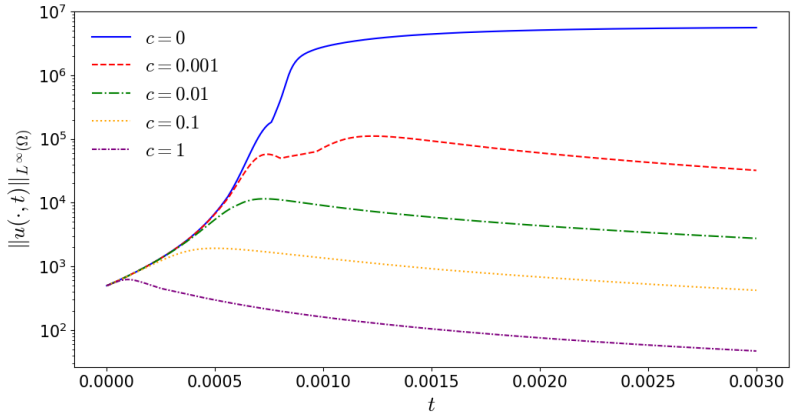

(a) $\gamma = 1.75$

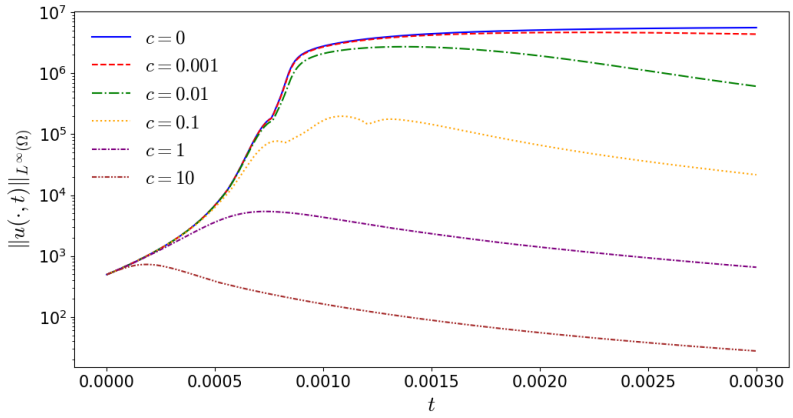

(b) $\gamma = 1.4$

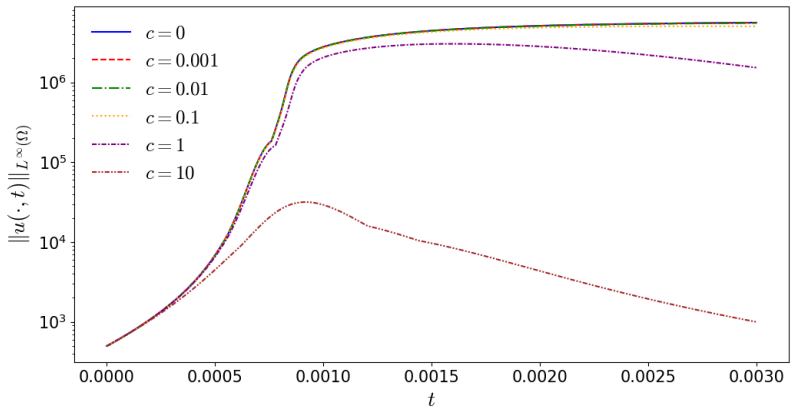

(c) $\gamma = 1.1$

Figure 4.2 Maximum of the approximation of u over time for different values of c and γ ($\chi = 5, \xi = 0$)

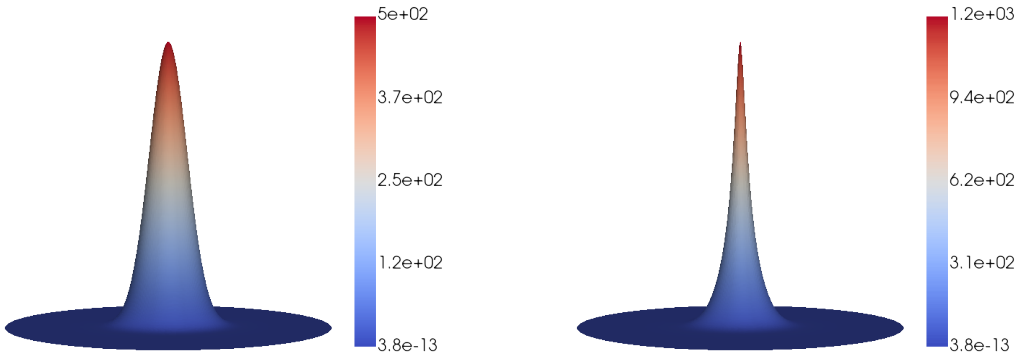

(a) $t = 0$ (b) $t = 5 \cdot 10^{-5}$

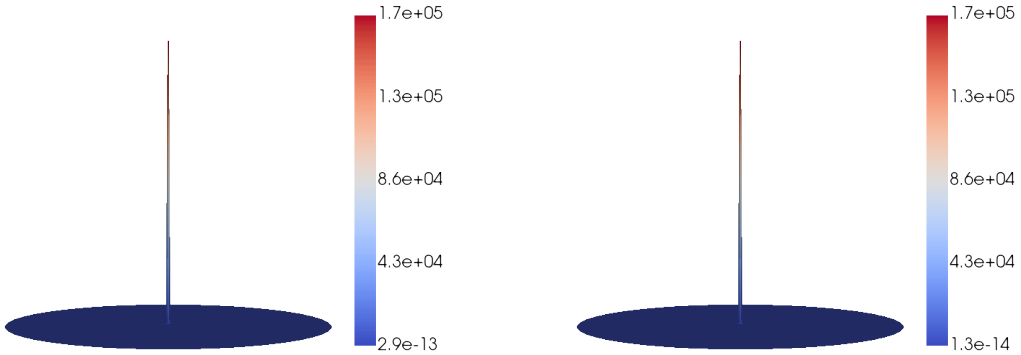

(c) $t = 10^{-4}$ (d) $t = 3 \cdot 10^{-4}$

Figure 4.3 Approximation of the solution u at different time steps ($n_1 = 1$, $c = 0$, $\alpha = 1.5$)

In fact, if we use a nonlinear diffusion term moving the value of n_1 we can observe in Figure 4.4 that we still obtain a chemotactic collapse but with different blow-up times. As expected, one may notice that the blow-up time increases with n_1.

Moreover, as it occurred with the previous example, if we introduce the dampening gradient nonlinearities using a strictly positive small value for c, such as $c = 10^{-3}$, the blow-up phenomenon is avoided if we stick to the bounds on γ given in 4.4, i.e. $1.67 \approx 5/3 < \gamma \leq 2$, as stated in Theorem 4.3.8. However, this singularity seems to remain for a small enough value of c if γ does not satisfy 4.4. See Figure 4.5.

4.4 Chemotactic processes in neuroblast migration

New neurons are generated in the adult rodent brain in specialized regions in which neural stem cells (NSC) are activated to produce neurons in a hierarchical process named neurogenesis. One of these regions is the subventricular zone (SVZ) [155]. Activation of NSC induce their cell cycle entrance

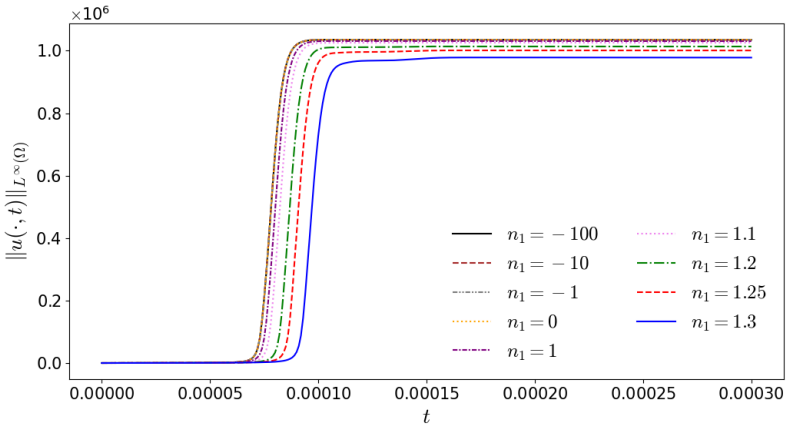

Figure 4.4 Maximum of the approximation of u for different values of n_1 ($c = 0$, $\alpha = 1.5$)

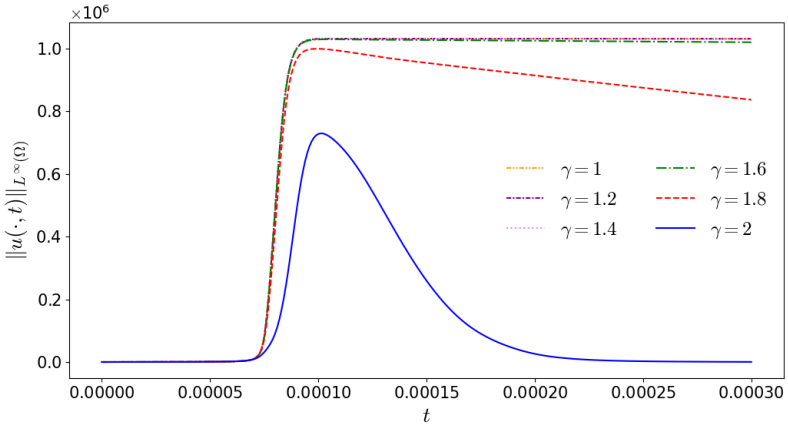

Figure 4.5 Maximum of the approximation of u for different values of γ ($n_1 = 1$, $c = 10^{-3}$, $\alpha = 1.5$)

and posterior division to produce transit amplifying actively dividing progenitors that will give rise to neuronal progenitors or neuroblasts [50]. Newly generated neuroblasts migrate from the SVZ toward the olfactory bulb (OB) through the rostral migratory stream (RMS) while still dividing [159] contributing to the continuous neuronal replacement in the OB. Neurons produced in this homeostatic mechanisms integrate into existing circuits and participate in olfaction [130].

Tens of thousands of neuroblasts migrate daily through the RMS travelling long distances toward the OB, where they integrate as inhibitory interneurons [15, 37, 143, 152]. These cells display an exploratory pattern while moving long distances [153]. On this way along the adult RMS, neuroblasts border the corpus callosum (CC), a bundle of nerve fibers located between the left and right cerebral

hemispheres, where the movement of neuroblasts is hindered due to the presence of a glial sheath deliniating the RMS and the low density of blood vessels in the CC, which they use as scaffold [131].

The importance of the homeostatic migration of neuroblasts toward the OB in the adult brain is highlighted by the fact that in models of brain damage an altered migration pattern is found. Several models of brain damage show an altered migration of SVZ neuroblasts that are different depending on the type of damage. Thus, in a murine model of Alzheimer's disease the proportion of migrating cells in the RMS is lower than in healthy mice [75]. In other models, such as murine models of Huntington's disease, migration toward the OB is reduced as well accompanied by an altered pattern of migration that direct neuroblasts toward the striatum avoiding the OB pathway [122, 129]. Alterations of neuroblast migration are also observed in cortical injuries generated by ischemic lesions, in which SVZ neurogenesis is stimulated in response to the injury and in some cases chains of neuroblast can be seen migrating toward the injured region [146].

All these reports suggest that stimulating neurogenesis in the SVZ and conducting neuroblasts toward the injured region may be of use at designing strategies to regenerate damaged brain regions. Notwithstanding, although neurogenesis and neuroblast migration in the adult brain of mammals has been studied in depth over the past two decades from an anatomical and physiological point of view, and despite the considerable amount of data available over the years, up to our knowledge no mathematical or computational model has been published to date describing the neuroblast migration toward the OB. This type of models could be of great value as a first approximation to describe more complex phenomena, such as the movement of neuroblasts towards brain lesions.

In Section 4.4.1 we present a mathematical model of neuroblast migration to the olfactory bulb, based on the following hypothesis: the movement of neuroblasts is due to a transport phenomenon exerted by certain attraction or *chemotaxis* velocity towards the OB. Altough technically not of chemotaxis type, our model is inspired by chemotactic biological processes through which a population of organisms (or cells) migrate in response to a chemical stimulus. More specifically, we suppose that there exists a function to be identified whose gradient drive the transport of neuroblasts. The PDE is supplemented with some extra reaction terms described below, modelling the birth of neuroblasts and their disappearance, for instance, due to their evolution into mature neurons.

Moreover, in Section 4.4.2 we have developed a discrete approximation of the proposed mathematical model of neuroblast migration in the mammalian brain using the ideas of the discrete upwind DG

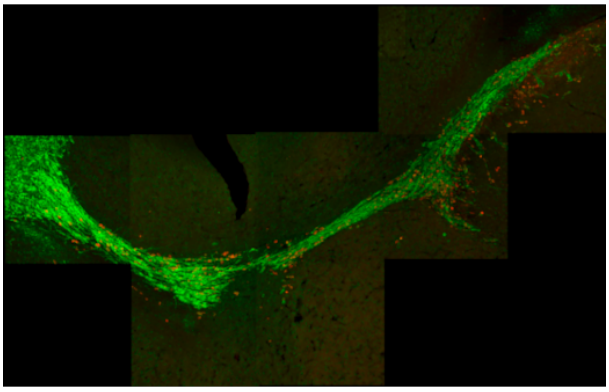

Figure 4.6 Original image (provided by the research group *INIBICA INCO-5*), obtained from real data, showing neuroblast distribution in a rodent brain

schemes in Section 2.3.2. Finally, we show several numerical simulations of the migration process in Section 4.4.3 where the model has been calibrated and validated using real data experimentally obtained by the research group *INIBICA INCO-5* led by Dr. Carmen Castro-González (the details can be consulted in [6]). The computational results match qualitatively the real neuroblasts distribution identified in experimental images of the rodent brain as the red spots in Figure 4.6. which are neuroblasts marked with the bromodeoxyuridine (BrdU).

A further discussion of the model, the results and the preliminary parameter fitting using real data can be read in [6].

4.4.1 Neuroblasts migration model

In this section, we present a model for migration of neuroblasts towards the OB along the RMS, starting from the SVZ and rounding the CC. Here we assume that the shape of this RMS path can be modeled by means of an attraction function which has been previously designed.

Let us fix a space-time domain $\Omega \times (0,T)$, where $\Omega \subset \mathbb{R}^2$, is an open set representing a rodent brain, with boundary $\partial\Omega$. We consider the following PDE for $u = u(\boldsymbol{x},t) \geq 0$ the density of neuroblasts,

$$\tau u_t + \chi \nabla \cdot (u \nabla \mathcal{O}) + \alpha\, u - \gamma\, u\, \mathbb{1}_{NZ} = \beta\, \mathbb{1}_{SVZ} \qquad \text{in } \Omega \times (0,T), \tag{4.13}$$

where $\mathcal{O} = \mathcal{O}(\boldsymbol{x}) \in \mathbb{R}$ is a potential function such that its gradient $\nabla\mathcal{O}$ models the attraction exerted by the olfactory bulb. Since we consider that neuroblasts cannot cross the brain boundary, we must choice $\mathcal{O}$

such that there is not entrance boundary, which mathematically means

$$\nabla \mathcal{O} \cdot \mathbf{n} \geq 0 \ \text{ on } \ \partial\Omega.$$

The precise definition of this function $\mathcal{O}$, reflecting the heterogeneity of the brain with respect to the neuroblast migration, is detailed in [6]. In any case, $\mathcal{O}$ depends on a parameter $\sigma > 0$, related to the spread of neuroblasts along the domain.

On the other hand, the parameter $\chi > 0$ is the amplitude of this attraction, $\alpha > 0$ is the death rate along the domain and $\beta > 0$ is related to the amount of neuroblasts which are generated in the SVZ. Also a source term, with coefficient $\gamma > 0$, has been added intended to model a narrowing zone (NZ) in the brain, where some neuroblast contribution occurs in our 2d domain arising from other regions in the real three-dimensional domain. Finally, the parameter $\tau \in \{0, 1\}$ distinguishes the stationary and evolutive cases, respectively.

The system (4.13) is supplemented with the initial condition

$$u(0) = u_0 \ \text{ in } \ \Omega, \tag{4.14}$$

where u_0 is the initial density of neuroblasts obtained as a steady state solution of the proposed model for certain experimentally chosen parameters.

4.4.2 Numerical solution of the neuroblasts model

Now, we introduce the discrete scheme which has been used to approximate the neuroblasts migration model (4.13), Again, here we will use the upwind discontinuous Galerkin method introduced in Section 2.3.2.

Assume that we have:

- An approximation of the initial condition $u_0 \in \mathbb{P}_0^{\text{disc}}(\mathcal{T}_h)$, computed for a certain set of parameters as detailed in [6].
- A chemoattractant function $\mathcal{O} \in \mathbb{P}_1^{\text{disc}}(\mathcal{T}_h)$, defined as the solution to the olfactory bulb problem that can be found in [6] and which depends on the parameter σ.

We approximate the solution of the evolution ($\tau = 1$) system (4.13)–(4.14) using an implicit Euler time scheme and an upwind DG space discretization as follows. For each $m \in \mathbb{N}$ and $u^m \in \mathbb{P}_0^{\text{disc}}(\mathcal{T}_h)$ with $u^m \geq 0$, find $u^{m+1} \in \mathbb{P}_0^{\text{disc}}(\mathcal{T}_h)$ such that, for every $\overline{u} \in \mathbb{P}_0^{\text{disc}}(\mathcal{T}_h)$,

$$\tau\left(\delta_t u^{m+1}, \overline{u}\right) + \chi a_h^{\text{upw}}(\nabla \mathcal{O}; u^{m+1}, \overline{u}) + \alpha\left(u^{m+1}, \overline{u}\right) = \beta\left(\mathbb{1}_{SVZ}, \overline{u}\right) + \gamma\left(\mathbb{1}_{NZ} u^m, \overline{u}\right), \tag{4.15}$$

where $a_h^{\text{upw}}(\cdot;\cdot,\cdot)$ is the bilinear form defined in (4.7). In practice, we are going to take $\beta = 0$, that is no new neuroblasts are generated in the SVZ. The reason is that the unknown u^m represents the density of those neuroblasts which, at the initial time, were marked with BrdU. And no new marked neuroblasts appear in later times.

The proof of the following theorem easily follows using the same techniques that have been previously introduced in Sections 2.3.2, 3.4 and 4.3.3.

Theorem 4.4.1. *There is a solution of the scheme* (4.15) *which satisfies* $u^{m+1} \geq 0$ *and*

$$\int_\Omega u^{m+1} \leq \frac{1}{\tau + \alpha\Delta t}\left(\tau \int_\Omega u^m + \beta\Delta t|\Omega_{SVZ}| + \gamma\Delta t \int_{\Omega_{NZ}} u^m\right).$$

In fact, again one can use a truncated scheme to enforce the positivity of the approximation in (4.15). However, in practice, like (4.6), the scheme (4.15) has been able to provide a positive approximation without heeding a specific restriction on the time step or the mesh size to enforce uniqueness of solution.

4.4.3 Numerical tests

The numerical scheme (4.15) described above has been applied to develop computer programs that allow solving the PDE model for simulation of migration of neuroblasts in the brain, yielding concrete data and comparing it to experimental data obtained from real rodent brains, see [6]. The final target is calibrating the model parameters so that its output is matched as closely as possible to the real data.

In this section, since the parameter fitting is beyond the scope of this work, we will just focus on the numerical approximation of the model (4.13).

We would like to thank and give credit to Noelia Ortega-Román for the parameter fitting, computing the numerical results and generating all the images shown in this section, in Figures 4.7, 4.8, 4.9, 4.10 and 4.11. These results and graphs can be also found in [6].

4.4.3.1 Computer implementation in a realistic domain

As to the computer implementation of the scheme (4.15), we have defined a mesh of a virtual rodent brain, see Figure 4.7. In this mesh, the triangles that are located in the CC have been identified (colored in black) and also those triangles laying in the SVZ and in the NZ (shown in red and green, respectively).

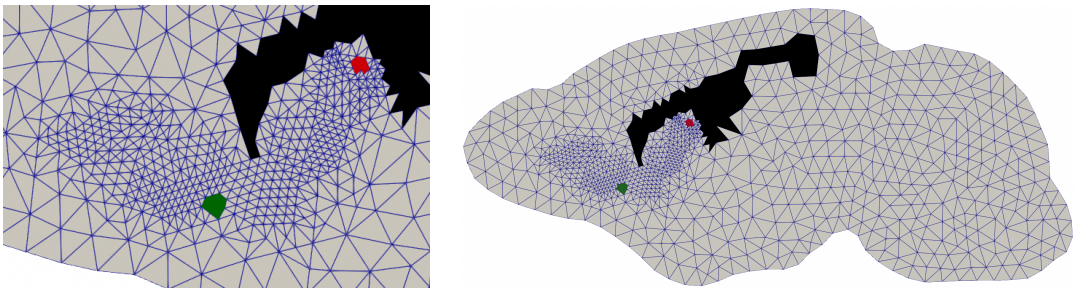

Figure 4.7 Right: mesh of a virtual rodent brain. Left: zoom around the RMS. Triangles defining the CC, SVZ and NZ are shown in black, red and green color, respectively

It is worth noting that the mesh shown in Figure 4.7 is actually the one resulting from refining and saving a coarser mesh that was initially built. Specifically, we build an initial mesh of the brain domain and then we refine it in the area where the RMS is expected to be located. We identify this area by a preliminar calculus of the initial condition u_0, obtained as a solution of the stationary ($\tau = 0$) equation (4.13), then we refine those triangles where $u_0 > \varepsilon$, where ε is a prescribed small constant. Using this refined mesh allows us to compute a more accurate solution for neuroblasts distribution in the region of interest, without significantly increasing the computational effort.

The final mesh we are using in our numerical tests, $\mathcal{T}_h$, is made of 2003 triangles with size $h \in [3.313 \cdot 10^{-3}, 4.814 \cdot 10^{-2}]$. For the time discretization, we define an uniform partition $t_0 < \ldots < t_m < \ldots < t_M$ of the time interval $[0, T]$ with $T = 4$ days and constant size $k = t_m - t_{m-1} = 0.04$. We use the library `FEniCS` [14] to load the mesh and code the scheme (4.15).

4.4.3.2 Computational results

More in detail, we follow the next steps in order to provide an approximation of the neuroblast migration process to the olfactory bulb:

1. For each olfactory bulb shape parameter σ, we compute a $\mathbb{P}_1^{\text{cont}}(\mathcal{T}_h)$ approximation of $\mathcal{O}$ as detailed in [6]. This olfactory bulb function $\mathcal{O}$ is one of the keys in our model and will determine the migration of neuroblasts, driven by $\nabla\mathcal{O}$ and thus orthogonal to the isolines of $\mathcal{O}$ (see Figure 4.8).

2. Given an attraction function $\mathcal{O}$ depending on parameter σ and given the positive parameters α, β, γ, χ an initial condition $u_0 \in \mathbb{P}_0^{\text{disc}}(\mathcal{T}_h)$ can be computed solving problem (4.15) with $\tau = 0$.

3. Then, for the same or different parameters, we can compute the neuroblast distribution $u^{m+1} \in \mathbb{P}_0^{\text{disc}}(\mathcal{T}_h)$ solving (4.15) with $\tau = 1$ at each time step in t_{m+1}.

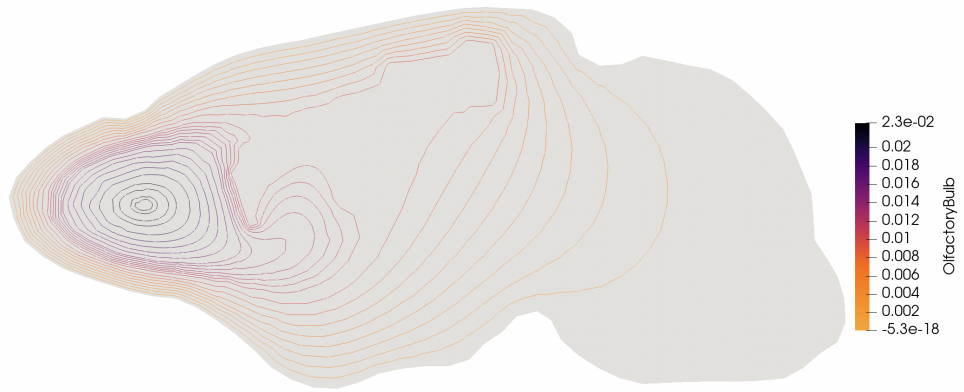

Figure 4.8 Isolines of the olfactory bulb function, $\mathcal{O}$, obtained from parameter optimization

Therefore, after a preliminary adjustment of the parameters and the computation of the suitable olfactory bulb attraction function in Figure 4.8 (see [6] for details) we obtain a satisfactory approximation of the initial condition shown in Figures 4.9, which agree with the real phenomena from Figure 4.10. This approximation of the initial distribution of neuroblasts not only qualitatively matches the behavior in the real picture of the brain but also quantitatively. The quantitative comparison between the model and the real data is shown in [6].

Then, starting from the initial solution u_0 that has been already computed and adjusting the parameters again so as to fit the real data, we can derive an approximation of the evolution of the neuroblasts migration process to the olfactory bulb. This process is shown in Figure 4.11.

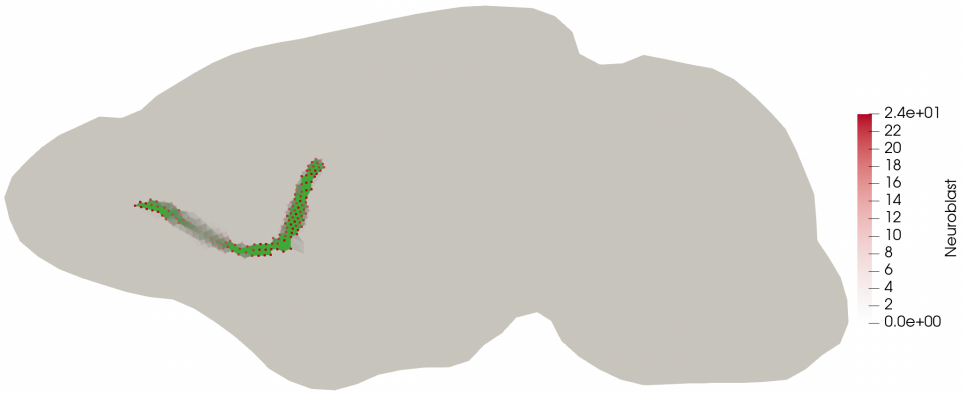

Figure 4.9 Steady neuroblast density (approximation of u_0)

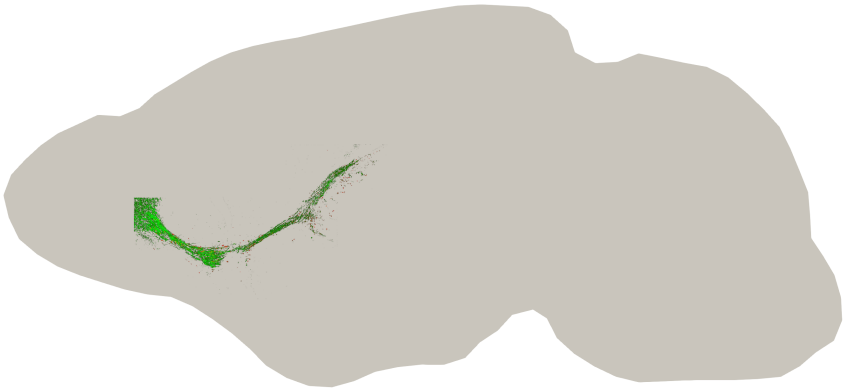

Figure 4.10 Real steady neuroblast density

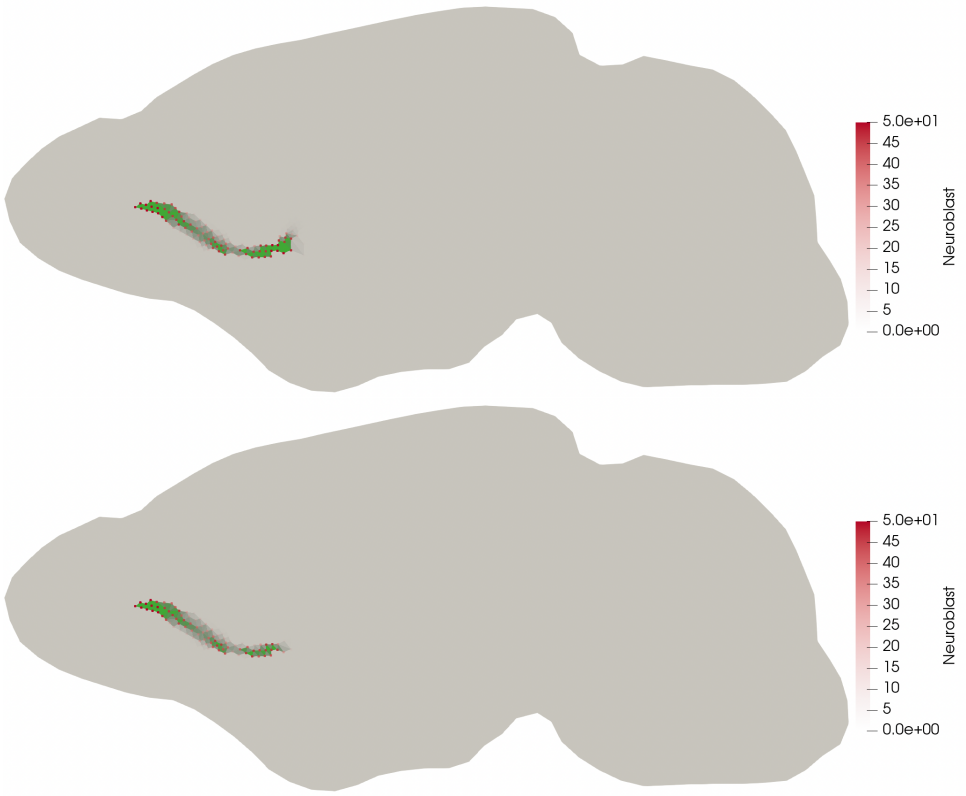

Figure 4.11 Evolution of neuroblast density after two days (top) and four days (bottom)

CHAPTER 5

A STRUCTURE-PRESERVING UPWIND DG SCHEME FOR A DEGENERATE PHASE-FIELD TUMOR MODEL

5.1 Abstract

In this chapter, we present a modification of the phase-field tumor growth model given in [113] that leads to bounded, more physically meaningful, volume fraction variables. In addition, we develop an upwind discontinuous Galerkin (DG) scheme preserving the mass conservation, pointwise bounds and energy stability of the continuous model. Finally, some computational tests in accordance with the theoretical results are introduced. In the first test, we compare our DG scheme with the finite element (FE) scheme related to the same time approximation. The DG scheme shows a well-behavior even for strong cross-diffusion effects in contrast with FE where numerical spurious oscillations appear. Moreover, the second test exhibits the behavior of the tumor-growth model under different choices of parameters and also of mobility and proliferation functions. The results of this chapter have been already published in [2].

5.2 Introduction

Lately, significant work on the mathematical modeling of tumor growth has been carried out. As a result, many different models have arisen, some of which have even been applied to predict the response of the tumor to its surrounding environment and possible medical treatments. Most of these models can be classified into micro-scale discrete models, macro-scale continuum models or hybrid models, [57, 145]. Regarding the continuum models, different approaches has been developed among which we can find models using both ODE, for instance, [46, 147], and PDE, for example, [79, 164].

In this sense, phase-field models such as the Cahn-Hilliard (CH) equation have become a very popular tool. This model describes the evolution of a thin, diffuse, interface between two different phases or states of a process [36, 154] through a so-called phase-field variable, which minimizes an adequate

free energy. Sometimes, this CH model is coupled with a degenerate mobility to impose phase-related pointwise bounds on this variable.

In particular, in the context of tumor modeling, the phase-field variable u is usually interpreted as a tumor volume-fraction (with $0 \leq u \leq 1$) and this model is coupled with other equations describing the interaction between the tumor and the surrounding environment. Some examples of these tumor models can be found in [19, 85, 88, 91, 113, 173, 189] and the references therein. Often, certain physical properties, inherited from the Cahn-Hilliard equation, are inherent to the solution of these models such as mass-conservation of a biological substance, pointwise bounds on some of the variables and some sort of energy-dissipation.

In this chapter, we consider the model (5.1) carefully derived from mixture theory by Hawkins-Daarud et al. in [113], which describes the interaction between a tumor and the nutrients in the extracellular water. To this aim, the CH equation for u is coupled with a diffusion equation for the nutrients n by means of some reaction and cross-diffusion terms. Although this model does not take into account some of the complex processes involved in the surrounding environment of the tumor, it allowed the authors to capture some irregular growth patterns that are typically associated with these processes. However, while this model is mass-conservative and energy-dissipative, it does not implicitly impose the necessary pointwise bounds on the volume fraction variables.

Therefore, we propose a modification of the aforementioned tumor model, see (5.3) below, in accordance with its physical interpretation. As a result of this modification, we obtain pointwise bounds on the tumor and the nutrient volume fractions ($0 \leq u, n \leq 1$) which are consistent with the physical meaning of the variables. This modification may help to a future application of this model (or a variant of it) for real tumor growth prediction.

This phase-field tumor model (5.3) consist of a system of coupled nonlinear equations where reaction and cross diffusion effects appear. Thus, dealing with this model is really challenging both from a theoretical and the computational point of view.

In the case of the Cahn-Hilliard equation itself, several advances have been published regarding the existence and regularity of solution, most of which can be found in [150] and the references therein. Also, one can find several results regarding the existence, regularity and long-time behavior of the solution of the tumor model (5.1) and variants in the literature in the case without cross-diffusion, see [51, 52,

53, 87]. Recently, the well-posedness and the long-time behavior of the model (5.1) with cross-diffusion have been addressed in the work by H. Garcke and S. Yayla, [96].

Regarding the numerical approximation of these equations, significant advances have been done both with respect to the time and the spatial discretizations.

On the one hand, the classical approach for the time discretization of the phase-field models is the convex-splitting decomposition introduced in [77] which preserves the energy stability. Nonetheless, other time-discrete schemes have been introduced in the literature (see, for instance, [105, 106, 180]). Among these time approximations we find the idea of introducing a Lagrange multiplier in the potential term in [24] which was extended in [105, 106, 180]. This idea led to the popular energy quadratization (EQ) schemes [192, 193, 194], later extended to the scalar auxiliary variable (SAV) approach [169].

On the other hand, in the case of the Cahn-Hilliard equation with degenerate mobility, designing a suitable spatial discretization consistent with the physical properties of the model, specially the pointwise bounds, is a difficult task and only a few works have been published in this regard. Among the currently available structure-preserving schemes we can find some schemes based on finite volumes, [25, 118], and on finite elements, [27, 103]. Moreover, we have developed in Chapter 2 a numerical scheme where the pointwise bounds of the CH model in the case with convection are preserved using an upwind discontinuous Galerkin (DG) approximation. To our best knowledge, no previous work has been published defining a fully discrete DG scheme preserving the mass conservation, pointwise bounds and energy stability of the CH model with degenerate mobility.

The difficulties of the discretization are emphasized in the case of phase-field tumor models. In particular, in [113] an energy-stable finite element scheme with a first-order convex-splitting scheme in time is proposed for (5.1) and extended in [190] to a second-order time discretization. Other types of approximations of this model (5.1) using meshless collocation methods, [62], stabilized element-free Galerkin method, [151], and SAV Fourier-spectral method, [171], can be found in the literature. However, no bounds are imposed on the discrete variables whatsoever.

In this sense, we introduce a well-suited convex-splitting DG scheme of the proposed model (5.3), based on [120] and the previous work in Chapters 2 and 3. This approximation preserves the physical properties of the phase-field tumor model (mass conservation, pointwise bounds and energy stability) and prevent numerical spurious oscillations. This scheme can be applied, in particular, to the more simple CH model with degenerate mobility itself preserving all of the aforementioned properties.

This chapter is organized as follows: in Section 5.3 we discuss the tumor model (5.1), which was derived in [113], and we introduce our modified version of this model, (5.3), showing its physical properties. In Section 5.4 we develop our numerical approximation of the tumor model (5.3). We introduce the convex-splitting time-discrete scheme (5.12) in Section 5.4.1. Moreover, we present the DG space approximation, (5.17), in Section 5.4.2, defining the upwind form (5.21) in Section 5.4.2.1. Then, we analyze the properties of the fully discrete scheme in Section 5.4.2.2. Finally, we compute a couple of numerical experiments in Section 5.5. Specifically, in Section (5.5.1), we present a numerical comparison between the robust DG scheme (5.17) and a FE discretization of (5.12), the latter of which fails in the case of strong cross-diffusion. In Section 5.5.2, we show the behavior of the model (5.3) under different choices of parameters and mobility/proliferation functions.

The results of this chapter have already been published in [2].

5.3 Modified tumor model

The following tumor-growth model was introduced in [113] and further studied in [190]:

$$\partial_t u = \nabla \cdot (M_u \nabla \mu_u) + \delta P(u)(\mu_n - \mu_u) \qquad \text{in } \Omega \times (0,T), \tag{5.1a}$$

$$\mu_u = F'(u) - \varepsilon^2 \Delta u - \chi_0 n \qquad \text{in } \Omega \times (0,T), \tag{5.1b}$$

$$\partial_t n = \nabla \cdot (M_n \nabla \mu_n) - \delta P(u)(\mu_n - \mu_u) \qquad \text{in } \Omega \times (0,T), \tag{5.1c}$$

$$\nabla u \cdot \mathbf{n} = (M_n \nabla \mu_n) \cdot \mathbf{n} = (M_u \nabla \mu_u) \cdot \mathbf{n} = 0 \qquad \text{on } \partial\Omega \times (0,T), \tag{5.1d}$$

$$u(0) = u_0, \quad n(0) = n_0 \qquad \text{in } \Omega, \tag{5.1e}$$

where

$$\mu_n = \frac{1}{\delta} n - \chi_0 u \quad \text{in } \Omega \times (0,T) \tag{5.2}$$

and $u_0, n_0 \in L^2(\Omega)$. In this model, u and n represent the tumor cells and the nutrient-rich extracellular water volume fractions, respectively. Therefore, these variables are assumed to be bounded in $[0,1]$. Moreover, μ_u and μ_n are the (chemical) potentials of u and n, respectively.

The behavior of the cells is modeled using a Cahn-Hilliard equation, where

$$F(u) = \frac{1}{4} u^2 (1-u)^2$$

is the Ginzburg-Landau double well potential and M_u is the mobility of the tumor, which is taken either as constant or degenerated at $u = 0$, for instance, $M_u(u) = \widehat{M}u^2$ with $\widehat{M} > 0$. The parameter $\varepsilon \geq 0$ is related to the thickness of the interface between the tumor phases $u = 1$ (fully saturated) and $u = 0$ (fully unsaturated).

On the other hand, the nutrients are modeled using a diffusion equation where the function M_n is the mobility of the nutrients, which is taken as constant in practice.

These equations are coupled by cross diffusion terms (multiplied by the coefficient $\chi_0 \geq 0$) introduced in (5.1b) and (5.2) that model the attraction between tumor cells and nutrients. In addition, reaction terms modeling the consumption of nutrients by the tumor cells appear in (5.1a) and (5.1c), where $P(u)$ is a proliferation term that vanishes when $u \leq 0$ in [113] or when $u \notin (0, 1)$ in [190]. These reaction terms depend on the difference between the potentials, which is assumed to be positive as the parameter $\delta > 0$ is very small, because one has the approximation

$$\delta P(u)(\mu_n - \mu_u) = P(u)(n - \delta(\chi_0 u - \mu_u)) \simeq P(u)n \quad \text{if } \delta \approx 0.$$

The well-posedness and long-time behavior of the model (5.1) and some variants have been considered in the case without cross-diffusion ($\chi_0 = 0$), see [51, 52, 53, 87], and only recently in the case with cross diffusion ($\chi_0 > 0$) in [96].

In this work, taking into account the previous considerations, we introduce the following modified phase-field tumor model

$$\partial_t u = C_u \nabla \cdot (M(u)\nabla \mu_u) + \delta P_0 P(u, n)(\mu_n - \mu_u)_{\oplus} \qquad \text{in } \Omega \times (0, T), \tag{5.3a}$$

$$\mu_u = F'(u) - \varepsilon^2 \Delta u - \chi_0 n \qquad \text{in } \Omega \times (0, T), \tag{5.3b}$$

$$\partial_t n = C_n \nabla \cdot (M(n)\nabla \mu_n) - \delta P_0 P(u, n)(\mu_n - \mu_u)_{\oplus} \qquad \text{in } \Omega \times (0, T), \tag{5.3c}$$

$$\nabla u \cdot \mathbf{n} = (M(n)\nabla \mu_n) \cdot \mathbf{n} = (M(u)\nabla \mu_u) \cdot \mathbf{n} = 0 \qquad \text{on } \partial\Omega \times (0, T), \tag{5.3d}$$

$$u(0) = u_0, \quad n(0) = n_0 \qquad \text{in } \Omega, \tag{5.3e}$$

where

$$\mu_n = \frac{1}{\delta} n - \chi_0 u \quad \text{in } \Omega \times (0, T), \tag{5.4}$$

$u_0, n_0 \in L^2(\Omega)$, $F(u) = \frac{1}{4}u^2(1-u)^2$ and all the parameters above are nonnegative with $\delta, C_u, C_n > 0$ and $\varepsilon, \chi_0, P_0 \geq 0$. Also, we define the following family of degenerate mobilities

$$M(v) \coloneqq h_{p,q}(v), \tag{5.5}$$

for certain $p, q \in \mathbb{N}$ where

$$h_{p,q}(v) \coloneqq K_{p,q} v_{\oplus}^{p}(1-v)_{\oplus}^{q} = \begin{cases} K_{p,q} v^p (1-v)^q, & v \in [0,1], \\ 0, & \text{elsewhere}, \end{cases}$$

with $K_{p,q} > 0$ a constant so that $\max_{x\in\mathbb{R}} h_{p,q}(v) = 1$, hence $M(v)$ is a degenerate and normalized mobility. In addition, we define the proliferation function depending on both cells and nutrients as

$$P(u,n) \coloneqq h_{r,s}(u) n_{\oplus}, \tag{5.6}$$

for certain $r, s \in \mathbb{N}$.

Notice that the mobility functions, defined in (5.5), for the tumor and for the nutrients do not necessarily need to be identical. One may consider the tumor mobility as $M_u(u) = h_{p,q}(u)$ with $p, q \in \mathbb{N}$ and the nutrients mobility as $M_n(n) = h_{p',q'}(n)$ with $p', q' \in \mathbb{N}$ and all the results below equally hold. However, for simplicity, we will assume that $M_u = M_n$ and denote the mobility function as M.

Remark 5.3.1. *This model introduces several changes with respect to the previous model* (5.1) *studied in [113, 190]. These modifications, described next, involve significant improvements. But also they lead to a more complex model, with degenerate mobility and proliferation functions and major difficulties regarding the analysis of the existence, regularity and long time behavior of solutions.*

Specifically:

- *The difference between the potentials, $\mu_n - \mu_u$ is assumed to be positive since δ is set to be a very small parameter. This difference could possible be negative in the regions where $n \simeq 0$ but, in this case, the reaction terms vanish due to the proliferation function $P(u,n)$ defined in* (5.6)*. Therefore, the positive part of $(\mu_n - \mu_u)$ is taken in* (5.3a) *and* (5.3c)*.*

- *When $\delta \to 0$, the reaction terms in equations* (5.3a) *and* (5.3c) *are assumed to grow with the square of the nutrients volume fraction. In fact*

$$\delta P_0 P(u,n)(\mu_n - \mu_u)_\oplus = P_0 P(u,n)(n - \delta(\chi_0 u - \mu_u))_\oplus \simeq P_0 P(u,n) n = P_0 h_{r,s}(u)(n_\oplus)^2.$$

- *A degenerate mobility,* (5.5)*, is considered for both the phase-field function u and the volume fraction of nutrients n.*

- *The aforementioned modifications imply that u and n must be bounded in the interval $[0,1]$ (see Theorem 5.3.3), what matches the physical assumptions of the model since u and n are assumed to be volume fractions. This is a clear improvement over previous approaches, such us the ones considered in [113, 190], where the solution does not necessarily satisfy these bounds.*

Remark 5.3.2. *In practice, $C_n = \delta D$ with $D > 0$ so that, when $\delta \to 0$, the n-equation is approached by*

$$\partial_t n \simeq D\nabla \cdot (M(n)\nabla n) - P_0 P(u,n) n.$$

Considering that μ_n is explicitly determined by (5.4), we can reduce the number of unknowns and define the weak formulation of (5.3) as: find (u, μ_u, n) with $u, n \in L^2(0,T; H^1(\Omega))$, $\partial_t u, \partial_t n \in L^2(0,T; H^1(\Omega)')$ and $\mu_u \in L^2(0,T; H^1(\Omega))$, which satisfies the following variational problem a.e. $t \in (0,T)$

$$\begin{aligned}
\langle \partial_t u(t), \overline{u} \rangle &= -C_u \left(M(u(t)) \nabla \mu_u(t), \nabla \overline{u} \right) \\
&\quad + \delta P_0 \left(P(u(t), n(t))(\mu_n(t) - \mu_u(t))_\oplus, \overline{u} \right), \qquad \forall \overline{u} \in H^1(\Omega), \qquad (5.7a) \\
(\mu_u(t), \overline{\mu}_u) &= \varepsilon^2 \left(\nabla u(t), \nabla \overline{\mu}_u \right) + \left(F'(u(t)) - \chi_0 n(t), \overline{\mu}_u \right), \qquad \forall \overline{\mu}_u \in H^1(\Omega), \qquad (5.7b) \\
\langle \partial_t n(t), \overline{n} \rangle &= -C_n \left(M(n(t)) \nabla \mu_n(t), \nabla \overline{n} \right) \\
&\quad - \delta P_0 \left(P(u(t), n(t))(\mu_n(t) - \mu_u(t))_\oplus, \overline{n} \right), \qquad \forall \overline{n} \in H^1(\Omega), \qquad (5.7c)
\end{aligned}$$

where

$$\mu_n(t) = \frac{1}{\delta} n(t) - \chi_0 u(t), \qquad (5.8)$$

$u(0) = u_0$, $n(0) = n_0$ and $\langle \cdot, \cdot \rangle$ denotes the dual product over $H^1(\Omega)$.

Since $u, n \in L^2(0,T,H^1(\Omega))$ with $\partial_t u, \partial_t n \in L^2(0,T,H^1(\Omega)')$, it is known, see for instance [61, 74], that $u, n \in \mathcal{C}^0([0,T], L^2(\Omega))$ and that $\langle \partial_t u(t), \overline{u}\rangle = \frac{d}{dt}(u(t), \overline{u})$, $\langle \partial_t n(t), \overline{n}\rangle = \frac{d}{dt}(n(t), \overline{n})$ for a.e. $t \in (0,T)$ and every $\overline{u}, \overline{n} \in H^1(\Omega)$.

Proposition 5.3.3. *Given $u_0, v_0 \in [0,1]$, any solution (u, μ_u, n) of the model* (5.7) *satisfies that $u(t)$ and $n(t)$ are bounded in $[0,1]$ for a.e. $t \in (0,T)$.*

Proof. Let (u, μ_u, n) be a solution of the model (5.7) and $u_0, v_0 \in [0,1]$.

- First, we prove that $u, n \geq 0$. Notice that $u_\ominus \in L^2(0,T,H^1(\Omega))$ and take $\overline{u} = u(t)_\ominus$ for a.e. $t \in (0,T)$ in (5.7a). We arrive at $\frac{1}{2}\frac{d}{dt}\|u(t)_\ominus\|^2_{L^2(\Omega)} = 0$, hence $\|u(t)_\ominus\|_{L^2(\Omega)} = \|u(0)_\ominus\|_{L^2(\Omega)} = 0$. Similarly, $\|n(t)_\ominus\|_{L^2(\Omega)} = 0$ for a.e. $t \in (0,T)$.
- Now, we prove that $u, n \leq 1$. Notice that $(1-u)_\ominus \in L^2(0,T,H^1(\Omega))$, $\partial_t u = \partial_t(u-1)$ and take $\overline{u} = (u(t)-1)_\oplus$ for a.e. $t \in (0,T)$ in (5.7a). We arrive at $\frac{1}{2}\frac{d}{dt}\|(u(t)-1)_\oplus\|^2_{L^2(\Omega)} = 0$, hence $\|(u(t)-1)_\oplus\|_{L^2(\Omega)} = \|(u(0)-1)_\oplus\|_{L^2(\Omega)} = 0$. Similarly, $\frac{1}{2}\frac{d}{dt}\|(n(t)-1)_\oplus\|^2_{L^2(\Omega)} \leq 0$ what implies $\|(n(t)-1)_\oplus\|_{L^2(\Omega)} \leq \|(n(0)-1)_\oplus\|_{L^2(\Omega)} = 0$ for a.e. $t \in (0,T)$.

□

Proposition 5.3.4. *Let (u, μ_u, n) be a solution of the problem* (5.7)*. Then, this solution conserves the total mass of tumor cells and nutrients in the sense of*

$$\frac{d}{dt}\int_\Omega (u(x,t) + n(x,t))dx = 0.$$

Proof. It is enough to take $\overline{u} = \overline{n} = 1$ in (5.7a) and (5.7c) and add the resulting expressions. □

Proposition 5.3.5. *If (u, μ_u, n) is a solution of the problem* (5.7) *with $\partial_t u \in L^2(0,T,H^1(\Omega))$, then it satisfies the following energy law*

$$\begin{aligned}\frac{dE(u(t),n(t))}{dt} &+ C_u\int_\Omega M(u(x,t))|\nabla\mu_u(x,t)|^2dx + C_n\int_\Omega M(n(x,t))|\nabla\mu_n(x,t)|^2dx \\ &+ \delta P_0\int_\Omega P(u(x,t),n(x,t))(\mu_u(x,t)-\mu_n(x,t))^2_\oplus dx = 0,\end{aligned} \tag{5.9}$$

where the energy functional is defined by

$$E(u,n) \coloneqq \int_\Omega \left(\frac{\varepsilon^2}{2}|\nabla u|^2 + F(u) - \chi_0 u\, n + \frac{1}{2\delta}n^2\right). \tag{5.10}$$

Therefore, the solution is energy stable in the sense

$$\frac{d}{dt}E(u(t), n(t)) \leq 0.$$

Proof. Take $\overline{u} = \mu_u(t)$, $\overline{\mu}_u = \partial_t u(t)$, $\overline{n} = \mu_n(t)$ in (5.7a)–(5.7c) and test (5.8) with $\partial_t n(t)$. Adding the resulting expressions we arrive at

$$\begin{aligned}\varepsilon^2 \left(\nabla u(t), \nabla(\partial_t u(t))\right) + \left(F'(u(t)), \partial_t u(t)\right) - \chi_0 \left[(n(t), \partial_t u(t)) + (u(t), \partial_t n(t))\right] + \frac{1}{\delta}\left(n(t), \partial_t n(t)\right) \\ + C_u \int_\Omega M(u(x,t))|\nabla \mu_u(t)|^2 dx + C_n \int_\Omega M(n(x,t))|\nabla \mu_n(t)|^2 dx \\ + \delta P_0 \int_\Omega P(u(x,t), n(x,t))(\mu_u(x,t) - \mu_n(x,t))_\oplus (\mu_u(x,t) - \mu_n(x,t)) dx = 0.\end{aligned}$$

Therefore, it is straightforward to check that (5.9) holds. □

5.4 Numerical approximation

In this section we will develop a well suited approximation of the tumor model (5.3) which preserves the physical properties presented in the previous section.

5.4.1 Time-discrete scheme

Now, we define a convex splitting of the double well potential $F(u)$ as follows:

$$F(u) \coloneqq F_i(u) + F_e(u), \quad F_i(u) \coloneqq \frac{3}{8}u^2, \quad F_e(u) \coloneqq \frac{1}{4}u^4 - \frac{1}{2}u^3 - \frac{1}{8}u^2, \quad u \in [0,1],$$

where we are going to treat the convex term, $F_i(u)$, implicitly and the concave term, $F_e(u)$, explicitly (see Section 2.4.1 and, for instance, [77, 105], for more details). For this, we define

$$f(u^{m+1}, u^m) \coloneqq F_i'(u^{m+1}) + F_e'(u^m) = \frac{1}{4}\left(3u^{m+1} + 4(u^m)^3 - 6(u^m)^2 - u^m\right). \tag{5.11}$$

We propose the following time-discrete scheme: given $(u^m, \mu_u^m, n^m) \in H^1(\Omega)^3$ with $u^m, n^m \in [0,1]$ in Ω, find $(u^{m+1}, \mu_u^{m+1}, n^{m+1}) \in H^1(\Omega)^3$ such that

$$\begin{aligned}
\left(\delta_t u^{m+1}, \overline{u}\right) &= -C_u \left(M(u^{m+1})\nabla \mu_u^{m+1}, \nabla \overline{u}\right) \\
&\quad + \delta P_0 \left(P(u^{m+1}, n^{m+1})(\mu_n^{m+1} - \mu_u^{m+1})_{\oplus}, \overline{u}\right), \qquad \forall \overline{u} \in H^1(\Omega), \quad (5.12a) \\
\left(\mu_u^{m+1}, \overline{\mu}_u\right) &= \varepsilon^2 \left(\nabla u^{m+1}, \nabla \overline{\mu}_u\right) + \left(f(u^{m+1}, u^m) - \chi_0 n^{m+1}, \overline{\mu}_u\right), \qquad \forall \overline{\mu}_u \in H^1(\Omega), \quad (5.12b) \\
\left(\delta_t n^{m+1}, \overline{n}\right) &= -C_n \left(M(n^{m+1})\nabla \mu_n^{m+1}, \nabla \overline{n}\right) \\
&\quad - \delta P_0 \left(P(u^{m+1}, n^{m+1})(\mu_n^{m+1} - \mu_u^{m+1})_{\oplus}, \overline{n}\right), \qquad \forall \overline{n} \in H^1(\Omega), \quad (5.12c)
\end{aligned}$$

where

$$\mu_n^{m+1} = \frac{1}{\delta} n^{m+1} - \chi_0 u^m \tag{5.13}$$

and $u^0 = u_0$, $n^0 = n_0$ in Ω.

Notice that the proposed scheme (5.12) is just a variation of backward Euler's method where we have treated explicitly the concave part of the splitting of $F(u)$ in (5.12b) and a part of the cross diffusion in (5.13).

The following results are the discrete in time versions of the Propositions 5.3.3, 5.3.4 and 5.3.5. We skip the proofs, because the same properties will be proved for the fully discrete scheme given in Section 5.4.2.

Proposition 5.4.1. *Any solution* $(u^{m+1}, \mu_u^{m+1}, n^{m+1})$ *of the time-discrete scheme* (5.12) *satisfies that* $u^{m+1}, n^{m+1} \in [0,1]$ *in* Ω.

Proposition 5.4.2. *Any solution* $(u^{m+1}, \mu_u^{m+1}, n^{m+1})$ *of the time-discrete scheme* (5.12) *conserves the total mass of tumor cells and nutrients in the sense of*

$$\delta_t \int_\Omega (u^{m+1}(x) + n^{m+1}(x))dx = 0.$$

Proposition 5.4.3. *Any solution* $(u^{m+1}, \mu_u^{m+1}, n^{m+1})$ *of the time-discrete scheme* (5.12) *satisfies the following discrete energy law*

$$\begin{aligned}\delta_t E(u^{m+1}, n^{m+1}) + C_u \int_\Omega M(u^{m+1})|\nabla \mu_u^{m+1}|^2 + C_n \int_\Omega M(n^{m+1})|\nabla \mu_n^{m+1}|^2 \\ + \frac{\Delta t\, \varepsilon^2}{2} \int_\Omega |\delta_t \nabla u^{m+1}|^2 + \frac{\Delta t}{2\delta} \int_\Omega |\delta_t n^{m+1}|^2 \\ + \delta\, P_0 \int_\Omega P(u^{m+1}, n^{m+1})(\mu_u^{m+1} - \mu_n^{m+1})_\oplus^2 \leq 0, \end{aligned} \tag{5.14}$$

where $E(u, n)$ *is defined in* (5.10)*.*

Therefore, the solution is energy stable in the sense

$$E(u^{m+1}, n^{m+1}) \leq E(u^m, n^m), \quad \forall\, m \geq 0.$$

Remark 5.4.4. *This first order nonlinear time-discrete scheme* (5.12) *preserves the properties of the continuous models, namely the conservation* $\int_\Omega (u^{m+1} + n^{m+1}) = \int_\Omega (u^m + n^m)$*, the point-wise bounds* $u^{m+1}, n^{m+1} \in [0, 1]$ *in* Ω *and the energy dissipation* $E(u^{m+1}, n^{m+1}) \leq E(u^m, n^m)$*. In particular, the convex-splitting technique used in* (5.11) *allows us to guarantee the dissipation of the discrete version of the exact energy of the model* (5.10)*.*

There exist other widely used techniques such as the SAV approach which does rely on the dissipation of a modified energy via an auxiliary variable that must be introduced in the scheme. An advantage of the SAV approach is that it usually leads, in more simple models, to linear schemes with decreasing modified energy but, in this case, since we want to preserve the pointwise bounds, we require anyway a nonlinear discretization as shown in (5.12)*.*

Therefore, in this context, we prefer the convex-splitting technique against the SAV approach. However, it would be interesting to explore whether it is possible to extend the ideas of this work to design a second-order in time approximation, which is not straightforward and may require a different approach such as a SAV-type discretization.

5.4.2 Fully discrete scheme

We assume, as in Section 3.4, the Hypothesis 3.4.1, i.e., the line between the barycenters of any adjacent triangles K and L is orthogonal to the interface $e = K \cap L \in \mathcal{E}_h^{\mathrm{i}}$. One example of a mesh

satisfying Hypothesis 3.4.1 is plotted in Figure 5.1. For other examples and a further insight on this property we refer the reader to Section 3.4.

In addition, we define the projection $\Pi_0 \colon L^1(\Omega) \to \mathbb{P}_0^{\text{disc}}(\mathcal{T}_h)$ and the regularization $\Pi_1^h \colon L^1(\Omega) \to \mathbb{P}_1^{\text{cont}}(\mathcal{T}_h)$ of a function $g \in L^1(\Omega)$ as the function satisfying the following:

$$(g, \overline{w}) = (\Pi_0 g, \overline{w}), \qquad \forall\, \overline{w} \in \mathbb{P}_0^{\text{disc}}(\mathcal{T}_h), \tag{5.15}$$

$$\left(g, \overline{\phi}\right) = \left(\Pi_1^h g, \overline{\phi}\right)_h, \qquad \forall\, \overline{\phi} \in \mathbb{P}_1^{\text{cont}}(\mathcal{T}_h), \tag{5.16}$$

where $(\cdot,\cdot)_h$ is the mass-lumping scalar product in $\mathbb{P}_1^{\text{cont}}(\mathcal{T}_h)$. In fact, $(\Pi_0 g)|_K = (\int_K g)/|K|$ for all $K \in \mathcal{T}_h$, and $(\Pi_1^h g)(a_j) = (\sum_{K \in \text{Sop}(a_j)} \int_K g\, \varphi_j)/(\sum_{K \in \text{Sop}(a_j)} |K|/(d+1))$ for all vertex a_j with φ_j the canonical basis of $\mathbb{P}_1^{\text{cont}}(\mathcal{T}_h)$.

We propose the following fully discrete scheme for the model (5.3): given $u^m, n^m \in \mathbb{P}_0^{\text{disc}}(\mathcal{T}_h)$ with $u^m, n^m \in [0,1]$ and $\mu_u^m \in \mathbb{P}_1^{\text{cont}}(\mathcal{T}_h)$, find $u^{m+1}, n^{m+1} \in \mathbb{P}_0^{\text{disc}}(\mathcal{T}_h)$ and $\mu_u^{m+1} \in \mathbb{P}_1^{\text{cont}}(\mathcal{T}_h)$, such that

$$\begin{aligned}
\left(\delta_t u^{m+1}, \overline{u}\right) &= -C_u a_h^{\text{upw}}(\Pi_0 \mu_u^{m+1}; M(u^{m+1}), \overline{u}) \\
&\quad + \delta P_0\left(P(u^{m+1}, n^{m+1})(\mu_n^{m+1} - \Pi_0 \mu_u^{m+1})_{\oplus}, \overline{u}\right), \qquad \forall \overline{u} \in \mathbb{P}_0^{\text{disc}}(\mathcal{T}_h), \quad (5.17a) \\
\left(\mu_u^{m+1}, \overline{\mu}_u\right)_h &= \varepsilon^2 \left(\nabla \Pi_1^h u^{m+1}, \nabla \overline{\mu}_u\right) + \left(f(\Pi_1^h u^{m+1}, \Pi_1^h u^m), \overline{\mu}_u\right) \\
&\quad - \chi_0\left(n^{m+1}, \overline{\mu}_u\right), \qquad \forall \overline{\mu}_u \in \mathbb{P}_1^{\text{cont}}(\mathcal{T}_h), \quad (5.17b) \\
\left(\delta_t n^{m+1}, \overline{n}\right) &= -C_n a_h^{\text{upw}}(\mu_n^{m+1}; M(n^{m+1}), \overline{n}) \\
&\quad - \delta P_0\left(P(u^{m+1}, n^{m+1})(\mu_n^{m+1} - \Pi_0 \mu_u^{m+1})_{\oplus}, \overline{n}\right), \qquad \forall \overline{n} \in \mathbb{P}_0^{\text{disc}}(\mathcal{T}_h), \quad (5.17c)
\end{aligned}$$

where

$$\mu_n^{m+1} = \frac{1}{\delta} n^{m+1} - \chi_0 \Pi_0(\Pi_1^h u^m), \tag{5.18}$$

$u^0 = u_0$, $n^0 = n_0$ and $a_h^{\text{upw}}(\cdot;\cdot,\cdot)$ is an upwind form defined in Section 5.4.2.1 below. Note that,

$$(\Pi_1^h u^m)(a_j) = \frac{\sum_{L \in \text{Sop}(a_j)} |L| u_L^m}{\sum_{L \in \text{Sop}(a_j)} |L|}, \quad \forall\, a_j, \tag{5.19}$$

and

$$\Pi_0(\Pi_1^h u^m)|_K = \frac{1}{d+1}\sum_{a_j\in K}(\Pi_1^h u^m)(a_j), \quad \forall\, K \in \mathcal{T}_h. \tag{5.20}$$

To ease the notation, we denote the solution of this fully discrete scheme in the same way than the time discrete scheme (5.12). From now on we will refer to the solution of the fully discrete scheme unless otherwise specified.

Notice that we have introduced the regularization of u^{m+1}, $\Pi_1^h u^{m+1}$ to preserve the diffusion term in (5.17b). In fact, this regularized variable will be regarded as our approximation of the tumor cells volume fraction as, according to the results in Section 5.4.2.2, it preserves the maximum principle and satisfies a discrete energy law. Moreover, in order to preserve the maximum principle and the dissipation of the energy, we consider mass lumping in the term $\left(\mu_u^{m+1}, \overline{\mu}\right)_h$.

Remark 5.4.5. *The homogeneous Neumann boundary conditions on u^m and n^m have been implicitly imposed in the definition of $a_h^{upw}(\cdot;\cdot,\cdot)$, see* (5.21)*. In addition, the boundary condition $\nabla\Pi_1^h u^m \cdot \boldsymbol{n} = 0$ on $\partial\Omega \times (0,T)$ is imposed implicitly by the term $\left(\nabla\Pi_1^h u^m, \nabla\overline{\mu}\right)$ in* (5.17b)*.*

Remark 5.4.6. *The scheme* (5.17) *is nonlinear so we will have to use an iterative procedure, such as Newton's method, to approach its solution.*

5.4.2.1 Definition of $a_h^{\text{upw}}(\cdot;\cdot,\cdot)$

First of all, following the ideas in Section 2.4.2, in order to preserve the maximum principle using an upwind approximation we will split the mobility function into its increasing and its decreasing part as follows:

$$M^{\uparrow}(v) = \begin{cases} M(v), & v \le v^*, \\ M(v^*), & v > v^*, \end{cases} \qquad M^{\downarrow}(v) = \begin{cases} 0, & v \le v^*, \\ M(v) - M(v^*), & v > v^*, \end{cases}$$

where $v^* \in \mathbb{R}$ is the point where the maximum of $M(v)$ is attained, which can be obtained by simple algebraic computations. Note that $M(v) = M^{\uparrow}(v) + M^{\downarrow}(v)$.

Now, we define the following upwind form for $v, \overline{v}, \mu \in \mathbb{P}_0(\mathcal{T}_h)$:

$$a_h^{\text{upw}}(\mu; M(v), \overline{v}) \coloneqq \sum_{e \in \mathcal{E}_h^i, e = K \cap L} \int_e \left(\left(-\nabla^0_{\boldsymbol{n}_e} \mu\right)_{\oplus} \left(M^{\uparrow}(v_K) + M^{\downarrow}(v_L) \right)_{\oplus} - \left(-\nabla^0_{\boldsymbol{n}_e} \mu\right)_{\ominus} \left(M^{\uparrow}(v_L) + M^{\downarrow}(v_K) \right)_{\oplus} \right) [\![\overline{v}]\!] \tag{5.21}$$

with

$$\nabla^0_{\boldsymbol{n}_e} \mu = \frac{-[\![\mu]\!]}{\mathcal{D}_e(\mathcal{T}_h)} = \frac{\mu_L - \mu_K}{\mathcal{D}_e(\mathcal{T}_h)}, \tag{5.22}$$

a reconstruction of the normal gradient using $\mathbb{P}_0(\mathcal{T}_h)$ functions for every $e \in \mathcal{E}_h^i$ with $e = K \cap L$ (see Section 3.4 for more details). We have denoted $\mathcal{D}_e(\mathcal{T}_h)$ the distance between the barycenters of the triangles K and L of the mesh $\mathcal{T}_h$ that share $e \in \mathcal{E}_h^{\text{i}}$. This way, we can rewrite (5.21) as

$$a_h^{\text{upw}}(\mu; M(v), \overline{v}) \coloneqq \sum_{e \in \mathcal{E}_h^i, e = K \cap L} \frac{1}{\mathcal{D}_e(\mathcal{T}_h)} \int_e \left([\![\mu]\!]_{\oplus} \left(M^{\uparrow}(v_K) + M^{\downarrow}(v_L) \right)_{\oplus} - [\![\mu]\!]_{\ominus} \left(M^{\uparrow}(v_L) + M^{\downarrow}(v_K) \right)_{\oplus} \right) [\![\overline{v}]\!] \,. \tag{5.23}$$

Remark 5.4.7. *The form $a_h^{upw}(\mu; M(v), \overline{v})$ is an upwind approximation of the convective term*

$$-\left(M(v)\nabla\mu, \nabla\overline{v}\right), \quad \overline{v} \in H^1(\Omega),$$

taking into consideration that the orientation of the flux is determined by both the orientation of $\nabla\mu$ and the sign of $M'(v)$ as follows:

$$\nabla \cdot (M(v)\nabla\mu) = M'(v)\nabla v \nabla\mu + M(v)\Delta\mu.$$

In order to develop this approximation we have followed the ideas of [120] and Sections 2.4.2 and 3.4, and we have considered an approximation of $M(v)$ in (5.21) *by means of its increasing and decreasing parts, $M^{\uparrow}(v)$ and $M^{\downarrow}(v)$, whose derivatives are positive and negative, respectively. However, unlike in Section 2.4.2, we have also truncated the mobility $M(v)$ to avoid negative approximations of $M(v)$ that may lead to a loss of energy stability.*

5.4.2.2 Properties of the fully discrete scheme

Proposition 5.4.8 (Conservation)**.** *The scheme* (5.17) *conserves the total mass of cells and nutrients in the following sense: for all* $m \geq 0$*,*

$$\int_\Omega (u^{m+1} + n^{m+1}) = \int_\Omega (u^m + n^m) \quad \textit{and} \quad \int_\Omega (\Pi_1^h u^{m+1} + n^{m+1}) = \int_\Omega (\Pi_1^h u^m + n^m).$$

Proof. Just need to take $\overline{u} = 1$ in (5.17a) and $\overline{n} = 1$ in (5.17c) and add both expressions to obtain:

$$\int_\Omega (u^{m+1} + n^{m+1}) = \int_\Omega (u^m + n^m).$$

Moreover, due to the definition of the regularization Π_1^h, we have that $\int_\Omega u^{m+1} = \int_\Omega \Pi_1^h u^{m+1}$ and $\int_\Omega u^m = \int_\Omega \Pi_1^h u^m$, what yields

$$\int_\Omega (\Pi_1^h u^{m+1} + n^{m+1}) = \int_\Omega (\Pi_1^h u^m + n^m).$$

□

Theorem 5.4.9 (Pointwise bounds)**.** *Let* $(u^{m+1}, \mu_u^{m+1}, n^{m+1})$ *be a solution of the scheme* (5.17)*, then* $u^{m+1}, n^{m+1} \in [0,1]$ *in* Ω *provided* $u^m, n^m \in [0,1]$ *in* Ω*.*

Proof. Firstly, we prove that $u^{m+1}, n^{m+1} \geq 0$ in Ω.

To prove that $u^{m+1} \geq 0$ we may take the following $\mathbb{P}_0^{\text{disc}}(\mathcal{T}_h)$ test function

$$\overline{u}^* = \begin{cases} (u_{K^*}^{m+1})_\ominus & \text{in } K^* \\ 0 & \text{out of } K^* \end{cases},$$

where K^* is an element of $\mathcal{T}_h$ such that $u_{K^*}^{m+1} = \min_{K \in \mathcal{T}_h} u_K^{m+1}$. Then, by definition of $P(u,n)$ in (5.6),

$$\delta P_0 \left(P(u^{m+1}, n^{m+1})(\mu_n^{m+1} - \mu_u^{m+1})_\oplus, \overline{u}^* \right) = 0,$$

equation (5.17a) becomes

$$|K^*| \delta_t u_{K^*}^{m+1} (u_{K^*}^{m+1})_\ominus = -C_u a_h^{\text{upw}}(\Pi_0 \mu_u^{m+1}; M(u^{m+1})_\oplus, \overline{u}^*). \tag{5.24}$$

Now, since $u_L^{m+1} \geq u_{K^*}^{m+1}$ we can assure that

$$M^{\uparrow}(u_L^{m+1}) \geq M^{\uparrow}(u_{K^*}^{m+1}) \quad \text{and} \quad M^{\downarrow}(u_L^{m+1}) \leq M^{\downarrow}(u_{K^*}^{m+1}).$$

Hence, using that the positive part is an increasing function, we obtain

$$a_h^{\text{upw}}(\Pi_0 \mu_u^{m+1}; M(u^{m+1}), \overline{u}^*) \leq 0,$$

which yields $|K^*| \delta_t u_{K^*}^{m+1} (u_{K^*}^{m+1})_{\ominus} \geq 0$.

Consequently,

$$0 \leq |K^*| (\delta_t u_{K^*}^{m+1})(u_{K^*}^{m+1})_{\ominus} = -\frac{|K^*|}{\Delta t} \left((u_{K^*}^{m+1})_{\ominus}^2 + u_{K^*}^m (u_{K^*}^{m+1})_{\ominus} \right) \leq 0,$$

which implies, since $u_{K^*}^m \geq 0$, that $(u_{K^*}^{m+1})_{\ominus} = 0$. Hence $u^{m+1} \geq 0$ in Ω.

Similarly, taking the following $\mathbb{P}_0^{\text{disc}}(\mathcal{T}_h)$ test function in (5.17c),

$$\overline{n}^* = \begin{cases} (n_{K^*}^{m+1})_{\ominus} & \text{in } K^* \\ 0 & \text{out of } K^* \end{cases}$$

where K^* is an element of $\mathcal{T}_h$ such that $n_{K^*}^{m+1} = \min_{K \in \mathcal{T}_h} n_K^{m+1}$ we get $n^{m+1} \geq 0$ in Ω.

Secondly, we prove that $u^{m+1}, n^{m+1} \leq 1$ in Ω.

To prove that $u^{m+1} \leq 1$, taking the following test function in (5.17a),

$$\overline{u}^* = \begin{cases} (u_{K^*}^{m+1} - 1)_{\oplus} & \text{in } K^* \\ 0 & \text{out of } K^* \end{cases},$$

where K^* is an element of $\mathcal{T}_h$ such that $u_{K^*}^{m+1} = \max_{K \in \mathcal{T}_h} u_K^{m+1}$ and using similar arguments than above, we arrive at

$$|K^*| \delta_t u_{K^*}^{m+1} (u_{K^*}^{m+1} - 1)_{\oplus} \leq 0.$$

Therefore, it is satisfied that

$$0 \geq |K^*|\delta_t u_{K^*}^{m+1}(u_{K^*}^{m+1}-1)_\oplus = \frac{|K^*|}{\Delta t}\left((u_{K^*}^{m+1}-1)+(1-u_{K^*}^{m})\right)(u_{K^*}^{m+1}-1)_\oplus$$
$$= \frac{|K^*|}{\Delta t}\left((u_{K^*}^{m+1}-1)_\oplus^2+(1-u_{K^*}^{m})(u_{K^*}^{m+1}-1)_\oplus\right) \geq 0,$$

what yields $(u_{K^*}^{m+1}-1)_\oplus = 0$ and, therefore, $u^{m+1} \leq 1$ in Ω.

Finally, taking the test function in (5.17c)

$$\overline{n}^* = \begin{cases} (n_{K^*}^{m+1}-1)_\oplus & \text{in } K^* \\ 0 & \text{out of } K^* \end{cases}$$

where K^* is an element of $\mathcal{T}_h$ such that $n_{K^*}^{m+1} = \max_{K\in\mathcal{T}_h} n_K^{m+1}$ we obtain, similarly, that $n^{m+1} \leq 1$ in Ω. □

The following result is a direct consequence of the previous Theorem 5.4.9 and the equality (5.19) of the regularization Π_1^h.

Corollary 5.4.10. *It satisfies* $\Pi_1^h u^{m+1} \in [0,1]$ *in* Ω *provided* $u^{m+1} \in [0,1]$ *in* Ω.

Theorem 5.4.11 (Energy law)**.** *Any solution of the scheme* (5.17) *satisfies the following* ***discrete energy law***

$$\delta_t E(\Pi_1^h u^{m+1}, n^{m+1}) + C_u a_h^{upw}(\Pi_0\mu_u^{m+1}; M(u^{m+1}), \Pi_0\mu_u^{m+1}) + C_n a_h^{upw}(\mu_n^{m+1}; M(n^{m+1}), \mu_n^{m+1})$$
$$+ \frac{\Delta t\,\varepsilon^2}{2}\int_\Omega |\delta_t \nabla \Pi_1^h u^{m+1}|^2 + \frac{\Delta t}{2\delta}\int_\Omega |\delta_t n^{m+1}|^2$$
$$+ \delta P_0 \int_\Omega P(u^{m+1}, n^{m+1})(\mu_n^{m+1} - \Pi_0\mu_u^{m+1})_\oplus^2 \leq 0, \tag{5.25}$$

where the energy $E(\Pi_1^h u, n)$ *is defined in* (5.10)*.*

Proof. By taking $\overline{u} = \Pi_0 \mu_u^{m+1}$, $\overline{\mu}_u = \delta_t \Pi_1^h u^{m+1}$, $\overline{n} = \mu_n^{m+1}$ in (5.17a)–(5.17c) and testing (5.18) by $\delta_t n^{m+1}$ we arrive at

$$\begin{aligned}
&\left(\delta_t u^{m+1}, \Pi_0 \mu_u^{m+1}\right) + C_u a_h^{\text{upw}}(\Pi_0 \mu_u^{m+1}; M(u^{m+1}), \Pi_0 \mu_u^{m+1}) \\
&\qquad = \delta P_0 \left(P(u^{m+1}, n^{m+1})(\mu_n^{m+1} - \Pi_0 \mu_u^{m+1})_{\oplus}, \Pi_0 \mu_u^{m+1}\right), \qquad (5.26a) \\
&\left(\mu_u^{m+1}, \delta_t \Pi_1^h u^{m+1}\right) = \varepsilon^2 \left(\nabla \Pi_1^h u^{m+1}, \delta_t \nabla \Pi_1^h u^{m+1}\right) + \left(f(\Pi_1^h u^{m+1}, \Pi_1^h u^m), \delta_t \Pi_1^h u^{m+1}\right) \\
&\qquad - \chi_0 \left(n^{m+1}, \delta_t \Pi_1^h u^{m+1}\right), \qquad (5.26b) \\
&\left(\delta_t n^{m+1}, \mu_n^{m+1}\right) + C_n a_h^{\text{upw}}(\mu_n^{m+1}; M(n^{m+1}), \mu_n^{m+1}) \\
&\qquad = -\delta P_0 \left(P(u^{m+1}, n^{m+1})(\mu_n^{m+1} - \Pi_0 \mu_u^{m+1})_{\oplus}, \mu_n^{m+1}\right), \qquad (5.26c) \\
&\left(\mu_n^{m+1}, \delta_t n^{m+1}\right) = \frac{1}{\delta} \left(n^{m+1}, \delta_t n^{m+1}\right) - \chi_0 \left(\Pi_1^h u^m, \delta_t n^{m+1}\right), \qquad (5.26d)
\end{aligned}$$

Observe that, by (5.15)–(5.16),

$$\begin{aligned}
\left(\delta_t \Pi_1^h u^{m+1}, \mu_u^{m+1}\right) &= \left(\delta_t u^{m+1}, \mu_u^{m+1}\right), \\
\left(\delta_t u^{m+1}, \mu_u^{m+1}\right) &= \left(\delta_t u^{m+1}, \Pi_0 \mu_u^{m+1}\right),
\end{aligned}$$

hence in particular

$$(\delta_t u^{m+1}, \Pi_0 \mu_u^{m+1}) = (\delta_t \Pi_1^h u^{m+1}, \mu_u^{m+1}).$$

Then, by adding (5.26a)–(5.26d), the previous terms cancel, remaining

$$\begin{aligned}
C_u a_h^{\text{upw}}(\Pi_0 \mu_u^{m+1}; M(u^{m+1}), \Pi_0 \mu_u^{m+1}) &+ C_n a_h^{\text{upw}}(\mu_n^{m+1}; M(n^{m+1}), \mu_n^{m+1}) \\
&+ \varepsilon^2 \left(\nabla \Pi_1^h u^{m+1}, \delta_t \nabla \Pi_1^h u^{m+1}\right) + \left(f(\Pi_1^h u^{m+1}, \Pi_1^h u^m), \delta_t \Pi_1^h u^{m+1}\right) \\
&+ \delta P_0 \left(P(u^{m+1}, n^{m+1})(\mu_n^{m+1} - \Pi_0 \mu_u^{m+1})_{\oplus}, \mu_n^{m+1} - \Pi_0 \mu_u^{m+1}\right) \\
&+ \frac{1}{\delta} \left(n^{m+1}, \delta_t n^{m+1}\right) - \chi_0 \left(n^{m+1}, \delta_t \Pi_1^h u^{m+1}\right) - \chi_0 \left(\Pi_1^h u^m, \delta_t n^{m+1}\right) = 0.
\end{aligned}$$

Taking into account that

$$\begin{aligned}
\varepsilon^2\left(\nabla\Pi_1^h u^{m+1}, \delta_t\nabla\Pi_1^h u^{m+1}\right) &= \frac{\varepsilon^2}{2}\delta_t\int_\Omega |\nabla\Pi_1^h u^{m+1}|^2 + \frac{\Delta t\,\varepsilon^2}{2}\int_\Omega |\delta_t\nabla\Pi_1^h u^{m+1}|^2,\\
\frac{1}{\delta}\left(n^{m+1}, \delta_t n^{m+1}\right) &= \frac{1}{2\delta}\delta_t\int_\Omega |n^{m+1}|^2 + \frac{\Delta t}{2\delta}\int_\Omega |\delta_t n^{m+1}|^2,\\
\chi_0\delta_t\int_\Omega u^{m+1}n^{m+1} &= \chi_0\left(n^m, \delta_t\Pi_1^h u^{m+1}\right) + \chi_0\left(\Pi_1^h u^{m+1}, \delta_t n^{m+1}\right),\\
\int_\Omega P(u^{m+1}, n^{m+1})(\mu_n^{m+1} - \Pi_0\mu_u^{m+1})_\oplus^2 &= \left(P(u^{m+1}, n^{m+1})(\mu_n^{m+1} - \Pi_0\mu_u^{m+1})_\oplus, \mu_n^{m+1} - \Pi_0\mu_u^{m+1}\right),
\end{aligned}$$

and by adding and subtracting $\delta_t\int_\Omega F(\Pi_1^h u^{m+1})$, we get the following equality

$$\begin{aligned}
\delta_t E(\Pi_1^h u^{m+1}, n^{m+1}) &+ C_u a_h^{\text{upw}}(\Pi_0\mu_u^{m+1}; M(u^{m+1}), \Pi_0\mu_u^{m+1}) + C_n a_h^{\text{upw}}(\mu_n^{m+1}; M(n^{m+1}), \mu_n^{m+1})\\
&+ \frac{\Delta t\,\varepsilon^2}{2}\int_\Omega |\delta_t\nabla\Pi_1^h u^{m+1}|^2 + \frac{\Delta t}{2\delta}\int_\Omega |\delta_t n^{m+1}|^2\\
&+ \delta P_0\int_\Omega P(u^{m+1}, n^{m+1})(\mu_n^{m+1} - \Pi_0\mu_u^{m+1})_\oplus^2\\
&= \delta_t\int_\Omega F(\Pi_1^h u^{m+1}) - \left(f(\Pi_1^h u^{m+1}, \Pi_1^h u^m), \delta_t\Pi_1^h u^{m+1}\right).
\end{aligned}$$

Finally, from the convex-splitting approximation (5.11) (see Section 2.4.1 and [77, 105]), one has that

$$\int_\Omega \delta_t F(\Pi_1^h u^{m+1}) - \left(f(\Pi_1^h u^{m+1}, \Pi_1^h u^m), \delta_t(\Pi_1^h u^{m+1})\right) \le 0,$$

which implies (5.25).

□

Corollary 5.4.12. *The scheme* (5.17) *is unconditionally energy stable in the sense*

$$E(\Pi_1^h u^{m+1}, n^{m+1}) \le E(\Pi_1^h u^m, n^m), \quad \forall\, m \ge 0.$$

Proof. It is straightforward to check (see Corollary 3.4.14) that

$$a_h^{\text{upw}}(\Pi_0\mu_u; M(u^{m+1}), \Pi_0\mu_u^{m+1}) \ge 0 \quad \text{and} \quad a_h^{\text{upw}}(\mu_n^{m+1}; M(n^{m+1}), \mu_n^{m+1}) \ge 0.$$

Hence, using (5.25) we conclude that $\delta_t E(\Pi_1^h u^{m+1}, n^{m+1}) \le 0$. □

Now, we focus on the existence of the scheme (5.17) for which we will use the Leray-Schauder fixed point theorem 2.3.6.

Theorem 5.4.13 (Existence)**.** *There is at least one solution of the scheme* (5.17)*.*

Proof. Given two functions $z_u, z_n \in \mathbb{P}_0^{\text{disc}}(\mathcal{T}_h)$ with $0 \leq z_u, z_n \leq 1$, we define the map

$$T\colon \mathbb{P}_0^{\text{disc}} \times \mathbb{P}_1^{\text{cont}} \times \mathbb{P}_0^{\text{disc}} \longrightarrow \mathbb{P}_0^{\text{disc}} \times \mathbb{P}_1^{\text{cont}} \times \mathbb{P}_0^{\text{disc}}$$

such that

$$T(\widehat{u}, \widehat{\mu}_u, \widehat{n}) = (u, \mu_u, n) \in \mathbb{P}_0^{\text{disc}}(\mathcal{T}_h) \times \mathbb{P}_1^{\text{cont}}(\mathcal{T}_h) \times \mathbb{P}_0^{\text{disc}}(\mathcal{T}_h)$$

is the unique solution of the linear (and decoupled, computing first μ_n, next n and u, and finally μ_u) scheme:

$$\begin{aligned}
\frac{1}{\Delta t}\left(u - z_u, \overline{u}\right) &= -C_u a_h^{\text{upw}}(\Pi_0 \widehat{\mu}; M(\widehat{u}), \overline{u}) \\
&\quad + \delta P_0\left(P(\widehat{u}, \widehat{n})(\mu_n - \Pi_0 \widehat{\mu}_u)_{\oplus}, \overline{u}\right), && \forall \overline{u} \in \mathbb{P}_0^{\text{disc}}(\mathcal{T}_h), && (5.27a) \\
(\mu_u, \overline{\mu}_u)_h &= \varepsilon^2 \left(\nabla \Pi_1^h u, \nabla \overline{\mu}_u\right) + \left(f(\Pi_1^h u, \Pi_1^h z_u), \overline{\mu}_u\right) \\
&\quad - \chi_0\left(n, \overline{\mu}_u\right), && \forall \overline{\mu}_u \in \mathbb{P}_1^{\text{cont}}(\mathcal{T}_h), && (5.27b) \\
\frac{1}{\Delta t}\left(n - z_n, \overline{n}\right) &= -C_n a_h^{\text{upw}}(\mu_n; M(\widehat{n}), \overline{n}) \\
&\quad - \delta P_0\left(P(\widehat{u}, \widehat{n})(\mu_n - \Pi_0 \widehat{\mu}_u)_{\oplus}, \overline{n}\right), && \forall \overline{n} \in \mathbb{P}_0^{\text{disc}}(\mathcal{T}_h), && (5.27c)
\end{aligned}$$

where

$$\mu_n = \frac{1}{\delta}\widehat{n} - \chi_0 \Pi_0(\Pi_h^1 z_u). \tag{5.28}$$

It is straightforward to check that, for any given $(\widehat{u}, \widehat{\mu}_u, \widehat{n}) \in \mathbb{P}_0^{\text{disc}}(\mathcal{T}_h) \times \mathbb{P}_1^{\text{cont}}(\mathcal{T}_h) \times \mathbb{P}_0^{\text{disc}}(\mathcal{T}_h)$, there is a unique solution $(u, \mu_u, n) \in \mathbb{P}_0^{\text{disc}}(\mathcal{T}_h) \times \mathbb{P}_1^{\text{cont}}(\mathcal{T}_h) \times \mathbb{P}_0^{\text{disc}}(\mathcal{T}_h)$. Therefore, the operator T is well defined.

Now we will prove that T is under the hypotheses of the Leray-Schauder fixed-point theorem 2.3.6.

First, we check that T is continuous. Let $\{(\widehat{u}_j, \widehat{\mu}_{u_j}, \widehat{n}_j)\}_{j \in \mathbb{N}} \subset \mathbb{P}_0^{\text{disc}}(\mathcal{T}_h) \times \mathbb{P}_1^{\text{cont}}(\mathcal{T}_h) \times \mathbb{P}_0^{\text{disc}}(\mathcal{T}_h)$ be a sequence such that $\lim_{j\to\infty}(\widehat{u}_j, \widehat{\mu}_{u_j}, \widehat{n}_j) = (\widehat{u}, \widehat{\mu}_u, \widehat{n})$. Taking into account that all norms are equivalent in $\mathbb{P}_0^{\text{disc}}(\mathcal{T}_h)$ since it is a finite-dimensional space, the convergences $\widehat{u}_j \to \widehat{u}$ and $\widehat{n}_j \to \widehat{n}$

are equivalent to the convergences elementwise $(\widehat{u}_j)_K \to \widehat{n}_K$ and $(\widehat{n}_j)_K \to \widehat{n}_K$ for every $K \in \mathcal{T}_h$ (this may be seen, for instance, by using the norm $\|\cdot\|_{L^\infty(\Omega)}$). Moreover, since Π_0 is continuous and $\Pi_0\widehat{\mu}_u \in \mathbb{P}_0^{\text{disc}}(\mathcal{T}_h)$, the convergence $\Pi_0\widehat{\mu}_{u_j} \to \Pi_0\widehat{\mu}_u$ is also equivalent to the convergence elementwise $(\Pi_0\widehat{\mu}_{u_j})_K \to (\Pi_0\widehat{\mu}_u)_K$ for every $K \in \mathcal{T}_h$. Finally, taking limits when $j \to \infty$ in (5.27) (with $\widehat{u} \coloneqq \widehat{u}_j$, $\widehat{\mu}_u \coloneqq \widehat{\mu}_{u_j}$, $\widehat{n} \coloneqq \widehat{n}_j$ and $(u_j, \mu_{u_j}, n_j) \coloneqq T(\widehat{u}_j, \widehat{\mu}_{u_j}, \widehat{n}_j)$), and using the notion of convergence elementwise, we get that

$$\lim_{j\to\infty} T(\widehat{u}_j, \widehat{\mu}_j, \widehat{n}_j) = T(\widehat{u}, \widehat{\mu}, \widehat{n}) = T\left(\lim_{j\to\infty}(\widehat{u}_j, \widehat{\mu}_j, \widehat{n}_j)\right),$$

hence T is continuous. Therefore, T is also compact since $\mathbb{P}_0^{\text{disc}}(\mathcal{T}_h)$ and $\mathbb{P}_1^{\text{cont}}(\mathcal{T}_h)$ have finite dimension.

Finally, let us prove that the set

$$B \;=\; \{(u, \mu_u, n) \;\in\; \mathbb{P}_0^{\text{disc}} \times \mathbb{P}_1^{\text{cont}} \times \mathbb{P}_0^{\text{disc}} \colon (u, \mu_u, n) \;=\; \alpha\, T(u, \mu_u, n) \text{ for some } 0 \;\leq\; \alpha \;\leq\; 1\}$$

is bounded (independent of α). The case $\alpha = 0$ is trivial so we will assume that $\alpha \in (0, 1]$.

If $(u, \mu_u, n) \in B$, then $(u, \mu_u, n) \in \mathbb{P}_0^{\text{disc}}(\mathcal{T}_h) \times \mathbb{P}_1^{\text{cont}}(\mathcal{T}_h) \times \mathbb{P}_0^{\text{disc}}(\mathcal{T}_h)$ is the solution of

$$\begin{aligned}
\frac{1}{\Delta t}\,(u - \alpha z_u, \overline{u}) &= -\alpha\, C_u\, a_h^{\text{upw}}(\Pi_0\mu_u; M(u), \overline{u}) \\
&\quad + \alpha\, \delta P_0\,(P(u, n)(\mu_n - \Pi_0\mu_u)_\oplus, \overline{u})\,, && \forall \overline{u} \in \mathbb{P}_0^{\text{disc}}(\mathcal{T}_h), && (5.29)\\
(\mu_u, \overline{\mu}_u)_h &= \varepsilon^2 \left(\nabla\Pi_1^h u, \nabla\overline{\mu}_u\right) + \left(f(\Pi_1^h u, \Pi_1^h z_u), \overline{\mu}_u\right) \\
&\quad - \chi_0\,(n, \overline{\mu}_u)\,, && \forall \overline{\mu}_u \in \mathbb{P}_1^{\text{cont}}(\mathcal{T}_h), && (5.30)\\
\frac{1}{\Delta t}\,(n - \alpha z_n, \overline{n}) &= -\alpha\, C_n\, a_h^{\text{upw}}(\mu_n; M(n), \overline{n}) \\
&\quad - \alpha\, \delta P_0\,(P(u, n)(\mu_n - \Pi_0\mu_u)_\oplus, \overline{n})\,, && \forall \overline{n} \in \mathbb{P}_0^{\text{disc}}(\mathcal{T}_h) && (5.31)
\end{aligned}$$

where

$$\mu_n = \frac{1}{\delta} n - \chi_0 \Pi_0(\Pi_h^1 z_u). \tag{5.32}$$

Now, testing (5.29) by $\overline{u} = 1$ and (5.31) by $\overline{n} = 1$, we obtain

$$\int_\Omega (u + n) = \alpha \int_\Omega (z_u + z_n).$$

Moreover, since $0 \leq z_u, z_n \leq 1$, it can be proved that $0 \leq u, n \leq 1$ using the same arguments than in Theorem 5.4.9. Therefore, we arrive at

$$\|u\|_{L^1(\Omega)} + \|n\|_{L^1(\Omega)} \leq \|z_u\|_{L^1(\Omega)} + \|z_n\|_{L^1(\Omega)}.$$

Hence, using properties of $\Pi_1^h u \in \mathbb{P}_1^{\text{cont}}(\mathcal{T}_h)$, since $0 \leq u \leq 1$ then $0 \leq \Pi_1^h u \leq 1$, and

$$\|\Pi_1^h u\|_{L^1(\Omega)} = \|u\|_{L^1(\Omega)} \leq \|z_u\|_{L^1(\Omega)} + \|z_n\|_{L^1(\Omega)}.$$

Now, we will check that μ_u is bounded. Testing (5.30) with $\overline{\mu}_u = \mu_u$ we obtain that

$$\|\mu_u\|^2_{L^2(\Omega)} \leq \varepsilon^2 \|\Pi_1^h u\|_{H^1(\Omega)} \|\mu_u\|_{H^1(\Omega)} + \|f(\Pi_1^h u, \Pi_1^h z_u)\|_{L^2(\Omega)} \|\mu_u\|_{L^2(\Omega)} + \|n\|_{L^2(\Omega)} \|\mu_u\|_{L^2(\Omega)}.$$

The norms are equivalent in the finite-dimensional space $\mathbb{P}_1^{\text{cont}}(\mathcal{T}_h)$, therefore, there are $K_1, K_2 \geq 0$ such that

$$\|\mu_u\|_{L^2(\Omega)} \leq \varepsilon^2 K_1 \|\Pi_1^h u\|_{L^1(\Omega)} + \|f(\Pi_1^h u, \Pi_1^h z_u)\|_{L^2(\Omega)} + K_2 \|n\|_{L^1(\Omega)}.$$

Consequently, since $\|f(\Pi_1^h u, \Pi_1^h z_u)\|_{L^2(\Omega)}$ is bounded due to $0 \leq \Pi_1^h u, \Pi_1^h z_u \leq 1$ and $\|\Pi_1^h u\|_{L^1(\Omega)}$ and $\|n\|_{L^1(\Omega)}$ are also bounded, we conclude that $\|\mu_u\|_{L^2(\Omega)}$ is bounded.

Since $\mathbb{P}_0^{\text{disc}}(\mathcal{T}_h)$ and $\mathbb{P}_1^{\text{cont}}(\mathcal{T}_h)$ are finite-dimensional spaces where all the norms are equivalent, we have proved that B is bounded.

Thus, using the Leray-Schauder fixed point theorem 2.3.6, there is a solution (u, μ_u, n) of the scheme (5.17). □

5.5 Numerical experiments

Now, we will present several numerical experiments that match the results presented in the previous section. We assume that $\Omega = [-10, 10]^2$, $\varepsilon = 0.1$, $\delta = 0.01$ and we consider the mesh is shown in Figure 5.1 which satisfies the Hypothesis 3.4.1. The nonlinear coupled scheme (5.17) is approximated by Newton's method.

These results have been computed using the Python interface of the library `FEniCSx`, [13, 166, 167], and the figures have been plotted using `PyVista`, [175].

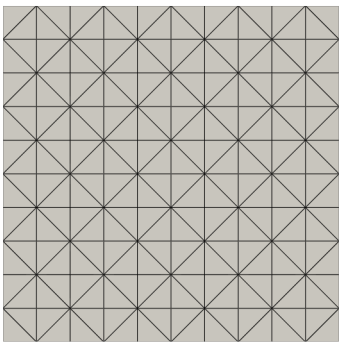

Figure 5.1 Mesh used for domain discretization

Notice that, as mentioned in Section 5.4.2, $\Pi_1^h u^m$ is considered the approximation of the phase-field variable u by the scheme (5.17). Therefore, all the results shown in this section correspond with this approximation. On the other hand, although n^m is taken as the approximation of the nutrients variable n, for the ease of visualization, $\Pi_1^h n^m$ has been plotted in Figures 5.2, 5.3, 5.4, 5.8 and 5.9.

5.5.1 Three tumors aggregation

We define the following initial conditions which are of the same type than those in [190]:

$$u_0 = \frac{1}{2}\left[\tanh\left(\frac{1-\sqrt{(x-2)^2+(y-2)^2}}{\sqrt{2}\varepsilon}\right)+\tanh\left(\frac{1-\sqrt{(x-3)^2+(y+5)^2}}{\sqrt{2}\varepsilon}\right)\right.$$
$$\left.+\tanh\left(\frac{1.73-\sqrt{(x+1.5)^2+(y+1.5)^2}}{\sqrt{2}\varepsilon}\right)+3\right],$$
$$n_0 = 1.0 - u_0.$$

These initial conditions are shown in Figure 5.2. As one may observe, we assume that, at the beginning, the nutrients are fully consumed in the area occupied by the initial tumor.

Moreover, we set $C_u = 100$, $C_n = 100 \cdot 10^{-4}$, $P_0 = 125\ h \approx 0.14$ and we use the following symmetric mobility and proliferation functions:

$$M(v) = h_{1,1}(v), \quad P(u,n) = h_{1,1}(u)n_{\oplus}. \tag{5.33}$$

We are going to compare the upwind DG scheme (5.17) and the $\mathbb{P}_1^{\text{pcont}}(\mathcal{T}_h)$-FE approximation of the time discrete scheme (5.12). We consider two different cases: $\chi_0 = 0$ and $\chi_0 = 10$, i.e. without and with cross-diffusion, respectively.

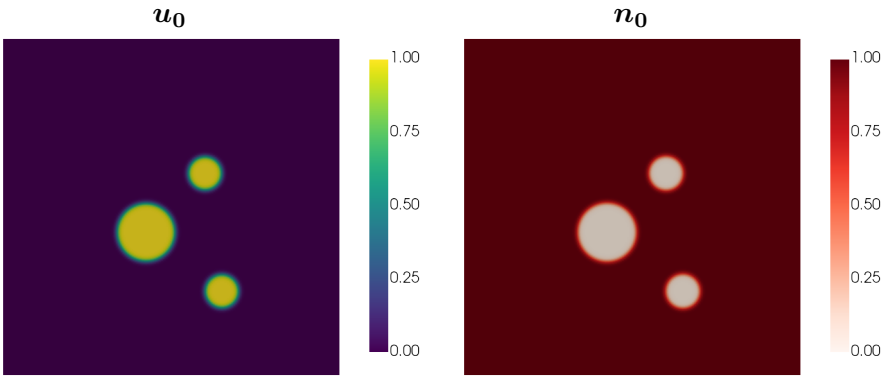

Figure 5.2 Initial conditions for test 5.5.1 (u_0 left, n_0 right)

On the one hand, the experiment without cross-diffusion ($\chi_0 = 0$ and $\Delta t = 10^{-5}$) is plotted in Figure 5.3. As one may notice, both schemes provide a similar approximation. The approximations preserve, approximately in the case of FE, the pointwise bounds of the variables u and n and the energy stability, see Figures 5.5 and 5.7 (left).

On the other hand, the test with cross-diffusion ($\chi_0 = 10$ and $\Delta t = 5 \cdot 10^{-6}$) is plotted in Figures 5.4. In this case, one may notice that, while DG scheme provides a good approximation of the solution, FE solution shows a lot of spurious oscillations. These numerical instabilities lead to a loss of the maximum principle while it is preserved by the DG scheme, see Figure 5.6. In both cases, the schemes preserve the energy stability of the model as expected, see Figure 5.7 (right).

Furthermore, it is remarkable to emphasize that the convergence of Newton's method for the FE scheme requires a very small time step. In this sense, the previous tests where shown for a small enough time step so that Newton's method converges for both schemes. Conversely, the upwind DG scheme (5.17) does converge for larger time steps. In practice, we have been able to compute the approximation given by the DG scheme for this test with time steps up to $\Delta t = 10^{-4}$.

5.5.2 Irregular tumor growth

In this test, we show the irregular growth of a tumor due to the irregular distribution of the nutrients over the domain. It is important to notice the well behavior of the scheme (5.17) which allow us to capture different irregular growth processes even in the cases with important cross-diffusion in which we cannot expect FE to work as shown in Section 5.5.1.

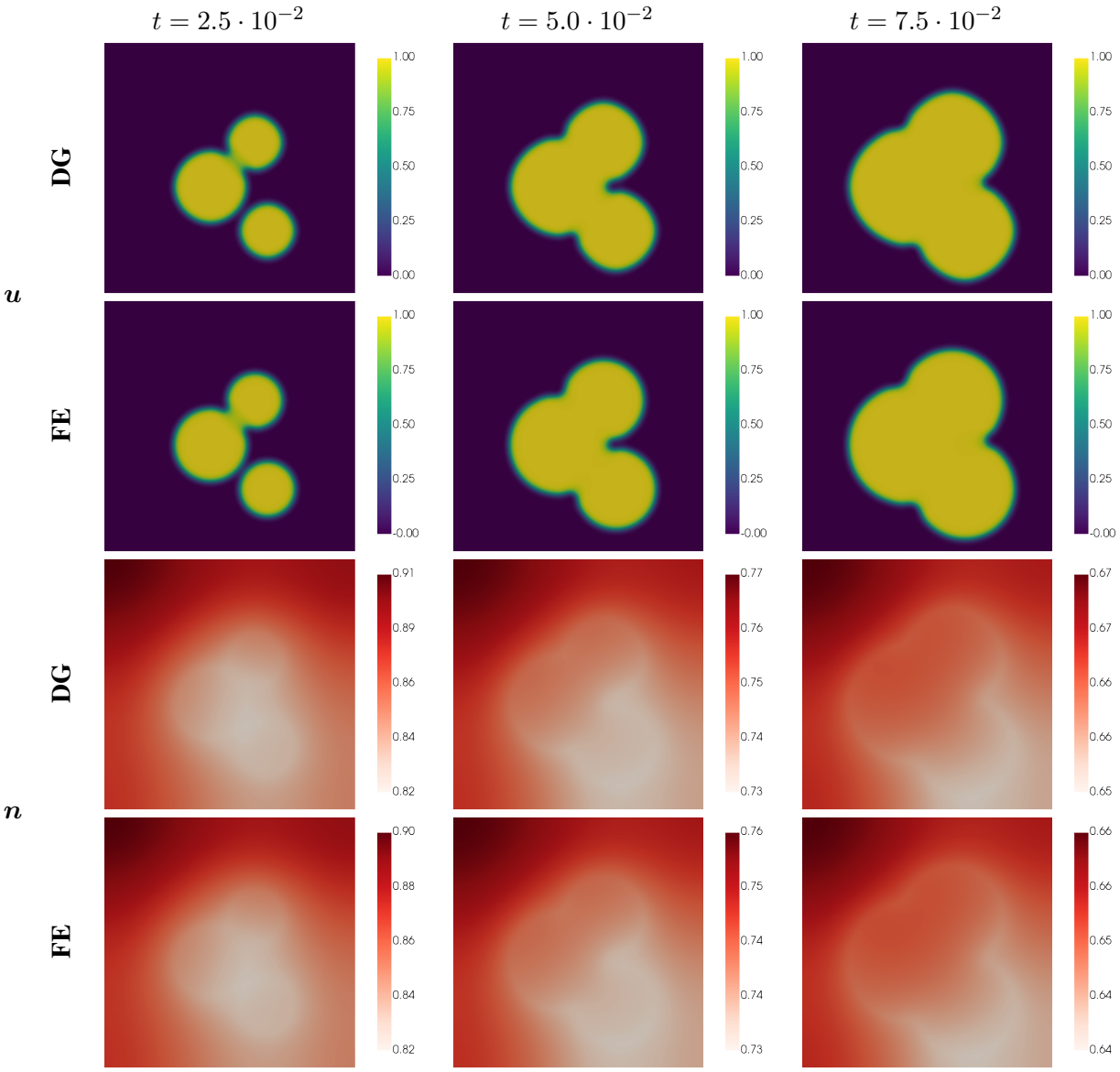

Figure 5.3 Tumor and nutrients for test (5.5.1) with $\chi_0 = 0$ at different time steps

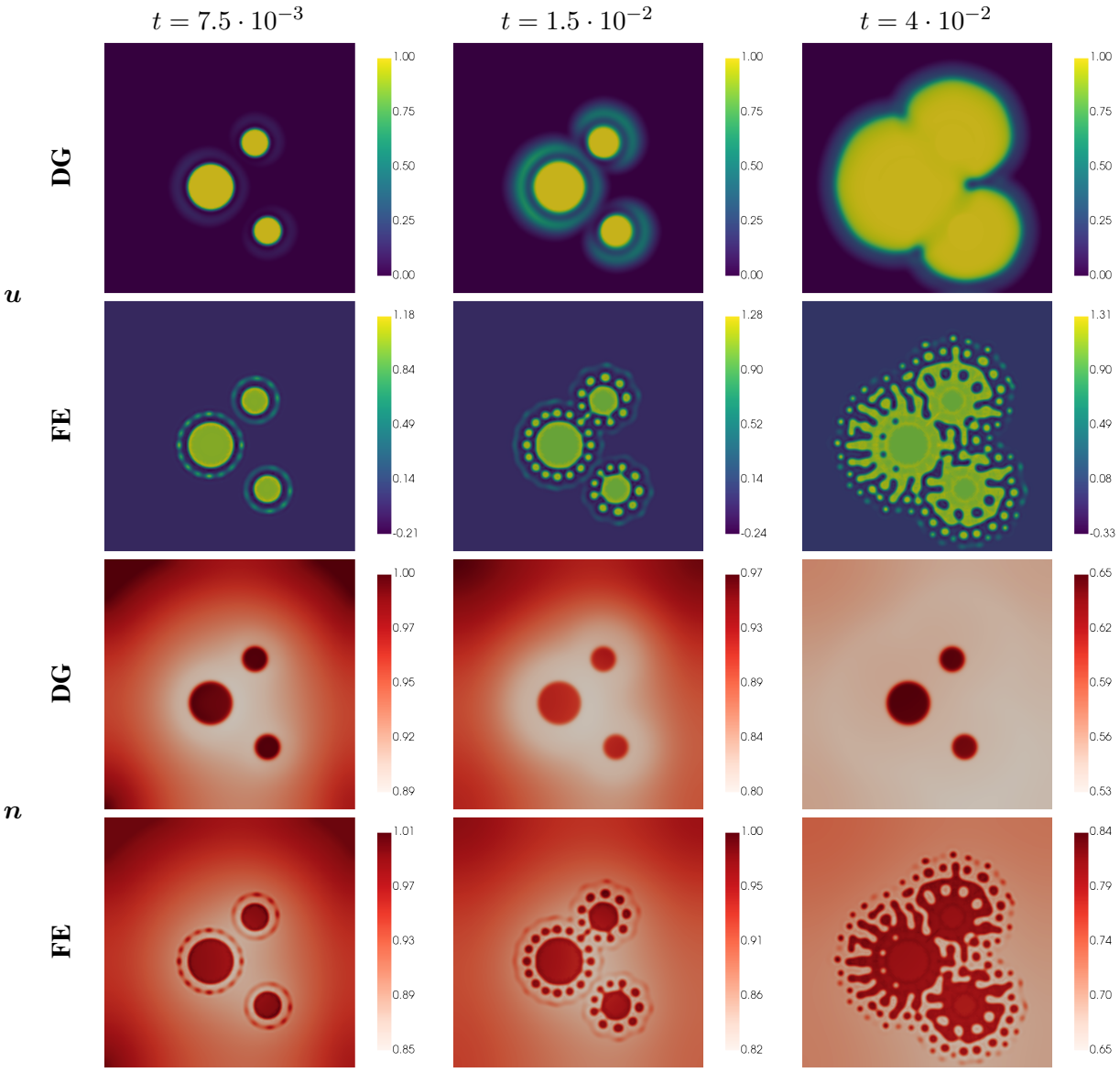

Figure 5.4 Tumor and nutrients for test (5.5.1) with $\chi_0 = 10$ at different time steps

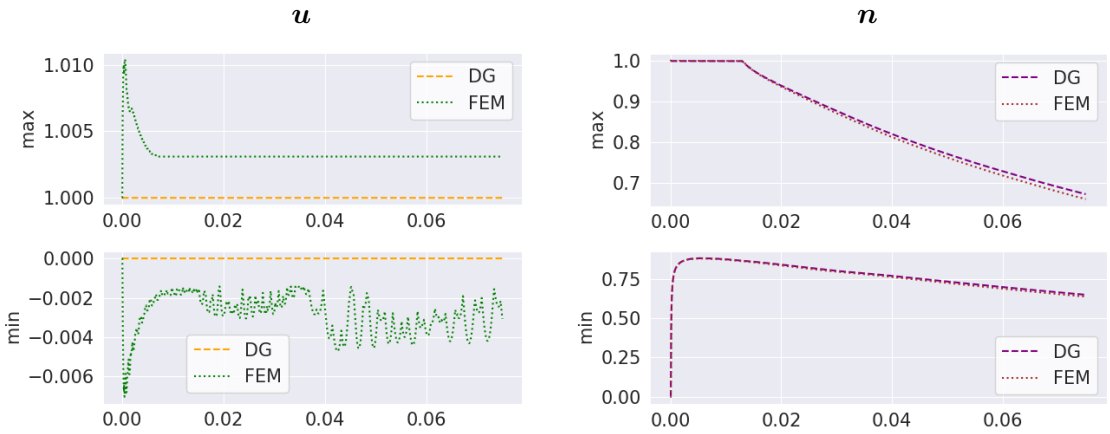

Figure 5.5 Pointwise bounds of the approximations for test 5.5.1 with $\chi_0 = 0$ (u left, n right)

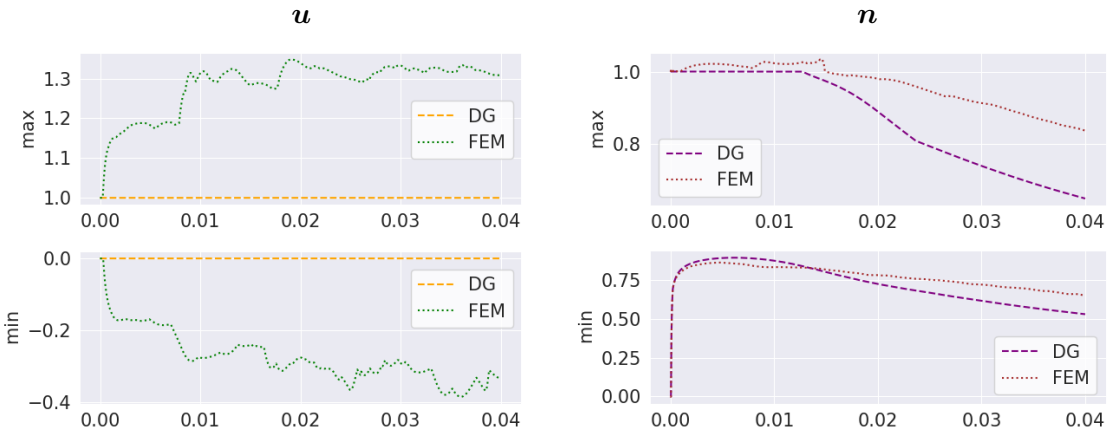

Figure 5.6 Pointwise bounds of the approximations for test 5.5.1 with $\chi_0 = 10$ (u left, n right)

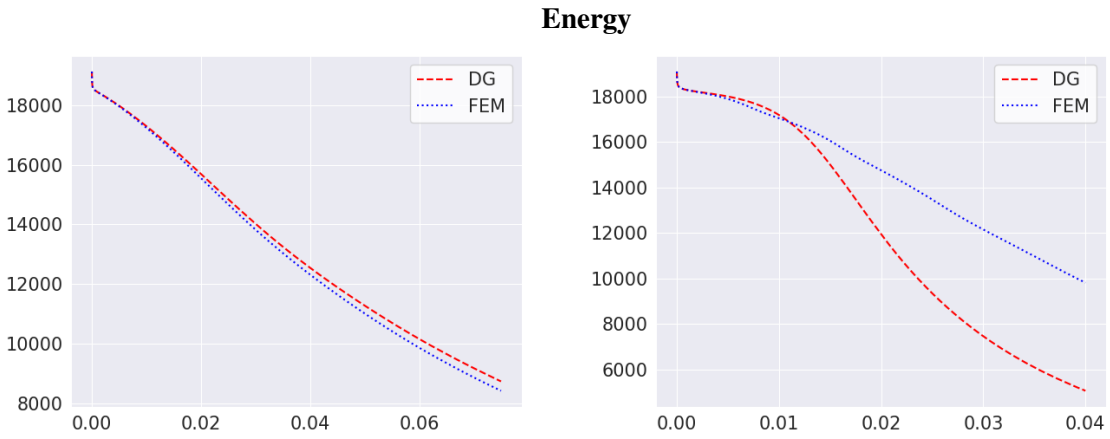

Figure 5.7 $E(\Pi_1^h u^m, n^m)$ for test 5.5.1 with $\chi_0 = 0$ (left) and with $\chi_0 = 10$ (right)

In particular, we consider the following initial conditions for tumor cells and nutrients:

$$u_0 = \frac{1}{2}\left[\tanh\left(\frac{1.75 - \sqrt{x^2+y^2}}{\sqrt{2}\varepsilon}\right) + 1\right],$$
$$n_0 = \frac{1}{2}(1-u_0) + \frac{1}{4}\left[\tanh\left(\frac{1 - \sqrt{(x-2.45)^2+(y-1.45)^2}}{\sqrt{2}\varepsilon}\right)\right.$$
$$\left. + \tanh\left(\frac{1.75 - \sqrt{(x+3.75)^2+(y-1)^2}}{\sqrt{2}\varepsilon}\right) + \tanh\left(\frac{2.5 - \sqrt{x^2+(y+5)^2}}{\sqrt{2}\varepsilon}\right) + 3\right],$$

which are shown in Figure 5.8.

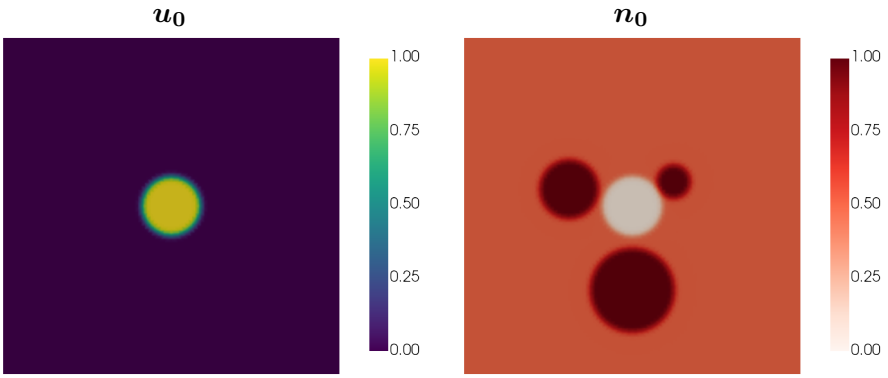

Figure 5.8 Initial conditions for test 5.5.2 (u_0 left, n_0 right)

We represent the behavior of the solution of the model under different set of parameters, see Figures 5.9–5.15. We set $C_u = 2.8$, $C_n = 2.8 \cdot 10^{-4}$, $h \approx 0.28$ for every experiment and we vary the rest of the parameters with respect to the reference test in Figure 5.9 ($P_0 = 0.5$, $\chi_0 = 0.1$ and $\Delta t = 0.1$). For the sake of brevity, we only show the nutrients variable for the reference test.

In fact, we have considered two different types of mobility and proliferation functions. On the one hand, the typical symmetric functions used in the previous experiment (5.33) have been used (see the top rows of Figures 5.9–5.15). However, on the other hand, we have considered the following non-symmetric choice of the mobility and proliferation functions

$$M(v) = h_{5,1}(v), \quad P(u,n) = h_{1,3}(u)n_{\oplus}, \tag{5.34}$$

whose associated results are plotted in the bottom row of Figures 5.9–5.15.

The proliferation function in (5.34) has been chosen to model a very quick tumor growth and nutrient consumption at the non-saturated state ($u \simeq 0$) that decays until the tumor is fully saturated ($u \simeq 1$). Moreover, the choice of the mobility function in (5.34) is thought to prevent the dissemination of the tumor and the nutrients in a non-saturated state ($u, n \simeq 0$) leading to a more local tumor/nutrient interaction due to the proliferation term.

Of course, the choice of these functions does not limit to those in (5.34) and other degenerated mobility and proliferation functions can be considered. In this sense, we would like to emphasize that the choice of these functions may be motivated by different types of tumor which might show particular growth and interaction with nutrients behaviors.

Indeed, we can observe the different expected behaviors of the solution for both choices of mobilities and proliferation functions in Figures 5.9–5.15. On the one hand, we may notice a local growth of the tumor where a proliferation area appears around the fully saturated tumor due to (5.34). Conversely, we can observe an eventual dissemination of the tumor all over the domain using (5.33) in the cases where the proliferation term is more significant than the cross-diffusion allowing the tumor to grow by consuming nutrients.

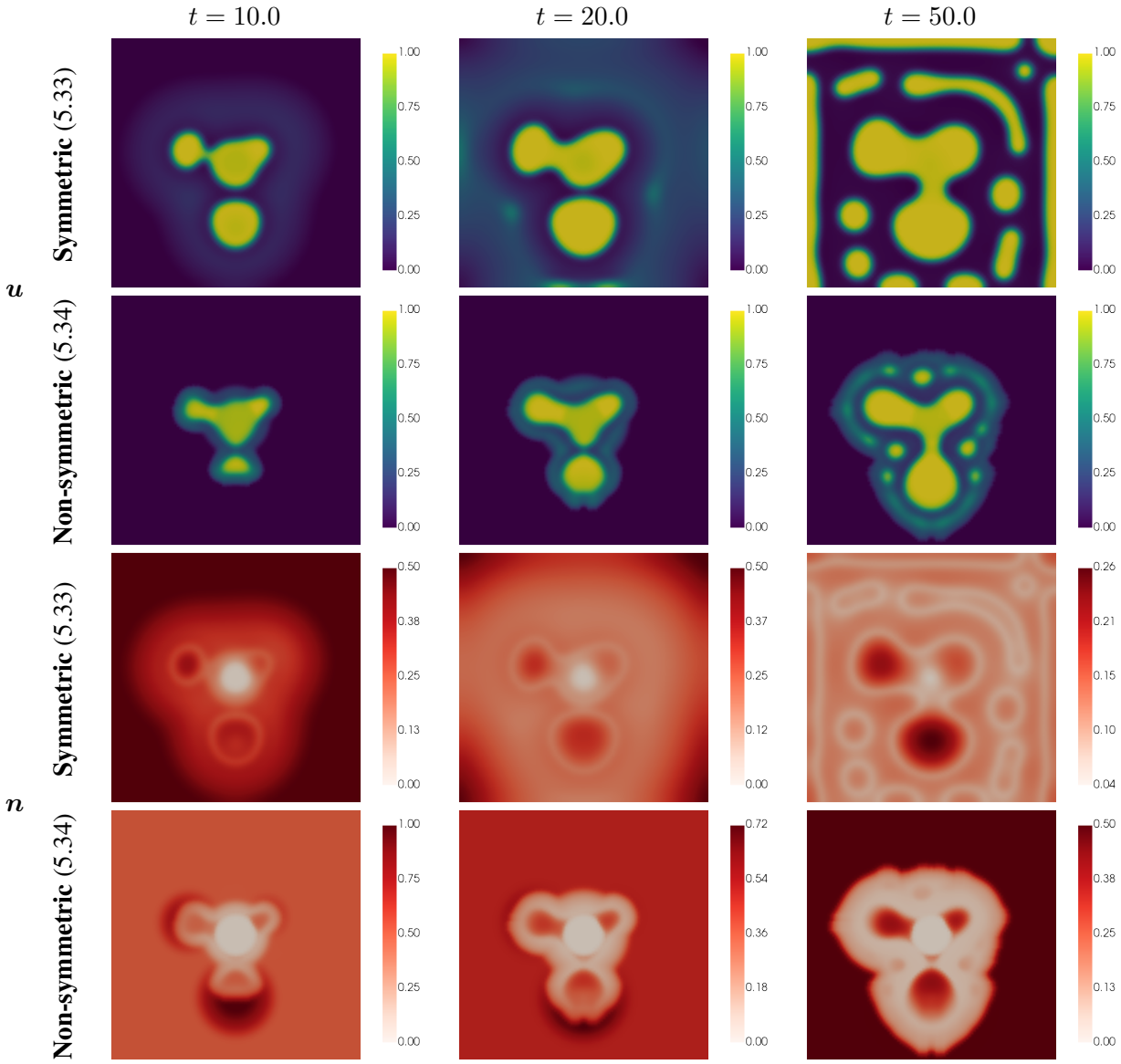

Figure 5.9 Tumor and nutrients for test (5.5.2) ($P_0 = 0.5$, $\chi_0 = 0.1$, $\Delta t = 0.1$) at different time steps

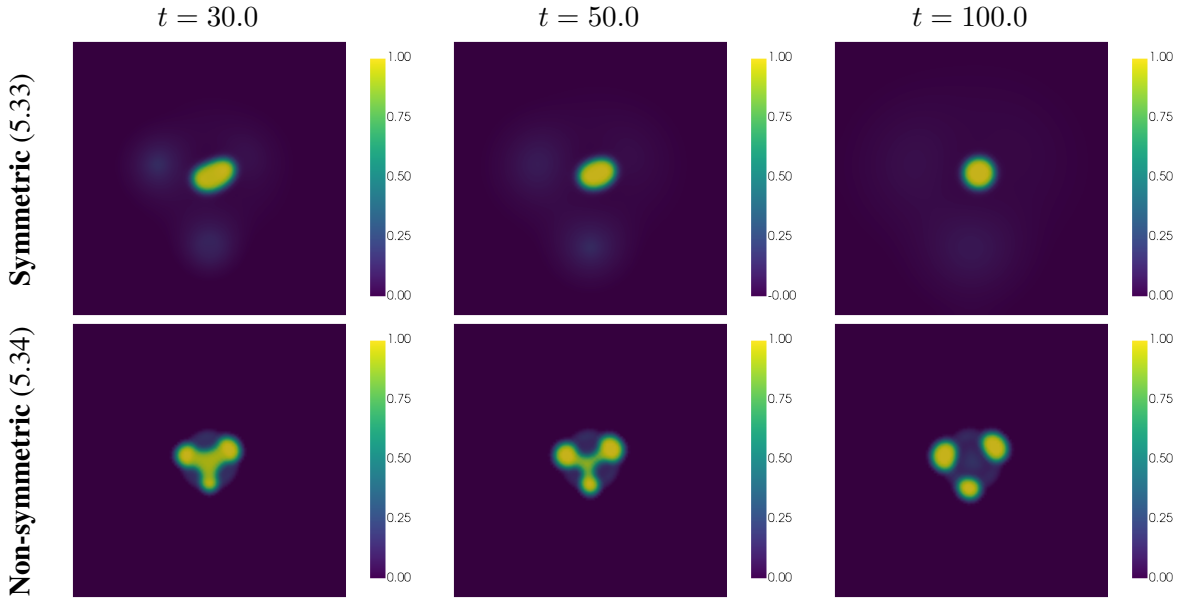

Figure 5.10 Tumor for test (5.5.2) ($P_0 = 0.001$, $\chi_0 = 0.1$, $\Delta t = 0.1$) at different time steps

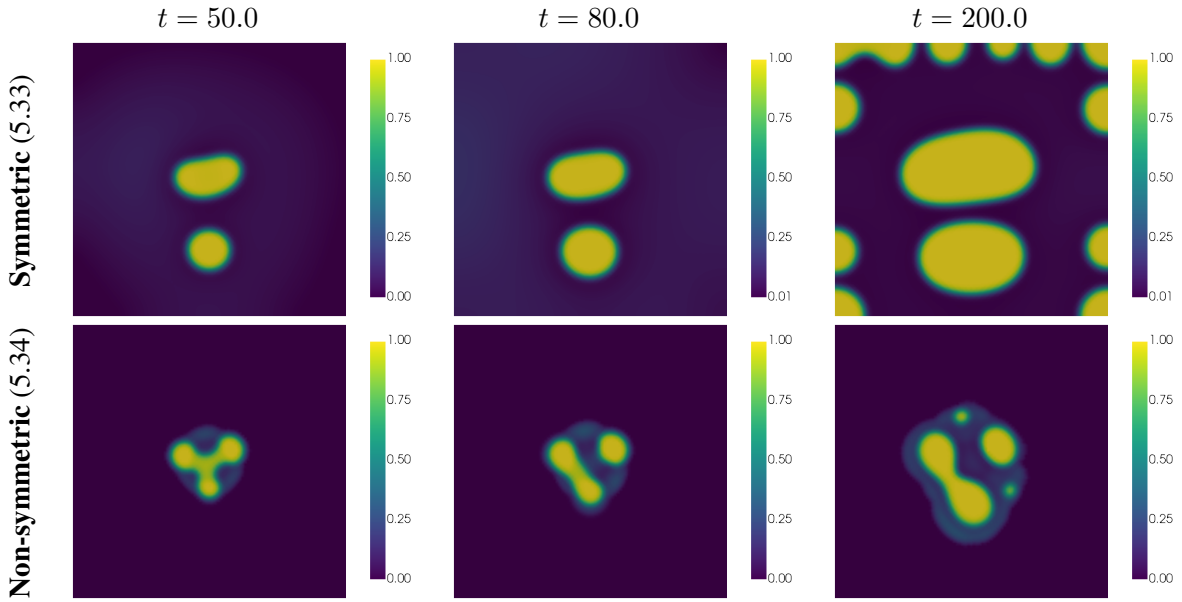

Figure 5.11 Tumor for test (5.5.2) ($P_0 = 0.05$, $\chi_0 = 0.1$, $\Delta t = 0.1$) at different time steps

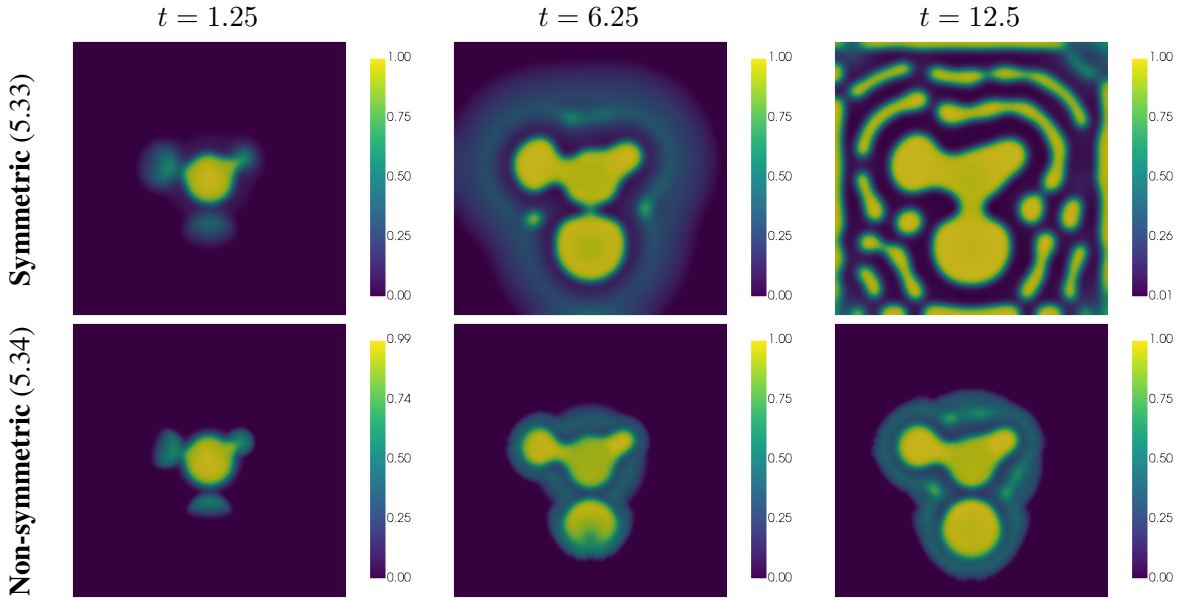

Figure 5.12 Tumor for test (5.5.2) ($P_0 = 2$, $\chi_0 = 0.1$, $\Delta t = 0.025$) at different time steps

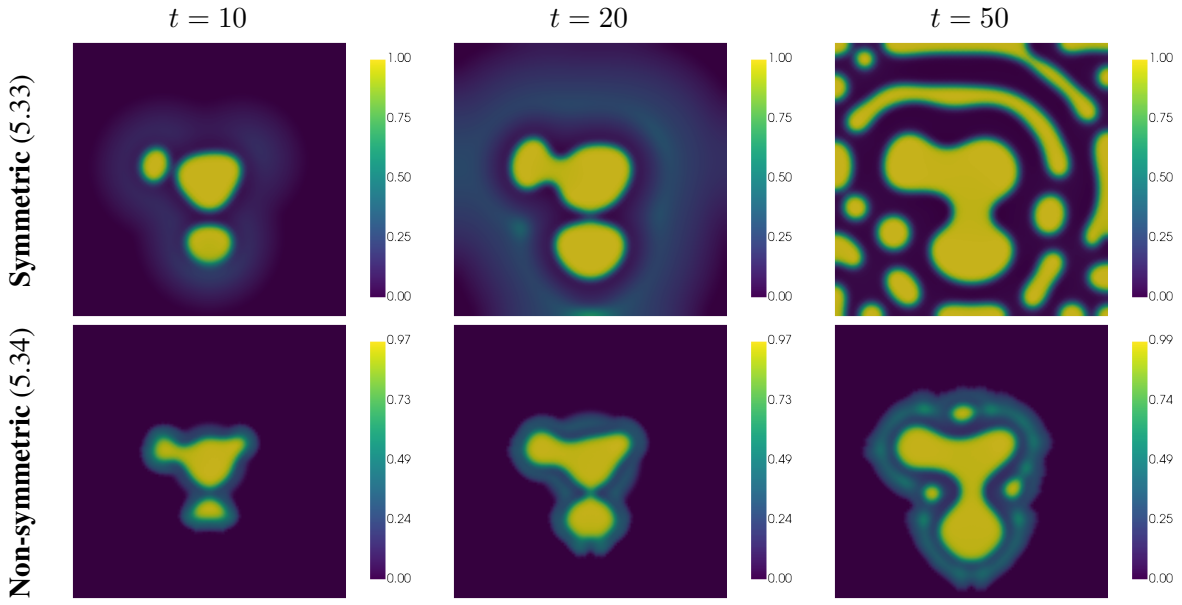

Figure 5.13 Tumor for test (5.5.2) ($P_0 = 0.5$, $\chi_0 = 0.01$, $\Delta t = 0.1$) at different time steps

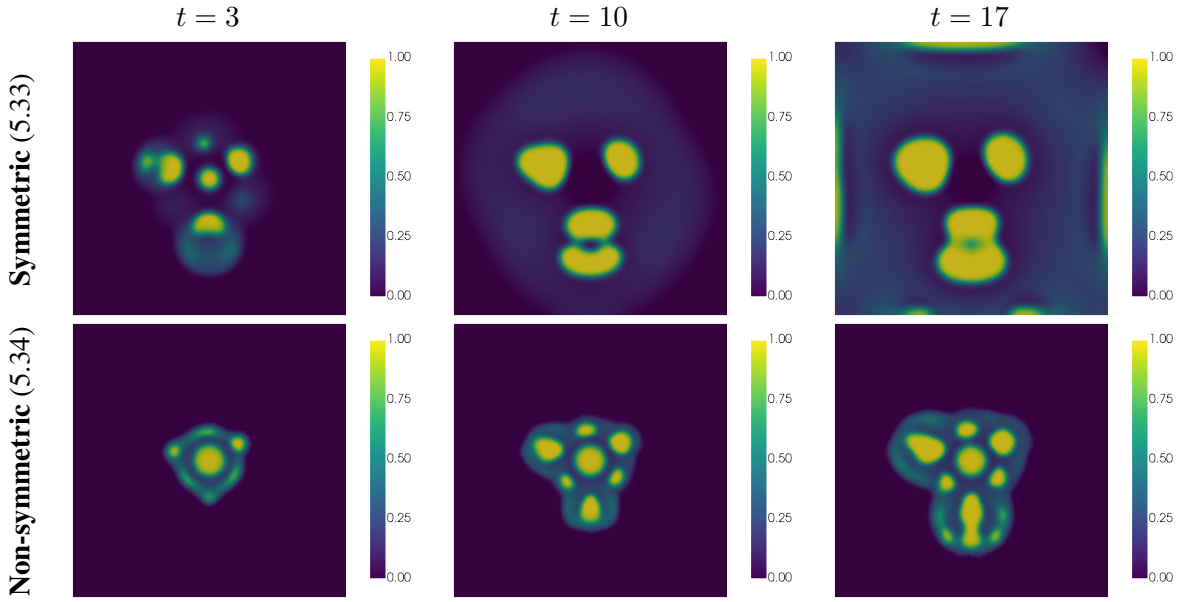

Figure 5.14 Tumor for test (5.5.2) ($P_0 = 0.5$, $\chi_0 = 0.5$, $\Delta t = 0.01$) at different time steps

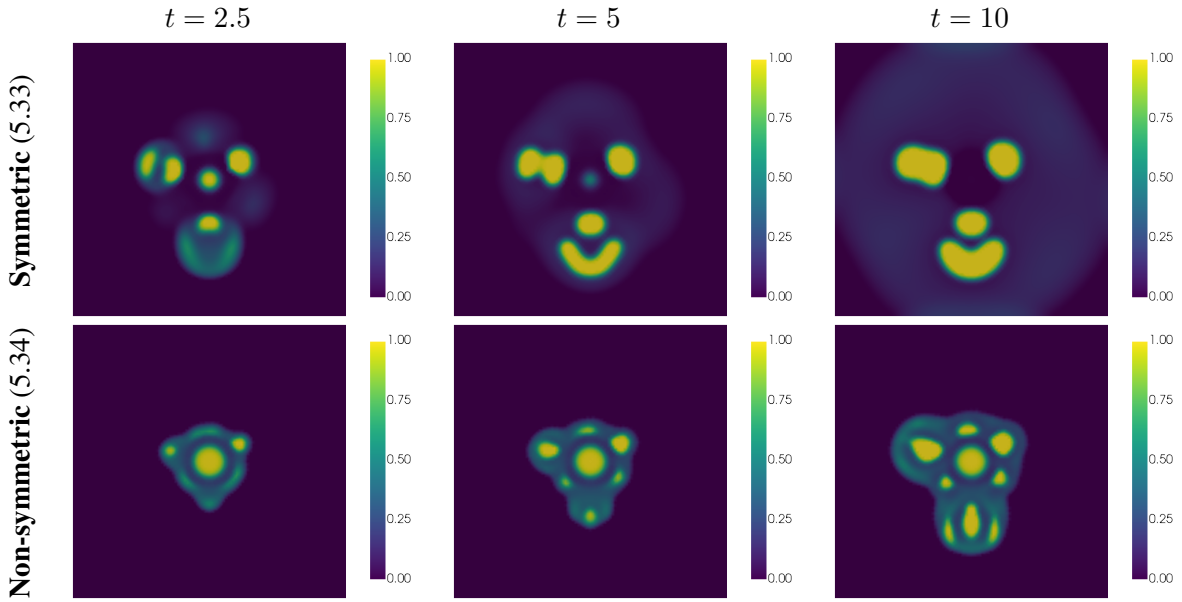

Figure 5.15 Tumor for test (5.5.2) ($P_0 = 0.5$, $\chi_0 = 1$, $\Delta t = 0.01$) at different time steps

CHAPTER 6

PROPERTY-PRESERVING NUMERICAL APPROXIMATIONS OF A CAHN–HILLIARD–NAVIER–STOKES MODEL WITH VARIABLE DENSITIES AND DEGENERATE MOBILITY

6.1 Abstract

In this chapter, we present a new computational framework using coupled and decoupled approximations for a Cahn–Hilliard–Navier–Stokes model with variable densities and degenerate mobility. In this sense, the coupled approximation is shown to conserve the mass of the fluid, preserve the pointwise bounds of the density and decrease an energy functional. In contrast, the decoupled scheme is presented as a more computationally efficient alternative but the discrete energy-decreasing property can not be assured. Both schemes are based on a finite element approximation for the Navier–Stokes fluid flow with discontinuous pressure and an upwind discontinuous Galerkin scheme for the Cahn–Hilliard part. Finally, several numerical experiments contrasting both approaches are conducted. In particular, results for a convergence test, a simple qualitative comparison and some well-known benchmark problems are shown. The results of this chapter have been already made available online as a preprint in [5].

6.2 Introduction

Hydrodynamics has been considered a research field of increasing interest among the scientific community during the last few decades. In this sense, diffuse interface models were proposed as a successful alternative to model fluid-solid interaction after van der Waals introduced the foundations in the pioneering paper [182]. Afterwards, these ideas were extended to fluid mixture and several works were published in this regard. In particular, both Hohelberg and Halpering, [115], and Gurtin et al., [110], arrived by different approaches to the same model, the well-known *Model H*, which would lead to the Cahn–Hilliard–Navier–Stokes (CHNS) system.

Since then, many different CHNS models have been developed using different techniques and extended to the case of fluids with different densities, see the model by Boyer [32] or by Ding et al. [65].

Moreover, several of these recent models satisfy some laws of thermodynamics. This is the case for the model by Lowengrub and Truskinovsky, [144], or the one by Abels et al., [1], which introduces an extra convective term in the momentum equation due to the different densities of the fluids. In [128] a careful revision of several CHNS models and their applications is provided. Also, recently, a very interesting survey has been published, [179], in which the authors, Eikelder et al., discuss different existing well-known CHNS models analyzing their advantages and disadvantages from a physical point of view. In fact, the authors of [179] provide some notions on properties a CHNS model has to satisfy in order to be physically consistent.

One characteristic that many of these models share is that the density of the mixture is usually interpolated as a linear function of the phase-field function. Hence, ensuring the pointwise bounds for this phase-field function in the Cahn-Hilliard equation, for instance, by using a degenerate mobility (see Chapter 2) is crucial to ensure a physically consistent model. Also, CHNS models conserve the total mass of the fluid and, as mentioned above, they tend to be thermodynamically consistent in the sense that the solutions of these models usually minimize an underlying energy law. Therefore, as these properties are extremely important for the physical meaning of the models it is likewise important to preserve them when approximating their solutions.

However, the transport of the diffuse interface by the velocity of the fluid is typically modeled by means of a convective term that is introduced into the Cahn-Hilliard equation and, as shown in Section 2.5, this term may lead to numerical instabilities in highly convective regimes if it is not treated carefully. The instabilities result in nonphysical spurious oscillations that make the approximation of the phase-field variable lose the pointwise bounds. In this regard, removing the numerical instabilities in the case of the convective Cahn-Hilliard model has been an object of study in recent works such as [81] or in Section 2.4.2, where we enforce the pointwise bounds by means of a discontinuous Galerkin (DG) upwind technique. Different ideas such as the use of limiters have been used in the case of the CHNS systems. For instance, in [140], the authors developed, by means of flux and slope limiters, a bound-preserving decoupled approximation of a CHNS simplified system with constant mobility. Later, the same model was approximated by high order polynomials using a decoupled scheme and a convex optimization technique with a scaling limiter to ensure the pointwise bounds, see [139].

In addition, designing an approximation that satisfies a discrete version of the continuous energy in the diffuse-interface models is not straightforward and usually requires the use of specific time-discrete

approximations such as the standard convex-splitting technique, [77], or the more recently developed SAV approach, [169]. In this sense, several advancements have been made towards the approximation of the CHNS models preserving the energy-stability constraint. For instance, we can find the work [107] where the authors propose an approximation of the model in [1] that decouples the phase-field equations from the fluid equations through a modified velocity. This approach was further studied in [100] and extended to a fully decoupled approximation that uses a pressure correction approach, [170].

Nevertheless, although it has been achieved in the case of a CHNS with a Flory-Huggins logarithmic potential (see [40]), to our best knowledge there is no published work on an approximation of a CHNS model with a Ginzburg-Landau polynomial potential and degenerate mobility that ensures both the mass-conservation, pointwise bounds and energy-stability properties.

To address this challenge, in this work, we provide an upwind DG approximation of the model by Abels et al. [1] where all the mass-conservation, the pointwise bounds and the energy-stability properties are preserved. Moreover, using similar ideas, a decoupled approximation of this model is developed. This decoupled approximation lacks the energy-stability property but is much more computationally efficient than the coupled counterpart.

Firstly, in Section 6.3 we introduce the CHNS model that we are going to consider and we present its properties. Then, in Section 6.4 we develop the coupled structure-preserving approximation of the aforementioned model, showing that it satisfies all the mass-conservation, pointwise bounds and energy-stability properties. On the other hand, in Section 6.5 we introduce the decoupled scheme as a computationally efficient alternative of the coupled counterpart showing that it satisfies both the mass-conservation and the pointwise bounds properties. Finally, in Section 6.6 we conduct several numerical experiments in which we compare both the coupled and the decoupled approaches. First, we compute a preliminary accuracy test in Section 6.6.1 that suggests that both schemes may have similar convergence order for all the variables in both $L^2(\Omega)$ and $H^1(\Omega)$ norms. Then, we provide a simple test where two bubbles are mixed in Section 6.6.2 to qualitatively compare both approaches. The results are in accordance with the previous theoretical analysis. Also, this test provides an example where the decoupled scheme becomes completely unstable due to the lack of the energy-stability property whereas the coupled counterpart provides a much more trustworthy, energy-decreasing solution. Finally, in Sections 6.6.3 and 6.6.4 we couple the CHNS system with a term modeling the action of gravitational

forces and conduct two benchmark tests: a heavier bubble in a lighter medium and the Rayleigh-Taylor instability.

The results of this chapter have been already made available online as a preprint in [5].

6.3 Cahn–Hilliard–Navier–Stokes model

We consider a mixture of two fluids with different densities $0 < \rho_1 < \rho_2$ and introduce a phase-field function $\phi = \phi(t, x) \in [-1, 1]$ such that $\phi = -1$ corresponds with fluid of density ρ_1, $\phi = 1$ with fluid of density ρ_2 and $\phi \in (-1, 1)$ in the interface between the two fluids. Then, the diffuse-interface Cahn–Hilliard–Navier–Stokes model proposed by Abels et al. in [1] and further numerically studied in [100, 107, 170], can be written as follows:

$$\rho(\phi)\boldsymbol{u}_t + ((\rho(\phi)\boldsymbol{u} - \boldsymbol{J}) \cdot \nabla)\,\boldsymbol{u} - \nabla \cdot (2\eta(\phi)\boldsymbol{D}\boldsymbol{u}) + \nabla p + \phi\nabla\mu = 0 \quad \text{in } \Omega \times (0,T), \tag{6.1a}$$

$$\nabla \cdot \boldsymbol{u} = 0 \quad \text{in } \Omega \times (0,T), \tag{6.1b}$$

$$\phi_t + \nabla \cdot (\phi\boldsymbol{u}) - \nabla \cdot (M(\phi)\nabla\mu) = 0 \quad \text{in } \Omega \times (0,T), \tag{6.1c}$$

$$-\lambda\varepsilon\Delta\phi + \frac{\lambda}{\varepsilon} f(\phi) = \mu \quad \text{in } \Omega \times (0,T), \tag{6.1d}$$

$$\boldsymbol{u}(0) = \boldsymbol{u}_0, \quad \phi(0) = \phi_0 \quad \text{in } \Omega, \tag{6.1e}$$

$$\boldsymbol{u} = 0, \quad \nabla\phi \cdot \boldsymbol{n} = 0, \quad M(\phi)\nabla\mu \cdot \boldsymbol{n} = 0 \quad \text{on } \partial\Omega. \tag{6.1f}$$

Here, $\boldsymbol{u}$ and p are the mean velocity and the pressure of the fluid respectively, and μ is the chemical potential related to the phase-field function ϕ. Also, $\boldsymbol{D}\boldsymbol{u} = \frac{1}{2}(\nabla\boldsymbol{u} + \nabla\boldsymbol{u}^t)$ is the strain tensor, $f(\phi)$ is the derivative of the Ginzburg-Landau double well potential $F(\phi) = \frac{1}{4}(\phi^2 - 1)^2$, i.e. $f(\phi) = F'(\phi) = (\phi^2 - 1)\phi$, $M(\phi) = (1 - \phi^2)_\oplus$ is the degenerate (truncated) mobility function and

$$\boldsymbol{J} = \frac{\rho_2 - \rho_1}{2} M(\phi)\nabla\mu$$

is the extra-convective term due to different densities. Moreover, the density of the mixture $\rho = \rho(\phi)$ depending on the phase-field variable ϕ, can be defined either as the solution of the mass balance equation

$$(\partial_t\rho, \overline{\rho}) - (\rho\boldsymbol{u} - \boldsymbol{J}, \nabla\overline{\rho}) = 0, \quad \forall\overline{\rho} \in H^1(\Omega), \quad \text{in } (0,T), \tag{6.2}$$

or, by taking into account the equation (6.1c), as the explicit relation

$$\rho(\phi) = \frac{\rho_1 + \rho_2}{2} + \frac{\rho_2 - \rho_1}{2}\phi \coloneqq \rho_{\text{avg}} + \rho_{\text{dif}}\phi. \tag{6.3}$$

Remark 6.3.1. *We have written the equation* (6.2) *in its more general variational formulation since* $\boldsymbol{J}$ *does not necessarily belong to* $H^1(\Omega)^d$. *It is clear from* (6.3) *that* $\rho_1 \leq \rho(\phi) \leq \rho_2$ *in* $\Omega \times (0,T)$ *is equivalent to* $-1 \leq \phi \leq 1$ *in* $\Omega \times (0,T)$. *Consequently, it is important the constraint* $\phi \in [-1,1]$ *to preserve the physical meaning of the model because the density of the mixture* $\rho(\phi)$ *must satisfy* $\rho(\phi) \in [\rho_1, \rho_2]$.

Finally, $\eta \in \mathcal{C}([-1,1])$ with $\eta(\phi) \geq C$ for certain $C > 0$ and for all $\phi \in [-1,1]$ is the viscosity of the mixture, $\lambda > 0$ is a constant related to the energy density and $\varepsilon > 0$ is a small parameter related to the thickness of the interface between the two fluids.

Since if p is a pressure function solution of (6.1) then $p + C$ is also solution for any constant C, it is usual to consider the zero mean-value pressure constraint $\int_\Omega p = 0$.

We can consider the following variational formulation of problem (6.1): Find $(\boldsymbol{u}, p, \phi, \mu)$ such that $\boldsymbol{u} \in L^\infty(0,T;L^2(\Omega)^d) \cap L^2(0,T;H_0^1(\Omega)^d)$, $p \in W^{-1,\infty}(0,T;L^2(\Omega))$ with $\int_\Omega p = 0$, $\phi \in L^\infty(0,T;H^1(\Omega))$ with $-1 \leq \phi \leq 1$ a.e. in $\Omega \times (0,T)$, $\mu : \Omega \times (0,T) \to \mathbb{R}$ with $\sqrt{M(\phi)}\nabla\mu \in L^2(0,T;L^2(\Omega))$, satisfying

$$\begin{aligned}
&\langle \rho(\phi)\boldsymbol{u}_t, \overline{\mathbf{u}}\rangle + \left([(\rho(\phi)\boldsymbol{u} - \rho_{\text{dif}} M(\phi)\nabla\mu)\cdot\nabla]\,\boldsymbol{u}, \overline{\mathbf{u}}\right) \\
&\quad + 2\left(\eta(\phi)\boldsymbol{D}\boldsymbol{u}, \boldsymbol{D}\overline{\mathbf{u}}\right) - (p, \nabla\cdot\overline{\mathbf{u}}) - (\mu, \nabla\cdot(\phi\overline{\mathbf{u}})) = 0, && \text{(6.4a)}\\
&\quad (\nabla\cdot\boldsymbol{u}, \overline{p}) = 0, && \text{(6.4b)}\\
&\langle \phi_t, \overline{\phi}\rangle + \left(\nabla\cdot(\phi\boldsymbol{u}), \overline{\phi}\right) + \left(M(\phi)\nabla\mu, \nabla\overline{\phi}\right) = 0, && \text{(6.4c)}\\
&\lambda\varepsilon\left(\nabla\phi, \nabla\overline{\mu}\right) + \frac{\lambda}{\varepsilon}\left(f(\phi), \overline{\mu}\right) - (\mu, \overline{\mu}) = 0, && \text{(6.4d)}
\end{aligned}$$

for each $(\overline{\mathbf{u}}, \overline{p}, \overline{\mu}, \overline{\phi}) \in (H_0^1(\Omega)\cap L^\infty(\Omega))^d \times L^2(\Omega) \times H^1(\Omega) \times H^1(\Omega)$. Above,

$$\left(\eta(\phi)\boldsymbol{D}\boldsymbol{u}, \boldsymbol{D}\overline{\mathbf{u}}\right) = \int_\Omega \eta(\phi)\boldsymbol{D}\boldsymbol{u} : \boldsymbol{D}\overline{\mathbf{u}},$$

where : denotes the Frobenius inner product.

Proposition 6.3.2. *The mass of the phase-field variable is conserved, because it holds*

$$\frac{d}{dt}\int_\Omega \phi(t,x)dx = 0.$$

In particular, the mass of the fluid is conserved, because using (6.3)*,*

$$\int_\Omega \rho(\phi(t,x))dx = |\Omega|\rho_{avg} + \rho_{dif}\int_\Omega \phi(t,x)dx = |\Omega|\rho_{avg} + \rho_{dif}\int_\Omega \phi_0(x)dx = \int_\Omega \rho(\phi_0(x))dx.$$

Proof. Just test (6.4c) by $\overline{\phi} = 1$. □

Proposition 6.3.3. *Assuming a sufficiently regular solution of* (6.4a)-(6.4d)*, the following energy law holds:*

$$\frac{d}{dt}E(\boldsymbol{u},\phi) + 2\int_\Omega \eta(\phi)|\boldsymbol{Du}|^2 + \int_\Omega M(\phi)|\nabla\mu|^2 = 0, \tag{6.5}$$

where $|\boldsymbol{Du}|^2 = \sum_{i=1}^d |\boldsymbol{Du}_i|^2$*, with* $\boldsymbol{Du}_i$ *denoting the* i*-th row of the stress tensor* $\boldsymbol{Du}$*, and*

$$E(\boldsymbol{u},\phi) \coloneqq \int_\Omega \rho(\phi)\frac{|\boldsymbol{u}|^2}{2} + \frac{\lambda\varepsilon}{2}\int_\Omega |\nabla\phi|^2 + \frac{\lambda}{\varepsilon}\int_\Omega F(\phi), \tag{6.6}$$

where the first term is associated to the kinetic energy and the others to the potential energy. In particular, the energy $E(\boldsymbol{u},\phi)$ *is time decreasing because*

$$\frac{d}{dt}E(\boldsymbol{u},\phi) \leq 0.$$

Proof. We argue formally, by considering that all the functions that appear below are regular enough so that the expressions are true. Moreover, they are regarded as functions to be evaluated at $t \in (0,T)$, although, for clarity, we will omit it.

If we test (6.4a)–(6.4d) by $\overline{\mathbf{u}} = \boldsymbol{u}$, $\overline{p} = p$, $\overline{\phi} = \mu$ and $\overline{\mu} = \phi_t$ and we add up the expressions, we obtain:

$$\begin{aligned}(\rho(\phi)\boldsymbol{u}_t,\boldsymbol{u}) + \lambda\varepsilon\left(\nabla\phi,\nabla\phi_t\right) + \frac{\lambda}{\varepsilon}\left(F'(\phi),\phi_t\right)& \\ + \left(\left[(\rho(\phi)\boldsymbol{u} - \boldsymbol{J})\cdot\nabla\right]\boldsymbol{u},\boldsymbol{u}\right) + 2\int_\Omega \eta(\phi)|\boldsymbol{Du}|^2 + \int_\Omega M(\phi)|\nabla\mu|^2 = 0.&\end{aligned}$$

Now, testing (6.2) by $\overline{\rho} = |\boldsymbol{u}|^2/2$, we have

$$\left(\partial_t \rho(\phi), \frac{|\boldsymbol{u}|^2}{2}\right) - ([(\rho(\phi)\boldsymbol{u} - \boldsymbol{J}) \cdot \nabla]\boldsymbol{u}, \boldsymbol{u}) = 0.$$

By adding the two previous expressions, the convective term $([(\rho(\phi)\boldsymbol{u} - \boldsymbol{J}) \cdot \nabla]\boldsymbol{u}, \boldsymbol{u})$ cancels. Hence, taking into account that

$$\begin{aligned}
\frac{d}{dt}\int_\Omega \rho(\phi)\frac{|\boldsymbol{u}|^2}{2} &= (\rho(\phi)\boldsymbol{u}_t, \boldsymbol{u}) + \left(\partial_t\rho(\phi), \frac{|\boldsymbol{u}|^2}{2}\right), \\
\frac{1}{2}\frac{d}{dt}\int_\Omega |\nabla\phi|^2 &= (\nabla\phi, \nabla\phi_t), \\
\frac{d}{dt}\int_\Omega F(\phi) &= \big(F'(\phi), \phi_t\big),
\end{aligned}$$

we can conclude that the energy law (6.5) holds. □

6.4 Coupled structure-preserving scheme

In this section we develop a fully coupled discretization of the model (6.1) that preserves all properties at the discrete level, including the mass conservation, pointwise bounds of the phase-field and density of the mixture variables, and the decreasing of the energy (also called energy-stability).

6.4.1 Discrete scheme

Following the ideas of Sections 2.4.2, 3.4 and 5.4.2 we define the projections $\Pi_0 \colon L^1(\Omega) \longrightarrow \mathbb{P}_0^{\text{disc}}(\mathcal{T}_h)$, $\Pi_1 \colon L^1(\Omega) \longrightarrow \mathbb{P}_1^{\text{cont}}(\mathcal{T}_h)$ and $\Pi_1^h \colon L^1(\Omega) \longrightarrow \mathbb{P}_1^{\text{cont}}(\mathcal{T}_h)$ as follows:

$$(\Pi_0 g, \overline{w}) = (g, \overline{w}), \qquad \forall\, \overline{w} \in \mathbb{P}_0^{\text{disc}}(\mathcal{T}_h) \tag{6.7}$$

$$(\Pi_1 g, \overline{v}) = (g, \overline{v}), \qquad \forall\, \overline{v} \in \mathbb{P}_1^{\text{cont}}(\mathcal{T}_h), \tag{6.8}$$

$$\left(\Pi_1^h g, \overline{v}\right)_h = (g, \overline{v}), \qquad \forall\, \overline{v} \in \mathbb{P}_1^{\text{cont}}(\mathcal{T}_h), \tag{6.9}$$

where $(\cdot,\cdot)$ and $(\cdot,\cdot)_h$ denote the usual scalar product in $L^2(\Omega)$ and the mass-lumping scalar product in $\mathbb{P}_1^{\text{cont}}(\mathcal{T}_h)$, respectively.

We propose the following numerical scheme: find $\boldsymbol{u}^{m+1} \in \mathcal{U}_h$, $p^{m+1} \in \mathcal{P}_h$ with $\int_\Omega p^{m+1} = 0$, $\phi^{m+1} \in \mathbb{P}_0^{\text{disc}}(\mathcal{T}_h)$ and $\mu^{m+1} \in \mathbb{P}_1^{\text{cont}}(\mathcal{T}_h)$ such that

$$\begin{aligned}
&\left(\rho(\Pi_1^h\phi^m)\delta_t\boldsymbol{u}^{m+1}, \overline{\mathbf{u}}\right) + \left(\left[\left(\rho(\Pi_1^h\phi^m)u^m - \boldsymbol{J}_h^m\right)\cdot\nabla\right]\boldsymbol{u}^{m+1}, \overline{\mathbf{u}}\right) \\
&+2\left(\eta(\phi^m)\boldsymbol{D}\boldsymbol{u}^{m+1}, \boldsymbol{D}\overline{\mathbf{u}}\right) - \left(p^{m+1}, \nabla\cdot\overline{\mathbf{u}}\right) + c_h(\phi^{m+1}, \Pi_0\mu^{m+1}, \overline{\mathbf{u}}) \\
&+s_h^1(\boldsymbol{u}^{m+1}, \boldsymbol{u}^m, \Pi_1^h\phi^{m+1}, \Pi_1^h\phi^m, \mu^m, \overline{\mathbf{u}}) + s_h^2(\boldsymbol{u}^{m+1}, \phi^{m+1}, \Pi_0\mu^{m+1}, \overline{\mathbf{u}}) = 0, \qquad (6.10a)\\
&\left(\nabla\cdot\boldsymbol{u}^{m+1}, \overline{p}\right) = 0, \qquad (6.10b)\\
&\left(\delta_t\phi^{m+1}, \overline{\phi}\right) + a_h^{\text{upw}}(\boldsymbol{u}^{m+1}; \phi^{m+1}, \overline{\phi}) + b_h^{\text{upw}}(\nabla_{\boldsymbol{n}}^0\mu^{m+1}; M(\phi^{m+1}), \overline{\phi}) = 0, \qquad (6.10c)\\
&\lambda\varepsilon\left(\nabla(\Pi_1^h\phi^{m+1}), \nabla\overline{\mu}\right) + \frac{\lambda}{\varepsilon}\left(f(\Pi_1^h\phi^{m+1}, \Pi_1^h\phi^m), \overline{\mu}\right) - \left(\mu^{m+1}, \overline{\mu}\right)_h = 0, \qquad (6.10d)
\end{aligned}$$

for each $\overline{\mathbf{u}} \in \mathcal{U}_h$, $\overline{p} \in \mathcal{P}_h$, $\overline{\phi} \in \mathbb{P}_0^{\text{disc}}(\mathcal{T}_h)$, $\overline{\mu} \in \mathbb{P}_1^{\text{cont}}(\mathcal{T}_h)$, where

$$\boldsymbol{J}_h^m = \rho_{\text{dif}} M(\Pi_1^h\phi^m)\Pi_1(\nabla\mu^m),$$

and

$$f(\phi_1, \phi_0) \coloneqq F_i'(\phi_1) + F_e'(\phi_0) \text{ with } F_i(\phi) \coloneqq \phi^2 + \frac{1}{4},\ F_e(\phi) \coloneqq \frac{1}{4}\phi^4 - \frac{3}{2}\phi^2 \qquad (6.11)$$

such that $F(\phi) = F_i(\phi) + F_e(\phi)$ is a convex splitting discretization of the Ginzburg-Landau double well potential $F(\phi)$ for any $\phi \in [-1, 1]$.

Also, $(\mathcal{U}_h, \mathcal{P}_h)$ is a compatible "inf-sup" pair of finite-dimensional spaces satisfying that $\mathcal{U}_h \subset (\mathcal{C}^0(\overline{\Omega}) \cap H_0^1(\Omega))^d$ and $\mathbb{P}_0^{\text{disc}}(\mathcal{T}_h) \subset \mathcal{P}_h$. In fact, the restriction $\mathbb{P}_0^{\text{disc}}(\mathcal{T}_h) \subset \mathcal{P}_h$ is needed in order to guarantee the local incompressibility of $\boldsymbol{u}^{m+1}$ in the following sense:

$$\sum_{e\in\mathcal{E}_h^{\text{i}}}\int_e (\boldsymbol{u}^{m+1}\cdot\boldsymbol{n}_e)\,[\![\overline{p}]\!] = 0, \quad \forall\,\overline{p} \in \mathbb{P}_0^{\text{disc}}(\mathcal{T}_h), \qquad (6.12)$$

which can be derived integrating by parts in (6.10b). This constraint will allow us to preserve the pointwise bounds of ϕ^{m+1}, see Theorem 6.4.5 below. Notice that the discretization of the pressure and the divergence term (6.10b) is the standard Stokes DG approach [63, 163] for continuous velocity and discontinuous pressure.

Remark 6.4.1. *Some possible choices of compatible spaces $(\mathcal{U}_h, \mathcal{P}_h)$ are the following (see [31, 74] for the details):*

- $(\mathcal{U}_h, \mathcal{P}_h) = ((\mathbb{P}_2^{cont}(\mathcal{T}_h) \cap H_0^1(\Omega))^d, \mathbb{P}_0^{disc}(\mathcal{T}_h))$ *which is stable for* $d = 2$ *but not for* $d = 3$*.*

- $(\mathcal{U}_h, \mathcal{P}_h) = ((\mathbb{P}_2^{bubble}(\mathcal{T}_h) \cap H_0^1(\Omega))^d, \mathbb{P}_1^{disc}(\mathcal{T}_h))$ *which is stable for* $d = 2, 3$ *but requires a higher computational effort. Here,* $\mathbb{P}_2^{bubble}(\mathcal{T}_h)$ *denotes the* $\mathbb{P}_2^{cont}(\mathcal{T}_h)$ *space enriched with a bubble of order 3.*

Notice that, for any choice of this pair $(\mathcal{U}_h, \mathcal{P}_h)$, the error bounds are expected to be determined by the lowest accuracy approximation of the phase-field function by $\mathbb{P}_0^{\text{disc}}(\mathcal{T}_h)$.

Moreover, $c_h(\phi, \mu, \overline{\mathbf{u}})$ is a centered discretization of the term $(\phi\nabla\mu, \overline{\mathbf{u}}) = -(\mu, \nabla\cdot(\phi\overline{\mathbf{u}}))$ in (6.4a) defined as

$$c_h(\phi, \mu, \overline{\mathbf{u}}) \coloneqq -\int_\Omega \nabla\cdot(\phi\overline{\mathbf{u}})\mu - \sum_{e\in\mathcal{E}_h^{\text{i}}}\int_e (\overline{\mathbf{u}}\cdot\boldsymbol{n}_e)\,\{\!\{\phi\}\!\}\,[\![\mu]\!]\,, \tag{6.13}$$

where the second term is a consistent stabilization term depending on the jumps of μ on the interior edges of the mesh $\mathcal{T}_h$.

In (6.10c) we have considered two different upwind formulas, the classical upwind

$$a_h^{\text{upw}}(\boldsymbol{u}; \phi, \overline{\phi}) \coloneqq \sum_{e\in\mathcal{E}_h^{\text{i}}, e=K\cap L}\int_e ((\boldsymbol{u}\cdot\boldsymbol{n}_e)_\oplus\phi_K - (\boldsymbol{u}\cdot\boldsymbol{n}_e)_\ominus\phi_L)\,[\![\overline{\phi}]\!] \tag{6.14}$$

whose properties were discussed in Section 2.3, and

$$b_h^{\text{upw}}(\nabla_{\boldsymbol{n}}^0\mu; M(\phi), \overline{\phi}),$$

which follows the ideas introduced in Sections 3.4 and 5.4.2, and which will be detailed in the Section 6.4.1.1.

Finally, we have introduced in (6.10a) two consistent stabilizations terms:

$$s_h^1(\boldsymbol{u}_1, \boldsymbol{u}_0, \phi_1, \phi_0, \mu, \overline{\mathbf{u}}) \coloneqq \frac{1}{2}\Big\{(\delta_t\rho(\phi_1), \boldsymbol{u}_1\cdot\overline{\mathbf{u}}) - (\rho(\phi_0)\boldsymbol{u}_0 - \rho_{\text{dif}}M(\phi_0)\Pi_1(\nabla\mu), \nabla(\boldsymbol{u}_1\cdot\overline{\mathbf{u}}))\Big\}, \tag{6.15}$$

which, following the ideas of [107], can be interpreted as a residual to the equation (6.2); and

$$s_h^2(\boldsymbol{u}, \phi, \mu, \overline{\mathbf{u}}) \coloneqq -\frac{1}{2}\sum_{e\in\mathcal{E}_h^{\text{i}}}\int_e (\overline{\mathbf{u}}\cdot\boldsymbol{n}_e)\,\text{sign}(\boldsymbol{u}\cdot\boldsymbol{n}_e)\,[\![\phi]\!]\,[\![\mu]\!]\,, \tag{6.16}$$

which is introduced to control the influence of the upwind term $a_h^{\text{upw}}(\boldsymbol{u}^{m+1};\phi^{m+1},\overline{\phi})$ in (6.10c). This latter stabilization together with the centered approximation $c_h(\phi^{m+1},\Pi_0\mu^{m+1},\overline{\mathbf{u}})$ of the phase-field force in the momentum equation (6.10a), cancel the effect of the transport of the phase-field function by the mean velocity $\boldsymbol{u}^{m+1}$ and allow us to obtain a discrete energy inequality, see Lemma 6.4.7 below.

To start the algorithm we take $\phi^0=\Pi_0\phi_0$ where ϕ_0 is the continuous initial data, which satisfies $\phi_0\in[-1,1]$. Notice that, one also has $\phi^0\in[-1,1]$.

Remark 6.4.2. *Observe that the* 0*-mean value constraint on the pressure has been removed from the discrete formulation* (6.10)*. This constraint will be enforced in practice by using an additional penalty term, see Section 6.6 below.*

6.4.1.1 Definition of the upwind form $b_h^{\text{upw}}(\cdot;\cdot,\cdot)$

In order to define the upwind form $b_h^{\text{upw}}(\cdot;\cdot,\cdot)$ we follow the ideas of Sections 3.4 and 5.4.2.

First, we split the mobility function $M(z)$ for $z\in\mathbb{R}$ into its increasing and decreasing parts, denoted respectively by $M^{\uparrow}(z)$ and $M^{\downarrow}(z)$, as follows:

$$
\begin{aligned}
M^{\uparrow}(z)&=\int_{-1}^{\min(z,1)}M'(s)_{\oplus}ds=\int_{-1}^{\min(z,1)}(-2s)_{\oplus}ds,\\
M^{\downarrow}(z)&=-\int_{-1}^{\min(z,1)}M'(s)_{\ominus}ds=-\int_{-1}^{\min(z,1)}(-2s)_{\ominus}ds
\end{aligned}
$$

Therefore,

$$
M^{\uparrow}(z)=\begin{cases}M(z) & \text{if } z\le 0\\ M(0) & \text{if } z>0\end{cases},\quad M^{\downarrow}(z)=\begin{cases}0 & \text{if } z\le 0\\ M(z)-M(0) & \text{if } z>0\end{cases}. \tag{6.18}
$$

Notice that $M^{\uparrow}(z)+M^{\downarrow}(z)=M(z)$.

Following the work in Section 2.4.2, we can define the following upwind form for any $\phi, \overline{\phi} \in \mathbb{P}_0^{\text{disc}}(\mathcal{T}_h)$ and $\mu \in \mathbb{P}_1^{\text{cont}}(\mathcal{T}_h)$:

$$b_h^{\text{upw}}(-\nabla_{\boldsymbol{n}}\mu; M(\phi), \overline{\phi}) \coloneqq \sum_{e \in \mathcal{E}_h^{\text{i}}, e=K\cap L} \int_e \Big((-\nabla_{\boldsymbol{n}}\mu)_{\oplus}(M^{\uparrow}(\phi_K) + M^{\downarrow}(\phi_L))_{\oplus} - (-\nabla_{\boldsymbol{n}}\mu)_{\ominus}(M^{\uparrow}(\phi_L) + M^{\downarrow}(\phi_K))_{\oplus} \Big) [\![\overline{\phi}]\!] \,, \tag{6.19}$$

where $\nabla_{\boldsymbol{n}}\mu \coloneqq \{\!\{\nabla\mu\}\!\} \cdot \boldsymbol{n}_e$ on every $e \in \mathcal{E}_h$.

Nonetheless, if we want to ensure a discrete energy law, as was done in Sections 3.4 and 5.4.2, we need to assume again Hypothesis 3.4.1.

Under this hypothesis, we can consider the following consistent approximation on every $e \in \mathcal{E}_h^i$, as done in Sections 3.4 and 5.4.2:

$$\nabla\mu \cdot \boldsymbol{n}_e \simeq \frac{-[\![\Pi_0\mu]\!]}{\mathcal{D}_e(\mathcal{T}_h)} \coloneqq \nabla_{\boldsymbol{n}}^0\mu|_e, \tag{6.20}$$

where $\mathcal{D}_e(\mathcal{T}_h)$ is the distance between the barycenters of the triangles of the mesh $\mathcal{T}_h$ that share $e \in \mathcal{E}_h^{\text{i}}$.

Therefore, we can extend the definition of the upwind form (6.19) as follows:

$$\begin{aligned} b_h^{\text{upw}}(-\nabla_{\boldsymbol{n}}^0\mu; M(\phi), \overline{\phi}) = \sum_{e \in \mathcal{E}_h^{\text{i}}, e=K\cap L} \frac{1}{\mathcal{D}_e(\mathcal{T}_h)} \int_e \Big(([\![\Pi_0\mu]\!])_{\oplus}(M^{\uparrow}(\phi_K) + M^{\downarrow}(\phi_L))_{\oplus} \\ - ([\![\Pi_0\mu]\!])_{\ominus}(M^{\uparrow}(\phi_L) + M^{\downarrow}(\phi_K))_{\oplus} \Big) [\![\overline{\phi}]\!] \,. \end{aligned} \tag{6.21}$$

This upwind approximation allows us to obtain both a discrete maximum principle and an energy-stability property as shown in Section 5.4.2 for a tumor model based on the Cahn-Hilliard equation with degenerate mobility.

Remark 6.4.3. *Notice that the upwind bilinear form $a_h^{upw}(\boldsymbol{u}; \phi, \overline{\phi})$ given in* (6.14)*, can be seen as a particular case of $b_h^{upw}(\cdot;\cdot,\cdot)$ given in* (6.19)*, changing $M(\phi)$ by ϕ, but now we have not truncated the transported variable ϕ. In fact, it is not necessary to truncate ϕ in $a_h^{upw}(\boldsymbol{u}; \phi, \overline{\phi})$ to preserve the pointwise bounds of ϕ due to the local incompressibility of $\mathbf{u}$ (see Chapter 2 for a more detailed explanation).*

6.4.1.2 Properties of the scheme (6.10)

Proposition 6.4.4 (Mass conservation)**.** *The mass of the phase-field variable and its regularization are conserved. In fact, one has*

$$\int_\Omega \phi^{m+1} = \int_\Omega \phi^m, \quad \int_\Omega \Pi_1^h \phi^{m+1} = \int_\Omega \Pi_1^h \phi^m.$$

As a consequence, since $\rho(\phi)$ is linear with respect to ϕ, the mass of the fluid is also conserved,

$$\int_\Omega \rho(\phi^{m+1}) = \int_\Omega \rho(\phi^m), \quad \int_\Omega \rho(\Pi_1^h \phi^{m+1}) = \int_\Omega \rho(\Pi_1^h \phi^m).$$

Proof. Just need to take $\overline{\phi} = 1$ in (6.10c) and consider the definitions of the regularization Π_1^h given in (6.9), and the density of the mixture $\rho(\phi)$ given in (6.3). □

Theorem 6.4.5 (pointwise bounds of the phase-field variable)**.** *Provided that $\phi^m \in [-1,1]$ in Ω, any solution ϕ^{m+1} of* (6.10) *and $\Pi_1^h \phi^{m+1}$ satisfy: $\phi^{m+1}, \Pi_1^h \phi^{m+1} \in [-1,1]$ in Ω.*

Proof. To prove that $\phi^{m+1} \geq -1$ in Ω we may take the following $\mathbb{P}_0^{\text{disc}}(\mathcal{T}_h)$ test function

$$\overline{\phi}^* = \begin{cases} (\phi_{K^*}^{m+1} + 1)_\ominus & \text{in } K^* \\ 0 & \text{out of } K^* \end{cases},$$

where K^* is an element of $\mathcal{T}_h$ such that $\phi_{K^*}^{m+1} = \min_{K \in \mathcal{T}_h} \phi_K^{m+1}$. We denote $\boldsymbol{n}_{K^*}$ the normal vector exterior to K^*. Then, since $\phi_L^{m+1} \geq \phi_{K^*}^{m+1}$ we can assure, using the local incompressibility constraint (6.12), that

$$\begin{aligned} a_h^{\text{upw}}(\boldsymbol{u}^{m+1}; \phi^{m+1}, \overline{\phi}^*) = \\ &= \sum_{e \in \mathcal{E}_h^{\text{i}}} \int_e \left((\boldsymbol{u}^{m+1} \cdot \boldsymbol{n}_e)_\oplus \phi_K^{m+1} - (\boldsymbol{u}^{m+1} \cdot \boldsymbol{n}_e)_\ominus \phi_L^{m+1} \right) \left[\!\left[\overline{\phi}^* \right]\!\right] \\ &= \sum_{e \in \mathcal{E}_h^{\text{i}}, e = K^* \cap L} \int_e \left((\boldsymbol{u}^{m+1} \cdot \boldsymbol{n}_{K^*})_\oplus \phi_{K^*}^{m+1} - (\boldsymbol{u}^{m+1} \cdot \boldsymbol{n}_{K^*})_\ominus \phi_L^{m+1} \right) (\phi_{K^*}^{m+1} + 1)_\ominus \\ &\leq \sum_{e \in \mathcal{E}_h^i, e \subset K^*} \int_e (\boldsymbol{u}^{m+1} \cdot \boldsymbol{n}_{K^*}) \phi_{K^*}^{m+1} (\phi_{K^*}^{m+1} + 1)_\ominus = \sum_{e \in \mathcal{E}_h^i} \int_e (\boldsymbol{u}^{m+1} \cdot \boldsymbol{n}_e) \left[\!\left[\phi^{m+1} \overline{\phi}^* \right]\!\right] = 0. \end{aligned}$$

On the other hand, using that the positive part is an increasing function and that

$$M^{\uparrow}(\phi_L^{m+1}) \geq M^{\uparrow}(\phi_{K^*}^{m+1}) \quad \text{and} \quad M^{\downarrow}(\phi_L^{m+1}) \leq M^{\downarrow}(\phi_{K^*}^{m+1}),$$

we can obtain (see Theorems 2.4.11 and 5.4.9)

$$b_h^{\text{upw}}(\nabla_{\boldsymbol{n}}^0 \mu^{m+1}; M(\phi^{m+1}), \overline{\phi}^*) \leq 0.$$

Consequently, $|K^*|\delta_t u_{K^*}^{m+1}(u_{K^*}^{m+1}+1)_{\ominus} \geq 0$. Therefore,

$$0 \leq |K^*|(\delta_t(\phi_{K^*}^{m+1}+1))(\phi_{K^*}^{m+1}+1)_{\ominus} = -\frac{|K^*|}{\Delta t}\left((\phi_{K^*}^{m+1}+1)_{\ominus}^2 + (\phi_{K^*}^{m}+1)(\phi_{K^*}^{m+1}+1)_{\ominus}\right) \leq 0,$$

which implies, since $\phi_{K^*}^m \geq -1$, that $(\phi_{K^*}^{m+1}+1)_{\ominus} = 0$. Hence, $\phi^{m+1} \geq -1$ in Ω.

Similarly, taking the following $\mathbb{P}_0^{\text{disc}}(\mathcal{T}_h)$ test function

$$\overline{\phi}^* = \begin{cases} (\phi_{K*}^{m+1} - 1)_{\oplus} & \text{in } K^* \\ 0 & \text{out of } K^* \end{cases},$$

where K^* is an element of $\mathcal{T}_h$ such that $\phi_{K^*}^{m+1} = \max_{K\in\mathcal{T}_h} \phi_K^{m+1}$, we can arrive at $\phi^{m+1} \leq 1$ in Ω.

Finally, $\Pi_1^h \phi^{m+1} \in [-1,1]$ in Ω is a direct consequence of the definition of the projection Π_1^h given in (6.9). □

The next Corollary is a direct consequence of the previous result.

Corollary 6.4.6 (pointwise bounds of the fluid density)**.** *Provided that $\rho(\phi^m) \in [\rho_1, \rho_2]$ in Ω, the density of the mixture satisfies $\rho(\phi^{m+1}), \rho(\Pi_1^h \phi^{m+1}) \in [\rho_1, \rho_2]$ in Ω.*

The following Lemma is a technical result that we are going to use when computing the discrete energy law.

Lemma 6.4.7. *The following expression holds*

$$a_h^{upw}(\boldsymbol{u}^{m+1}; \phi^{m+1}, \Pi_0\mu^{m+1}) + c_h(\phi^{m+1}, \Pi_0\mu^{m+1}, \boldsymbol{u}^{m+1}) + s_h^2(\boldsymbol{u}^{m+1}, \phi^{m+1}, \Pi_0\mu^{m+1}, \boldsymbol{u}^{m+1}) = 0. \tag{6.22}$$

Proof. First, notice that we can rewrite the term $a_h^{\mathrm{upw}}(\boldsymbol{u}^{m+1};\phi^{m+1},\Pi_0\mu^{m+1})$ as follows

$$a_h^{\mathrm{upw}}(\boldsymbol{u}^{m+1};\phi^{m+1},\Pi_0\mu^{m+1}) = \sum_{e\in\mathcal{E}_h}\int_e(\boldsymbol{u}^{m+1}\cdot\boldsymbol{n}_e)\left\{\!\!\left\{\phi^{m+1}\right\}\!\!\right\}\left[\!\left[\Pi_0\mu^{m+1}\right]\!\right] + \frac{1}{2}\sum_{e\in\mathcal{E}_h^{\mathrm{i}}}\int_e|\boldsymbol{u}^{m+1}\cdot\boldsymbol{n}_e|\left[\!\left[\phi^{m+1}\right]\!\right]\left[\!\left[\Pi_0\mu^{m+1}\right]\!\right].$$

Then, by definition and due to $\phi^{m+1}\in\mathbb{P}_0^{\mathrm{disc}}(\mathcal{T}_h)$,

$$\begin{aligned} c_h(\phi^{m+1},\Pi_0\mu^{m+1},\boldsymbol{u}^{m+1}) &= -\int_\Omega(\nabla\cdot\boldsymbol{u}^{m+1})\phi^{m+1}\Pi_0\mu^{m+1} \\ &\quad -\sum_{e\in\mathcal{E}_h}\int_e(\boldsymbol{u}^{m+1}\cdot\boldsymbol{n}_e)\left\{\!\!\left\{\phi^{m+1}\right\}\!\!\right\}\left[\!\left[\Pi_0\mu^{m+1}\right]\!\right], \\ s_h^2(\boldsymbol{u}^{m+1},\phi^{m+1},\Pi_0\mu^{m+1},\boldsymbol{u}^{m+1}) &= -\frac{1}{2}\sum_{e\in\mathcal{E}_h^{\mathrm{i}}}\int_e|\boldsymbol{u}^{m+1}\cdot\boldsymbol{n}_e|\left[\!\left[\phi^{m+1}\right]\!\right]\left[\!\left[\Pi_0\mu^{m+1}\right]\!\right]. \end{aligned}$$

Finally, using (6.10b),

$$c_h(\phi^{m+1},\Pi_0\mu^{m+1},\boldsymbol{u}^{m+1}) = -\sum_{e\in\mathcal{E}_h}\int_e(\boldsymbol{u}^{m+1}\cdot\boldsymbol{n}_e)\left\{\!\!\left\{\phi^{m+1}\right\}\!\!\right\}\left[\!\left[\Pi_0\mu^{m+1}\right]\!\right],$$

what yields (6.22). □

Theorem 6.4.8 (Discrete energy law)**.** *The following discrete energy law holds:*

$$\begin{aligned} &\delta_t E(\boldsymbol{u}^{m+1},\Pi_1^h\phi^{m+1}) + 2\left(\eta(\phi^{m+1})\boldsymbol{D}\boldsymbol{u}^{m+1},\boldsymbol{D}\boldsymbol{u}^{m+1}\right) + b_h^{upw}(-\nabla_{\boldsymbol{n}}^0\mu^{m+1};M(\phi^{m+1}),\Pi_0\mu^{m+1}) \\ &\quad + \frac{\Delta t}{2}\int_\Omega\rho(\Pi_1^h\phi^m)|\delta_t\boldsymbol{u}^{m+1}|^2 + \frac{\Delta t\lambda\varepsilon}{2}\int_\Omega|\delta_t\nabla\Pi_1^h\phi^{m+1}|^2 \\ &\quad + \frac{\lambda}{\varepsilon}\int_\Omega\Big(f(\Pi_1^h\phi^{m+1},\Pi_1^h\phi^m)\delta_t\Pi_1^h\phi^{m+1} - F(\Pi_1^h\phi^{m+1})\Big) = 0, \end{aligned} \tag{6.23}$$

where the energy functional $E(\boldsymbol{u},\phi)$ is defined in (6.6)*.*

Proof. First, take $\overline{\mathbf{u}} = \boldsymbol{u}^{m+1}$ and $\overline{p} = p^{m+1}$ in (6.10a)–(6.10b). Consider that

$$\Big(\rho(\Pi_1^h\phi^m)\delta_t\boldsymbol{u}^{m+1},\boldsymbol{u}^{m+1}\Big) = \frac{1}{2}\int_\Omega\rho(\Pi_1^h\phi^m)\delta_t|\boldsymbol{u}^{m+1}|^2 + \frac{\Delta t}{2}\int_\Omega\rho(\Pi_1^h\phi^m)|\delta_t\boldsymbol{u}^{m+1}|^2, \tag{6.24}$$

and, by definition of $s_h^1(\cdot,\cdot,\cdot,\cdot,\cdot,\cdot)$ given in (6.15),

$$\frac{1}{2}\int_\Omega \delta_t\left(\rho(\Pi_1^h\phi^{m+1})\right)|\boldsymbol{u}^{m+1}|^2 = \left(\left[\left(\rho(\Pi_1^h\phi^m)u^m - \boldsymbol{J}_h^m\right)\cdot\nabla\right]\boldsymbol{u}^{m+1},\boldsymbol{u}^{m+1}\right) + s_h^1(\boldsymbol{u}^{m+1},\boldsymbol{u}^m,\Pi_1^h\phi^{m+1},\Pi_1^h\phi^m,\mu^m,\boldsymbol{u}^{m+1}). \tag{6.25}$$

Then, using (6.24) and (6.25) we can arrive at the following expression

$$\delta_t\int_\Omega \rho(\Pi_1^h\phi^{m+1})\frac{|\boldsymbol{u}^{m+1}|^2}{2} + \frac{\Delta t}{2}\int_\Omega \rho(\Pi_1^h\phi^m)|\delta_t\boldsymbol{u}^{m+1}|^2 + 2\left(\eta(\phi^{m+1})\boldsymbol{D}\boldsymbol{u}^{m+1},\boldsymbol{D}\boldsymbol{u}^{m+1}\right) + c_h(\phi^{m+1},\Pi_0\mu^{m+1},\boldsymbol{u}^{m+1}) + s_h^2(\boldsymbol{u}^{m+1},\phi^{m+1},\Pi_0\mu^{m+1},\boldsymbol{u}^{m+1}) = 0. \tag{6.26}$$

Now, if we test (6.10c)–(6.10d) with $\overline{\phi} = \Pi_0\mu^{m+1}$ and $\overline{\mu} = \delta_t\Pi_1^h\phi^{m+1}$ and we add the resulting expressions and (6.26), we obtain, using (6.22),

$$\begin{aligned}&\delta_t\int_\Omega \rho(\Pi_1^h\phi^{m+1})\frac{|\boldsymbol{u}^{m+1}|^2}{2} + \frac{\Delta t}{2}\int_\Omega \rho(\Pi_1^h\phi^m)|\delta_t\boldsymbol{u}^{m+1}|^2 + 2\left(\eta(\phi^{m+1})\boldsymbol{D}\boldsymbol{u}^{m+1},\boldsymbol{D}\boldsymbol{u}^{m+1}\right)\\ &+\left(\delta_t\phi^{m+1},\Pi_0\mu^{m+1}\right) + b_h^{\text{upw}}(-\nabla_{\boldsymbol{n}}^0\mu^{m+1};M(\phi^{m+1}),\Pi_0\mu^{m+1}) + \lambda\varepsilon\left(\nabla\Pi_1^h\phi^{m+1},\delta_t\nabla\Pi_1^h\phi^{m+1}\right)\\ &+\frac{\lambda}{\varepsilon}\left(f(\Pi_1^h\phi^{m+1},\Pi_1^h\phi^m),\delta_t\Pi_1^h\phi^{m+1}\right) - \left(\mu^{m+1},\delta_t\Pi_1^h\phi^{m+1}\right)_h = 0.\end{aligned}$$

Finally, the following equalities

$$\begin{aligned}\left(\delta_t\phi^{m+1},\Pi_0\mu^{m+1}\right) &= \left(\delta_t\phi^{m+1},\mu^{m+1}\right) = \left(\delta_t\Pi_1^h\phi^{m+1},\mu^{m+1}\right)_h,\\ \lambda\varepsilon\left(\nabla\Pi_1^h\phi^{m+1},\delta_t\nabla\Pi_1^h\phi^{m+1}\right) &= \frac{\lambda\varepsilon}{2}\delta_t\int_\Omega|\nabla\Pi_1^h\phi^{m+1}|^2 + \frac{\Delta t\lambda\varepsilon}{2}\int_\Omega|\delta_t\nabla\Pi_1^h\phi^{m+1}|^2,\end{aligned}$$

yield (6.23). □

Using the definition of the upwind form $b_h^{\text{upw}}(\cdot;\cdot,\cdot)$ and the standard procedure for the convex-splitting technique (see e.g. [77, 105]), one can show the following Lemma.

Lemma 6.4.9. *The following two inequalities hold:*

$$b_h^{upw}(-\nabla_{\boldsymbol{n}}^0\mu^{m+1};M(\phi^{m+1}),\Pi_0\mu^{m+1}) \geq 0, \tag{6.27}$$

$$\int_\Omega\left(f(\Pi_1^h\phi^{m+1},\Pi_1^h\phi^m)\delta_t\Pi_1^h\phi^{m+1} - \delta_t F(\Pi_1^h\phi^{m+1})\right) \geq 0. \tag{6.28}$$

The following result is a direct consequence of Theorem 6.4.8 and Lemma 6.4.9.

Corollary 6.4.10 (Discrete energy stability)**.** *The scheme* (6.10) *satisfies*

$$\delta_t E(\boldsymbol{u}^{m+1}, \Pi_1^h \phi^{m+1}) + 2\left(\eta(\phi^{m+1})\boldsymbol{D}\boldsymbol{u}^{m+1}, \boldsymbol{D}\boldsymbol{u}^{m+1}\right) + b_h^{upw}(-\nabla_{\boldsymbol{n}}^0 \mu^{m+1}; M(\phi^{m+1}), \Pi_0 \mu^{m+1}) \leq 0. \tag{6.29}$$

In particular, scheme (6.10) *is unconditionally energy stable, i.e.,* $\delta_t E(\boldsymbol{u}^{m+1}, \Pi_1^h \phi^{m+1}) \leq 0$.

The scheme (6.10) is nonlinear so we will need to approximate its solution by means of an iterative procedure such as the nonsmooth Newton's method (see [49]).

However, the function $\operatorname{sign}(\phi)$ that appears in the stabilization term $s_h^2(\cdot,\cdot,\cdot,\cdot)$ is not subdifferentiable at $\phi = 0$ and, although it is rare in practice that $\phi = 0$ holds exactly due to round-off errors, one might eventually find convergence issues.

In this case, several approaches can be carried out to improve the convergence of the algorithm. For instance, one may use an iterative procedure that does not rely on the Jacobian of the whole system such as a fixed point algorithm. Conversely, if we want to use a higher order procedure depending on the Jacobian like the nonsmooth Newton's method, one may avoid the use of the $\operatorname{sign}(\cdot)$ function regularizing the term $s_h^2(\cdot,\cdot,\cdot,\cdot)$ as follows

$$s_h^{2,\delta}(\boldsymbol{u}, \phi, \mu, \overline{\mathbf{u}}) \coloneqq \frac{1}{2} \sum_{e \in \mathcal{E}_h^{\mathrm{i}}} \int_e (\overline{\mathbf{u}} \cdot \boldsymbol{n}_e) \frac{\boldsymbol{u} \cdot \boldsymbol{n}_e}{|\boldsymbol{u} \cdot \boldsymbol{n}_e| + \delta} [\![\Pi_0 \mu]\!] [\![\phi]\!], \tag{6.30}$$

for $\delta > 0$ small. This modification preserves the mass conservation and the pointwise bounds but introduces a modification in the discrete energy law, see Theorem 6.4.11.

The following result can be proved using the same procedure in Theorem 6.4.8 and Corollary 6.4.10.

Theorem 6.4.11. *If we regularize the stabilization term* $s_h^2(\cdot,\cdot,\cdot,\cdot)$ *in the equation* (6.10a)*, using* $s_h^{2,\delta}(\cdot,\cdot,\cdot,\cdot)$ *defined in* (6.30) *for a certain* $\delta > 0$*, the following discrete energy law holds:*

$$\begin{aligned} \delta_t E(\boldsymbol{u}^{m+1}, \Pi_1^h \phi^{m+1}) + 2\left(\eta(\phi^{m+1})\boldsymbol{D}\boldsymbol{u}^{m+1}, \boldsymbol{D}\boldsymbol{u}^{m+1}\right) + b_h^{upw}(-\nabla_{\boldsymbol{n}}^0 \mu^{m+1}; M(\phi^{m+1}), \Pi_0 \mu^{m+1}) \\ \leq -\frac{\delta}{2} \sum_{e \in \mathcal{E}_h^i} \int_e \frac{|\boldsymbol{u}^{m+1} \cdot \boldsymbol{n}_e|}{|\boldsymbol{u}^{m+1} \cdot \boldsymbol{n}_e| + \delta} \left[\!\left[\Pi_0 \mu^{m+1}\right]\!\right] \left[\!\left[\phi^{m+1}\right]\!\right]. \end{aligned} \tag{6.31}$$

6.5 Decoupled bound-preserving scheme

Now, we develop a decoupled approximation of the model (6.1) that reduces significantly the computational effort with respect to the previous coupled approach (6.10), while still preserving the mass conservation and the pointwise bounds.

Nonetheless, it is not clear whether a discrete energy law directly holds even for the time semidiscrete scheme (6.32) given below. Hence, we will not focus on the energy stability of the decoupled fully discrete scheme and we leave this study for a future work.

6.5.1 Time discrete scheme

For clarity in the exposition, we are going to introduce first the time semidiscretization used to decouple the equations. In particular, we apply a rotational pressure-correction method based on the work in [140] to decouple the fluid equations.

Consider the following steps:

Step 1: given $(\phi^m, \mu^m, \boldsymbol{u}^m, p^m)$ compute $\boldsymbol{v}^{m+1}$ satisfying

$$\rho(\phi^m)\frac{\boldsymbol{v}^{m+1}-\boldsymbol{u}^m}{\Delta t} + \left[(\rho(\phi^m)\boldsymbol{v}^m - \rho_{dif}M(\phi^m)\nabla\mu^m)\cdot\nabla\right]\boldsymbol{v}^{m+1}$$
$$-2\nabla\cdot(\eta(\phi^m)\boldsymbol{D}\boldsymbol{v}^{m+1}) + \nabla p^m + \phi^m\nabla\mu^m = 0 \quad \text{in } \Omega, \tag{6.32a}$$
$$\boldsymbol{v}^{m+1} = 0 \quad \text{on } \partial\Omega. \tag{6.32b}$$

Step 2: given $(\phi^m, \boldsymbol{v}^{m+1})$ compute τ^{m+1}, with $\int_\Omega \tau^{m+1} = 0$ and satisfying

$$-\nabla\cdot\left(\frac{1}{\rho(\phi^m)}\nabla\tau^{m+1}\right) = -\frac{1}{\Delta t}\nabla\cdot\boldsymbol{v}^{m+1}, \quad \text{in } \Omega, \tag{6.32c}$$
$$\nabla\tau^{m+1}\cdot\boldsymbol{n} = 0, \quad \text{on } \partial\Omega. \tag{6.32d}$$

Step 3: given $(\phi^m, \tau^{m+1}, \boldsymbol{v}^{m+1}, p^m)$ compute $(p^{m+1}, \boldsymbol{u}^{m+1})$ satisfying

$$p^{m+1} = p^m + \tau^{m+1} - 2\eta(\phi^m)\nabla\cdot\boldsymbol{v}^{m+1}, \tag{6.32e}$$
$$\boldsymbol{u}^{m+1} = \boldsymbol{v}^{m+1} - \frac{\Delta t}{\rho(\phi^m)}\nabla\tau^{m+1}, \tag{6.32f}$$

where p^{m+1} is post-processed to ensure the 0-mean constraint.

Step 4: given $(\phi^m, \boldsymbol{u}^{m+1})$, compute (ϕ^{m+1}, μ^{m+1}) satisfying:

$$\delta_t \phi^{m+1} + \nabla \cdot (\phi^{m+1} \boldsymbol{u}^{m+1}) - \nabla \cdot (M(\phi^{m+1}) \nabla \mu^{m+1}) = 0 \quad \text{in } \Omega, \tag{6.32g}$$

$$-\lambda \varepsilon \Delta \phi^{m+1} + \frac{\lambda}{\varepsilon} f(\phi^{m+1}, \phi^m) - \mu^{m+1} = 0 \quad \text{in } \Omega, \tag{6.32h}$$

$$\nabla \phi^{m+1} \cdot \boldsymbol{n} = M(\phi^{m+1}) \nabla \mu^{m+1} \cdot \boldsymbol{n} = 0 \quad \text{on } \partial\Omega, \tag{6.32i}$$

where $f(\cdot, \cdot)$ is defined in (6.11).

Notice that this projection method only leads to an inaccurate boundary condition on the velocity variable $\boldsymbol{u}^{m+1}$ in the tangential direction due to the terms depending on $\nabla \tau^{m+1}$ in (6.32f), in fact, one only has the so-called slip boundary condition $\boldsymbol{u}^{m+1} \cdot \boldsymbol{n} = 0$ on $\partial\Omega$. For further insight on this issue with projection methods, see, for instance, [101].

6.5.2 Fully discrete scheme

We will use the well known SIP method (see [63, 163]) to discretize the term $-\nabla \cdot (\kappa \nabla \tau)$ in (6.32c), where $\kappa = \kappa(x) \in L^\infty(\Omega)$ with $\kappa \geq C > 0$ in Ω, by means of the bilinear form

$$\begin{aligned} a_h^{\text{sip},\sigma}(\kappa; \tau, \overline{\tau}) \coloneqq \int_\Omega \kappa \nabla \tau \cdot \nabla \overline{\tau} - \left(\sum_{e \in \mathcal{E}_h^{\text{i}}} \int_e \{\!\{ \kappa \nabla \tau \}\!\} \cdot \boldsymbol{n}_e \, [\![\overline{\tau}]\!] + \sum_{e \in \mathcal{E}_h^{\text{i}}} \int_e \{\!\{ \kappa \nabla \overline{\tau} \}\!\} \cdot \boldsymbol{n}_e \, [\![\tau]\!] \right) \\ + \sum_{e \in \mathcal{E}_h^{\text{i}}} \int_e \frac{\sigma}{|e|} [\![\tau]\!] [\![\overline{\tau}]\!], \end{aligned} \tag{6.33}$$

where $\sigma > 0$ is a parameter large enough to ensure the coercivity of the bilinear form $a_h^{\text{sip},\sigma}(\kappa; \cdot, \cdot)$.

Then, we propose the following decoupled fully discrete scheme based on the previous time-discrete approach. In order to simplify the notation, we will denote the fully discrete functions the same way as the time-semidiscrete functions in (6.32).

Step 1: given $(\phi^m, \mu^m, \boldsymbol{u}^m, p^m) \in \mathbb{P}_0^{\text{disc}}(\mathcal{T}_h) \times \mathbb{P}_1^{\text{cont}}(\mathcal{T}_h) \times \mathcal{U}_h \times \mathcal{P}_h$ compute $\boldsymbol{v}^{m+1} \in \mathcal{V}_h$ satisfying

$$\begin{aligned} \left(\rho(\phi^m) \frac{\boldsymbol{v}^{m+1} - \boldsymbol{u}^m}{\Delta t}, \overline{\mathbf{v}} \right) + \left([(\rho(\phi^m) \boldsymbol{v}^m - \rho_{dif} M(\phi^m) \nabla \mu^m) \cdot \nabla] \, \boldsymbol{v}^{m+1}, \overline{\mathbf{v}} \right) \\ + \left(2\eta(\phi^m) \boldsymbol{D} \boldsymbol{v}^{m+1}, \boldsymbol{D} \overline{\mathbf{v}} \right) - (p^m, \nabla \cdot \overline{\mathbf{v}}) + (\phi^m \nabla \mu^m, \overline{\mathbf{v}}) = 0, \quad \forall \overline{\mathbf{v}} \in \mathcal{V}_h, \end{aligned} \tag{6.34a}$$

with $\boldsymbol{v}^{m+1} = 0$ on $\mathcal{E}_h^{\mathrm{b}}$.

Step 2: given $(\phi^m, \boldsymbol{v}^{m+1}) \in \mathbb{P}_0^{\mathrm{disc}}(\mathcal{T}_h) \times \mathcal{V}_h$ compute $\tau^{m+1} \in \mathbb{P}_1^{\mathrm{disc}}(\mathcal{T}_h)$ satisfying

$$a_h^{\mathrm{sip},\sigma}(1/\rho(\phi^m); \tau^{m+1}, \overline{\tau}) = -\frac{1}{\Delta t}\left(\nabla \cdot \boldsymbol{v}^{m+1}, \overline{\tau}\right), \quad \forall \overline{\tau} \in \mathbb{P}_1^{\mathrm{disc}}(\mathcal{T}_h). \tag{6.34b}$$

Step 3: given $(\phi^m, \tau^{m+1}, \boldsymbol{v}^{m+1}, p^m) \in \mathbb{P}_0^{\mathrm{disc}}(\mathcal{T}_h) \times \mathbb{P}_1^{\mathrm{disc}}(\mathcal{T}_h) \times \mathcal{V}_h \times \mathcal{P}_h$ compute $\boldsymbol{u}^{m+1} \in \mathcal{U}_h$ and $p^{m+1} \in \mathcal{P}_h$ as follows

$$\left(p^{m+1}, \overline{p}\right) = (p^m, \overline{p}) + \left(\tau^{m+1}, \overline{p}\right) - 2\left(\eta(\phi^m)\nabla \cdot \boldsymbol{v}^{m+1}, \overline{p}\right) \quad \forall \overline{p} \in \mathcal{P}_h, \tag{6.34c}$$

$$\boldsymbol{u}^{m+1} = \boldsymbol{v}^{m+1} - \frac{\Delta t}{\rho(\phi^m)}\nabla \tau^{m+1}. \tag{6.34d}$$

Step 4: given $(\phi^m, \boldsymbol{u}^{m+1}) \in \mathbb{P}_0^{\mathrm{disc}}(\mathcal{T}_h) \times \mathcal{U}_h$ compute $(\phi^{m+1}, \mu^{m+1}) \in \mathbb{P}_0^{\mathrm{disc}}(\mathcal{T}_h) \times \mathbb{P}_1^{\mathrm{cont}}(\mathcal{T}_h)$ satisfying:

$$\left(\delta_t \phi^{m+1}, \overline{\phi}\right) + a_h^{\mathrm{upw}}(\widetilde{\boldsymbol{u}}^{m+1}; \phi^{m+1}, \overline{\phi}) + b_h^{\mathrm{upw}}(-\nabla_{\boldsymbol{n}}\mu^{m+1}; M(\phi^{m+1}), \overline{\phi}) = 0, \quad \forall \overline{\phi} \in \mathbb{P}_0^{\mathrm{disc}}(\mathcal{T}_h), \tag{6.34e}$$

$$\lambda\varepsilon\left(\nabla(\Pi^h\phi^{m+1}), \nabla\overline{\mu}\right) + \frac{\lambda}{\varepsilon}\left(f(\phi^{m+1}, \phi^m), \overline{\mu}\right) - \left(\mu^{m+1}, \overline{\mu}\right) = 0, \quad \forall \overline{\mu} \in \mathbb{P}_1^{\mathrm{cont}}(\mathcal{T}_h), \tag{6.34f}$$

where the velocity $\widetilde{\boldsymbol{u}}^{m+1}$ in (6.34e) is defined on every $e \in \mathcal{E}_h^{\mathrm{i}}$ as follows

$$\widetilde{\boldsymbol{u}}_{|e}^{m+1} \cdot \boldsymbol{n}_e \coloneqq \left\{\!\!\left\{\boldsymbol{u}^{m+1}\right\}\!\!\right\} \cdot \boldsymbol{n}_e + \Delta t \frac{\sigma}{|e|}\left[\!\left[\tau^{m+1}\right]\!\right], \tag{6.34g}$$

and then this modified velocity $\widetilde{\boldsymbol{u}}^{m+1}$ is locally incompressible. Hence, $\phi^{m+1}, \Pi^h\phi^{m+1} \in [-1, 1]$ can be preserved, see Proposition 6.5.3 and Theorem 6.5.5 below. Note that, for every $e \in \mathcal{E}_h^{\mathrm{i}}$, the stabilization term $\Delta t(\sigma/|e|)\left[\!\left[\tau^{m+1}\right]\!\right]$ is consistent and vanishes as $\Delta t, h \to 0$. The upwind forms $a_h^{\mathrm{upw}}(\boldsymbol{u}; \phi, \overline{\phi})$ and $b_h^{\mathrm{upw}}(-\nabla_{\boldsymbol{n}}\mu; M(\phi), \overline{\phi})$ have been already defined in (6.14) and (6.19), respectively.

We have denoted $(\mathcal{V}_h, \mathcal{U}_h, \mathcal{P}_h)$ to any triple of discrete spaces such that $\mathcal{U}_h = \mathcal{V}_h + \mathbb{P}_0^{\mathrm{disc}}(\mathcal{T}_h)^d$ with $\mathcal{V}_h \subset (\mathcal{C}^0(\overline{\Omega}) \cap H_0^1(\Omega))^d$.

In this case, the triple $(\mathcal{V}_h, \mathcal{U}_h, \mathcal{P}_h)$ needs to satisfy $\mathcal{V}_h \subset (\mathcal{C}^0(\overline{\Omega}) \cap H_0^1(\Omega))^d$ in order to strongly impose the no-slip boundary condition on $\boldsymbol{v}^{m+1}$ and $\mathcal{U}_h = \mathcal{V}_h + \mathbb{P}_0^{\text{disc}}(\mathcal{T}_h)$, directly derived from equation (6.34d), to preserve the local incompressibility of the variable $\boldsymbol{u}^{m+1}$ (see Lemma 6.5.2).

Although we do not know if the solution of this decoupled scheme (6.34) satisfies any discrete energy law, in case that we achieve estimates for the velocity $\boldsymbol{u}^{m+1}$, it is preferable to choose an inf-sup compatible pair of spaces $(\mathcal{V}_h, \mathcal{P}_h)$ as was mentioned in Section 6.4. For more information on the inf-sup condition for projection methods we refer the reader to [101, 102].

Again, as in the fully coupled approximation scheme (6.10), the error bounds are expected to be determined by the lowest accuracy approximation of the phase-field function given by $\mathbb{P}_0^{\text{disc}}(\mathcal{T}_h)$.

To start the algorithm we take again $\phi^0 = \Pi_0\phi_0$ hence $\phi^0 \in [-1, 1]$. Also, we take $\boldsymbol{u}^0$ as the projection of $\boldsymbol{u}_0$ on $\mathcal{V}_h$ and $p^0 = 0$.

Remark 6.5.1. *Notice that in step 4 of* (6.34) *we do not need to solve any linear system of equations for* $\boldsymbol{u}^{m+1}$. *Instead, this function can be directly computed by adjusting the degrees of freedom of the resulting polynomial on the right hand side of* (6.34d). *In fact, the computation of* $\boldsymbol{u}^{m+1}$ *can be avoided, and in* (6.34a) *take* $\boldsymbol{u}^m = \boldsymbol{v}^m - \Delta t/\rho(\phi^{m-1})\nabla\tau^m$ *for* $m > 1$, *given for instance* $\tau^0 = 0$ *as initialization.*

Since we are not certain about if an energy law can be derived for the solution of the semidiscrete scheme (6.32), we have omitted in this case the constraints and stabilization terms needed for the fully coupled scheme (6.10) to be energy-stable. Indeed, we have not used the approximation of the normal derivative of the chemical potential (6.20) in (6.34e) and, consequently, we can omit Hypothesis 3.4.1 for the decoupled scheme (6.34). Therefore, the approximation given by the decoupled scheme (6.34) can be computed in more general meshes than its coupled counterpart (6.10).

Moreover, since only the equation (6.34e) is nonlinear in the decoupled fully discrete scheme (6.34), we will only need to use an iterative procedure such as Newton's method to approximate the solution in Step 1. This improvement reduces significantly the computational cost with respect to the fully coupled scheme (6.10) which requires an iterative procedure to be carried out for the whole system.

6.5.2.1 Properties of the scheme (6.34)

In this section, we will only show the proof of the local incompressibility of $\boldsymbol{u}^{m+1}$ and we will just state the other results as they are analogous to the ones in Section 6.4.1.2.

Lemma 6.5.2 (Approximated local incompressibility)**.** *The velocity variable* $\boldsymbol{u}^{m+1}$ *computed from* (6.34d) *is approximately locally incompressible in the following sense:*

$$\sum_{e\in\mathcal{E}_h^i}\int_e \left\{\!\!\left\{\boldsymbol{u}^{m+1}\right\}\!\!\right\}\cdot\boldsymbol{n}_e\left[\!\left[\overline{\varphi}\right]\!\right]=-\Delta t\sum_{e\in\mathcal{E}_h^i}\int_e\frac{\sigma}{|e|}\left[\!\left[\tau^{m+1}\right]\!\right]\left[\!\left[\overline{\varphi}\right]\!\right],\quad\forall\,\overline{\varphi}\in\mathbb{P}_0^{disc}(\mathcal{T}_h),\tag{6.35}$$

where the right hand side of (6.35) *tends to 0 as* $\Delta t, h\to 0$*.*

Proof. Let $\overline{\varphi}\in\mathbb{P}_0^{\text{disc}}(\mathcal{T}_h)$. Taking the (broken) divergence of (6.34d) and testing by $\overline{\varphi}$ we arrive at

$$\left(\nabla\cdot\boldsymbol{u}^{m+1},\overline{\varphi}\right)=\left(\nabla\cdot\boldsymbol{v}^{m+1},\overline{\varphi}\right)-\left(\nabla\cdot\left(\frac{\Delta t}{\rho(\phi^m)}\nabla\tau^{m+1}\right),\overline{\varphi}\right).\tag{6.36}$$

Now, substituting (6.34b) into (6.36),

$$\left(\nabla\cdot\boldsymbol{u}^{m+1},\overline{\varphi}\right)=-\Delta t\left[a_h^{\text{sip},\sigma}(1/\rho(\phi^m);\tau^{m+1},\overline{\varphi})+\left(\nabla\cdot\left(\frac{1}{\rho(\phi^m)}\nabla\tau^{m+1}\right),\overline{\varphi}\right)\right].\tag{6.37}$$

Since $\overline{\varphi}$ is piecewise constant in $\mathcal{T}_h$,

$$a_h^{\text{sip},\sigma}(1/\rho(\phi^m);\tau^{m+1},\overline{\varphi})=-\sum_{e\in\mathcal{E}_h^{\text{i}}}\int_e\left\{\!\!\left\{(1/\rho(\phi^m))\nabla\tau^{m+1}\right\}\!\!\right\}\cdot\boldsymbol{n}_e\left[\!\left[\overline{\varphi}\right]\!\right]+\sum_{e\in\mathcal{E}_h^{\text{i}}}\int_e\frac{\sigma}{|e|}\left[\!\left[\tau^{m+1}\right]\!\right]\left[\!\left[\overline{\varphi}\right]\!\right],$$

integrating by parts, we obtain

$$\begin{aligned}\left(\nabla\cdot\left(\frac{1}{\rho(\phi^m)}\nabla\tau^{m+1}\right),\overline{\varphi}\right)=&\sum_{e\in\mathcal{E}_h}\int_e\left\{\!\!\left\{(1/\rho(\phi^m))\nabla\tau^{m+1}\right\}\!\!\right\}\cdot\boldsymbol{n}_e\left[\!\left[\overline{\varphi}\right]\!\right]\\&+\sum_{e\in\mathcal{E}_h}\int_e\left[\!\left[(1/\rho(\phi^m))\nabla\tau^{m+1}\right]\!\right]\cdot\boldsymbol{n}_e\left\{\!\!\left\{\overline{\varphi}\right\}\!\!\right\}.\end{aligned}$$

Hence, returning to (6.37) and using (6.34d) and that $\left[\!\left[\boldsymbol{v}^{m+1}\right]\!\right] = 0$ on $\mathcal{E}_h$ due to the choice of $\mathcal{V}_h$, we have

$$\begin{aligned}
\left(\nabla\cdot\boldsymbol{u}^{m+1},\overline{\varphi}\right) &= -\Delta t\sum_{e\in\mathcal{E}_h}\int_e\left[\!\left[(1/\rho(\phi^m))\nabla\tau^{m+1}\right]\!\right]\cdot\boldsymbol{n}_e\left\{\!\!\left\{\overline{\varphi}\right\}\!\!\right\} - \Delta t\sum_{e\in\mathcal{E}_h^{\mathrm{b}}}\int_e(1/\rho(\phi^m))(\nabla\tau^{m+1}\cdot\boldsymbol{n}_e)\overline{\varphi}\\
&\quad - \Delta t\sum_{e\in\mathcal{E}_h^{\mathrm{i}}}\int_e\frac{\sigma}{|e|}\left[\!\left[\tau^{m+1}\right]\!\right]\left[\!\left[\overline{\varphi}\right]\!\right]\\
&= \sum_{e\in\mathcal{E}_h}\int_e\left[\!\left[\boldsymbol{u}^{m+1}\right]\!\right]\cdot\boldsymbol{n}_e\left\{\!\!\left\{\overline{\varphi}\right\}\!\!\right\} - \Delta t\sum_{e\in\mathcal{E}_h^{\mathrm{b}}}\int_e(1/\rho(\phi^m))(\nabla\tau^{m+1}\cdot\boldsymbol{n}_e)\overline{\varphi}\\
&\quad - \Delta t\sum_{e\in\mathcal{E}_h^{\mathrm{i}}}\int_e\frac{\sigma}{|e|}\left[\!\left[\tau^{m+1}\right]\!\right]\left[\!\left[\overline{\varphi}\right]\!\right]\\
&= \sum_{e\in\mathcal{E}_h}\int_e\left[\!\left[\boldsymbol{u}^{m+1}\right]\!\right]\cdot\boldsymbol{n}_e\left\{\!\!\left\{\overline{\varphi}\right\}\!\!\right\} + \sum_{e\in\mathcal{E}_h^{\mathrm{b}}}(\boldsymbol{u}^{m+1}\cdot\boldsymbol{n}_e)\overline{\varphi} - \Delta t\sum_{e\in\mathcal{E}_h^{\mathrm{i}}}\int_e\frac{\sigma}{|e|}\left[\!\left[\tau^{m+1}\right]\!\right]\left[\!\left[\overline{\varphi}\right]\!\right].
\end{aligned} \tag{6.38}$$

Now, integrate by parts the left-hand side of (6.38),

$$\left(\nabla\cdot\boldsymbol{u}^{m+1},\overline{\varphi}\right) = \sum_{e\in\mathcal{E}_h}\int_e\left\{\!\!\left\{\boldsymbol{u}^{m+1}\right\}\!\!\right\}\cdot\boldsymbol{n}_e\left[\!\left[\overline{\varphi}\right]\!\right] + \sum_{e\in\mathcal{E}_h}\int_e\left[\!\left[\boldsymbol{u}^{m+1}\right]\!\right]\cdot\boldsymbol{n}_e\left\{\!\!\left\{\overline{\varphi}\right\}\!\!\right\}. \tag{6.39}$$

Consequently, due to (6.38) and (6.39), we arrive at (6.35). □

The following result is a direct consequence of the previous lemma.

Proposition 6.5.3 (Local incompressibility)**.** *The modified velocity $\widetilde{\boldsymbol{u}}^{m+1}$ defined in* (6.34g) *is locally incompressible in the sense that*

$$\sum_{e\in\mathcal{E}_h^i}\int_e\widetilde{\boldsymbol{u}}^{m+1}\cdot\boldsymbol{n}_e\left[\!\left[\overline{\varphi}\right]\!\right] = 0,\quad\forall\,\overline{\varphi}\in\mathbb{P}_0^{disc}(\mathcal{T}_h). \tag{6.40}$$

Proposition 6.5.4 (Mass conservation)**.** *The mass of the phase-field variable and its regularization are conserved, i.e.,*

$$\int_\Omega\phi^{m+1} = \int_\Omega\phi^m,\quad \int_\Omega\Pi_1^h\phi^{m+1} = \int_\Omega\Pi_1^h\phi^m.$$

As a consequence, since $\rho(\phi)$ is linear with respect to ϕ, the mass of the fluid is also conserved,

$$\int_\Omega\rho(\phi^{m+1}) = \int_\Omega\rho(\phi^m),\quad \int_\Omega\rho(\Pi_1^h\phi^{m+1}) = \int_\Omega\rho(\Pi_1^h\phi^m).$$

Theorem 6.5.5 (Bounds of the phase-field variable)**.** *Provided that* $\phi^m \in [-1,1]$ *in* Ω*, any solution* ϕ^{m+1} *and its* $\mathbb{P}_1^{cont}(\mathcal{T}_h)$*-regularization* $\Pi_1^h\phi^{m+1}$ *in* (6.34e) *satisfy* $\phi^{m+1}, \Pi_1^h\phi^{m+1} \in [-1,1]$ *in* Ω*.*

Corollary 6.5.6 (Bounds of the fluid density)**.** *Provided that* $\rho(\phi^m) \in [\rho_1,\rho_2]$ *in* Ω*, the density of the mixture* $\rho(\phi^{m+1})$ *or* $\rho(\Pi_1^h\phi^{m+1})$ *in* (6.34) *satisfy* $\rho(\phi^{m+1}), \rho(\Pi_1^h\phi^{m+1}) \in [\rho_1,\rho_2]$ *in* Ω*.*

6.6 Numerical experiments

We have carried out the following numerical experiments in the spatial domain $\Omega = [-0.5, 0.5]^2$. Moreover, we have set the following values of the parameters $\varepsilon = 0.01$, $\lambda = 0.01$, $\rho_1 = 1$ and $\rho_2 = 100$, unless otherwise specified. Also, the penalty parameter σ has been chosen as $\sigma = 4$ in (6.34), although other choices might have been possible.

Following the Remark 6.4.1, we have chosen the pair of "inf-sup" stable spaces $(\mathcal{U}_h, \mathcal{P}_h) = ((\mathbb{P}_2^{\text{bubble}}(\mathcal{T}_h) \cap H_0^1(\Omega))^d, \mathbb{P}_1^{\text{disc}}(\mathcal{T}_h))$ for the coupled scheme (6.10) and $(\mathcal{V}_h, \mathcal{P}_h) = ((\mathbb{P}_2^{\text{bubble}}(\mathcal{T}_h) \cap H_0^1(\Omega))^d, \mathbb{P}_1^{\text{disc}}(\mathcal{T}_h))$ regarding the decoupled approach (6.34), where $\mathcal{U}_h = (\mathbb{P}_2^{\text{bubble}}(\mathcal{T}_h) \cap H_0^1(\Omega))^d + \mathbb{P}_0^{\text{disc}}(\mathcal{T}_h)^d$.

To compute the approximations we have used the finite element library `FEniCSx` (see [13, 166, 167]) coupled with `PyVista` for the visualization of the results (see [175]).

On the one hand, an iterative Newton solver has been used to approximate the nonlinear problem. In this sense, the modified stabilization term $s_h^{2,\delta}(\cdot,\cdot,\cdot,\cdot)$ with $\delta = 10^{-6}$ has been used in the coupled scheme (6.10) to avoid convergence issues.

On the other hand, we have used the default iterative linear solver, GMRES (generalized minimal residual method), and preconditioner, computed using an incomplete LU factorization (ILU), of `PETSc` (see [26, 60]) for solving the resulting linear systems except (6.34a). In the case of (6.34a), this combination provided some instabilities in several examples. Therefore, we opted for a different approach and used an LU parallel solver implemented in `MUMPS`, [16, 17], for (6.34a), which provided much more accurate results shown in the figures below.

Remark 6.6.1. *In the case of the decoupled approach* (6.34)*, enforcing the* 0*-mean constraint on the approximation of the potential* τ *is rather straightforward as the linear Krylov solvers can handle singular matrices and provide a solution of the linear system. Therefore, we compute a solution of the linear system and then post-process it so that it satisfies the constraint.*

However, we must be careful when dealing with an ill-posed nonlinear problem if we want Newton's method to converge. To overcome this issue in the case of the coupled approximation (6.10)*, we have added a penalty term* $\xi\left(p^{m+1}, \overline{p}\right)$ *to the LHS of* (6.10b) *with* ξ *very small (in practice, we have chosen* $\xi = 10^{-10}$*). In this way, we enforce the* 0*-mean constraint on the approximation of* p *and Newton's method does converge. In fact, a posteriori, we can check that this additional term has not severely affected the approximation obtained in two different manners. On the one hand, taking into account the* $\|\cdot\|_{L^\infty(\Omega)}$ *of the approximation of* p *we observe that the term* ξp *has been at most of order* 10^{-5}*. On the other hand, the pointwise bounds have been preserved despite the crucial role that the local incompressibility constraint* (6.12) *plays in Theorem 6.4.5.*

Certainly, many other ways of enforcing the 0*-mean pressure constraint in the coupled nonlinear system can be explored.*

In all the figures shown in this section, we plot both the phase field variable (in red/blue) and the following scaled vector field (in white)

$$\boldsymbol{u}_s^{m+1} = \begin{cases} \frac{5\cdot 10^{-2}}{\|\boldsymbol{u}^{m+1}\|_{L^\infty(\Omega)}}\boldsymbol{u}^{m+1}, & \text{if } \|\boldsymbol{u}^{m+1}\|_{L^\infty(\Omega)} \geq 5\cdot 10^{-2}, \\ \boldsymbol{u}^{m+1}, & \text{otherwise.} \end{cases}$$

6.6.1 Accuracy test

In this case, we define the following initial conditions

$$\begin{aligned} \phi_0(x,y) = 2\tanh\Bigg(&\frac{(0.25 - \sqrt{(x-0.1)^2+(y-0.1)^2})_\oplus}{\sqrt{2}\varepsilon} \\ &+ \frac{(0.15 - \sqrt{(x+0.15)^2+(y+0.15)^2})_\oplus}{\sqrt{2}\varepsilon}\Bigg) - 1.0, \\ \boldsymbol{u}_0(x,y) = \chi(&y(0.16 - (x^2+y^2))_\oplus, -x(0.16-(x^2+y^2))_\oplus), \end{aligned}$$

with $\chi = 1$, which are plotted in Figure 6.1.

We conduct a preliminary convergence test in which we compare a reference solution given by each of the coupled, (6.10), and decoupled, (6.34), approaches in a very refined mesh ($h \approx 7\cdot 10^{-3}$) with the approximation given by the same approach in a less refined mesh. In this way, with $\Delta t = 10^{-5}$ fixed, we can remove the error introduced by the time discretization in each of the different schemes. In

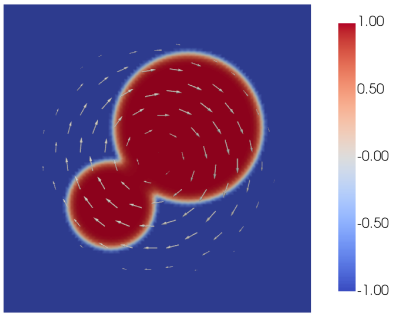

Figure 6.1 Initial condition of tests 6.6.1 and 6.6.2

any case, we would like to emphasize that such a test for these sophisticated schemes involving several different discrete spaces and projection operators is nontrivial and the results obtained only provide an estimation of the possible order of convergence of the proposed approximations.

The results of the test at $T = 5 \cdot 10^{-4}$ are shown in Tables 6.1 and 6.2, where similar orders of convergence have been achieved for both schemes (6.10) and (6.34). It is worth mentioning that, as in Section 2.5 for the convective Cahn-Hilliard model, order 2 in $\|\cdot\|_{L^2(\Omega)}$ and order 1 in $\|\cdot\|_{H^1(\Omega)}$ for the approximation of the variable $\Pi_1^h\phi$ have been approached. On the other hand, order around 2 in $\|\cdot\|_{L^2(\Omega)}$ has been obtained for the approximations of p and $\boldsymbol{u}$, the latter probably affected by the order of convergence in the approximation of $\Pi_1^h\phi$. Finally, order around 2 in $\|\cdot\|_{H^1(\Omega)}$ seems to have been achieved by the approximation of $\boldsymbol{u}$.

Table 6.1 Errors and convergence orders at $T = 5 \cdot 10^{-4}$ in $\|\cdot\|_{L^2(\Omega)}$

Variable	Scheme	$h \approx 2.36 \cdot 10^{-2}$	$3h/4 \approx 1.77 \cdot 10^{-2}$		$4h/7 \approx 1.35 \cdot 10^{-2}$		$h/2 \approx 1.18 \cdot 10^{-2}$	
		Error	Error	**Order**	Error	**Order**	Error	**Order**
$\Pi_1^h\phi$	Coupled	$8.48e-03$	$5.40e-03$	1.57	$3.38e-03$	1.73	$2.62e-03$	1.89
	Decoupled	$8.80e-03$	$5.59e-03$	1.58	$3.21e-03$	2.05	$2.54e-03$	1.74
$\boldsymbol{u}$	Coupled	$5.91e-04$	$4.89e-04$	0.66	$3.31e-04$	1.44	$2.43e-04$	2.30
	Decoupled	$2.57e-04$	$6.98e-05$	4.53	$3.09e-05$	3.01	$2.46e-05$	1.69
p	Coupled	$2.24e-01$	$1.14e-01$	2.35	$5.47e-02$	2.71	$4.37e-02$	1.67
	Decoupled	$9.26e-02$	$1.90e-02$	5.51	$1.14e-02$	1.89	$8.87e-03$	1.86

6.6.2 Mixing bubbles

For this test we keep the same initial conditions as in the previous test but with $\chi = 100$. Again, this initial condition can be seen in Figure 6.1.

In Figure 6.2 we have plotted the evolution in time of the approximation obtained using both the coupled and the decoupled schemes, (6.10) and (6.34), respectively, with $h \approx 1.41 \cdot 10^{-2}$ and $\Delta t = 10^{-3}$.

On the other hand, in Figure 6.3 (left) we can observe how the bounds are preserved as predicted by the previous analytical results. In addition, in Figure 6.3 (right) one may observe how the energy decreases both using the coupled approximation, as predicted by the theory above, and the decoupled approximation. In this case, the decoupled scheme is around 73% faster than the coupled scheme when run in series (using 8 threads to solve the linear systems) in the same computer.

Table 6.2 Errors and convergence orders at $T = 5 \cdot 10^{-4}$ in $\|\cdot\|_{H^1(\Omega)}$

Variable	Scheme	$h \approx 2.36 \cdot 10^{-2}$	$3h/4 \approx 1.77 \cdot 10^{-2}$		$3h/5 \approx 1.41 \cdot 10^{-2}$		$h/2 \approx 1.18 \cdot 10^{-2}$	
		Error	Error	**Order**	Error	**Order**	Error	**Order**
$\Pi_1^h \phi$	Coupled	$1.22e+00$	$1.17e+00$	0.15	$9.12e-01$	0.92	$8.09e-01$	0.89
	Decoupled	$1.34e+00$	$1.25e+00$	0.24	$9.43e-01$	1.04	$8.31e-01$	0.94
$\boldsymbol{u}$	Coupled	$9.61e-02$	$7.98e-02$	0.65	$4.90e-02$	1.80	$3.75e-02$	1.99
	Decoupled	$2.06e-02$	$8.82e-03$	2.95	$4.03e-03$	2.89	$3.30e-03$	1.48

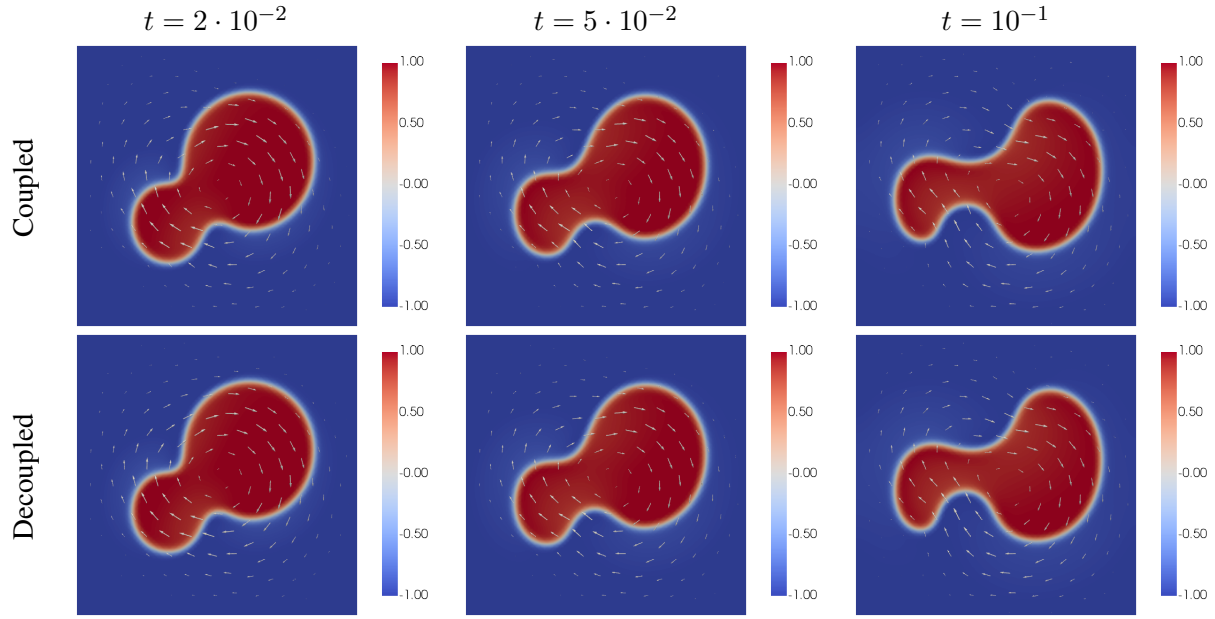

Figure 6.2 Evolution of $\Pi^h \phi$ over time in test 6.6.2 ($\rho_1 = 1$, $\rho_2 = 100$)

We would like to highlight that even with this simple test one can find situations where the discrete energy of the decoupled scheme (6.34) increases exponentially while the approximation becomes completely unstable. In particular, in the case of two fluids with very different densities, for instance $\rho_1 = 1$ and $\rho_2 = 1000$, the approximation given by the decoupled scheme is totally nonphysical (see Figure 6.4) as its energy grows to infinity (see Figure 6.5, left) until the nonlinear solver is not able to converge to an approximation. Conversely, the energy stability property of the coupled scheme

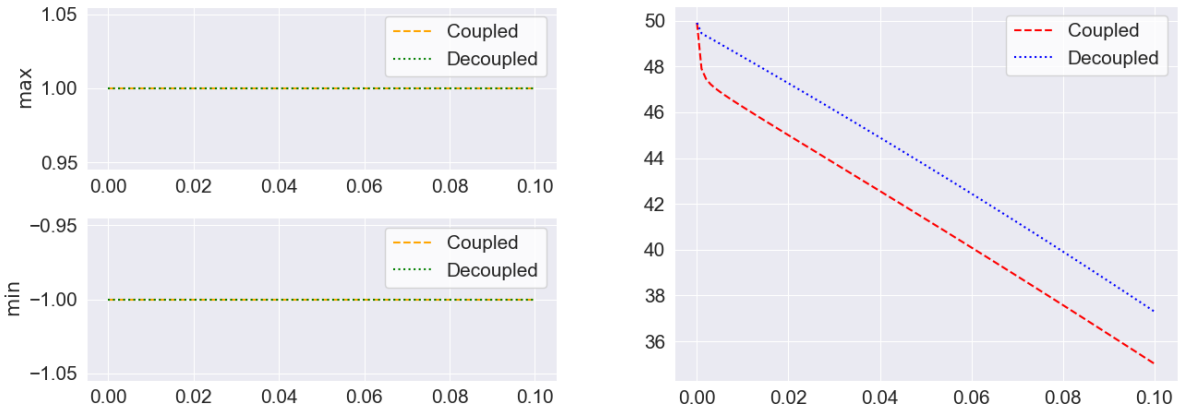

Figure 6.3 Left, maximum and minimum of $\Pi^h\phi$. Right, discrete energy. Test 6.6.2 ($\rho_1 = 1$, $\rho_2 = 100$)

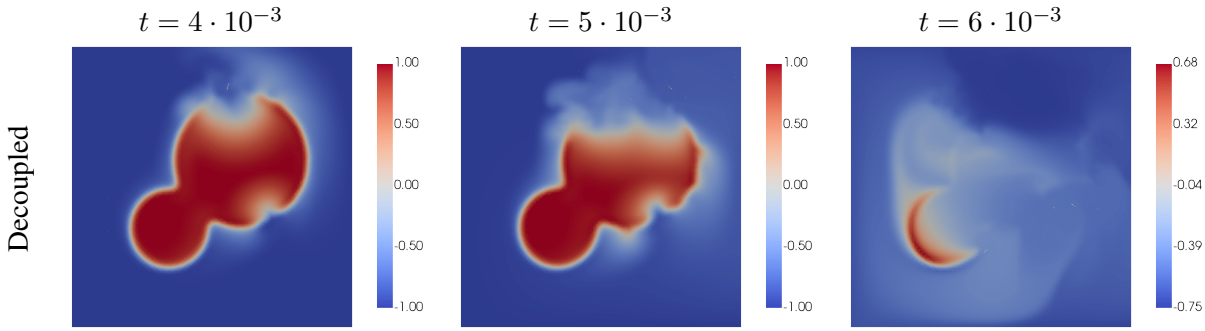

Figure 6.4 Evolution of $\Pi^h\phi$ over time in test 6.6.2 for the decoupled scheme ($\rho_1 = 1$, $\rho_2 = 1000$)

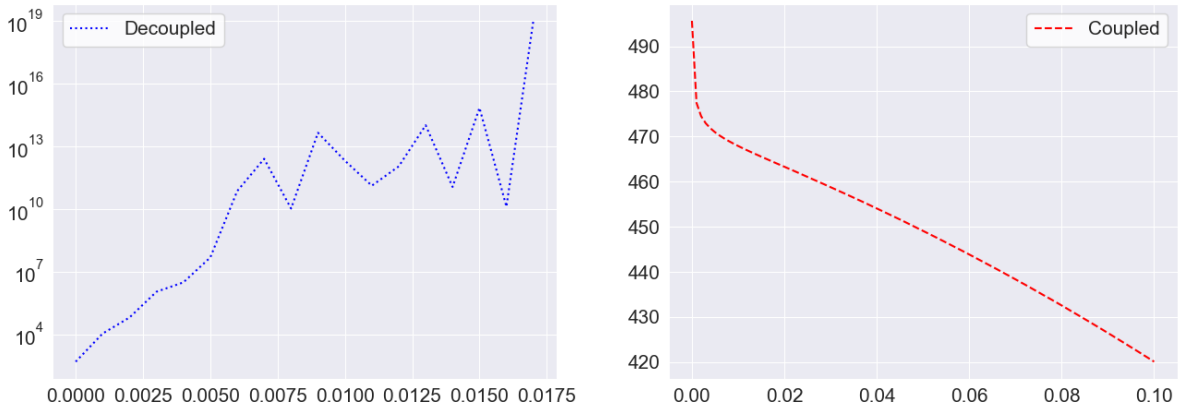

Figure 6.5 Left, discrete energy of the decoupled scheme. Right, discrete energy of the coupled scheme. Test 6.6.2 ($\rho_1 = 1$, $\rho_2 = 1000$)

(6.10) makes it much more robust and, in this case, this approach is capable of providing a physical approximation where the energy does decrease over time as predicted by the theoretical results (see Figure 6.5, right). We omit the figures of the solution given by the coupled scheme as it is barely distinguishable from those shown in Figure 6.2.

6.6.3 A heavier bubble falling in a lighter medium

Now, we perform a test in which we define the following initial condition: $\boldsymbol{u}_0 = 0$ and

$$\phi_0(x, y) = \tanh\left(\frac{0.2 - \sqrt{x^2 + y^2}}{\sqrt{2}\varepsilon}\right),$$

a bubble of density $\rho_2 = 100$ in a lighter medium of density $\rho_1 = 1$, plotted in Figure 6.6. Moreover, we have added a term $-\rho(\phi)\boldsymbol{g}$ on the right-hand side of equation (6.1a) acting as the gravitational forces pushing the heavier bubble down to the bottom of the domain Ω. In our case, we have chosen $\boldsymbol{g} = (0, 1)$ and we have treated this term implicitly in (6.10) and explicitly in (6.34).

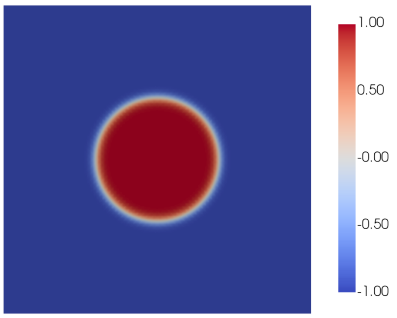

Figure 6.6 Initial condition of test 6.6.3

In this case, we have shown in Figure 6.7 the evolution in time of the solution using (6.10) and (6.34) with $h \approx 1.41 \cdot 10^{-2}$ and $\Delta t = 10^{-4}$. The result is qualitatively similar to the ones shown in previous studies such as [107]. Also, the bounds are preserved as shown in Figure 6.8 (left). In this case, the energy does not necessarily decrease due to the gravitational forces but, as one may observe in Figure 6.8 (right), the behavior of the energy is similar using both approaches.

We have noticed that the decoupled scheme is around 75% faster than the coupled approach in this test.

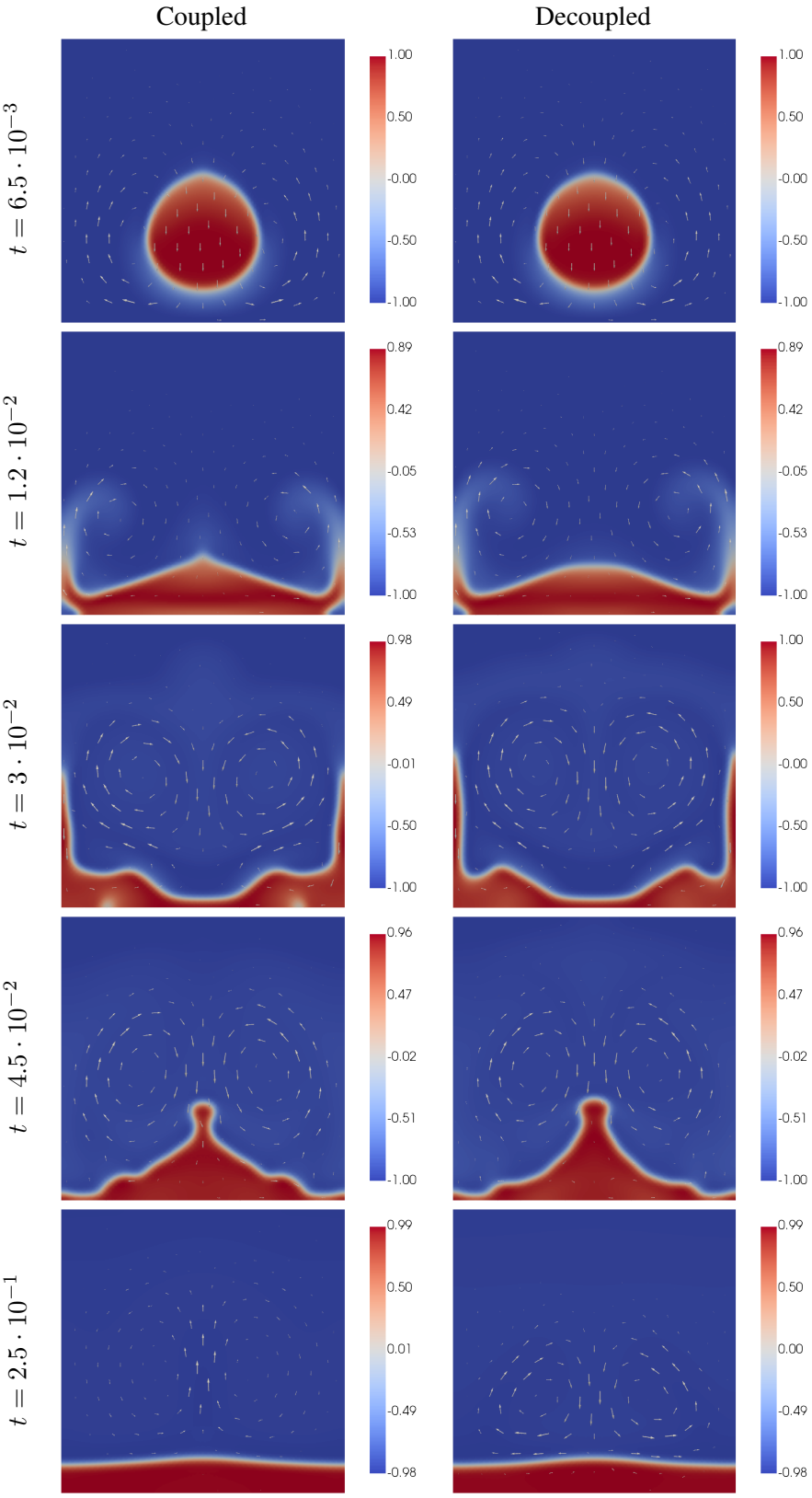

Figure 6.7 Evolution of $\Pi^h \phi$ over time in test 6.6.3

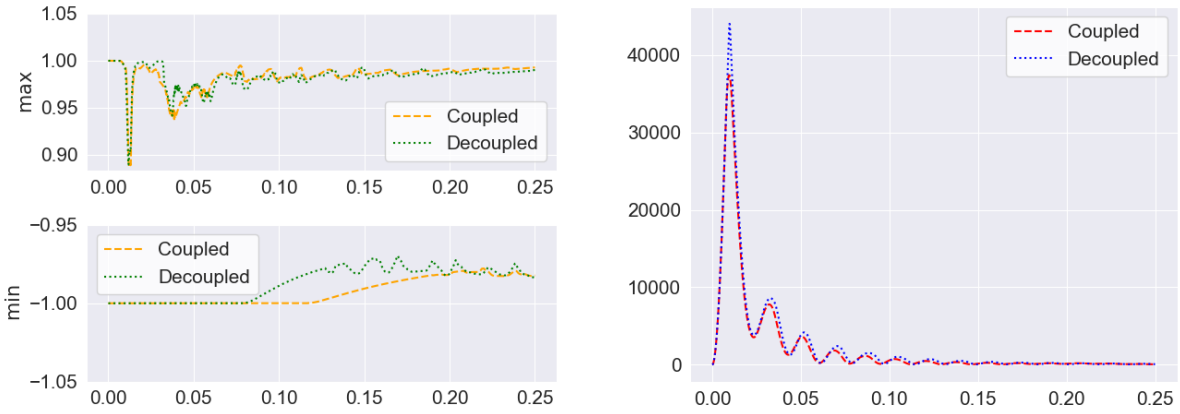

Figure 6.8 Left, maximum and minimum of $\Pi^h\phi$. Right, discrete energy. Test 6.6.3

6.6.4 Rayleigh-Taylor instability

Finally, we carry out the benchmark Rayleigh-Taylor instability test for which we define the following initial condition: $\boldsymbol{u}_0 = 0$ and

$$\phi_0(x, y) = \tanh\left(\frac{y - (0.1\exp(-(x+0.2)^2/0.1))}{\sqrt{2}\varepsilon}\right),$$

plotted in Figure 6.9. Again, we add the gravity term $-\rho(\phi)\boldsymbol{g}$ with $\boldsymbol{g} = (0, 1)$ in the RHS of equation (6.1a).

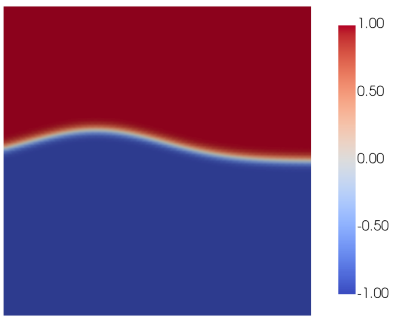

Figure 6.9 Initial condition of test 6.6.4

The evolution in time of the solution using (6.10) and (6.34) with $h \approx 1.41 \cdot 10^{-2}$ and $\Delta t = 10^{-4}$ can be seen in Figure 6.11. Again, despite the difficulty of this test due to the fast dynamics involved, the results are qualitatively similar to the ones shown in previous works such as [107]. In Figure 6.10 (left) we plot the evolution of the maximum and minimum of the regularized phase-field function, where

we can observe that the bounds are indeed preserved as predicted by the theory. In addition, one may observe in Figure 6.10 (right), the behavior of the energy is similar using both approaches.

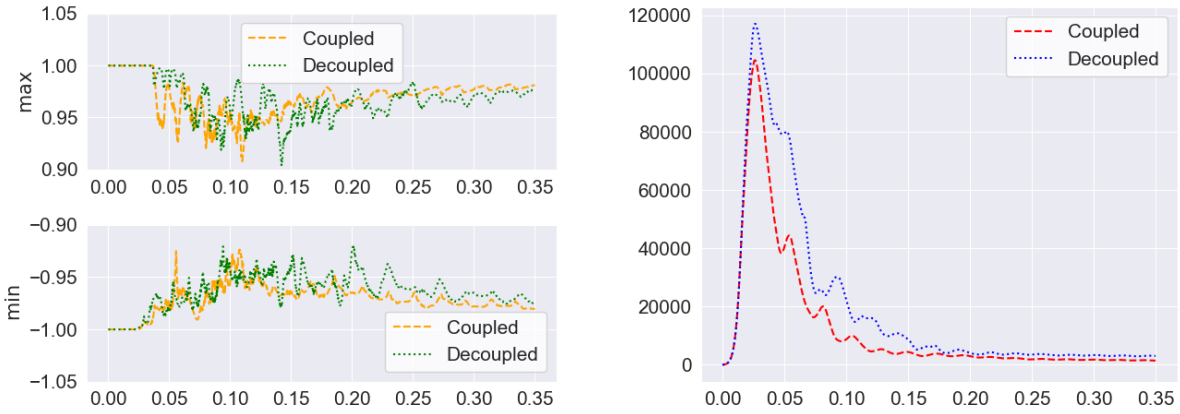

Figure 6.10 Left, maximum and minimum of $\Pi^h \phi$. Right, discrete energy. Test 6.6.4

The decoupled scheme is around 39% faster than the coupled scheme in this test.

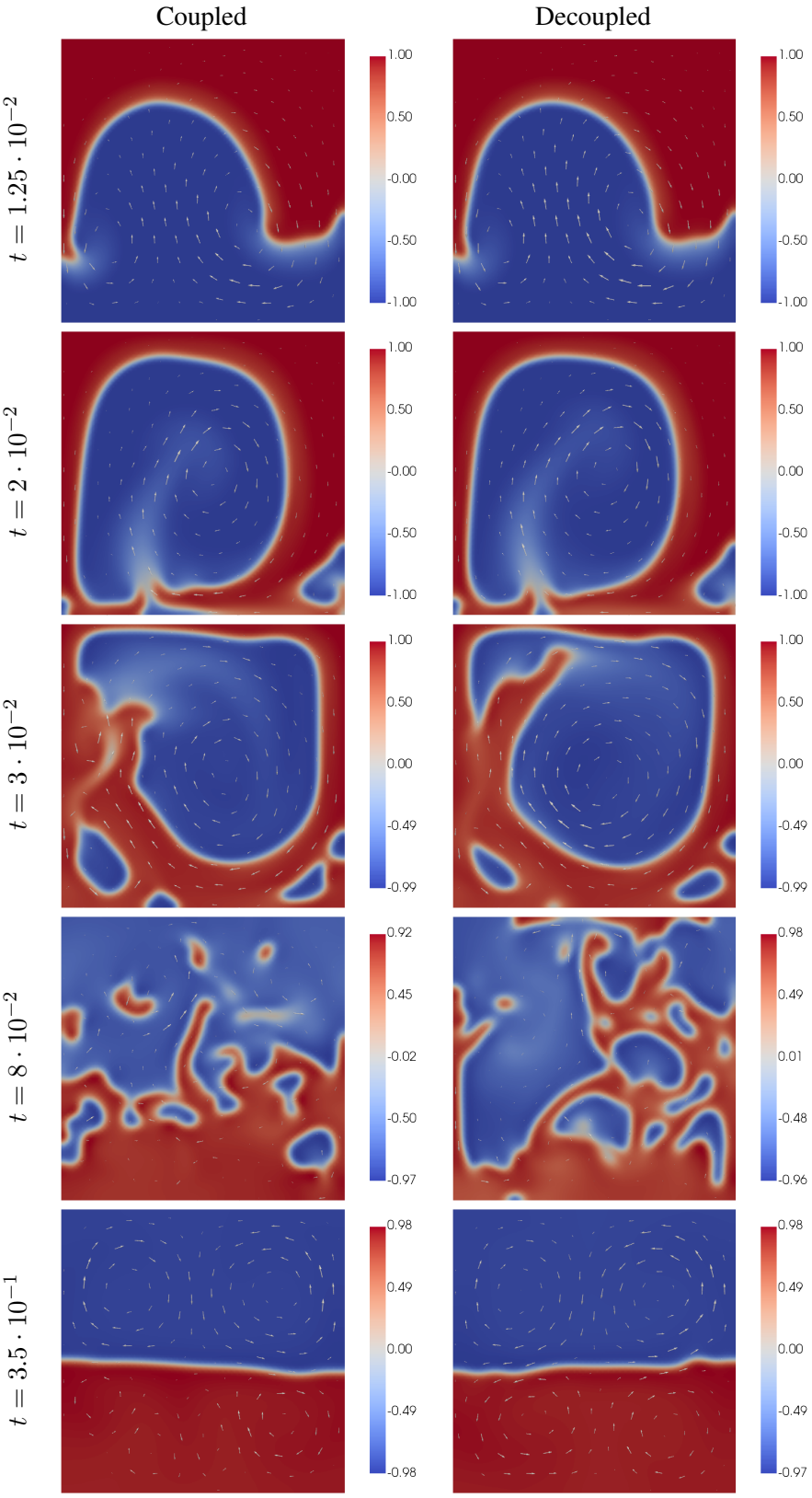

Figure 6.11 Evolution of $\Pi^h \phi$ over time in test 6.6.4

CHAPTER 7

POSSIBLE EXTENSION OF THE STRUCTURE-PRESERVING UPWIND DG SCHEME TO A CAHN–HILLIARD–DARCY MODEL OF TUMOR GROWTH

7.1 Abstract

In this chapter, we present an ongoing work where we aim to extend the ideas in Chapter 5 to a diffuse-interface tumor model including the effects of the surrounding fluid on the cells and nutrients. To this end, in Section 7.3, we develop a particular Cahn–Hilliard–Darcy model from the general framework proposed in [95] that extends the tumor model shown in Section 5.3 including the nonsymmetric mobility and proliferation functions. The proposed model is mass-conservative, pointwise-bounded and energy-stable and seems perfectly suitable to be approximated combining the ideas in Sections 5.4.2 and 6.4.

7.2 Introduction

Diffuse-interface models have recently been appointed as a successful alternative for tumor growth modeling. In this sense, considerable effort has been made in describing a general framework for the correct modeling and calibration of the diffuse-interface models of tumor growth, oriented to their possible physical application, as summarized in [88, 112, 156, 157] and the references therein. So far, there are several examples of success in this direction as different approaches have been capable of providing accurate enough results to be compared with real clinical data. Among these celebrated models we can find the work by Pozzi et al. [160] where a Cahn–Hilliard equation is coupled with a Keller–Segel system; the works by Agosti et al. [7, 8, 9] where a Cahn-Hilliard equation for the tumor with nonsymmetric degenerate mobility (as the one shown in Chapter 5) is coupled with a diffusion-reaction equation for the nutrients; or the works of Lima et al. [137, 138] where phase-field models are compared against reaction-diffusion models regarding data prediction.

The complexity of these models vary depending on their constitutive assumptions and intrinsic limitations, but most of them are based on multicomponent mixture theory, where the phase-field variable is assumed to be a pointwise-bounded tumor volume fraction, and which accounts for the mass, momentum

and energy balances for each of the constituents. One can trace back these kind of thermodynamically consistent mixture models to the work of Wise et al., [189] and the references therein. As a consequence of this pioneering work, many other models have arisen taking into account different kind of processes and proposing simplifications. For instance, we can find [85] where the model in [189] is extended to describe angiogenesis and tumor invasion, the work by [113] where the nutrients are included as a component of the mixture, or the more recent model in [94] where mechanical effects are also taken into account, just to mention a few.

Among the existing literature, one can find different works which have tried to model the tumor tissue immersed in a fluid that transports the mixture of cells and nutrients. On the one hand, as initially proposed in [189], some authors have derived models relying on the Cahn–Hilliard–Darcy equations, [86, 92, 93, 95], where the tissue is assumed to behave as a porous medium. On the other hand, some alternatives have arisen for the cases where the tissue cannot be modeled as porous medium, for instance, a Cahn–Hilliard–Brinkman model [54, 67, 68] and, very recently, a Cahn–Hilliard–Navier–Stokes system [69]. In this sense, even more general models have been proposed where the previous approaches have been generalized to satisfy the Darcy–Forchheimer–Brinkman law, [89], or to introduce viscoelastic effects, [91].

However, increasing the complexity of the model leads to more challenging mathematical problem. As a consequence, not many works have been able to provide a successful, unconditionally physically meaningful approximation of these kind of models involving tumor-nutrient interactions and fluid flows. In this regard, the works [68, 93, 95] propose a finite element bound-preserving discretization that involves solving a discrete variational inequality following the ideas in [27] whereas [91] introduce a finite element approximation that mimic some entropies of the model at the discrete level. On the contrary, in [69], a combination of a suitable phase-field variable transformation, the time-discrete SAV approach and an upwind finite volume spatial discretization is used to preserve the pointwise bounds and the energy-stability in their approximations, although a CFL condition that is difficult to check beforehand is required.

In this chapter, we introduce a possible extension of the results presented in Sections 5.4.2 and 6.4 with the purpose of developing a physically meaningful approximation for a tumor system coupled with a fluid equation. In this sense, we derive a mass-conservative, pointwise-bounded and energy-stable Cahn–Hilliard–Darcy model from the more general model introduced by Garcke et al. in [95] under

certain constitutive assumptions by means of the non-symmetric mobility and proliferation functions used in Chapter 5 to modify the tumor model in [113]. The resulting model lies in the framework of the previous tumor model studied in Chapter 5 and the CHNS studied in Chapter 6, hence a successful approximation using the upwind DG ideas developed throughout this work is likely to be obtained.

7.3 Cahn–Hilliard–Darcy model

In this section we derive a particular continuous Cahn–Hilliard–Darcy model from the general equations proposed in [95] using the ideas that we presented in Section 5.3 to modify the tumor model introduced in [113]. Moreover, we present the physical properties of the resulting model.

7.3.1 General model

H. Garcke et al. introduced in [95] the following diffuse interface model of tumor growth:

$$\boldsymbol{v} = -K(\nabla p + u\nabla\mu_u + n\nabla\partial_n N(u,n)) \qquad \text{in } \Omega\times(0,T), \tag{7.1a}$$

$$\nabla\cdot\boldsymbol{v} = \Gamma_{\boldsymbol{v}} \qquad \text{in } \Omega\times(0,T), \tag{7.1b}$$

$$\partial_t u + \nabla\cdot(u\boldsymbol{v}) = \nabla\cdot(M_u\nabla\mu_u) + \frac{\Gamma_u}{2} \qquad \text{in } \Omega\times(0,T), \tag{7.1c}$$

$$\mu_u = AF'(u) - B\Delta u + \partial_u N(u,n) \qquad \text{in } \Omega\times(0,T), \tag{7.1d}$$

$$\partial_t n + \nabla\cdot(n\boldsymbol{v}) = \nabla\cdot(M_n\nabla\partial_n N(u,n)) - \mathcal{S} \qquad \text{in } \Omega\times(0,T), \tag{7.1e}$$

$$\boldsymbol{v}\cdot\boldsymbol{n} = g \qquad \text{on } \partial\Omega\times(0,T), \tag{7.1f}$$

$$\nabla u\cdot\mathbf{n} = (M_u\nabla\mu_u)\cdot\mathbf{n} = 0 \qquad \text{on } \partial\Omega\times(0,T), \tag{7.1g}$$

$$(M_n\nabla\partial_n N(u,n))\cdot\mathbf{n} = c(n_\infty - n) \qquad \text{on } \partial\Omega\times(0,T), \tag{7.1h}$$

$$u(0) = u_0, \quad n(0) = n_0 \qquad \text{in } \Omega, \tag{7.1i}$$

where a change of variables have been made so that u is a phase-field function whose domain lies in $[0,1]$.

Here, $\boldsymbol{v}$ is the volume-averaged velocity; p represents the pressure; u is a phase-field variable that represents the volume fraction of tumor cells, where the region $\{x\in\Omega\colon u(x)=1\}$ represents the unmixed tumor and $\{x\in\Omega\colon u(x)=0\}$, the pure healthy cells; n is the concentration of chemicals that supply nutrients to the tumor; and μ_u is the chemical potential of u.

On the other hand, $u_0, n_0 \in L^2(\Omega)$ are the initial conditions of the tumor and the nutrients and the boundary condition (7.1h) with $c \geq 0$ and the given supply at the boundary n_∞ allows the entrance of nutrients through the boundary. Therefore, if $c = 0$ we obtain the zero flux boundary condition and as long as $c \to \infty$ we approach the Dirichlet boundary condition $n = n_\infty$ on $\partial\Omega$.

Moreover, $F(u)$ is the potential of the phase-field equation, typically the Ginzburg-Landau double well potential, i.e $F(u) = \frac{1}{4}u^2(1-u)^2$, although other choices are possible (see [95]). Also, $N(u, n)$ models the contribution to the energy of the system of the interaction between the tumor tissue and the nutrients due to different phenomena such as chemotaxis (tumor cells are attracted by nutrients) or active transport of the nutrients (mechanism by which the nutrients are attracted by the tumors).

The terms $\Gamma_{\boldsymbol{v}}$ and Γ_u are related to the densities of the healthy and the tumor tissues, ρ_1 and ρ_2, respectively, as follows

$$\Gamma_{\boldsymbol{v}} = \rho_1^{-1}\Gamma_1 + \rho_2^{-1}\Gamma_2, \quad \Gamma_u = \rho_2^{-1}\Gamma_2 - \rho_1^{-1}\Gamma_1.$$

Here, Γ_1 and Γ_2 are the source terms of the mass balance equations for each of the components of the mixture, healthy and tumor cells, respectively. On the other hand, $\mathcal{S}$ is a source/sink term for the nutrients.

The density of the mixture ρ satisfies the mass balance equation

$$\partial_t \rho + \nabla \cdot (\boldsymbol{v} - \boldsymbol{J}) = \Gamma_1 + \Gamma_2, \tag{7.2}$$

where $\boldsymbol{J} = \rho_{\text{dif}} M_u \nabla \mu_u$, and it can be explicitly determined as

$$\rho(u) = \rho_1 + (\rho_2 - \rho_1)u. \tag{7.3}$$

In addition, K, permeability tensor of the tissue, and A, B are constants with $K > 0$, $A, B \geq 0$.

Notice that the natural Dirichlet boundary condition in the normal direction (7.1f) implies the compatibility restriction

$$\int_{\partial\Omega} g = \int_\Omega \Gamma_{\boldsymbol{v}}, \tag{7.4}$$

due to (7.10b).

Remark 7.3.1. *Notice that we can regard the equations* (7.10a)–(7.10b) *as an elliptic problem for the pressure variable. In fact, if we take the divergence of* (7.10a) *we obtain, using* (7.10b)*, that*

$$\Gamma_v = -K(\Delta p + \nabla \cdot (u\nabla\mu_u) + \nabla \cdot (n\nabla\partial_n N(u,n))) \text{ in } \Omega \times (0,T).$$

7.3.2 Constitutive assumptions

From now on we will make several considerations that will lead us to a generalized version of the model in Chapter 5. We refer the reader to [95] to explore other possibilities.

First, we assume that the total mass of the mixture may vary depending on the relation between the densities of each of the states (tumor and healthy cells) as $\Gamma_1 = -\frac{\rho_1}{\rho_2}\Gamma$, where $\Gamma \coloneqq \Gamma_2$ so that (7.2) becomes

$$\partial_t \rho + \nabla(\boldsymbol{v} - \boldsymbol{J}) = \left(1 - \frac{\rho_1}{\rho_2}\right)\Gamma,$$

and the terms $\Gamma_{\boldsymbol{v}}$ and Γ_u satisfy

$$\Gamma_{\boldsymbol{v}} = 0, \quad \Gamma_u = \frac{2}{\rho_2}\Gamma.$$

Then, following the ideas in Section 5.3, we define the following family of degenerate and normalized mobilities

$$M(v) \coloneqq h_{p,q}(v), \tag{7.5}$$

for certain $p, q \in \mathbb{N}$ where

$$h_{p,q}(v) \coloneqq K_{p,q} v_{\oplus}^{p}(1-v)_{\oplus}^{q} = \begin{cases} K_{p,q} v^p (1-v)^q, & v \in [0,1], \\ 0, & \text{elsewhere}, \end{cases}$$

with $K_{p,q} > 0$ a constant so that $\max_{x\in\mathbb{R}} h_{p,q}(v) = 1$. Although one may consider the tumor mobility as $M_u(u) = h_{p,q}(u)$ with $p, q \in \mathbb{N}$ and the nutrients mobility as $M_n(n) = h_{p',q'}(n)$ with $p', q' \in \mathbb{N}$ and all the results below equally hold, for simplicity, we will assume that $M_u = M_n$ and denote the mobility function as M. In addition, we define the proliferation function

$$P(u,n) \coloneqq h_{r,s}(u) n_{\oplus}, \tag{7.6}$$

for certain $r, s \in \mathbb{N}$, which depends on both cells and nutrients, and take

$$\mathcal{S} = \delta P_0 P(u,n)(\mu_n - \mu_u)_\oplus, \tag{7.7}$$

$$\Gamma = \rho_2 \mathcal{S}, \tag{7.8}$$

which leads to $\Gamma_u = 2\mathcal{S}$. Following this choice of the mobility and proliferation functions, we restrict both the variables u and n to interval $[0,1]$ as they represent the volume fraction of tumors and nutrients, respectively.

Moreover, following the previous work [113] we take

$$N(u,n) = \frac{1}{2\delta} n^2 - \chi_0 u n$$

for certain small parameter $\delta > 0$ and $\chi_0 \geq 0$. To abbreviate the notation, we define the nutrients chemical potential as

$$\mu_n \coloneqq \partial_n N(u,n) = \frac{1}{\delta} n - \chi_0 u. \tag{7.9}$$

As we expect δ to be small, we assume that the active transport of the nutrients towards the tumor is barely negligible with respect to the diffusion of the nutrients in the medium Ω (see [113] and Section 5.3 for more details).

Finally, with a proper choice of the remaining parameters, we can arrive at the following model, which is a extension of the work in Chapter 5:

$$\boldsymbol{v} = -K(\nabla p + u\nabla\mu_u + n\nabla\mu_n) \qquad \text{in } \Omega \times (0,T), \tag{7.10a}$$

$$\nabla \cdot \boldsymbol{v} = 0 \qquad \text{in } \Omega \times (0,T), \tag{7.10b}$$

$$\partial_t u + \nabla \cdot (u\boldsymbol{v}) = C_u \nabla \cdot (M(u)\nabla\mu_u) + \delta P_0 P(u,n)(\mu_n - \mu_u)_\oplus \qquad \text{in } \Omega \times (0,T), \tag{7.10c}$$

$$\mu_u = F'(u) - \varepsilon^2 \Delta u - \chi_0 n \qquad \text{in } \Omega \times (0,T), \tag{7.10d}$$

$$\partial_t n + \nabla \cdot (n\boldsymbol{v}) = C_n \nabla \cdot (M(n)\nabla\mu_n) - \delta P_0 P(u,n)(\mu_n - \mu_u)_\oplus \qquad \text{in } \Omega \times (0,T), \tag{7.10e}$$

$$\boldsymbol{v} \cdot \boldsymbol{n} = \nabla u \cdot \mathbf{n} = (M_n \nabla\mu_n) \cdot \mathbf{n} = (M_u \nabla\mu_u) \cdot \mathbf{n} = 0 \qquad \text{on } \partial\Omega \times (0,T), \tag{7.10f}$$

$$u(0) = u_0, \quad n(0) = n_0 \qquad \text{in } \Omega, \tag{7.10g}$$

where $u, n \in [0,1]$ in Ω, $u_0, n_0 \in L^2(\Omega)$ with $u_0, n_0 \in [0,1]$ in Ω, μ_n is defined in (7.9) and all the parameters above are nonnegative with $\delta, C_u, C_n, K > 0$ and $\varepsilon, \chi_0, P_0 \geq 0$.

Notice that we have imposed the boundary condition $\boldsymbol{v} \cdot \boldsymbol{n} = 0$ on $\partial\Omega$ in (7.10f) which now satisfies the compatibility condition (7.4).

Furthermore, the density of the mixture ρ, defined in (7.3), satisfies the equation

$$\partial_t \rho + \nabla(\boldsymbol{v} - \boldsymbol{J}) = (\rho_2 - \rho_1)\delta P_0 P(u,n)(\mu_n - \mu_u)_\oplus, \tag{7.11}$$

which implies that the variation of mass of the mixture follows

$$\partial_t \int_\Omega \rho = \left(1 - \frac{\rho_1}{\rho_2}\right) \int_\Omega \Gamma = (\rho_2 - \rho_1)\delta P_0 \int_\Omega P(u,n)(\mu_n - \mu_u)_\oplus = (\rho_2 - \rho_1)\partial_t \int_\Omega u.$$

Therefore, since $\Gamma \geq 0$ if $u, n \in [0,1]$, only the tumor cells proliferate by consuming nutrients, we can observe that the tissue will gain mass if the density of the tumor cells is bigger than the density of the healthy cells, $\rho_1 < \rho_2$, and will lose mass in the opposite case, $\rho_1 > \rho_2$. In the case of matching densities, $\rho_1 = \rho_2$, we assume that the tissue will gain no mass during the process.

7.3.3 Variational formulation and properties

We define the weak formulation of (7.10) as follows: find $(\boldsymbol{v}, p, u, \mu_u, n)$ such that $\boldsymbol{v} \in L^2(0,T; L^2(\Omega)^d)$; $p \in L^2(0,T; H^1(\Omega))$ with $\int_\Omega p = 0$; $u, n \in L^2(0,T; H^1(\Omega))$ with $0 \leq u, n \leq 1$ in $\Omega \times (0,T)$ and $\partial_t u, \partial_t n \in L^2(0,T; H^1(\Omega)')$; and $\mu_u \in L^2(0,T; H^1(\Omega))$; which satisfies the following variational problem a.e. $t \in (0,T)$

$$(\boldsymbol{v}, \overline{\mathbf{v}}) = -K\left((\nabla p, \overline{\mathbf{v}}) + (u\nabla\mu_u + n\nabla\mu_n, \overline{\mathbf{v}})\right) \qquad \forall \overline{\mathbf{v}} \in L^2(\Omega)^d, \tag{7.12a}$$

$$(\boldsymbol{v}, \nabla\overline{p}) = 0 \qquad \forall \overline{p} \in H^1(\Omega), \tag{7.12b}$$

$$\begin{aligned}\langle \partial_t u(t), \overline{u}\rangle = {} & (u\boldsymbol{v}, \nabla\overline{u}) - C_u\left(M(u(t))\nabla\mu_u(t), \nabla\overline{u}\right) \\ & + \delta P_0\left(P(u(t), n(t))(\mu_n(t) - \mu_u(t))_\oplus, \overline{u}\right), \qquad \forall \overline{u} \in H^1(\Omega),\end{aligned} \tag{7.12c}$$

$$(\mu_u(t), \overline{\mu}_u) = \varepsilon^2\left(\nabla u(t), \nabla\overline{\mu}_u\right) + \left(F'(u(t)), \overline{\mu}_u\right) - \chi_0\left(n(t), \overline{\mu}_u\right), \qquad \forall \overline{\mu}_u \in H^1(\Omega), \tag{7.12d}$$

$$\begin{aligned}\langle \partial_t n(t), \overline{n}\rangle = {} & (n\boldsymbol{v}, \nabla\overline{n}) - C_n\left(M(n(t))\nabla\mu_n(t), \nabla\overline{n}\right) \\ & - \delta P_0\left(P(u(t), n(t))(\mu_n(t) - \mu_u(t))_\oplus, \overline{n}\right), \qquad \forall \overline{n} \in H^1(\Omega),\end{aligned} \tag{7.12e}$$

where

$$\mu_n(t) = \frac{1}{\delta} n(t) - \chi_0 u(t), \tag{7.13}$$

$u(0) = u_0$, $n(0) = n_0$ and $\langle \cdot, \cdot \rangle$ denotes the dual product over $H^1(\Omega)$.

For the next results we are going to assume that the solution of (7.12) is regular enough so that the expressions that appear below hold.

Proposition 7.3.2. *Let $(\boldsymbol{v}, p, u, \mu_u, n)$ be a solution of the problem* (7.12)*. Then, this solution conserves the total mass of tumor cells and nutrients in the sense of*

$$\frac{d}{dt} \int_\Omega (u(x,t) + n(x,t)) dx = 0.$$

Proof. It is enough to take $\overline{u} = \overline{n} = 1$ in (7.12c) and (7.12e) and add the resulting expressions. □

Proposition 7.3.3. *Let $(\boldsymbol{v}, p, u, \mu_u, n)$ be a solution of the problem* (7.12)*. Then, it satisfies the following energy law*

$$\begin{aligned} \frac{dE(u(t), n(t))}{dt} &+ C_u \int_\Omega M(u(x,t)) |\nabla \mu_u(x,t)|^2 dx + C_n \int_\Omega M(n(x,t)) |\nabla \mu_n(x,t)|^2 dx \\ &+ \delta P_0 \int_\Omega P(u(x,t), n(x,t)) (\mu_u(x,t) - \mu_n(x,t))_\oplus^2 dx + \frac{1}{K} \int_\Omega |\boldsymbol{v}(x,t)|^2 dx = 0, \end{aligned} \tag{7.14}$$

where the energy functional is defined by

$$E(u,n) \coloneqq \int_\Omega \left(\frac{\varepsilon^2}{2} |\nabla u|^2 + F(u) - \chi_0 u\, n + \frac{1}{2\delta} n^2 \right). \tag{7.15}$$

Therefore, the solution is energy stable in the sense

$$\frac{d}{dt} E(u(t), n(t)) \leq 0.$$

Proof. Take $\overline{\mathbf{v}} = \frac{1}{K}\boldsymbol{v}$, $\overline{p} = p$, $\overline{u} = \mu_u(t)$, $\overline{\mu}_u = \partial_t u(t)$, $\overline{n} = \mu_n(t)$ in (7.12a)–(7.12e) and test (7.13) with $\partial_t n(t)$. Adding the resulting expressions we arrive at

$$
\begin{aligned}
0 =& \varepsilon^2 \left(\nabla u(t), \nabla(\partial_t u(t))\right) + \left(F'(u(t)), \partial_t u(t)\right) \\
&- \chi_0 \left[(n(t), \partial_t u(t)) + (u(t), \partial_t n(t))\right] + \frac{1}{\delta}\left(n(t), \partial_t n(t)\right) \\
&+ C_u \int_\Omega M(u(x,t))|\nabla \mu_u(x,t)|^2 dx + C_n \int_\Omega M(n(x,t))|\nabla \mu_n(x,t)|^2 dx \\
&+ \delta P_0 \int_\Omega P(u(x,t), n(x,t))(\mu_u(x,t) - \mu_n(x,t))_\oplus (\mu_u(x,t) - \mu_n(x,t)) dx + \frac{1}{K}\int_\Omega |\boldsymbol{v}(x,t)|^2 dx.
\end{aligned}
$$

Therefore, it is straightforward to check that (7.14) holds. □

CHAPTER 8

CONCLUSIONS AND FUTURE WORK

In this dissertation we have addressed the development of physically meaningful and property-preserving numerical approximations of diffuse-interface tumor models that can lead to a successful application of the results in order to predict how tumors behave in real life.

To this purpose, we have divided this goal in several smaller steps in which we have dealt with more affordable problems that have been introduced in the different chapters of this work. The results obtained for each of these steps served as the starting point to address more difficult tasks and, ultimately, to achieve the proposed objective.

First, in Chapter 2 we have addressed the problem of designing a numerical approximation of the convective Cahn–Hilliard (CCH) equation (2.1) that avoids the nonphysical spurious oscillations in the convection-dominated regimes. This approximation was based on a piecewise constant upwind discontinuous Galerkin approach that conserves the mass and preserves the pointwise bounds for the simple linear transport equation (Sections 2.3.2 and 2.3.3). Then, these ideas were extended to the CCH equation with degenerate mobility in Section 2.4 and again proved to preserve the pointwise bounds. Finally, several numerical tests comparing the proposed approximation of the CCH with other approaches in the literature were presented in Section 2.5 showing the improvements introduced by the new technique.

After, in Chapter 3 we studied the classical Keller–Segel equations for chemotaxis. Using the ideas in Chapter 2 we were able to develop a numerical approximation of this system rewritten as a gradient flow problem in Section 3.4 which not only conserves the mass and preserves the positivity but also guarantees a discrete energy-stability property under certain restriction on the mesh. This scheme was tested in practice in Section 3.5 in different computationally demanding blow-up and pattern formation situations where it was shown to be successful in capturing very high peaks involving very steep gradients. In addition, these ideas were extended to other models related to chemotaxis in Chapter 4, providing really good numerical results. On the one hand, the results obtained for a generalization of the Keller–Segel equations in Section 4.3 are in complete accordance with the previously described theoretical analysis

and, on the other hand, the simulations of a neuroblast migration process shown in Section 4.4 could be fit using real data so that they are qualitatively and quantitatively comparable to the experimental results. The latter experience, in collaboration to neuroscientists, is important because it suggests that more complex models, including our tumor ones, might become a valuable tool for biomedical research in a not far future.

Then, in Chapter 5 we studied a diffuse-interface tumor model. First, in Section 5.3, we proposed a modification of an existing model in the literature by means of nonsymmetric degenerate mobility and proliferation functions that leads to bounded, more physically meaningful solutions. Then, in Section 5.4 we discretized this model using the techniques developed in Chapters 2 and 3 which allowed us to obtain a mass-conservative, pointwise-bounded and energy-stable numerical approximation of the system. Finally, we carried out several numerical experiments in Section 5.5 comparing the results with those obtained using the standard finite element discretization and showing the qualitative behavior of the model under different choices of mobility and proliferation functions. Among these tests we explored scenarios where the cross-diffusion is dominant, what would be prohibitive for other more standard approximations as indicated in Section 5.5.1.

Afterwards, we wanted to address the problem of generalizing the aforementioned tumor model considering the effects of the flow driven by the fluid that surrounds the tumor tissue. In this regard, we first analyzed and designed two different numerical schemes of a Cahn–Hilliard–Navier–Stokes (CHNS) model in Chapter 6, using again the ideas in Chapters 2 and Chapter 3. On the one hand, we presented a fully-coupled approximation in Section 6.4 that is mass-conservative, pointwise bounded and energy stable and, on the other hand, we proposed a decoupled approximation in Section 6.5 as a more computationally-efficient alternative but for which an energy-dissipation property is not known. These two approaches were compared through different benchmark tests and by means of a preliminary accuracy test in Section 6.6. Finally, in Chapter 7 we introduced an extension of the tumor model studied in Chapter 5 where we incorporate the fluid effects by means of a Cahn–Hilliard–Darcy system. The resulting framework might be seen as to be a natural step where the results derived in Chapters 5 and 6 are likely to be applied to derive a numerical scheme that guarantees mass-conservation, pointwise bounds and energy-stability properties.

In conclusion, this dissertation presents several advances towards the numerical approximation of diffuse-interface tumor growth models as well as other closely connected topics. However, the work

in this field is far from been completed and the natural question that arises is: what comes next? In this sense, the aforementioned results and discussion motivates the following lines of research that we would like to address in the near future.

- First, we are currently working on the project presented in Chapter 7, where the ultimate objective is to propose a structure-preserving approximation of the Cahn–Hilliard–Darcy model (7.10). Furthermore, we would like to compare the computational results obtained in Section 5.5 for the model (5.3) with the results for the model (7.10) that incorporates the effects of the fluid flow via the Darcy system.

- Can the condition (2.17) presented in Section 2.3.2 to ensure uniqueness of solution of the upwind DG approximation of the linear convection equation (2.16) be weakened? Removing this condition would mean that one may use the linear scheme (2.16) ensuring a positive approximation. Analogously, uniqueness of solution in the case of the linear scheme (4.6) presented in Section 4.3.3 to discretize the generalized Keller–Segel models (4.1) or (4.2), would ensure that the approximation obtained is always positive as observed in the numerical experiments in Section 4.3.4.

- In this work we have addressed the tumor models and related problems mostly from a purely numerical point of view. However, if we want to explore whether the results obtained can be applied to describing real phenomena, we need to use data, as it is done in previous works as [7, 8, 9, 137, 138, 160]. Unfortunately, fitting the models and the discrete approximations to real data is not simple and specifically developed techniques are required in order to obtain good results. In fact, even obtaining the specific real data needed to adjust the models is rather difficult. In our case, we have started exploring how to introduce the information obtained from real data, provided by the group of neuroscientists *INIBICA INCO-5*, led by Dr. Carmen Castro-González, with which there is already a strong collaboration, into a more simple chemotaxis model in [6]. However, this is still an ongoing work to be further studied in another PhD dissertation which is under development in our group. In this regard, we would like to work closely with the aforementioned group of neuroscientists in order to explore how real data of glioblastomas, a common type of brain cancer where they have previous experience (see, e.g. [98]), can be incorporated into the diffuse-interface tumor models that we have studied. Moreover, we believe that recently developed tools such as Neural Networks (NNs), see e.g. [99], or, more specifically, Physics Informed Neural Network

(PINNs), see [59, 162], that we are currently studying, can be of really good help to adjust the parameters of the models to real data.

- The techniques presented throughout the dissertation are based on a piecewise constant approximation of the pointwise bounded variable. This approximation plays a a crucial role in the proof of the pointwise bounds of the approximation. Extending these ideas to higher order approximations and therefore improving the computational efficiency of the algorithms is one of our next goals. In this sense, we would like to explore whether the ideas introduced in [196] by X. Zhang and C.-W. Shu and further developed in [161, 172, 197, 198] and the references therein, where a limiter is used to reconstruct high-order pointwise bounded approximations from cell-averaged pointwise bounded approximations under a CFL condition, can be combined with the ideas that we have presented.

- Moreover, in order to ensure the energy stability property we have used an approximation of the flow using the barycenters of the meshes that satisfy the geometrical constraint given in Hypothesis 3.4.3. We would like to study if this restriction can be weakened or removed by means of a more sophisticated approximation of the flow as shown in [63, Section 5.4].

- Regarding the decoupled scheme (6.34) presented in Chapter 6 to approximate the Cahn–Hilliard–Navier–Stokes model (6.1), we would like to explore whether this approximation can be improved by ensuring a discrete energy-stability property as it was done with the coupled counterpart (6.10). In this sense, the decoupled energy-stable schemes for a CHNS model with degenerate mobility found in the existing literature, such as the ones in [100, 107, 170], impose several restrictions that make them unlikely to be extended and combined with the ideas presented in this dissertation in order to preserve the pointwise bounds. Therefore, since we have not found any ideas that could lead, at least in a straightforward manner, to decoupled, pointwise-bounded and energy-stable schemes for the CHNS model (6.1), we believe this is a rather challenging task.

8.1 Scientific production directly connected to the dissertation

Finally, we present the publications, preprints and finished works that we have already developed in relation to this dissertation.

- Published:

- D. Acosta-Soba, F. Guillén-González, and J. R. Rodríguez-Galván. An upwind DG scheme preserving the maximum principle for the convective Cahn–Hilliard model. *Numerical Algorithms*, 92(3):1589–1619, 2022. DOI: 10.1007/s11075-022-01355-2.
  JCR category: Mathematics, Applied | Year: 2022 | Rank: 59/267 (Q1)
- D. Acosta-Soba, F. Guillén-González, and J. R. Rodríguez-Galván. An Unconditionally Energy Stable and Positive Upwind DG Scheme for the Keller–Segel Model. *Journal of Scientific Computing*, 97(1):18, 2023. DOI: 10.1007/s10915-023-02320-4.
  JCR category: Mathematics, Applied | Year: 2022 | Rank: 42/267 (Q1)
- D. Acosta-Soba, F. Guillén-González, and J. R. Rodríguez-Galván. A structure-preserving upwind DG scheme for a degenerate phase-field tumor model. *Computers & Mathematics with Applications*, 152:317–333, 2023. DOI: 10.1016/j.camwa.2023.10.028.
  JCR category: Mathematics, Applied | Year: 2022 | Rank: 29/267 (Q1)

- Submitted:
  - D. Acosta-Soba, F. Guillén-González, J. R. Rodríguez-Galván, and J. Wang. Property-preserving numerical approximations of a Cahn–Hilliard–Navier–Stokes model with variable densities and degenerate mobility. *Submitted, arXiv preprint*, 2023. DOI: 10.48550/arXiv.2310.01522.

- To be submitted:
  - D. Acosta-Soba, C. González-Castro, N. Geribaldi-Doldán, F. Guillén-González, P. Núnez-Abades, N. Ortega-Román, P. Pérez-García, and J. R. Rodríguez-Galván. Mathematical Modelling of Neuroblast Migration towards the Olfactory Bulb. *To be submitted, arXiv preprint*, 2022. DOI: 10.48550/arXiv.2211.06166.
  - T. Li, D. Acosta-Soba, A. Columbu, and G. Viglialoro. Dampening gradient nonlinearities prevent δ-formations in attraction-repulsion chemotaxis models. *To be submitted*, 2023.

CONCLUSIONES Y TRABAJOS FUTUROS

En esta tesis hemos abordado el desarrollo de aproximaciones numéricas físicamente significativas y que preservan las propiedades de los modelos tumorales de interfaz difusa que pueden conducir a una aplicación exitosa de los resultados para predecir cómo se comportan los tumores en la vida real.

Para ello, hemos dividido este objetivo en varios pasos más pequeños en los que hemos abordado problemas más asequibles que se han ido introduciendo en los diferentes capítulos de este trabajo. Los resultados obtenidos en cada uno de estos pasos han servido como punto de partida para abordar tareas más difíciles y, en última instancia, para conseguir del objetivo propuesto.

En primer lugar, en el Capítulo 2 hemos abordado el problema de diseñar una aproximación numérica de la ecuación de Cahn–Hilliard con convección (CCH), (2.1), que evite las oscilaciones espurias no físicas en situaciones de convección dominante. Esta aproximación se basa en una discretización de la ecuación, más simple, de transporte lineal (Secciones 2.3.2 y 2.3.3) de tipo Galerkin discontinuo aguas arriba con funciones constantes a trozos que conserva la masa y preserva las cotas puntuales. A continuación, estas ideas fueron extendidas a la ecuación CCH con movilidad degenerada en la Sección 2.4 y se demostró de nuevo que se preservan las cotas puntuales. Por último, mostramos varios experimentos numéricos en la Sección 2.5 en los que se compara la aproximación propuesta de CCH con otras posibilidades presentes en la literatura poniendo de manifiesto las mejoras introducidas por la nueva técnica.

Tras esto, en el Capítulo 3 estudiamos las ecuaciones clásicas de Keller–Segel para la quimiotaxis. Utilizando las ideas del Capítulo 2 pudimos desarrollar una aproximación numérica de este sistema reescrito como un problema de flujo gradiente en la Sección 3.4, la cual no sólo conserva la masa y preserva la positividad, sino que también garantiza una propiedad de estabilidad de energía discreta bajo cierta restricción en la malla. Este esquema se probó en la práctica en la Sección 3.5 en diferentes situaciones computacionalmente exigentes de explosión y formación de patrones, donde se mostró que es capaz de capturar de picos muy altos que implican gradientes muy pronunciados. Además, estas ideas se extendieron a otros modelos relacionados con la quimiotaxis en el Capítulo 4, proporcionando

resultados numéricos realmente buenos. Por un lado, los resultados obtenidos en la Sección 4.3 para una generalización de las ecuaciones de Keller–Segel están en total consonancia con el análisis teórico descrito anteriormente y, por otro, las simulaciones de un proceso de migración de neuroblastos mostradas en la Sección 4.4 pudieron ajustarse utilizando datos reales de forma que sean cualitativa y cuantitativamente comparables a los resultados experimentales. Esta última experiencia, en colaboración con neurocientíficos, es importante porque sugiere que los modelos más complejos, incluidos nuestros modelos de tumores, podrían convertirse en una herramienta valiosa para la investigación biomédica en un futuro no muy lejano.

Luego, en el Capítulo 5 estudiamos un modelo de tumor con interfaz difusa. En primer lugar, en la Sección 5.3, proponemos una modificación de un modelo existente en la literatura mediante funciones de movilidad y proliferación degeneradas y no simétricas que conducen a soluciones acotadas y más significativas desde el punto de vista físico. Después, en la Sección 5.4 discretizamos este modelo utilizando las técnicas desarrolladas en los Capítulos 2 y 3 que nos permiten obtener una aproximación numérica del sistema que conserva la masa, está acotada puntualmente y es estable energéticamente. Finalmente, realizamos varios experimentos numéricos en la Sección 5.5 comparando los resultados con los obtenidos utilizando la discretización de elementos finitos estándar y mostrando el comportamiento cualitativo del modelo con diferentes elecciones de funciones de movilidad y proliferación. En estos tests exploramos escenarios donde la difusión cruzada es dominante, lo que sería prohibitivo para otras aproximaciones más estándar como se indica en la Sección 5.5.1.

Posteriormente, quisimos abordar el problema de generalizar el modelo de tumor anterior considerando los efectos del flujo impulsado por el fluido que rodea al tejido tumoral. En este sentido, primero analizamos y diseñamos dos esquemas numéricos diferentes de un modelo Cahn–Hilliard–Navier–Stokes (CHNS) en el Capítulo 6, utilizando de nuevo las ideas de los Capítulos 2 y 3. Por un lado presentamos una aproximación totalmente acoplada en la Sección 6.4 que conserva la masa, está acotada puntualmente y es estable energéticamente y, por otro lado, propusimos una aproximación desacoplada en la Sección 6.5 como una alternativa más eficiente desde el punto de vista computacional, pero para la cual no se conoce una propiedad de disipación de energía. Estas dos aproximaciones se comparan en diferentes tests de referencia y mediante un test preliminar de convergencia en la Sección 6.6. Por último, en el Capítulo 7 presentamos una extensión del modelo de tumor estudiado en el Capítulo 5 donde incorporamos los efectos del fluido mediante un sistema Cahn–Hilliard–Darcy. El problema resultante se

puede ver como un paso natural en el que parece que los resultados obtenidos en los Capítulos 5 y 6 se pueden aplicar para desarrollar un esquema numérico que garantice las propiedades de conservación de la masa, cotas puntuales y estabilidad de energía.

En conclusión, esta tesis presenta varios avances en relación a la aproximación numérica de los modelos de crecimiento tumoral de interfaz difusa, así como en otros temas estrechamente relacionados. Sin embargo, el trabajo en este campo está lejos de estar concluido y la pregunta natural que surge es: ¿qué viene después? En este sentido, los resultados y la discusión anteriores motivan las siguientes líneas de investigación que nos gustaría abordar en un futuro próximo.

- En primer lugar, actualmente estamos trabajando en el proyecto presentado en el Capítulo 7, donde el objetivo final es proponer una aproximación que preserve las propiedades del modelo de Cahn–Hilliard–Darcy (7.10). Además, nos gustaría comparar los resultados computacionales obtenidos en la Sección 5.5 para el modelo (5.3) con los resultados para el modelo (7.10) que incorpora los efectos del flujo del fluido a través del sistema de Darcy.

- ¿Puede debilitarse la condición (2.17) presentada en la Sección 2.3.2 para garantizar la unicidad de solución de la aproximación DG de la ecuación de convección lineal (2.16)? La eliminación de esta condición significaría que se puede utilizar el esquema lineal (2.16) garantizando una aproximación positiva. Análogamente, la unicidad de la solución en el caso del esquema lineal (4.6) presentado en la Sección 4.3.3 para discretizar los modelos generalizados de Keller–Segel (4.1) o (4.2), garantizaría que la aproximación obtenida es siempre positiva como se observa en los experimentos numéricos de la Sección 4.3.4.

- En este trabajo hemos abordado los modelos de tumores y los problemas relacionados principalmente desde un punto de vista puramente numérico. Sin embargo, si queremos explorar si los resultados obtenidos pueden aplicarse a la descripción de fenómenos reales, necesitamos utilizar datos, como se hace en trabajos anteriores como [7, 8, 9, 137, 138, 160]. Desafortunadamente, ajustar los modelos y las aproximaciones discretas a datos reales no es sencillo y se requieren técnicas específicamente desarrolladas para obtener buenos resultados. De hecho, incluso obtener los datos reales específicos necesarios para ajustar los modelos es bastante difícil. En nuestro caso, hemos empezado a explorar cómo introducir la información obtenida de datos reales, proporcionada por el grupo de neurocientíficos *INIBICA INCO-5*, dirigido por la Dra. Carmen Castro-González,

con el que ya existe una fuerte colaboración, en un modelo de quimiotaxis más simple en [6]. Sin embargo, este trabajo está todavía en desarrollo y se estudiará con más profundidad en otra tesis doctoral que se está desarrollando en nuestro grupo. En este sentido, nos gustaría colaborar estrechamente con el grupo de neurocientíficos mencionado anteriormente para explorar cómo los datos reales de glioblastomas, un tipo común de cáncer cerebral en el que ellos tienen experiencia previa (véase, por ejemplo, [98]), pueden incorporarse a los modelos tumorales de interfaz difusa que hemos estudiado. Además, creemos que las herramientas desarrolladas recientemente, como las redes neuronales (NNs), véase por ejemplo [99], o, más específicamente, las redes neuronales físicamente informadas (PINNs), véase [59, 162], que estamos estudiando actualmente, pueden ser de gran ayuda para ajustar los parámetros de los modelos a los datos reales.

- Las técnicas presentadas a lo largo de la tesis se basan en una aproximación con funciones constantes a trozos de la variable acotada puntualmente. Esta aproximación desempeña un papel crucial en la demostración de los cotas puntuales de la aproximación. Uno de nuestros próximos objetivos es extender estas ideas a aproximaciones de orden superior y, por tanto, mejorar la eficiencia computacional de los algoritmos. En este sentido, nos gustaría explorar si las ideas introducidas en [196] por X. Zhang y C.-W. Shu y desarrolladas posteriormente en [161, 172, 197, 198] y las referencias allí mencionadas, donde se utiliza un limitador para reconstruir aproximaciones acotadas puntualmente de orden alto a partir de aproximaciones con cotas puntuales en la media de las celdas bajo una condición CFL, pueden combinarse con las ideas que hemos presentado.

- Además, para asegurar la propiedad de estabilidad de energía hemos utilizado una aproximación del flujo utilizando los baricentros de las mallas que satisfacen la restricción geométrica dada en la Hipótesis 3.4.3. Nos gustaría estudiar si esta restricción puede debilitarse o eliminarse mediante una aproximación más sofisticada del flujo como se muestra en [63, Sección 5.4].

- Con respecto al esquema desacoplado (6.34) presentado en el Capítulo 6 para aproximar el modelo de Cahn–Hilliard–Navier–Stokes (6.1), nos gustaría explorar si esta aproximación puede mejorarse asegurando una propiedad de estabilidad de energía discreta como se hizo con el esquema acoplado (6.10). En este sentido, los esquemas desacoplados estables energéticamente para un modelo CHNS con movilidad degenerada encontrados en la literatura existente, como los de [100, 107, 170], imponen varias restricciones que hacen improbable que se puedan generalizar y combinar

con las ideas presentadas en esta tesis para preservar las cotas puntuales. Por lo tanto, dado que no hemos encontrado ninguna idea que pueda conducir, al menos de forma directa, a esquemas desacoplados, con cotas puntuales y estables energéticamente para el modelo CHNS (6.1), creemos que se trata de una tarea bastante difícil.

Producción científica directamente relacionada con la tesis

Finalmente, presentamos las publicaciones, *preprints* y trabajos terminados que hemos desarrollado en relación con esta tesis.

- Publicados:
  - D. Acosta-Soba, F. Guillén-González, and J. R. Rodríguez-Galván. An upwind DG scheme preserving the maximum principle for the convective Cahn–Hilliard model. *Numerical Algorithms*, 92(3):1589–1619, 2022. DOI: 10.1007/s11075-022-01355-2. Categoría JCR: "Mathematics, Applied" | Año: 2022 | Rango: 59/267 (Q1)
  - D. Acosta-Soba, F. Guillén-González, and J. R. Rodríguez-Galván. An Unconditionally Energy Stable and Positive Upwind DG Scheme for the Keller–Segel Model. *Journal of Scientific Computing*, 97(1):18, 2023. DOI: 10.1007/s10915-023-02320-4. Categoría JCR: "Mathematics, Applied" | Año: 2022 | Rango: 42/267 (Q1)
  - D. Acosta-Soba, F. Guillén-González, and J. R. Rodríguez-Galván. A structure-preserving upwind DG scheme for a degenerate phase-field tumor model. *Computers & Mathematics with Applications*, 152:317–333, 2023. DOI: 10.1016/j.camwa.2023.10.028. Categoría JCR: "Mathematics, Applied" | Año: 2022 | Rango: 29/267 (Q1)
- Enviados:
  - D. Acosta-Soba, F. Guillén-González, J. R. Rodríguez-Galván, and J. Wang. Property-preserving numerical approximations of a Cahn–Hilliard–Navier–Stokes model with variable densities and degenerate mobility. *Submitted, arXiv preprint*, 2023. DOI: 10.48550/arXiv.2310.01522.
- Por enviar:

– D. Acosta-Soba, C. González-Castro, N. Geribaldi-Doldán, F. Guillén-González, P. Núnez-Abades, N. Ortega-Román, P. Pérez-García, and J. R. Rodríguez-Galván. Mathematical Modelling of Neuroblast Migration towards the Olfactory Bulb. *To be submitted, arXiv preprint*, 2022. DOI: 10.48550/arXiv.2211.06166.

– T. Li, D. Acosta-Soba, A. Columbu, and G. Viglialoro. Dampening gradient nonlinearities prevent δ-formations in attraction-repulsion chemotaxis models. *To be submitted*, 2023.

REFERENCES

[1] H. Abels, H. Garcke, and G. Grün. Thermodynamically consistent, frame indifferent diffuse interface models for incompressible two-phase flows with different densities. *Mathematical Models and Methods in Applied Sciences*, 22(03):1150013, 2012. DOI: 10.1142/S0218202511500138.

[2] D. Acosta-Soba, F. Guillén-González, and J. R. Rodríguez-Galván. A structure-preserving upwind DG scheme for a degenerate phase-field tumor model. *Computers & Mathematics with Applications*, 152:317–333, 2023. DOI: 10.1016/j.camwa.2023.10.028.

[3] D. Acosta-Soba, F. Guillén-González, and J. R. Rodríguez-Galván. An Unconditionally Energy Stable and Positive Upwind DG Scheme for the Keller–Segel Model. *Journal of Scientific Computing*, 97(1):18, 2023. DOI: 10.1007/s10915-023-02320-4.

[4] D. Acosta-Soba, F. Guillén-González, and J. R. Rodríguez-Galván. An upwind DG scheme preserving the maximum principle for the convective Cahn–Hilliard model. *Numerical Algorithms*, 92(3):1589–1619, 2022. DOI: 10.1007/s11075-022-01355-2.

[5] D. Acosta-Soba, F. Guillén-González, J. R. Rodríguez-Galván, and J. Wang. Property-preserving numerical approximations of a Cahn–Hilliard–Navier–Stokes model with variable densities and degenerate mobility. *Submitted, arXiv preprint*, 2023. DOI: 10.48550/arXiv.2310.01522.

[6] D. Acosta-Soba et al. Mathematical Modelling of Neuroblast Migration towards the Olfactory Bulb. *To be submitted, arXiv preprint*, 2022. DOI: 10.48550/arXiv.2211.06166.

[7] A. Agosti, P. Ciarletta, H. Garcke, and M. Hinze. Learning patient-specific parameters for a diffuse interface glioblastoma model from neuroimaging data. *Mathematical Methods in the Applied Sciences*, 43(15):8945–8979, 2020. DOI: 10.1002/mma.6588.

[8] A. Agosti et al. A computational framework for the personalized clinical treatment of glioblastoma multiforme. *ZAMM-Journal of Applied Mathematics and Mechanics / Zeitschrift für Angewandte Mathematik und Mechanik*, 98(12):2307–2327, 2018. DOI: 10.1002/zamm.201700294.

[9] A. Agosti et al. A personalized mathematical tool for neuro-oncology: A clinical case study. *International Journal of Non-Linear Mechanics*, 107:170–181, 2018. DOI: 10.1016/j.ijnonlinmec.2018.06.004.

[10] J. Ahrens, B. Geveci, and C. Law. 36 - ParaView: An End–User Tool for Large–Data Visualization. In C. D. Hansen and C. R. Johnson, editors, *Visualization Handbook*, pages 717–731. Elsevier, 2005. DOI: 10.1016/B978-012387582-2/50038-1.

[11] M. Aida et al. Lower estimate of the attractor dimension for a chemotaxis growth system. *Journal of the London Mathematical Society*, 74(2):453–474, 2006. DOI: 10.1112/S0024610706023015.

[12] R. Almeda, H. van Someren Gréve, and T. Kiørboe. Behavior is a major determinant of predation risk in zooplankton. *Ecosphere*, 8(2):e01668, 2017. DOI: 10.1002/ecs2.1668.

[13] M. S. Alnaes et al. Unified Form Language: A domain-specific language for weak formulations of partial differential equations. *ACM Transactions on Mathematical Software*, 40(2):1–37, 2014. DOI: 10.1145/2566630.

[14] M. Alnæs et al. The FEniCS Project Version 1.5. *Archive of Numerical Software*, 3(100), 2015. DOI: 10.11588/ans.2015.100.20553.

[15] J. Altman. Autoradiographic and histological studies of postnatal neurogenesis. IV. Cell proliferation and migration in the anterior forebrain, with special reference to persisting neurogenesis in the olfactory bulb. *J Comp Neurol*, 137(4):433–57, 1969. DOI: 10.1002/cne.901370404.

[16] P. R. Amestoy, I. S. Duff, J.-Y. L'Excellent, and J. Koster. A Fully Asynchronous Multifrontal Solver Using Distributed Dynamic Scheduling. *SIAM Journal on Matrix Analysis and Applications*, 23(1):15–41, 2001. DOI: 10.1137/S0895479899358194.

[17] P. R. Amestoy, A. Guermouche, J.-Y. L'Excellent, and S. Pralet. Hybrid scheduling for the parallel solution of linear systems. *Parallel computing*, 32(2):136–156, 2006. DOI: 10.1016/j.parco.2005.07.004.

[18] B. Andreianov, M. Bendahmane, and M. Saad. Finite volume methods for degenerate chemotaxis model. *Journal of Computational and Applied Mathematics*, 235(14):4015–4031, 2011. DOI: 10.1016/j.cam.2011.02.023.

[19] A. C. Aristotelous. *Adaptive Discontinuous Galerkin Finite Element Methods for a Diffuse Interface Model of Biological Growth*. PhD thesis, University of Tennessee, 2011. URL: http://trace.tennessee.edu/utk_graddiss/1051/.

[20] A. C. Aristotelous, O. A. Karakashian, and S. M. Wise. Adaptive, second-order in time, primitive-variable discontinuous Galerkin schemes for a Cahn–Hilliard equation with a mass source. *IMA Journal of Numerical Analysis*, 35(3):1167–1198, 2015. DOI: 10.1093/imanum/dru035.

[21] G. Arumugam and J. Tyagi. Keller-Segel Chemotaxis Models: A Review. *Acta Applicandae Mathematicae*, 171:6, 2021. DOI: 10.1007/s10440-020-00374-2.

[22] V. Badalassi, H. Ceniceros, and S. Banerjee. Computation of multiphase systems with phase field models. *Journal of Computational Physics*, 190(2):371–397, 2003. DOI: 10.1016/S0021-9991(03)00280-8.

[23] S. Badia, J. Bonilla, and J. V. Gutiérrez-Santacreu. Bound-preserving finite element approximations of the Keller–Segel equations. *Mathematical Models and Methods in Applied Sciences*, 33(03):609–642, 2023. DOI: 10.1142/S0218202523500148.

[24] S. Badia, F. Guillén-González, and J. V. Gutiérrez-Santacreu. Finite element approximation of nematic liquid crystal flows using a saddle-point structure. *Journal of Computational Physics*, 230(4):1686–1706, 2011. DOI: 10.1016/j.jcp.2010.11.033.

[25] R. Bailo, J. A. Carrillo, S. Kalliadasis, and S. P. Perez. Unconditional Bound-Preserving and Energy-Dissipating Finite-Volume Schemes for the Cahn-Hilliard Equation. *Communications in Computational Physics*, 34(3):713–748, 2023. DOI: https://doi.org/10.4208/cicp.OA-2023-0049.

[26] S. Balay et al. PETSc/TAO Users Manual. Technical report ANL-21/39 - Revision 3.19, Argonne National Laboratory, 2023. DOI: 10.2172/1968587.

[27] J. W. Barrett, J. F. Blowey, and H. Garcke. Finite element approximation of the Cahn–Hilliard equation with degenerate mobility. *SIAM Journal on Numerical Analysis*, 37(1):286–318, 1999. DOI: 10.1137/S0036142997331669.

[28] N. Bellomo, A. Bellouquid, Y. Tao, and M. Winkler. Toward a mathematical theory of Keller–Segel models of pattern formation in biological tissues. *Mathematical Models and Methods in Applied Sciences*, 25(09):1663–1763, 2015. DOI: 10.1142/S021820251550044X.

[29] A. L. Bertozzi, S. Esedoglu, and A. Gillette. Inpainting of Binary Images Using the Cahn–Hilliard Equation. *IEEE Transactions on Image Processing*, 16(1):285–291, 2007. DOI: 10.1109/tip.2006.887728.

[30] A. Blanchet et al. A hybrid variational principle for the Keller–Segel system in $\mathbb{R}^2$. *ESAIM: Mathematical Modelling and Numerical Analysis*, 49(6):1553–1576, 2015. DOI: 10.1051/m2an/2015021.

[31] D. Boffi, F. Brezzi, and M. Fortin. *Mixed finite element methods and applications*, number 44 in Springer Series in Computational Mathematics. Springer, 2013. DOI: 10.1007/978-3-642-36519-5.

[32] F. Boyer. A theoretical and numerical model for the study of incompressible mixture flows. *Computers & fluids*, 31(1):41–68, 2002. DOI: 10.1016/s0045-7930(00)00031-1.

[33] F. Boyer and F. Nabet. A DDFV method for a Cahn-Hilliard/Stokes phase field model with dynamic boundary conditions. *ESAIM: Mathematical Modelling and Numerical Analysis*, 51(5):1691–1731, 2017. DOI: 10.1051/m2an/2016073.

[34] S. C. Brenner and L. R. Scott. *The Mathematical Theory of Finite Element Methods*, number 15 in Texts in Applied Mathematics. Springer, 2008. DOI: 10.1007/978-0-387-75934-0.

[35] J. W. Cahn. On spinodal decomposition. *Acta Metallurgica*, 9(9):795–801, 1961. DOI: 10.1016/0001-6160(61)90182-1.

[36] J. W. Cahn and J. E. Hilliard. Free Energy of a Nonuniform System. I. Interfacial Free Energy. *The Journal of Chemical Physics*, 28(2):258–267, 1958. DOI: 10.1063/1.1744102.

[37] A. Carleton et al. Becoming a new neuron in the adult olfactory bulb. *Nature Neuroscience*, 6(5):507–518, 2003. DOI: 10.1038/nn1048.

[38] G. Chamoun, M. Saad, and R. Talhouk. Monotone combined edge finite volume-finite element scheme for Anisotropic Keller–Segel model. *Numerical Methods for Partial Differential Equations*, 30(3):1030–1065, 2014. DOI: 10.1002/num.21858.

[39] M. Chen, S. Lu, and Q. Liu. Uniqueness of weak solutions to a Keller-Segel-Navier-Stokes model with a logistic source. *Applications of Mathematics*, 67(1):93–101, 2022. DOI: 10.21136/AM.2021.0069-20.

[40] W. Chen, J. Jing, C. Wang, and X. Wang. A positivity preserving, energy stable finite difference scheme for the Flory–Huggins–Cahn–Hilliard–Navier-Stokes system. *Journal of Scientific Computing*, 92(2):31, 2022. DOI: 10.1007/s10915-022-01872-1.

[41] W. Chen, Q. Liu, and J. Shen. Error Estimates and Blow-Up Analysis of a Finite–Element Approximation for the Parabolic–Elliptic Keller–Segel System. *International Journal of Numerical Analysis and Modeling*, 19(2-3):275–298, 2022. URL: http://global-sci.org/intro/article_detail/ijnam/20481.html.

[42] W. Chen, C. Wang, X. Wang, and S. M. Wise. Positivity-preserving, energy stable numerical schemes for the Cahn-Hilliard equation with logarithmic potential. *Journal of Computational Physics: X*, 3:100031, 2019. DOI: 10.1016/j.jcpx.2019.100031.

[43] Y. Chen and J. Shen. Efficient, adaptive energy stable schemes for the incompressible Cahn–Hilliard Navier–Stokes phase-field models. *Journal of Computational Physics*, 308:40–56, 2016. DOI: 10.1016/j.jcp.2015.12.006.

[44] K. Cheng, W. Feng, C. Wang, and S. M. Wise. An energy stable fourth order finite difference scheme for the Cahn–Hilliard equation. *Journal of Computational and Applied Mathematics*, 362:574–595, 2019. DOI: 10.1016/j.cam.2018.05.039.

[45] A. Chertock and A. Kurganov. A second-order positivity preserving central-upwind scheme for chemotaxis and haptotaxis models. *Numerische Mathematik*, 111(2):169–205, 2008. DOI: 10.1007/s00211-008-0188-0.

[46] S. Chulián, A Martínez-Rubio, M. Rosa, and V. M. Pérez-García. Mathematical models of Leukaemia and its treatment: A review. *SeMA Journal*, 79(3):441–486, 2022. DOI: 10.1007/s40324-022-00305-1.

[47] P. Ciarlet and P. Raviart. Maximum principle and uniform convergence for the finite element method. *Computer Methods in Applied Mechanics and Engineering*, 2(1):17–31, 1973. DOI: 10.1016/0045-7825(73)90019-4.

[48] P. G. Ciarlet. *The Finite Element Method for Elliptic Problems*. Classics in Applied Mathematics. SIAM, 2002. DOI: 10.1137/1.9780898719208.

[49] F. H. Clarke. *Optimization and nonsmooth analysis*. Classics in Applied Mathematics. SIAM, 1990. DOI: 10.1137/1.9781611971309.

[50] P. Codega et al. Prospective identification and purification of quiescent adult neural stem cells from their in vivo niche. *Neuron*, 82(3):545–59, 2014. DOI: 10.1016/j.neuron.2014.02.039.

[51] P. Colli, G. Gilardi, and D. Hilhorst. On a Cahn–Hilliard type phase field system related to tumor growth. *Discrete and Continuous Dynamical Systems*, 35(6):2423–2442, 2015. DOI: 10.3934/dcds.2015.35.2423.

[52] P. Colli, G. Gilardi, E. Rocca, and J. Sprekels. Asymptotic analyses and error estimates for a Cahn-Hilliard type phase field system modelling tumor growth. *Discrete & Continuous Dynamical Systems-Series S*, 10(1):37–54, 2017. DOI: 10.3934/dcdss.2017002.

[53] P. Colli, G. Gilardi, E. Rocca, and J. Sprekels. Vanishing viscosities and error estimate for a Cahn–Hilliard type phase field system related to tumor growth. *Nonlinear Analysis: Real World Applications*, 26:93–108, 2015. DOI: 10.1016/j.nonrwa.2015.05.002.

[54] P. Colli, G. Gilardi, A. Signori, and J. Sprekels. Cahn–Hilliard–Brinkman model for tumor growth with possibly singular potentials. *Nonlinearity*, 36(8):4470, 2023. DOI: 10.1088/1361-6544/ace2a7.

[55] A. Columbu, S. Frassu, and G. Viglialoro. Properties of given and detected unbounded solutions to a class of chemotaxis models. *Studies in Applied Mathematics*, 151(4):1349–1379, 2023. DOI: 10.1111/sapm.12627.

[56] A. Columbu, R. D. Fuentes, and S. Frassu. Uniform-in-time boundedness in a class of local and nonlocal nonlinear attraction-repulsion chemotaxis models with logistics. *arXiv preprint*, 2023. DOI: 10.48550/arXiv.2311.06526.

[57] V. Cristini and J. Lowengrub. *Multiscale Modeling of Cancer: An Integrated Experimental and Mathematical Modeling Approach*. Cambridge University Press, 2010. DOI: 10.1017/CBO9780511781452.

[58] L. Cueto-Felgueroso and J. Peraire. A time-adaptive finite volume method for the Cahn–Hilliard and Kuramoto–Sivashinsky equations. *Journal of Computational Physics*, 227(24):9985–10017, 2008. DOI: 10.1016/j.jcp.2008.07.024.

[59] S. Cuomo et al. Scientific Machine Learning Through Physics–Informed Neural Networks: Where we are and What's Next. *Journal of Scientific Computing*, 92(3):88, 2022. DOI: 10.1007/s10915-022-01939-z.

[60] L. D. Dalcin, R. R. Paz, P. A. Kler, and A. Cosimo. Parallel distributed computing using Python. *Advances in Water Resources*, 34(9):1124–1139, 2011. DOI: 10.1016/j.advwatres.2011.04.013.

[61] R. Dautray and J.-L. Lions. *Mathematical Analysis and Numerical Methods for Science and Technology: Evolution Problems I*, volume 5. Springer, 1999. ISBN: 9783540661016.

[62] M. Dehghan and V. Mohammadi. Comparison between two meshless methods based on collocation technique for the numerical solution of four-species tumor growth model. *Communications*

in Nonlinear Science and Numerical Simulation, 44:204–219, 2017. DOI: 10.1016/j.cnsns.2016.07.024.

[63] D. A. Di Pietro and A. Ern. *Mathematical Aspects of Discontinuous Galerkin Methods*, number 69 in Mathématiques et Applications. Springer, 2012. DOI: 10.1007/978-3-642-22980-0.

[64] J. I. Díaz and T Nagai. Symmetrization in a parabolic-elliptic system related to chemotaxis. *Advances in Mathematical Sciences and Applications*, 5(2):659–680, 1995. URL: https://blogs.mat.ucm.es/jidiaz/wp-content/uploads/sites/31/2017/09/A_059.pdf.

[65] H. Ding, P. D. M. Spelt, and C. Shu. Diffuse interface model for incompressible two-phase flows with large density ratios. *Journal of Computational Physics*, 226(2):2078–2095, 2007. DOI: 10.1016/j.jcp.2007.06.028.

[66] V. Dolejší and M. Feistauer. *Discontinuous Galerkin Method*, number 48 in Springer Series in Computational Mathematics. Springer, 2015. DOI: 10.1007/978-3-319-19267-3.

[67] M. Ebenbeck and H. Garcke. Analysis of a Cahn–Hilliard–Brinkman model for tumour growth with chemotaxis. *Journal of Differential Equations*, 266(9):5998–6036, 2019. DOI: 10.1016/j.jde.2018.10.045.

[68] M. Ebenbeck, H. Garcke, and R. Nürnberg. Cahn–Hilliard–Brinkman systems for tumour growth. *Discrete and Continuous Dynamical Systems-S*, 14(11):3989–4033, 2021. DOI: 10.3934/dcdss.2021034.

[69] C. Elbar and A. Poulain. Analysis and numerical simulation of a generalized compressible Cahn-Hilliard-Navier-Stokes model with friction effects. *arXiv preprint*, 2023. DOI: 10.48550/arXiv.2305.05623.

[70] C. M. Elliott and D. A. French. A nonconforming finite-element method for the two-dimensional Cahn–Hilliard equation. *SIAM Journal on Numerical Analysis*, 26(4):884–903, 1989. DOI: 10.1137/0726049.

[71] C. M. Elliott and H. Garcke. On the Cahn–Hilliard equation with degenerate mobility. *SIAM Journal on Mathematical Analysis*, 27(2):404–423, 1996. DOI: 10.1137/S0036141094267662.

[72] Y. Epshteyn. Discontinuous Galerkin methods for the chemotaxis and haptotaxis models. *Journal of Computational and Applied Mathematics*, 224(1):168–181, 2009. DOI: 10.1016/j.cam.2008.04.030.

[73] Y. Epshteyn and A. Kurganov. New Interior Penalty Discontinuous Galerkin Methods for the Keller–Segel Chemotaxis Model. *SIAM Journal on Numerical Analysis*, 47(1):386–408, 2009. DOI: 10.1137/07070423X.

[74] A. Ern and J.-L. Guermond. *Theory and Practice of Finite Elements*, number 159 in Applied mathematical sciences. Springer, 2004. DOI: 10.1007/978-1-4757-4355-5.

[75] D. Esteve et al. Adult Neural Stem Cell Migration Is Impaired in a Mouse Model of Alzheimer's Disease. *Molecular Neurobiology*, 59(2):1168–1182, 2022. DOI: 10.1007/s12035-021-02620-6.

[76] L. C. Evans. *Partial differential equations*, number 19 in Graduate Studies in Mathematics. American Mathematical Society, 2010. ISBN: 978-1-4704-6942-9.

[77] D. J. Eyre. An unconditionally stable one-step scheme for gradient systems. *Unpublished article*, 1998. URL: https://citeseerx.ist.psu.edu/document?repid=rep1&type=pdf&doi=4f016a98fe25bfc06b9bcab3d85eeaa47d3ad3ca.

[78] I. Fatkullin. A study of blow-ups in the Keller–Segel model of chemotaxis. *Nonlinearity*, 26(1):81–94, 2013. DOI: 10.1088/0951-7715/26/1/81.

[79] A. Fernández-Romero, F. Guillén-González, and A. Suárez. A Glioblastoma PDE–ODE model including chemotaxis and vasculature. *ESAIM: Mathematical Modelling and Numerical Analysis*, 56(2):407–431, 2022. DOI: 10.1051/m2an/2022012.

[80] A. Fernández-Romero, F. Guillén-González, and A. Suárez. Theoretical and numerical analysis for a hybrid tumor model with diffusion depending on vasculature. *Journal of Mathematical Analysis and Applications*, 503(2):125325, 2021. DOI: 10.1016/j.jmaa.2021.125325.

[81] F. Frank, C. Liu, F. O. Alpak, and B. Riviere. A finite volume / discontinuous Galerkin method for the advective Cahn–Hilliard equation with degenerate mobility on porous domains stemming from micro-CT imaging. *Computational Geosciences*, 22(2):543–563, 2018. DOI: 10.1007/s10596-017-9709-1.

[82] F. Frank, A. Rupp, and D. Kuzmin. Bound-preserving flux limiting schemes for DG discretizations of conservation laws with applications to the Cahn–Hilliard equation. *Computer Methods in Applied Mechanics and Engineering*, 359:112665, 2020. DOI: 10.1016/j.cma.2019.112665.

[83] S. Frassu, T. Li, and G. Viglialoro. Improvements and generalizations of results concerning attraction-repulsion chemotaxis models. *Mathematical Methods in the Applied Sciences*, 45(17):11067–11078, 2022. DOI: 10.1002/mma.8437.

[84] S. Frassu, R. Rodríguez Galván, and G. Viglialoro. Uniform in time L^∞-estimates for an attraction-repulsion chemotaxis system with double saturation. *Discrete and Continuous Dynamical Systems - Series B*, 28(3):1886–1904, 2023. DOI: 10.3934/dcdsb.2022151.

[85] H. Frieboes et al. Three-dimensional multispecies nonlinear tumor growth-II: Tumor invasion and angiogenesis. *Journal of Theoretical Biology*, 264(4):1254–1278, 2010. DOI: 10.1016/j.jtbi.2010.02.036.

[86] S Frigeri, K. Lam, E Rocca, G Schimperna, et al. On a multi-species Cahn-Hilliard-Darcy tumor growth model with singular potentials. *Communications in Mathematical Sciences*, 16(3):821–856, 2018. DOI: 10.4310/CMS.2018.v16.n3.a11.

[87] S. Frigeri, M. Grasselli, and E. Rocca. On a diffuse interface model of tumour growth. *European Journal of Applied Mathematics*, 26(2):215–243, 2015. DOI: 10.1017/S0956792514000436.

[88] M. Fritz. Tumor evolution models of phase-field type with nonlocal effects and angiogenesis. *Bulletin of Mathematical Biology*, 85(6):44, 2023. DOI: 10.1007/s11538-023-01151-6.

[89] M. Fritz, E. A. Lima, J Tinsley Oden, and B. Wohlmuth. On the unsteady Darcy–Forchheimer–Brinkman equation in local and nonlocal tumor growth models. *Mathematical Models and Methods in Applied Sciences*, 29(09):1691–1731, 2019. DOI: 10.1142/S0218202519500325.

[90] D. Furihata. A stable and conservative finite difference scheme for the Cahn–Hilliard equation. *Numerische Mathematik*, 87(4):675–699, 2001. DOI: 10.1007/PL00005429.

[91] H. Garcke, B. Kovács, and D. Trautwein. Viscoelastic Cahn–Hilliard models for tumor growth. *Mathematical Models and Methods in Applied Sciences*, 32(13):2673–2758, 2022. DOI: 10.1142/S0218202522500634.

[92] H. Garcke and K. F. Lam. *On a Cahn–Hilliard–Darcy System for Tumour Growth with Solution Dependent Source Terms*. In *Trends in Applications of Mathematics to Mechanics*. E. Rocca, U. Stefanelli, L. Truskinovsky, and A. Visintin, editors. Springer, 2018, pages 243–264. DOI: 10.1007/978-3-319-75940-1_12.

[93] H. Garcke, K. F. Lam, R. Nürnberg, and E. Sitka. A multiphase Cahn–Hilliard–Darcy model for tumour growth with necrosis. *Mathematical Models and Methods in Applied Sciences*, 28(03):525–577, 2018. DOI: 10.1142/S0218202518500148.

[94] H. Garcke, K. F. Lam, and A. Signori. On a phase field model of Cahn–Hilliard type for tumour growth with mechanical effects. *Nonlinear Analysis: Real World Applications*, 57:103192, 2021. DOI: 10.1016/j.nonrwa.2020.103192.

[95] H. Garcke, K. F. Lam, E. Sitka, and V. Styles. A Cahn–Hilliard–Darcy model for tumour growth with chemotaxis and active transport. *Mathematical Models and Methods in Applied Sciences*, 26(06):1095–1148, 2016. DOI: 10.1142/S0218202516500263.

[96] H. Garcke and S. Yayla. Long-time dynamics for a Cahn–Hilliard tumor growth model with chemotaxis. *Zeitschrift für angewandte Mathematik und Physik*, 71(4):123, 2020. DOI: 10.1007/s00033-020-01351-3.

[97] I. Geipel et al. Predation risks of signalling and searching: bats prefer moving katydids. *Biology Letters*, 16(4):20190837, 2020. DOI: 10.1098/rsbl.2019.0837.

[98] R. Gómez-Oliva et al. Evolution of Experimental Models in the Study of Glioblastoma: Toward Finding Efficient Treatments. *Frontiers in Oncology*, 10:614295, 2021. DOI: 10.3389/fonc.2020.614295.

[99] I. Goodfellow, Y. Bengio, and A. Courville. *Deep learning*. MIT Press, 2016. ISBN: 9780262035613.

[100] G. Grün, F. Guillén-González, and S. Metzger. On Fully Decoupled, Convergent Schemes for Diffuse Interface Models for Two-Phase Flow with General Mass Densities. *Communications in Computational Physics*, 19(5):1473–1502, 2016. DOI: 10.4208/cicp.scpde14.39s.

[101] J. L. Guermond, P. Minev, and J. Shen. An overview of projection methods for incompressible flows. en. *Computer Methods in Applied Mechanics and Engineering*, 195(44-47):6011–6045, 2006. DOI: 10.1016/j.cma.2005.10.010.

[102] J. L. Guermond and J. Shen. A new class of truly consistent splitting schemes for incompressible flows. *Journal of computational physics*, 192(1):262–276, 2003. DOI: 10.1016/j.jcp.2003.07.009.

[103] F. Guillén-González and G. Tierra. Energy-stable and boundedness preserving numerical schemes for the Cahn-Hilliard equation with degenerate mobility. *Applied Numerical Mathematics*, 196:62–82, 2024. DOI: 10.1016/j.apnum.2023.10.006.

[104] F. Guillén-González and G. Tierra. Finite element numerical schemes for a chemo-attraction and consumption model. *Journal of Computational and Applied Mathematics*, 441:115676, 2024. DOI: 10.1016/j.cam.2023.115676.

[105] F. Guillén-González and G. Tierra. On linear schemes for a Cahn–Hilliard diffuse interface model. *Journal of Computational Physics*, 234:140–171, 2013. DOI: 10.1016/j.jcp.2012.09.020.

[106] F. Guillén-González and G. Tierra. Second order schemes and time-step adaptivity for Allen–Cahn and Cahn–Hilliard models. *Computers & Mathematics with Applications*, 68(8):821–846, 2014. DOI: 10.1016/j.camwa.2014.07.014.

[107] F. Guillén-González and G. Tierra. Splitting Schemes for a Navier-Stokes-Cahn-Hilliard Model for Two Fluids with Different Densities. *Journal of Computational Mathematics*, 32(6):643–664, 2014. DOI: 10.4208/jcm.1405-m4410.

[108] L. Guo, X. H. Li, and Y. Yang. Energy Dissipative Local Discontinuous Galerkin Methods for Keller–Segel Chemotaxis Model. *Journal of Scientific Computing*, 78(3):1387–1404, 2019. DOI: 10.1007/s10915-018-0813-8.

[109] Z. Guo, P. Lin, J. Lowengrub, and S. M. Wise. Mass conservative and energy stable finite difference methods for the quasi-incompressible Navier–Stokes–Cahn–Hilliard system: Primitive variable and projection-type schemes. *Computer Methods in Applied Mechanics and Engineering*, 326:144–174, 2017. DOI: 10.1016/j.cma.2017.08.011.

[110] M. E. Gurtin, D. Polignone, and J. Vinals. Two-phase binary fluids and immiscible fluids described by an order parameter. *Mathematical Models and Methods in Applied Sciences*, 6(6):815–831, 1996. DOI: 10.1142/S0218202596000341.

[111] J. V. Gutiérrez-Santacreu and J. R. Rodríguez-Galván. Analysis of a fully discrete approximation for the classical Keller–Segel model: Lower and a priori bounds. *Computers & Mathematics with Applications*, 85:69–81, 2021. DOI: 10.1016/j.camwa.2021.01.009.

[112] A. Hawkins-Daarud, S. Prudhomme, K. G. van der Zee, and J. T. Oden. Bayesian calibration, validation, and uncertainty quantification of diffuse interface models of tumor growth. *Journal of Mathematical Biology*, 67(6–7):1457–1485, 2013. DOI: 10.1007/s00285-012-0595-9.

[113] A. Hawkins-Daarud, K. G. van der Zee, and J. Tinsley Oden. Numerical simulation of a thermodynamically consistent four-species tumor growth model. *International Journal for Numerical Methods in Biomedical Engineering*, 28(1):3–24, 2012. DOI: 10.1002/cnm.1467.

[114] M. A. Herrero and J. J. Velázquez. A blow-up mechanism for a chemotaxis model. *Annali della Scuola Normale Superiore di Pisa - Classe di Scienze*, 24(4):633–683, 1997. URL: https://eudml.org/doc/84273.

[115] P. C. Hohenberg and B. I. Halperin. Theory of dynamic critical phenomena. *Reviews of Modern Physics*, 49(3):435–479, 1977. DOI: 10.1103/RevModPhys.49.435.

[116] D. Horstmann and G. Wang. Blow-up in a chemotaxis model without symmetry assumptions. *European Journal of Applied Mathematics*, 12(2):159–177, 2001. DOI: 10.1017/S0956792501004363.

[117] F. Huang and J. Shen. Bound/Positivity Preserving and Energy Stable Scalar auxiliary Variable Schemes for Dissipative Systems: Applications to Keller–Segel and Poisson–Nernst–Planck Equations. *SIAM Journal on Scientific Computing*, 43(3):A1832–A1857, 2021. DOI: 10.1137/20M1365417.

[118] Q.-A. Huang, W. Jiang, J. Z. Yang, and C. Yuan. A structure-preserving, upwind-SAV scheme for the degenerate Cahn–Hilliard equation with applications to simulating surface diffusion. *Journal of Scientific Computing*, 97(3):64, 2023. DOI: 10.1007/s10915-023-02380-6.

[119] J. D. Hunter. Matplotlib: A 2D Graphics Environment. *Computing in Science & Engineering*, 9(3):90–95, 2007. DOI: 10.1109/MCSE.2007.55.

[120] M. Ibrahim and M. Saad. On the efficacy of a control volume finite element method for the capture of patterns for a volume-filling chemotaxis model. *Computers & Mathematics with Applications*, 68(9):1032–1051, 2014. DOI: 10.1016/j.camwa.2014.03.010.

[121] S. Ishida, J. Lankeit, and G. Viglialoro. A Keller-Segel type taxis model with ecological interpretation and boundedness due to gradient nonlinearities. *arXiv preprint*, 2023. DOI: 10.48550/arXiv.2306.12137.

[122] M. Kandasamy et al. Reduction in subventricular zone-derived olfactory bulb neurogenesis in a rat model of Huntington's disease is accompanied by striatal invasion of neuroblasts. *PLoS One*, 10(2):e0116069, 2015. DOI: 10.1371/journal.pone.0116069.

[123] P. Kareiva and G. Odell. Swarms of Predators Exhibit "Preytaxis" if Individual Predators Use Area-Restricted Search. *The American Naturalist*, 130(2):233–270, 1987. DOI: 10.1086/284707.

[124] D. Kay, V. Styles, and E. Süli. Discontinuous Galerkin Finite Element Approximation of the Cahn–Hilliard Equation with Convection. *SIAM Journal on Numerical Analysis*, 47(4):2660–2685, 2009. DOI: 10.1137/080726768.

[125] E. F. Keller and L. A. Segel. Initiation of slime mold aggregation viewed as an instability. *Journal of Theoretical Biology*, 26(3):399–415, 1970. DOI: 10.1016/0022-5193(70)90092-5.

[126] E. F. Keller and L. A. Segel. Model for chemotaxis. *Journal of Theoretical Biology*, 30(2):225–234, 1971. DOI: 10.1016/0022-5193(71)90050-6.

[127] J. Kim. A numerical method for the Cahn–Hilliard equation with a variable mobility. *Communications in Nonlinear Science and Numerical Simulation*, 12(8):1560–1571, 2007. DOI: 10.1016/j.cnsns.2006.02.010.

[128] J. Kim. Phase-Field Models for Multi-Component Fluid Flows. *Communications in Computational Physics*, 12(3):613–661, 2012. DOI: 10.4208/cicp.301110.040811a.

[129] Z. Kohl et al. Impaired adult olfactory bulb neurogenesis in the R6/2 mouse model of Huntington's disease. *BMC Neuroscience*, 11:114, 2010. DOI: 10.1186/1471-2202-11-114.

[130] F. Lazarini and P. M. Lledo. Is adult neurogenesis essential for olfaction? *Trends in Neurosciences*, 34(1):20–30, 2011. DOI: 10.1016/j.tins.2010.09.006.

[131] C. Le Magueresse et al. Subventricular zone-derived neuroblasts use vasculature as a scaffold to migrate radially to the cortex in neonatal mice. *Cerebral Cortex*, 22(10):2285–2296, 2012. DOI: 10.1093/cercor/bhr302.

[132] R. J. LeVeque. *Finite Volume Methods for Hyperbolic Problems*. Cambridge Texts in Applied Mathematics. Cambridge University Press, 2002. DOI: 10.1017/CBO9780511791253.

[133] R. Li et al. Discontinuous finite volume element method for a coupled Navier-Stokes-Cahn-Hilliard phase field model. *Advances in Computational Mathematics*, 46(2):25, 2020. DOI: 10.1007/s10444-020-09764-4.

[134] T. Li, D. Acosta-Soba, A. Columbu, and G. Viglialoro. Dampening gradient nonlinearities prevent δ-formations in attraction-repulsion chemotaxis models. *To be submitted*, 2023.

[135] T. Li, S. Frassu, and G. Viglialoro. Combining effects ensuring boundedness in an attraction–repulsion chemotaxis model with production and consumption. *Zeitschrift für angewandte Mathematik und Physik*, 74(3):109, 2023. DOI: 10.1007/s00033-023-01976-0.

[136] X. H. Li, C.-W. Shu, and Y. Yang. Local Discontinuous Galerkin Method for the Keller-Segel Chemotaxis Model. *Journal of Scientific Computing*, 73(2-3):943–967, 2017. DOI: 10.1007/s10915-016-0354-y.

[137] E. Lima et al. Selection and validation of predictive models of radiation effects on tumor growth based on noninvasive imaging data. *Computer Methods in Applied Mechanics and Engineering*, 327:277–305, 2017. DOI: 10.1016/j.cma.2017.08.009.

[138] E. Lima et al. Selection, calibration, and validation of models of tumor growth. *Mathematical Models and Methods in Applied Sciences*, 26(12):2341–2368, 2016. DOI: 10.1142/S0218202516500550X.

[139] C. Liu, B. Rivière, J. Shen, and X. Zhang. A simple and efficient convex optimization based bound-preserving high order accurate limiter for Cahn–Hilliard–Navier–Stokes system. *arXiv preprint*, 2023. DOI: 10.48550/arXiv.2307.09726.

[140] C. Liu et al. A pressure-correction and bound-preserving discretization of the phase-field method for variable density two-phase flows. *Journal of Computational Physics*, 449:110769, 2022. DOI: 10.1016/j.jcp.2021.110769.

[141] H. Liu and P. Yin. Unconditionally energy stable discontinuous Galerkin schemes for the Cahn–Hilliard equation. *Journal of Computational and Applied Mathematics*, 390:113375, 2021. DOI: 10.1016/j.cam.2020.113375.

[142] A. Logg, K.-A. Mardal, G. N. Wells, et al. *Automated Solution of Differential Equations by the Finite Element Method*, number 84 in Lecture Notes in Computational Science and Engineering. Springer, 2012. DOI: 10.1007/978-3-642-23099-8.

[143] C. Lois and A. Alvarez-Buylla. Long-distance neuronal migration in the adult mammalian brain. *Science*, 264(5162):1145–1148, 1994. DOI: 10.1126/science.8178174.

[144] J. Lowengrub and L. Truskinovsky. Quasi–incompressible Cahn–Hilliard fluids and topological transitions. *Proceedings of the Royal Society of London. Series A: Mathematical, Physical and Engineering Sciences*, 454(1978):2617–2654, 1998. DOI: 10.1098/rspa.1998.0273.

[145] J. S. Lowengrub et al. Nonlinear modelling of cancer: bridging the gap between cells and tumours. *Nonlinearity*, 23(1):R1–R91, 2010. DOI: 10.1088/0951-7715/23/1/R01.

[146] S. S. Magavi, B. R. Leavitt, and J. D. Macklis. Induction of neurogenesis in the neocortex of adult mice. *Nature*, 405(6789):951–955, 2000. DOI: 10.1038/35016083.

[147] S. McDougall, A. Anderson, and M. Chaplain. Mathematical modelling of dynamic adaptive tumour-induced angiogenesis: Clinical implications and therapeutic targeting strategies. *Journal of Theoretical Biology*, 241(3):564–589, 2006. DOI: 10.1016/j.jtbi.2005.12.022.

[148] M. Mimura and T. Tsujikawa. Aggregating pattern dynamics in a chemotaxis model including growth. *Physica A: Statistical Mechanics and its Applications*, 230(3-4):499–543, 1996. DOI: 10.1016/0378-4371(96)00051-9.

[149] A. Miranville. The Cahn–Hilliard equation and some of its variants. *AIMS Mathematics*, 2(3):479–544, 2017. DOI: 10.3934/Math.2017.2.479.

[150] A. Miranville. *The Cahn–Hilliard equation: recent advances and applications*, number 95 in CBMS-NSF Regional Conference Series in Applied Mathematics. SIAM, 2019. DOI: 10.1137/1.9781611975925.

[151] V. Mohammadi and M. Dehghan. Simulation of the phase field Cahn–Hilliard and tumor growth models via a numerical scheme: Element-free Galerkin method. *Computer Methods in Applied Mechanics and Engineering*, 345:919–950, 2019. DOI: 10.1016/j.cma.2018.11.019.

[152] C. M. Morshead and D. van der Kooy. Postmitotic death is the fate of constitutively proliferating cells in the subependymal layer of the adult mouse brain. *J Neurosci*, 12(1):249–56, 1992. DOI: 10.1523/JNEUROSCI.12-01-00249.1992.

[153] S. C. Nam et al. Dynamic features of postnatal subventricular zone cell motility: a two-photon time-lapse study. *Journal of Comparative Neurology*, 505(2):190–208, 2007. DOI: 10.1002/cne.21473.

[154] A. Novick-Cohen. Chapter 4 The Cahn–Hilliard Equation. In C. M. Dafermos and M. Pokorny, editors, *Handbook of Differential Equations: Evolutionary Equations*. Volume 4, pages 201–228. Elsevier, 2008. DOI: 10.1016/S1874-5717(08)00004-2.

[155] K. Obernier and A. Alvarez-Buylla. Neural stem cells: origin, heterogeneity and regulation in the adult mammalian brain. *Development*, 146(4):dev156059, 2019. DOI: 10.1242/dev.156059.

[156] J. T. Oden, A. Hawkins, and S. Prudhomme. General diffuse-interface theories and an approach to predictive tumor growth modeling. *Mathematical Models and Methods in Applied Sciences*, 20(03):477–517, 2010. DOI: 10.1142/S0218202510004313.

[157] J. T. Oden et al. Toward Predictive Multiscale Modeling of Vascular Tumor Growth: Computational and Experimental Oncology for Tumor Prediction. *Archives of Computational Methods in Engineering*, 23(4):735–779, 2016. DOI: 10.1007/s11831-015-9156-x.

[158] O. Pironneau. *Finite element methods for fluids*. Wiley, 1989. ISBN: 978-0471922551.

[159] G. Ponti, K. Obernier, and A. Alvarez-Buylla. Lineage progression from stem cells to new neurons in the adult brain ventricular-subventricular zone. *Cell Cycle*, 12(11):1649–1650, 2013. DOI: 10.4161/cc.24984.

[160] G. Pozzi et al. T cell therapy against cancer: A predictive diffuse-interface mathematical model informed by pre-clinical studies. *Journal of Theoretical Biology*, 547:111172, 2022. DOI: 10.1016/j.jtbi.2022.111172.

[161] T. Qin and C.-W. Shu. Implicit positivity-preserving high-order discontinuous Galerkin methods for conservation laws. *SIAM Journal on Scientific Computing*, 40(1):A81–A107, 2018. DOI: 10.1137/17M112436X.

[162] M. Raissi, P. Perdikaris, and G. E. Karniadakis. Physics-informed neural networks: A deep learning framework for solving forward and inverse problems involving nonlinear partial differential equations. *Journal of Computational physics*, 378:686–707, 2019. DOI: 10.1016/j.jcp.2018.10.045.

[163] B. Rivière. *Discontinuous Galerkin methods for solving elliptic and parabolic equations: theory and implementation*. Frontiers in applied mathematics. SIAM, 2008. DOI: 10.1137/1.9780898717440.

[164] T. Roose, S. J. Chapman, and P. K. Maini. Mathematical models of avascular tumor growth. *SIAM review*, 49(2):179–208, 2007. DOI: 10.1137/S0036144504446291.

[165] N. Saito. Conservative upwind finite-element method for a simplified Keller–Segel system modelling chemotaxis. *IMA Journal of Numerical Analysis*, 27(2):332–365, 2007. DOI: 10.1093/imanum/drl018.

[166] M. W. Scroggs, I. A. Baratta, C. N. Richardson, and G. N. Wells. Basix: a runtime finite element basis evaluation library. *Journal of Open Source Software*, 7(73):3982, 2022. DOI: 10.21105/joss.03982.

[167] M. W. Scroggs, J. S. Dokken, C. N. Richardson, and G. N. Wells. Construction of Arbitrary Order Finite Element Degree-of-Freedom Maps on Polygonal and Polyhedral Cell Meshes. *ACM Transactions on Mathematical Software*, 48(2):18, 2022. DOI: 10.1145/3524456.

[168] J. Shen and J. Xu. Unconditionally Bound Preserving and Energy Dissipative Schemes for a Class of Keller–Segel Equations. *SIAM Journal on Numerical Analysis*, 58(3):1674–1695, 2020. DOI: 10.1137/19M1246705.

[169] J. Shen, J. Xu, and J. Yang. The scalar auxiliary variable (SAV) approach for gradient flows. *Journal of Computational Physics*, 353:407–416, 2018. DOI: 10.1016/j.jcp.2017.10.021.

[170] J. Shen and X. Yang. Decoupled, Energy Stable Schemes for Phase-Field Models of Two-Phase Incompressible Flows. *SIAM Journal on Numerical Analysis*, 53(1):279–296, 2015. DOI: 10.1137/140971154.

[171] X. Shen, L. Wu, J. Wen, and J. Zhang. SAV Fourier-spectral method for diffuse-interface tumor-growth model. *Computers & Mathematics with Applications*, 140:250–259, 2023. DOI: 10.1016/j.camwa.2022.09.031.

[172] C.-W. Shu. High order WENO and DG methods for time-dependent convection-dominated PDEs: A brief survey of several recent developments. *Journal of Computational Physics*, 316:598–613, 2016. DOI: 10.1016/j.jcp.2016.04.030.

[173] A. Signori. *Understanding the Evolution of Tumours, a Phase-field Approach: Analytic Results and Optimal Control*. PhD thesis, University of Milano Bicocca, 2020. URL: https://signori.faculty.polimi.it/files/PhDthesis.pdf.

[174] P. Souplet. Finite Time Blow-up for a Non-linear Parabolic Equation with a Gradient Term and Applications. *Mathematical methods in the applied sciences*, 19(16):1317–1333, 1996. DOI: 10.1002/(SICI)1099-1476(19961110)19:16%3C1317::AID-MMA835%3E3.0.CO;2-M.

[175] C. B. Sullivan and A. Kaszynski. PyVista: 3D plotting and mesh analysis through a streamlined interface for the Visualization Toolkit (VTK). *Journal of Open Source Software*, 4(37):1450, 2019. DOI: 10.21105/joss.01450.

[176] H. Sung et al. Global cancer statistics 2020: GLOBOCAN estimates of incidence and mortality worldwide for 36 cancers in 185 countries. *CA: A Cancer Journal for Clinicians*, 71(3):209–249, 2021. DOI: 10.3322/caac.21660.

[177] Y. Tao and M. Winkler. Global existence and boundedness in a Keller–Segel–Stokes model with arbitrary porous medium diffusion. *Discrete & Continuous Dynamical Systems*, 32(5):1901–1914, 2012. DOI: 10.3934/dcds.2012.32.1901.

[178] J. I. Tello and M. Winkler. A Chemotaxis System with Logistic Source. *Communications in Partial Differential Equations*, 32(6):849–877, 2007. DOI: 10.1080/03605300701319003.

[179] M. F. P. Ten Eikelder, K. G. van der Zee, I. Akkerman, and D. Schillinger. A unified framework for Navier–Stokes Cahn–Hilliard models with non-matching densities. *Mathematical Models and Methods in Applied Sciences*, 33(1):175–221, 2023. DOI: 10.1142/S0218202523500069.

[180] G Tierra and F Guillén-González. Numerical methods for solving the Cahn–Hilliard equation and its applicability to related energy-based models. *Archives of Computational Methods in Engineering*, 22(2):269–289, 2015. DOI: 10.1007/s11831-014-9112-1.

[181] R. Tyson, L. Stern, and R. J. LeVeque. Fractional step methods applied to a chemotaxis model. *Journal of Mathematical Biology*, 41:455–475, 2000. DOI: 10.1007/s002850000038.

[182] J. D. van der Waals. The thermodynamic theory of capillarity flow under the hypothesis of a continuous variation of density. *Verhandel. Konink. Akad. Weten. Amsterdam*, 1(8), 1893. In Dutch. English translation by J. S. Rowlinson. *Journal of Statistical Physics*, 20:197–200, 1979. DOI: 10.1007/BF01011513.

[183] A. W. Visser. Motility of zooplankton: fitness, foraging and predation. *Journal of Plankton research*, 29(5):447–461, 2007. DOI: 10.1093/plankt/fbm029.

[184] C. Wang and S. M. Wise. An Energy Stable and Convergent Finite-Difference Scheme for the Modified Phase Field Crystal Equation. *SIAM Journal on Numerical Analysis*, 49(3):945–969, 2011. DOI: 10.1137/090752675.

[185] G. N. Wells, E. Kuhl, and K. Garikipati. A discontinuous Galerkin method for the Cahn–Hilliard equation. *Journal of Computational Physics*, 218(2):860–877, 2006. DOI: 10.1016/j.jcp.2006.03.010.

[186] M. Winkler. Aggregation vs. global diffusive behavior in the higher-dimensional Keller–Segel model. *Journal of Differential Equations*, 248(12):2889–2905, 2010. DOI: 10.1016/j.jde.2010.02.008.

[187] M. Winkler. Finite-time blow-up in low-dimensional Keller–Segel systems with logistic-type superlinear degradation. *Zeitschrift für Angewandte Mathematik und Physik*, 69(2):40, 2018. DOI: 10.1007/s00033-018-0935-8.

[188] M. Winkler. Global large-data solutions in a chemotaxis-(Navier–)Stokes system modeling cellular swimming in fluid drops. *Communications in Partial Differential Equations*, 37(2):319–351, 2012. DOI: 10.1080/03605302.2011.591865.

[189] S. Wise, J. Lowengrub, H. Frieboes, and V. Cristini. Three-dimensional multispecies nonlinear tumor growth-I: Model and numerical method. *Journal of Theoretical Biology*, 253(3):524–543, 2008. DOI: 10.1016/j.jtbi.2008.03.027.

[190] X. Wu, G. J. Zwieten, and K. G. van der Zee. Stabilized second-order convex splitting schemes for Cahn–Hilliard models with application to diffuse-interface tumor-growth models. *International Journal for Numerical Methods in Biomedical Engineering*, 30(2):180–203, 2014. DOI: 10.1002/cnm.2597.

[191] Y. Xia, Y. Xu, and C.-W. Shu. Local discontinuous Galerkin methods for the Cahn–Hilliard type equations. *Journal of Computational Physics*, 227(1):472–491, 2007. DOI: 10.1016/j.jcp.2007.08.001.

[192] X. Yang. Linear, first and second-order, unconditionally energy stable numerical schemes for the phase field model of homopolymer blends. *Journal of Computational Physics*, 327:294–316, 2016. DOI: 10.1016/j.jcp.2016.09.029.

[193] X. Yang and L. Ju. Efficient linear schemes with unconditional energy stability for the phase field elastic bending energy model. *Computer Methods in Applied Mechanics and Engineering*, 315:691–712, 2017. DOI: 10.1016/j.cma.2016.10.041.

[194] X. Yang, J. Zhao, and Q. Wang. Numerical approximations for the molecular beam epitaxial growth model based on the invariant energy quadratization method. *Journal of Computational Physics*, 333:104–127, 2017. DOI: 10.1016/j.jcp.2016.12.025.

[195] R. Zhang, J. Zhu, A. F. Loula, and X. Yu. Operator splitting combined with positivity-preserving discontinuous Galerkin method for the chemotaxis model. *Journal of Computational and Applied Mathematics*, 302:312–326, 2016. DOI: 10.1016/j.cam.2016.02.018.

[196] X. Zhang and C.-W. Shu. On maximum-principle-satisfying high order schemes for scalar conservation laws. *Journal of Computational Physics*, 229(9):3091–3120, 2010. DOI: 10.1016/j.jcp.2009.12.030.

[197] X. Zhang, Y. Xia, and C.-W. Shu. Maximum-principle-satisfying and positivity-preserving high order discontinuous Galerkin schemes for conservation laws on triangular meshes. *Journal of Scientific Computing*, 50(1):29–62, 2012. DOI: 10.1007/s10915-011-9472-8.

[198] Y. Zhang, X. Zhang, and C.-W. Shu. Maximum-principle-satisfying second order discontinuous Galerkin schemes for convection–diffusion equations on triangular meshes. *Journal of Computational Physics*, 234:295–316, 2013. DOI: 10.1016/j.jcp.2012.09.032.

VITA

Daniel Acosta Soba was born and raised in San Fernando (Cádiz), Spain. He received a bachelor's and master's degree in Mathematics from the Universidad de Cádiz (UCA), Spain, in 2019 and 2020, respectively. Then, he earned his doctoral degrees in Mathematics at the UCA and in Computational Science, with a Computational and Applied Mathematics concentration, at the University of Tennessee at Chattanooga (UTC), USA, in 2024 under the international joint supervision agreement by UCA and UTC. His doctoral program has been supervised by Dr. Francisco Guillén González (Universidad de Sevilla, Spain), Dr. J. Rafael Rodríguez Galván (UCA) and Dr. Jin Wang (UTC).

Daniel has worked as a predoctoral fellow and as a substitute teaching tutor at the UCA, teaching linear algebra, real analysis, differential equations and numerical analysis courses. During his doctoral program, he has gained significant experience coding in Python and he, with his advisors, has published three papers in very high ranked journals and submitted another one. At the time of submitting this dissertation, he is about to submit other two papers in collaboration with two different research groups and he is working on other two publications with his advisors. He has visited the UTC for 9 months under the supervision of his advisor Dr. Jin Wang and the Università degli Studi di Cagliari for 3 months under the supervision of Dr. Silvia Frassu and Dr. Giuseppe Viglialoro. He was an invited speaker at the following international conferences: CEDYA 2020 and 2022, BYMAT 2020 and 2022, UTC Research Dialogues 2022, CANA 2023, FEniCS 2023 and ICIAM 2023. Moreover, he has been invited to give a talk in the seminar series "VI Jornadas Doctorales del Programa de Doctorado en Matemáticas" at the UCA in 2020, in the series "Advanced Modeling and Simulation Thrust Seminar" of the SimCenter at the UTC in 2021 and in the series sponsored by the research project "Analysis of PDEs in connection with real phenomena" at the Università degli Studi di Cagliari in 2023. Also, he has been invited to participate in the "Oberwolfach Seminar: Control of PDEs Models for Living Systems" organized by the Mathematisches Forschungsinstitut Oberwolfach in 2023.